The effects of PPARβ/δ ligands on lung inflammation and vascular reactivity

Noelia Perez Diaz

Submitted to the University of Hertfordshire in partial fulfilment of the requirements of the degree of Doctor of Philosophy (PhD)

August 2019

Abstract

Introduction: The peroxisome proliferator activated receptor beta/delta (PPARβ/δ) is a transcription factor ubiquitously expressed in cells, although more highly active in skeletal muscle, arteries and endothelium. Signalling via PPARβ/δ is involved in lipid metabolism, glucose metabolism, insulin sensitivity, inflammation, and cell proliferation and therefore it is emerging as a therapeutic target for the treatment of disorders associated with metabolic syndrome or diabetes. However, there are great discrepancies in the literature about the role of PPARβ/δ and scientists describe both anti- and pro-effects on inflammation, cell migration and cell proliferation after ligand-activation of PPARβ/δ. Understanding the PPARβ/δ mode of action is of great interest and may provide new molecular mechanisms for treating a variety of inflammation-related diseases. This thesis aims to expand the knowledge on PPARβ/δ to better understand its mechanism of action at genomic and non-genomic level, which might give some clues for new therapeutic drug developments targeting PPARβ/δ.

Methods: Pharmacological techniques including organ bath and myography were used for the study of the non-genomic effects of PPARβ/δ on vascular tone, comparing aorta and mesenteric arteries as a model of systemic and resistance vasculature respectively from healthy and streptozotocin (STZ)-induced diabetic rats. Molecular biology techniques including Griess assay, ELISA and qRT-PCR were used for the study of the regulation of lung inflammation by PPARβ/δ, focusing on the PPARβ/δ molecular switch between induction and trans-repression, two different pathways of gene regulation. Computational methods such as docking were used for the study of the PPARβ/δ binding pocket and how

PPARβ/δ is activated/repressed after ligand binding as well as the possibility of accommodating more than one ligand simultaneously into the binding pocket.

Results: In large STZ-diabetic systemic aorta arteries, PPARβ/δ inhibits the contraction through the PI3K/Akt/eNOS pathway. GW0742, a PPARβ/δ agonist, improves vasodilation through the RhoA/ROCK pathway in Naïve aorta and through potassium channels in STZ-diabetic aorta. In resistance arteries such as mesenteric arteries, PPARβ/δ inhibits the contraction through the PI3K/Akt/eNOS pathway in Naïve and possibly STZ-diabetic tissues. In contrast, GW0742 inhibits the RhoA/ROCK pathway on STZ-diabetic mesentery arteries and regulates the potassium channels in Naïve mesenteric arteries in a PPARβ/δ independent manner. In the model of lung inflammation used, the presence of agonist (GW0742 or L-165041) and antagonist (GSK3787 or GSK0660) at same time has anti-inflammatory effects and switches the PPARβ/δ mode of action from induction to trans-repression, therefore it was concluded that, at least in this model, the PPARβ/δ induction mode of action is pro-inflammatory and the trans-repression anti-inflammatory. PPARβ/δ agonists and antagonists bind differently to the PPARβ/δ receptor pocket. PPARβ/δ agonists form polar interactions with the residues His287, His413 and Tyr437 whilst PPARβ/δ antagonists form polar interactions with the residues Thr252 and Asn307. Further, our modelling indicates favourable binding energies and the feasibility of two ligands binding at same time into the PPARβ/δ binding pocket.

Conclusion: A multidisciplinary approach was designed for the study of PPARβ/δ and provided novel information about its functioning both at genomic and non-genomic level. The findings of this thesis can help the drug discovery industry for a better prediction of the modelling behaviour of new PPARβ/δ drugs and can support the rationale for developing new treatments targeting PPARβ/δ for hypertension and/or cardiovascular complications.

Acknowledgement

Firstly, I would like to give my gratitude to my supervisory team Dr Lisa Lione, Dr Louise Mackenzie and Dr Victoria Hutter for your guide, support and help during the development of this project. Thank you for understanding my fluctuating circumstances and demands, without you this thesis would have not been possible.

Thanks to my Biochemistry work colleagues Nathan Davies, Magdalena Liszka and Ravi Joshi for your support and patience with me all these years. I would also like to extend my gratitude to the rest of the technical teams of LMS, specially Microbiology, Molecular Biology and Pharmacology teams.

A big thank you to Professor Francisco Perez-Vizcaino, Dr Laura Moreno Gutierrez and the rest of the Pharmacology group from the Complutense de Madrid University for making me feel part of the team from day one and your continuous support in the distance every time a needed your help. I learnt a great deal from all of you and I hope to keep collaborating with you in the future.

Thanks to Dr Cristina Barrero Sicilia for being there every time I needed help with the PCRs but most importantly for your friendship. And thank you to John Davis and Michelle Botha, your help was crucial to get to the end of this thesis.

Thank you, Sara, for being at the other side of the screen every time I needed you even when we were literally one world apart. Words are not needed. Everything is said.

I would like to thank my parents, family and friends. Thank you for your support through all my life, for cheering me up when I am down and believe in me no matter what. I cannot thank you enough in one lifetime.

Thank you, Carlos, for your patience and generosity. I know that it has not been easy for you but still you always respected and supported all my decisions. But I am more grateful for keeping me in touch with the human part of me, without you I would be a cold emotionless robot only worried about work.

And the most special thank you is to our son Gabinin for coming at the right time. You gave me the final push and strength that I needed to complete this thesis.

Publications

Scientific papers

· **Perez-Diaz N.,** Pushkarsky I., Oweis N., Lione L. A. and Mackenzie L. S. (2018). "The non-genomic effects of the PPARβ/δ; Agonist GW0742 on streptozotocin treated rat aorta." Current Molecular Pharmacology 11: 149-154.

· **Perez-Diaz N.,** Zloh M., Patel P. and Mackenzie L. S. (2016). "In silico modelling of prostacyclin and other lipid mediators to nuclear receptors reveal novel thyroid hormone receptor antagonist properties." Prostaglandins Other Lipid Mediat 122: 18-27.

· Zloh M., **Perez-Diaz N.,** Tang L., Patel P. and Mackenzie L. S. (2016). "Evidence that diclofenac and celecoxib are thyroid hormone receptor beta antagonists." Life Sciences 146: 66-72.

· **Perez-Diaz N.** and Mackenzie L. S. (2015). "Linking induction and transrepression of PPARβ/δ with cellular function." Annual Research & Review in Biology 6: 253-263.

Poster presentation and abstract publication at external research conferences

· **Perez-Diaz N.,** Barakat J., Perez-Vizcaino F., Moreno L., Mackenzie L. S. "The PPARβ/δ agonist GW0742 prevents LPS-induced nitrite production in rat parenchyma but not in aorta or pulmonary arteries". International conference of the British Pharmacology Society (BPS), London 2014; pA2 online, Vol. 12, No. 3.

· **Perez-Diaz N**., Zloh M., Tang L., Patel P., Mackenzie S. L. "Evidence that diclofenac and celecoxib are thyroid hormone receptor beta antagonists; use of in silico, molecular and pharmacological techniques". International conference of the British Pharmacology Society (BPS), London 2015; pA2 online, Vol. 13, No.3

Table of contents

List of figures

x

List of tables

Abbreviations

8-HETE	8-hydroxyeicosatetraenoic acid
9-HODE	9-hydroxyoctadecadienoic acid
13-HODE	13-hydroxyoctadecadienoic acid
Aa	Amino acid
Ach	Acetylcholine
AF-1	Ligand-independent transactivation motif
AF-2	Ligand-dependent transactivation motif
Akt	Protein kinase B
ALI	Acute lung injury
AM	Alveolar macrophages
AP-1	Activator protein 1
BB	Biobreeding rat
BCA	Bicinchoninic acid
Bcl-6	B cell lymphoma-6
BSA	Bovine serum albumin
cGMP	Cyclic guanosine monophosphate
ChIP	Chromatin immunoprecipitation
CLP	Cecal ligation and puncture operation
Co-IP	Co-immunoprecipitation
CVD	Cardiovascular disease
DBD	DNA binding domain
DMEM	Dulbecco's Modified Eagle's Medium
DMSO	Dimethyl sulfoxide
DTT	Dithiothreitol
EC	Endothelial cell
ECL	Enhanced chemiluminescence
ELISA	Enzyme-linked immunosorbent assay
eNOS	Endothelial nitric oxide synthase
ER	Endoplasmic reticulum
ERK1/2	Extracellular signal-regulated kinase 1/2
ETYA	Eicosatetranoic acid
FBS	Foetal bovine serum
FT	Flow through

FXR	Farnesoid X receptor
GAP	GTPase activation protein
GDP	Guanosine diphosphate
GEF	Guanine nucleotide exchange
GK	Goto kakizaki rat
GSK-3β	Glycogen synthase kinase 3β
GTP	Guanosine triphosphate
HBO_2	Hyperbaric oxygen therapy
HDAC	Histone deacetylases
HDL-cholesterol	High density lipoprotein-cholesterol
HEPES	4-(2-hydroxyethyl)-1-piperazineethanesulfonic acid
HUVEC	Human umbilical vascular endothelium cell
IκB-α	Inhibitor of NF-κB alpha
IFN-γ	Interferon gamma
IL-1β	Interleukin 1-β
IL-6	Interleukin 6
iNOS	Inducible nitric oxide synthase
IP	Immunoprecipitation
IR	Insulin receptor
JAK	Janus kinase
KK	Kyoji Kondo
KPSS	High potassium physiological saline solution
Kv7	Voltage-dependent potassium channel
LBD	Ligand binding domain
LDL-cholesterol	Low density lipoprotein-cholesterol
LPS	Lipopolysaccharide
LXR	Liver X receptor
MAPK	Mitogen-activated protein kinase
MD simulation	Molecular dynamics simulation
MLCK	Myosin light chain kinase
MLCP	Myosin light chain phosphorylse
MNU	N-methyl-N-nitrosurea moiety
MS	Mass spectometry
NCo-R	Nuclear receptor co-repressor
NF-κB	Nuclear factor κB
NMR	Nuclear magnetic resonance
NO	Nitric oxide

NOD	Non-obese diabetic mice
NSY	Nagoya shibata yasuda mice
NTD	N-terminal domain
OEA	Oleoylethanomamide
OLETF	Otsuka long-evants tokoshima fatty rat
PA	Pulmonary artery
PASMC	Pulmonary artery smooth muscle cell
PBP	PPAR binding protein
PBS	Phosphate buffered saline
PCR	Polymerase chain reaction
PDB	Protein data bank
PDGF	Platelet derived growth factor
PDK-1	Phosphoinositide-dependent protein kinase-1
PE	Phenylephrine
PGC1-α	PPAR gamma co-activator 1-alpha
PI3K	Phosphatidylinositol 3-kinase
PKCα	Protein kinase C α
PMVEC	Pulmonary microvascular endothelial cells
PPAR	Peroxisome proliferator activated receptor
PPRE	Peroxisome proliferator response element
PSMCs	Pulmonary smooth muscle cells
PSS	Physiological saline solution
PVDF	Polyvinylidene difluoride
PXR	Pregnane X receptor
qRT-PCR	Quantitative real time polymerase chain reaction
RAR	Retinoid acid receptor
RhoA	Ras homolog gene family, member A
RIP140	Receptor interacting protein 140
ROCK	RhoA kinase
ROS	Reactive oxygen species
RT	Reverse transcription
RXR	Retinoid X receptor
SDS-PAGE	Sodium dodecylsulfate polyacrylamide gel electrophoresis
SEM	Standard error of the mean
SMRT	Silencing mediator of retinoid and thyroid signalling
SOD1	Superoxide dismutase 1

SRC-1	Steroid receptor co-activator-1
SRC-2	Steroid receptor co-activator-2
STAT-3	Signal transducer and activator of transcription 3
STZ	Streptozotocin
T1DM	Type 1 diabetes mellitus
T2DM	Type 2 diabetes mellitus
TBS	Tris-buffered saline
TBS-T	Tris-buffered saline with Tween 20
TNF-α	Tumour necrosis factor alpha
TR	Thyroid receptor
TZD	Thiazolidinedione
VCAM-1	Vascular cell adhesion molecule 1
VDCC	Voltage dependent calcium channel
VDR	Vitamin D receptor
VSMC	Vascular smooth muscle cell

Chapter 1: Introduction

1.1 Peroxisome Proliferator Activated Receptors (PPARs)

Peroxisome proliferator activated receptors (PPARs) are ligand-activated transcription factors and members of the nuclear hormone receptor superfamily. PPARs were originally found to be activated by peroxisome proliferators, whereby they received their name (Issemann and Green 1990). The PPAR family consists of three isoforms, PPARα (NR1C1), PPARβ/δ (NR1C2) and PPARγ (NR1C3), which are encoded by different genes and its expression is tissue dependent: PPARα is expressed in tissues of high fatty acid catabolism, most importantly the liver, kidneys, heart and brown adipose tissue (Braissant *et al.* 1996); PPARγ is found as three isoforms, PPARγ1 is expressed in the gut, brain, vascular cells and immune cells, PPARγ2 in adipose tissue, and PPARγ3 in adipose tissue and large intestine (Fajas *et al.* 1998); PPARβ/δ is present in all animal cells, from *C. elegans* and drosophila to all mammals tested (Mandard and Patsouris 2013) and it is ubiquitously expressed, although more highly active in skeletal muscle, arteries and endothelium (Coll *et al.* 2009, Hamblin *et al.* 2009).

PPARs can be activated by numerous endogenous ligands, mainly fatty acids and eicosanoids (Yu *et al.* 1995). Some of them are common to all PPAR, like arachidonic acid, and others are subtype specific (Krey *et al.* 1997). Natural ligands specific of PPARα includes leukotriene B4 (Krey *et al.* 1997), 8-hydroxyeicosatetraenoic acids (8-HETE) (Krey *et al.* 1997), eicosatetraionic acid (ETYA)(Keller *et al.* 1997) and oleoylethanolamide (OEA) (Moraes *et al.* 2006); PPARγ natural ligands are, 9- and 13-hydroxyoctadecadienoic acid (9-HODE and 13-HODE) (Schild *et al.* 2002) and prostaglandin J2 (Krey *et al.* 1997); and

PPARβ/δ natural ligands includes prostacyclin, (Li *et al.* 2012), omega 3 (Forman *et al.* 1997), and linoleic acid C6-C8 (Moraes *et al.* 2006).

PPARs control key biological functions such as lipid metabolism, glucose metabolism, immune response, inflammation, cell proliferation, cell migration, apoptosis and carcinogenesis (reviewed by Bishop-Bailey (2000), Neels and Grimaldi (2014) and Tan *et al.* (2016)). Dysregulation of PPARs contributes to the pathogenesis of metabolic diseases such as obesity, metabolic syndrome, diabetes, non-alcoholic fatty liver disease and atherosclerosis. Thus, PPARs represent important molecular targets for the development of new drugs to treat metabolic diseases.

1.1.1 PPARα

PPARα regulates lipid metabolism acting as a lipid sensor. High concentrations of fatty acids activate PPARα which promotes the uptake and thus lowers the levels of these acids (Grygiel-Gorniak 2014). For that reason, PPARα is used as a target molecule for the treatment of dyslipidemias.

Fibrates are a synthetic family of PPARα agonists which clinically proved to lower circulating triglycerides and small dense fraction of low density lipoprotein (LDL)-cholesterol, raise high density lipoprotein (HDL)-cholesterol, and improve the overall atherogenic plasma lipid profile (Ito 2015). They also show to have beneficial effects on inflammation, insulin resistance and metabolic syndrome (Feng *et al.* 2016, Moreno-Indias *et al.* 2017). Moreover, increasing evidence suggests that the fibrate class of drugs also decreases the rate of cardiovascular disease (CVD) events, especially in patients with dyslipidemia and type 2 diabetes mellitus (T2DM) (Burgess *et al.* 2010, Lee *et al.* 2011).

Fibrates have been used to treat patients with dyslipidemia for decades. Fenofibrate, gemfibrozil, bezafibrate and ciprofibrate were the first fibrates synthesised in the 1970's and 1980's (Goldberg *et al.* 1989, Pauciullo *et al.* 1990), and more fibrates continue developing nowadays, like pemafibrate which is currently undergoing Phase III clinical trials (Araki *et al.* 2018). However, the use of fibrates is controversial due to the adverse side effects including gastrointestinal bleeding (Schelleman *et al.* 2010), increased liver function tests (Ahmad *et al.* 2017), venous thromboembolic events (Humbert *et al.* 2017) or increased serum creatinine level (Zhao *et al.* 2012).

The efficacy of fibrates in improving the lipid profile of the patients raised interest on its use as a treatment for the metabolic syndrome (Gomaraschi *et al.* 2015, Moreno-Indias *et al.* 2017). However, it is becoming clear that the combination of fibrate and statin drugs - a family of drugs that inhibits the 3-hydroxy-3-methyl-glutaryl-coenzyme A reductase (HMG-CoA reductase) and thus reduces the production of cholesterol - results in a more effective therapy for lipid disorders than either monotherapy (Choi and Shin 2014). Moreover, several clinical trials have shown that the combined administration of fenofibrate/simvastatin to patients with mixed dyslipidemia is not associated with significantly increased incidence of severe undesirable effects compared with either monotherapy (Filippatos and Elisaf 2015) and in general, fibrates seem to be safe to use in combination with other lipid lowering medications. However, the metabolic syndrome is a multifaceted metabolic disorder composed of the combination of numerous risk factors including atherogenic dyslipidemia, elevated blood pressure, insulin resistance, elevated glucose, and a pro-thrombotic and pro-inflammatory state (Grundy 2016), and in this complex scenario fibrates and statin drugs only ameliorates the hyperlipidemia, and consequently its use as a therapy for the metabolic syndrome is very limited.

To improve the treatment strategies in the management of metabolic syndrome, T2DM and associated CVD, dual and pan PPARα agonists are currently being developed (Chen *et al.* 2017, Patel *et al.* 2017, An *et al.* 2018). The logic behind is that the simultaneous activation of two or all three PPARs by one single agonist will trigger overlapping and complementary mechanisms that will target multiple components of metabolic syndrome and other metabolic diseases at same time. A large number of structurally diverse dual PPARα agonists, such as muraglitazar (Nissen *et al.* 2005), naveglitazar (Long *et al.* 2009), tesaglitazar (Hellmold *et al.* 2007), and aleglitazar (Henry *et al.* 2015), has been synthesized and evaluated, but further clinical development showed serious safety concerns, such as myocardial infarction, transient ischemic attack or stroke, and its use as potential therapy was discontinued. Encouraging, the PPARα/γ agonist saroglitazar has successfully passed the preliminary safety controls and is currently in clinical use in India (Jani *et al.* 2014).

1.1.2 PPARγ

PPARγ is involved in many physiological processes including the regulation of insulin sensitivity, inflammation, fatty acid storage and glucose metabolism, thus represents a high clinical interest as a target of insulin sensitizer drugs for the treatment of T2DM (Grygiel-Gorniak 2014).

Thiazolidinedione (TZD) class of drugs are full agonists of PPARγ that improve insulin sensitivity, decrease fasting blood glucose, promote the utilization of glucose by peripheral tissues, and additionally increase serum levels of HDL-cholesterol and decrease triglycerides and LDL-cholesterol levels (Fonseca *et al.* 1998, Kawamori *et al.* 1998, Aronoff *et al.* 2000, Juhl *et al.* 2003, Chiquette *et al.* 2004, Berhanu *et al.* 2006). Two of the most common TZD drugs currently used in the clinic for the treatment of T2DM are Rosiglitazone (Avandia), introduced in 1999 and widely used as monotherapy or in fixed-dose combinations with either

metformin (Avandamet, GlaxoSmithKline) or glimepiride (Avandaryl, GlaxoSmithKline), and pioglitazone (Actos) (Grygiel-Gorniak 2014, Soccio *et al.* 2014).

However, TZDs are known to cause severe side effects such as increased water retention, increased cardiovascular events, bladder tumours, bone fractures, oedema, weight gain, heart enlargement and hepatotoxicity, consequently some TZDs drugs, such as troglitazone and rosiglitazone, have been withdrawn from the market (Nesto *et al.* 2004, Kahn *et al.* 2006, Nissen and Wolski 2007, Home *et al.* 2009, Lewis *et al.* 2014, Soccio *et al.* 2014). Pioglitazone was also found to increase the risk of bladder cancer (Neumann *et al.* 2012) although it is still the most used TZD. New TZD are in clinical development. For example, rivoglitazone is undergoing phase III trials in the US and China and has been reported to improve the glycemic control in a safe manner (Truitt *et al.* 2010, Kong *et al.* 2011), although further studies with longer duration are needed to fully assess the risks associated with this drug.

The unwanted side effects of TZDs mentioned above have been associated with their behaviour as full agonists of PPARγ. In contrast, partial PPARγ agonists such as balaglitazone were found to be safer compounds while maintaining the insulin-sensitizing effect (Henriksen *et al.* 2011, DePaoli *et al.* 2014). Crystal structures as well as *in silico* docking studies showed different binding profiles of the PPARγ agonists to the ligand binding domain which might explain the different co-activators recruited and different effects (Bruning *et al.* 2007, Montanari *et al.* 2008). Consequently, there is a growing interest on the development of partial PPARγ agonists with antidiabetic effects. For example, balaglitazone showed 50% PPARγ activation capacity (Larsen *et al.* 2008) and was used on a phase III clinical trial resulting on glycemic with a lower incidence of fat accumulation and fluid retention, when compared to pioglitazone (Henriksen *et al.* 2011). Similarly

INT131, a non-TZD selective for PPARγ modulator, has completed phase IIb clinical trial showing an improvement of hyperglycaemia in T2DM patients, with effects comparable to those of pioglitazone, but with less fluid accumulation and weight gain (DePaoli *et al.* 2014).

Alternatively, dual PPARα/γ activators are being developed to combine the regulation of lipid plasma profile by PPARα with the increased insulin sensitivity effect of PPARγ, although with little success so far (Ratner *et al.* 2007, Erdmann *et al.* 2015). Aleglitazar is a dual PPARα/γ activator that has successfully completed phase II clinical trial (SYNCHRONY) (Henry *et al.* 2009). The results showed that aleglitazar treatment produced significant improvements in fasting plasma glucose and significant improvements in all lipid parameters compared with placebo. Also, for doses of aleglitazar less than 300 μg the frequency of oedema was similar to placebo, and bodyweight gain was less, compared with pioglitazone (Henry *et al.* 2009). The positive effects observed with aleglitazar together with the minor side effects provided enough evidence to move on to phase III of clinical trial (ALEPREVENT). Phase III was a randomized double-blind trial design to study aleglitazar 150 μg in patients with T2DM or prediabetes with stable cardiovascular disease compared with placebo. Unfortunately this study was halted early due to an excess of hypoglycaemia, oedema and gastrointestinal haemorrhage, and the authors raised severe concerns about any further clinical use for this drug (Erdmann *et al.* 2015).

Saroglitazar, commercially known as Ligaglyn, is a new dual PPARα/γ agonist used for the treatment of dyslipidemia on patients with T2DM in India, though larger studies are yet needed for long term safety (Agrawal 2014).

1.1.3   PPARβ/δ

PPARβ/δ is widely expressed in most tissues and is a major regulator of lipid metabolism, glucose metabolism, cell migration, proliferation and differentiation, hence it has been linked to very serious diseases such as metabolic syndrome, diabetes or cancer (Oliver *et al.* 2001, Kim *et al.* 2010, Quintela *et al.* 2014). Consequently, PPARβ/δ is emerging as a therapeutic target for the treatment of disorders associated with metabolic syndrome, although there are no marketed drugs targeting PPARβ/δ yet.

Research reported mainly on animal models such as mice, rats or rhesus monkeys indicates that PPARβ/δ agonists results in a number of favourable pharmacological effects including reduced weight gain, increased metabolism in the skeletal muscle and cardiovascular function, suppression of atherogenic inflammation and improvement of the blood lipid profile, which are common abnormalities in patients with metabolic syndrome (Oliver *et al.* 2001, Tanaka *et al.* 2003, Wang *et al.* 2003).

These encouraging results lead to the first clinical trials on humans. Glaxo Smith Kline (GSK) developed the agonist GW501516 (Endurobol), a promising compound that completed proof-of-concept clinical trials successfully for dyslipidaemia (Ooi *et al.* 2011) and hypocholesteraemia (Olson *et al.* 2012). However, some studies with GW501516 showed a suspected link with tumour development (Geiger *et al.* 2009, Pollock *et al.* 2011), and any further clinical trial was suspended.

Nevertheless, the interest on PPARβ/δ continues and in the last years several compounds targeting PPARβ/δ were developed, although just a few of these molecules reached clinical trials. One of them was MBX-8025, which was tested on overweight men and women around 50 years old with mixed dyslipidemia. After 8 weeks of treatment, MBX-8025 significantly reduced triglyceride and LDL-

cholesterol, raised HDL-cholesterol, improved insulin sensitivity and decreased waist circumference and body fat compared with placebo, with the benefit of being safe and generally well tolerated (Bays *et al.* 2011).

In a very recent study, a new PPARβ/δ agonist (Compound 1) was compared with GW501516 using a thermal injury mouse model for muscle regeneration, both of them showing an improvement on muscle regeneration compared with control (Lagu *et al.* 2017). After 14 days of treatment with either GW501516, Compound 1 or vehicle, the marker for cancer ki-67 was measured showing a significant increase in those animals treated with GW501516 compared with vehicle and no significant in those animals treated with Compound 1, suggesting that this compound can be a safer alternative to GW501516. There are other PPARβ/δ agonists, such as HPP593, that are currently under various stages of development (Fedorova *et al.* 2013).

At present there are no therapies available to treat metabolic syndrome, and extensive efforts are being devoted to develop new dual or pan PPAR agonists. The aim is to obtain a super agonist that holds combined properties of any of the two or all three PPARs that will target multiple components of metabolic syndrome simultaneously. That is the case of GFT505 (Elafibranor) and its main active circulating metabolite GFT1007, a PPARα/β activator used in a clinical phase IIa study with patients with either combined dyslipidemia or prediabetes and abdominal obesity. After 35 days treatment, GFT505 significantly improved lipid homeostasis and insulin sensitivity, and no serious adverse events were reported. (Cariou *et al.* 2011). This study was followed by another study 8 weeks long with twenty-two abdominally obese insulin-resistant males. GFT505 improved plasma lipid parameters and significantly decreased both TG and LDL cholesterol levels with no reported serious adverse events (Cariou *et al.* 2013). Although these

clinical trials are promising, further studies are needed to assess the long-term safety of GFT505 in a larger and more diverse sample group.

1.2 Molecular structure of PPAR

PPARs, as any other nuclear transcription factor, are organized in four functional domains (Figure 1.1): the N-terminal domain (NTD), the DNA binding domain (DBD), the hinge domain, and the ligand binding domain (LBD) which accommodates the ligand binding pocket.

1- The NTD is the most varied domain among the different PPARs. This domain is relatively short and is believed to mediate ligand-independent activity through the ligand-independent transactivation motif (AF-1) by promoting protein-protein interactions with co-activators or co-suppressors, which induces conformational modifications that allow allosteric interactions (Xu *et al.* 1999). However, AF-1 has a very weak activity especially in PPARβ/δ, and is a target of kinase phosphorylation (Neels and Grimaldi 2014, Usuda and Kanda 2014, Vazquez-Carrera 2016).

2- The DBD is the most conserved domain among the various PPARs. The core structure is composed of two zinc fingers: the α-helix in the first zinc finger promotes the recognition of a specific sequence in the peroxisome proliferator response element (PPRE) in the DNA, and the second zinc finger mediates the heterodimerization with retinoid X receptor (RXR). The rest of the DBD domain further stabilize the DNA-PPAR complex by direct interactions with the minor groove of the DNA and/or, alternatively, by stabilizing the interactions with other partner in the dimer complex (Xu *et al.* 1999).

3- The hinge domain separates the DBD from the LBD. It also contains a nuclear localization signal and amino acid side chains susceptible of post-translational modifications (Xu *et al.* 1999).

4- The structure of the LBD is similar among the various PPAR. This domain contains the pocket that accommodates the ligands, and the ligand-dependent transactivation motif (AF-2), which promotes the recruitment of co-activators for gene transcription (Neels and Grimaldi 2014). Protein X-ray crystallographic structures of PPARβ/δ identified a Y-like shaped ligand binding cavity of ~1300Å^3 (Xu *et al.* 1999), larger than other members of the nuclear receptor superfamily.
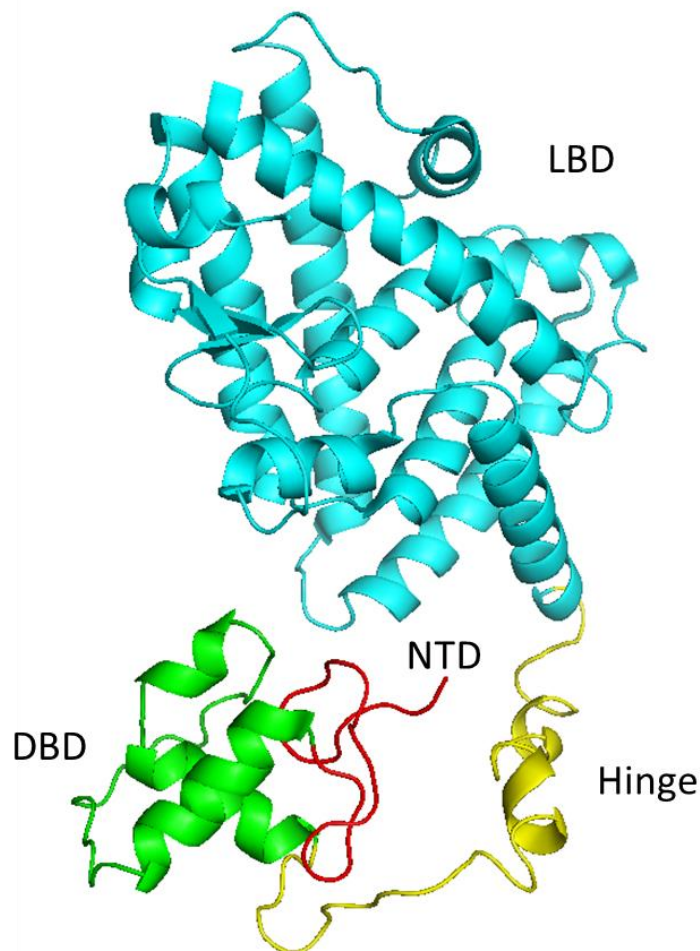
Figure 1.1 Structure of PPARs. PPARs have the classical structure of a nuclear transcription factor composed of a ligand binding domain (LBD), DNA binding domain (DBD), hinge domain and an N-Terminal domain (NTD). The structure above belongs to the PDB file 3DZY (Chandra *et al.* 2008).

Among all three PPARs, PPARβ/δ is the most unknown and controversial, besides is the subject of interest in the present thesis. Therefore, all the evidence presented from this point will exclusively focus on PPARβ/δ.

1.3 PPARβ/δ multiple mechanisms of action

PPARβ/δ is a transcription factor that regulate genes by two different mechanisms, induction and trans-repression (Figure 1.2):

1.3.1 Induction mode

In the induction mode, PPARβ/δ forms a complex with RXR and together, as a heterodimer, regulate the target genes by binding to the promoter PPRE. The promoter is composed of the repetition of the consensus sequence AGGTCA separated by one nucleotide, where PPARs are orientated to the 5'-end and RXR to the 3'-end (IJpenberg *et al.* 1997). In the absence of ligand, co-repressor proteins and histone deacetylases (HDACs) are bound to the heterodimer which tight the chromatin and prevents its binding to the PPRE sites (Neels and Grimaldi 2014). The presence of ligand induces a conformational change of PPARβ/δ which makes helix 12 act as a lid of the ligand-binding pocket. This conformation of helix 12 promotes the binding of co-activators, releases the co-repressor proteins, induces histone acetylation and methylation and finally allows the transcription of the target genes (Figure 1.2) (Cronet *et al.* 2001, Helsen and Claessens 2014).

A large number of co-activator and co-repressor complexes interacting with PPARβ/δ have been identified and summarised in Table 1.1. The expression of these complexes is cell and tissue specific, adding another level in the regulation of PPARβ/δ.

Table 1.1 PPARβ/δ co-activators and co-repressors

PPARβ/δ co-activators	References
SRC-1 (Steroid receptor co-activator-1)	(Zhu *et al.* 1996)
SRC-2 (Steroid receptor co-activator-2)	(Lim *et al.* 2004)
CBP/p300 (cAMP response element binding proteins)	(Misra *et al.* 2002)
PGC1-α (PPAR gamma co-activator 1-alpha)	(Puigserver *et al.* 1998)
PBP (PPAR binding protein)	(Zhu *et al.* 1997)
PPARβ/δ co-repressors	**References**
HDAC (Histone deacetylases)	(Aarenstrup *et al.* 2008)
NCo-R (Nuclear receptor co-repressor)	(Krogsdam *et al.* 2002)
SMRT (Silencing mediator of retinoid and thyroid signalling)	(Lim *et al.* 2004)
RIP140 (Receptor interacting protein 140)	(Seth *et al.* 2007)

On the other side, RXR forms heterodimers with other nuclear transcription factors such as liver X receptor (LXR) (Széles *et al.* 2010), vitamin D receptor (VDR) (Széles *et al.* 2010), farnesoid X receptor (FXR) (Forman *et al.* 1995), pregnane X receptor (PXR) (Toell *et al.* 2002), retinoid acid receptor (RAR) (Széles *et al.* 2010), thyroid receptor (TR) (Kojetin *et al.* 2015), PPARα and PPARγ (Kliewer *et al.* 1992), being direct competitors of PPARβ/δ for RXR. This means that high concentrations of these receptors decrease the availability of RXR, which indirectly represses the induction activity of PPARβ/δ.
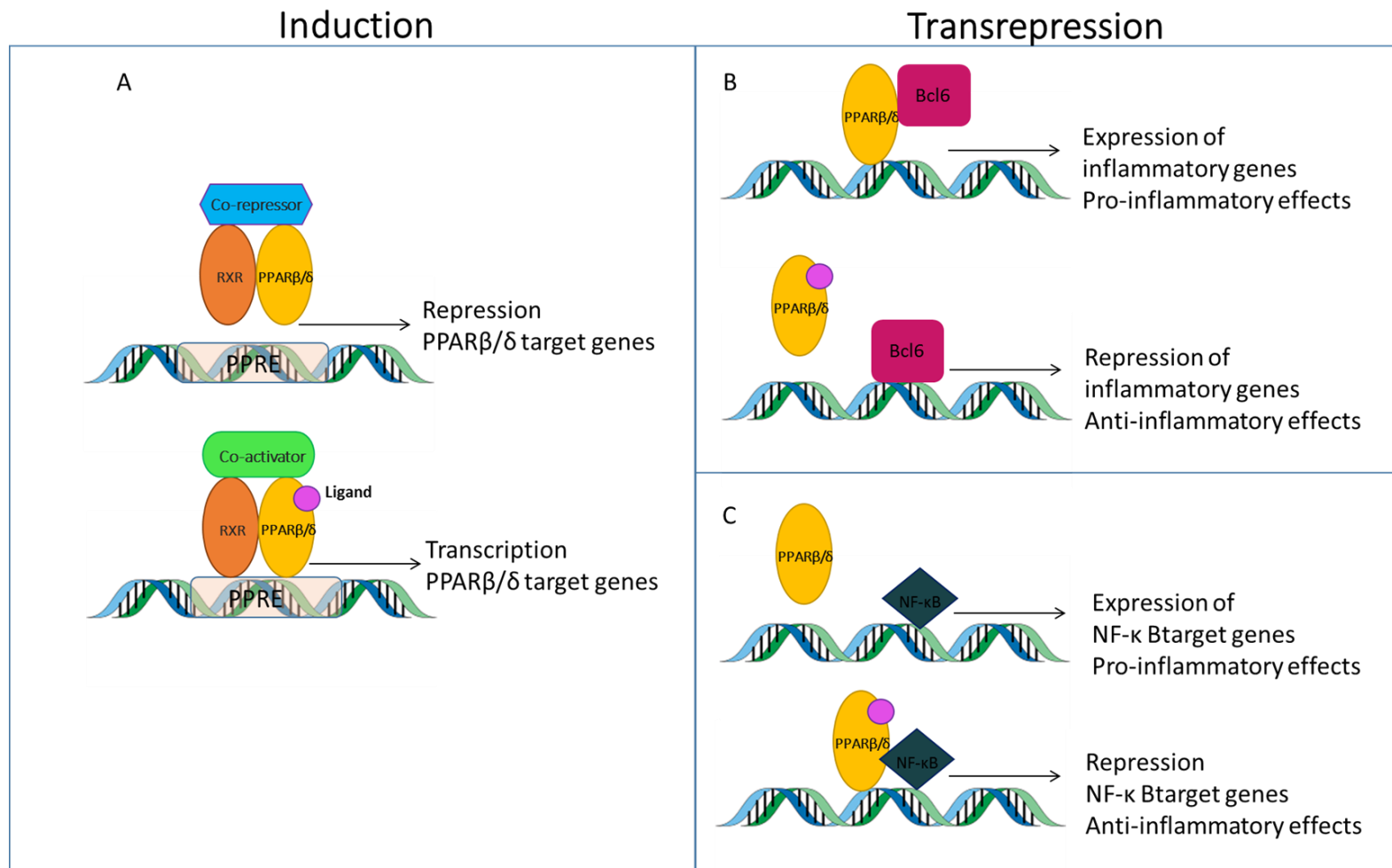
Figure 1.2 Induction and trans-repression mode of action of PPARβ/δ. Modified from Neels and Grimaldi (2014).

1.3.2   Trans-repression mode

PPARβ/δ regulates gene expression in a PPRE independent manner through the regulation (mostly suppression) of other transcription factors, including nuclear factor-κB (NF-κB) (Rodriguez-Calvo *et al.* 2008), activator protein (AP-1) (Schnegg *et al.* 2012) and B cell lymphoma 6 (Bcl6) (Fan *et al.* 2008) (Figure 1.2).

Control over other nuclear factors can occur different ways:

1- Direct competition between PPARs and other transcription factors for limiting amounts of shared co-activators (Sheppard *et al.* 1998).

2- Direct interaction of the PPAR-RXR heterodimer with other transcription factors preventing binding with their promoters and thus inhibiting gene transcription (Desreumaux *et al.* 2001).

3- PPAR-RXR heterodimer inhibition of mitogen-activated protein kinase (MAPK) phosphorylation and activation, resulting in the inhibition of transcription factors (Wu *et al.* 2016).

1.3.3   PPARβ/δ synthetic ligands

Synthetic PPARβ/δ ligands have been developed in the last few years and widely used as a chemical tool for the pharmacological study of PPARβ/δ. The most commonly used are the following:

1.3.3.1   L-165041

L-165041 is a non-selective PPARβ/α agonist with a human PPARβ/α (hPPARβ/α) activity of $Ki = 6$ nM and a weaker human PPARγ (hPPARγ) activity of $Ki = 730$ nM (Berger *et al.* 1999).

1.3.3.2 GW0742

GW0742 is a PPARβ/δ agonist that showed hPPARβ/δ activity of EC_{50} = 1 nM and selectivity of ~1100-fold against hPPARα and ~2000-fold against hPPARγ. In mice, the PPARβ/δ activity of GW0742 was EC_{50} = 30 nM and the selectivity ~290-fold against PPARα and ~330-fold against PPARγ (Sznaidman *et al.* 2003).

1.3.3.3 GW501516

GW501516 is another PPARβ/δ agonist developed at same time as GW0742 which showed a hPPARβ/δ activity EC_{50} = 1 nM and a selectivity of ~1100-fold against hPPARα, and ~850-fold against hPPARγ. GW501516 also showed excellent selectivity on the murine receptors of EC_{50} = 2.5, 1.0, 0.02 mM for PPARα, PPARγ, and PPARβ/δ, respectively (Sznaidman *et al.* 2003).

1.3.3.4 GSK0660

The PPARβ/δ ligand GSK0660 was developed as the first specific PPARβ/δ antagonist (Shearer *et al.* 2008). GSK0660 pIC_{50} and selectivity for the PPARs was determined in an *in vitro* ligand displacement assay. GSK0660 showed to be a potent binder of PPARβ/δ with a pIC_{50} of 6.8 (IC_{50} = ~160 nM) and nearly inactive on PPARγ and PPARα, with IC_{50}s above 10 M. The GSK0660 antagonism activity on PPARβ/δ was 100% at pIC_{50} of 6.53 (IC_{50} = ~100 nM). However, it has the disadvantage that is not bioavailable (Shearer *et al.* 2008).

1.3.3.5 GSK3787

GSK3787 was developed later by Shearer *et al.* (2010) as a bioavailable and irreversible PPARβ/δ antagonist that covalently modifies Cys249 within the ligand binding pocket. The ability of GSK3787 to bind to each of the PPAR subtypes was measured *in vitro* in a ligand displacement assay showing no binding activity for hPPARα and hPPARγ; however, it showed a potent binding to hPPARβ/δ with a

pIC_{50} = 6.7 (IC_{50} = ~0.1 μM) and 100% hPPARβ/δ antagonism activity with a pIC_{50}

= 6.9 (IC_{50} = ~0.1 μM).

1.4 Genomic regulation of the inflammatory response by PPARβ/δ

Signalling via PPARβ/δ has been shown to be involved in lipid metabolism (Olson *et al.* 2012), glucose metabolism (Lee *et al.* 2006), insulin sensitivity (Lee *et al.* 2006), inflammation (Barish *et al.* 2008, Bishop-Bailey and Bystrom 2009) and cell proliferation (Kim *et al.* 2004); however, its role remains controversial and scientists do not agree on its function, as shown in a number of contradictions reviewed by Perez-Diaz and Mackenzie (2015) and summarised in the Table 1.2 below.

Table 1.2 Controversy of the function of PPARβ/δ in different biological activities.

Biological activity	Pro-	Anti-
Inflammation	(Wang *et al.* 2014, Degueurce *et al.* 2016, Wang *et al.* 2016)	(Di Paola *et al.* 2010, Kapoor *et al.* 2010, Schnegg *et al.* 2012)
Cell proliferation	(Zhang *et al.* 2002, Stephen *et al.* 2004, Piqueras *et al.* 2007)	(Wang *et al.* 2006, Romanowska *et al.* 2008, Lim *et al.* 2009, Kim *et al.* 2010)
Cell migration	(Tan *et al.* 2007, Ham *et al.* 2014, Park *et al.* 2015)	(Lim *et al.* 2009, Kim *et al.* 2010, He *et al.* 2011)
Atherosclerosis	(Vosper *et al.* 2001, Zhang *et al.* 2002, Mou *et al.* 2016)	(Barish *et al.* 2008, Takata *et al.* 2008, Chin *et al.* 2010)
Angiogenesis	(Piqueras *et al.* 2007, Han *et al.* 2013, Quintela *et al.* 2014)	(Meissner *et al.* 2011, Liu *et al.* 2013, Yang *et al.* 2013)
Apoptosis	(Foreman *et al.* 2011, Pechery *et al.* 2016, Wu *et al.* 2016)	(Di-Poi *et al.* 2002, Barlaka *et al.* 2015, Hwang *et al.* 2015)
Senescence	(Zhu *et al.* 2014, Zhu *et al.* 2014, Riahi *et al.* 2015)	(Altieri *et al.* 2012, Kim *et al.* 2012, Jung *et al.* 2015)

Among these biological activities, the regulation of inflammation by PPARβ/δ has been extensively studied.

1.4.1 Role of PPARβ/δ in the inflammatory responses

Inflammation is a complex and dynamic process that happens when the body detects an infection or injury. The inflammatory response is a sequential release of mediators that leads to vasodilation, increased blood flow and increased vascular permeability which provokes the accumulation of a fluid exudate, and the activation of neurosensory pain fibres, resulting in the classical signs of acute inflammation of heat, redness, swelling and pain (Moraes *et al.* 2006).

Several inflammatory cellular pathways regulated by PPARβ/δ have been identified (Fan *et al.* 2008, Piqueras *et al.* 2009, Kapoor *et al.* 2010, Schnegg *et al.* 2012, Serrano-Marco *et al.* 2012, Zhang *et al.* 2014), but how exactly they are regulated remains unknown. The trans-repression of Bcl6 has been proposed as a key mechanism (Kapoor *et al.* 2010). When PPARβ/δ is in the trans-repression mode and in the absence of agonist, it sequesters Bcl6 which leads to a pro-inflammatory response; however, the presence of agonist activates PPARβ/δ and releases Bcl6 (Figure 1.3 B), which is then free to repress the inflammatory gene expression (Fan *et al.* 2008). Following the same principle, the absence of PPARβ/δ would free Bcl6, resembling the PPARβ/δ-activated anti-inflammatory response. Surprisingly, Kapoor *et al.* (2010) showed that PPARβ/δ KO mice do not mimic the effect of the free Bcl6 in the presence of PPARβ/δ ligand, and concluded that there are additional major anti-inflammatory pathways regulated by PPARβ/δ.

NF-κB has been extensively studied as one of the main responsible molecules for the inflammatory response (Lawrence 2009, Schnegg *et al.* 2012, Chang *et al.* 2013, Yue *et al.* 2016). NF-κB is a transcriptional factor that regulates the transcription of genes involved in local and systemic inflammation, such as

cytokines, chemokines, cell adhesion molecules, apoptotic factors and other mediators (Lawrence 2009). PPARβ/δ can regulate NF-κB, and therefore its inflammatory response, at different levels (Figure 1.3-1): inhibition of the NF-κB translocation to the nucleus (Jove *et al.* 2005, Kapoor *et al.* 2010), physical interaction with NF-κB (Schnegg *et al.* 2012) , and reduction of NF-κB acetylation (Barroso *et al.* 2011).

Alternatively, Kapoor *et al.* (2010) proposed the regulation of the Akt/GSK-3β/NF-κB inflammatory pathway by PPARβ/δ (Figure 1.3-2). Akt is a member of the phosphoinositide 3-kinases signal transduction enzyme family that reduces apoptosis and inflammation when phosphorylated. Ligand activated PPARβ/δ contributes to the phosphorylation of Akt, and hence, contributes to the anti-inflammatory effects. On the other hand, GSK-3β is a serine-threonine kinase which is inactivated by phosphorylation and regulated by multiple signalling pathways, including the Akt pathway; several studies have reported an association between GSK-3β and NF-κB (Chang *et al.* 2013, Zhang *et al.* 2014). Taking this together, it is likely that the activation of PPARβ/δ phosphorylates and activates the Akt pathway, which goes on to phosphorylate and hence inhibit GSK-3β, resulting in the inhibition of NF-κB.

There are a few studies involving PPARβ/δ-regulated interleukin 6 (IL-6) that suggest a similar anti-inflammatory mechanism (Figure 1.3-3). IL-6 is a cytokine related to the development of rheumatoid arthritis and other inflammatory disorders, atherosclerosis, osteoporosis and septic shock (Pathan *et al.* 2004, Edwards and Williams 2010, Yue *et al.* 2016). The activation of PPARβ/δ inhibits IL-6-mediated inflammatory responses and subsequent acute phase reaction in the liver by increasing the phosphorylation of STAT-3 (Kapoor *et al.* 2010), or by inhibiting NF-kB in adipocytes (Serrano-Marco *et al.* 2012).

The tumour necrosis factor alpha (TNF-α) contributes to reactive oxygen species (ROS) production and induces the expression of the pro-inflammatory molecules vascular cell adhesion molecule 1 (VCAM-1) and E-selectin in endothelial cells (ECs), which is suppressed by PPARβ/δ activation (Fan *et al.* 2008, Piqueras *et al.* 2009) (Figure 1.3-4). Interestingly, the 5'-flanking regulatory regions of VCAM-1 and E-selectin genes lack PPRE, which means that these proteins are regulated via trans-repression rather than induction mechanism of PPARβ/δ, and other transcription factors might play an important role (Fan *et al.* 2008).
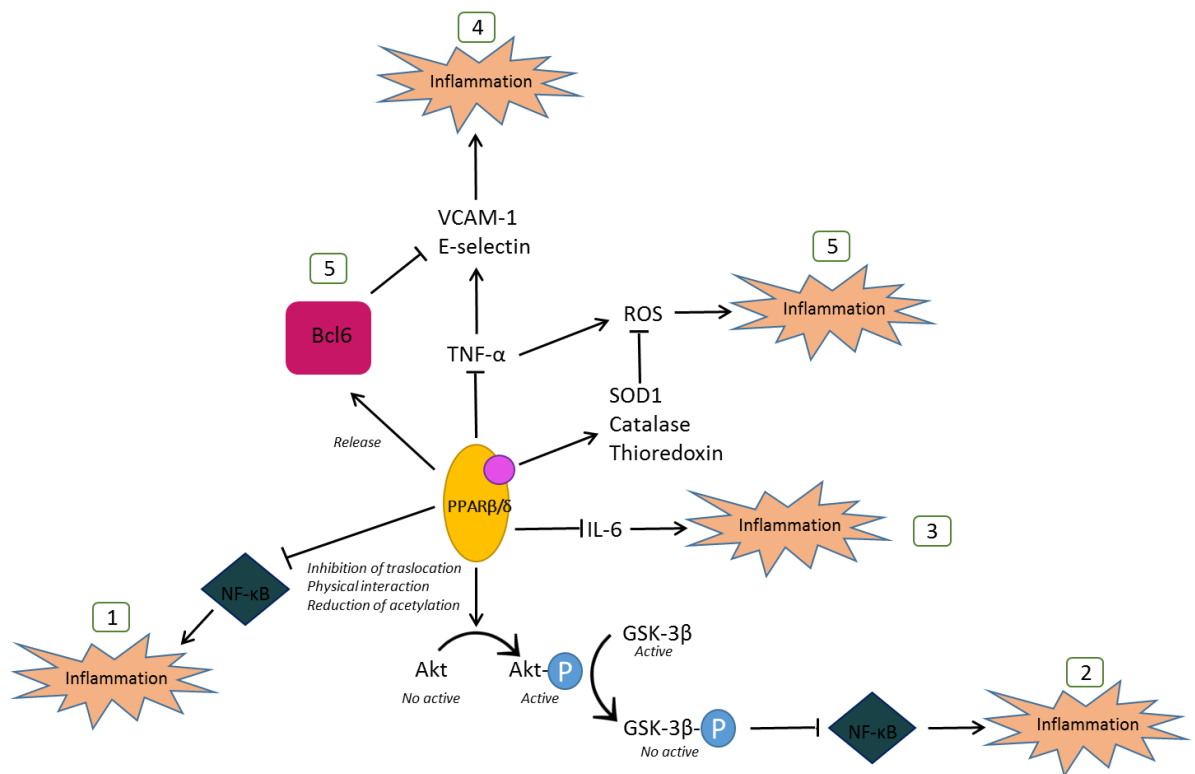
Figure 1.3 Regulation of the inflammatory pathways by PPARβ/δ. The inflammatory response frequently involves several molecules, which can be regulated by PPARβ/δ at different levels: 1) PPARβ/δ can inhibit NF-κB by: inhibition of the NF-κB translocation to the nucleus (Jove *et al.* 2005), physical interaction with NF-κB (Schnegg *et al.* 2012), and reduction of NF-κB acetylation (Barroso *et al.* 2011). 2) Ligand activated PPARβ/δ contributes to the phosphorylation of Akt, which becomes active. Activated Akt phosphorylates GSK-3β which ultimately results in the inhibition of NF-κB (Kapoor *et al.* 2010, Chang *et al.* 2013, Zhang *et al.* 2014). 3) PPARβ/δ inhibits the IL-6 mediated inflammatory response (Kapoor *et al.* 2010, Serrano-Marco *et al.* 2012). 4) Activated PPARβ/δ supresses TNF-α, which induces the expression of the pro-inflammatory molecules VCAM-1 and E-selectin and contributes to ROS production (Fan *et al.* 2008). 5) At same time, ligand activated PPARβ/δ leads to the expression of the anti-oxidative genes *SOD1*, catalase and thioredoxin, which eliminate ROS and releases Bcl-6, that is then free to repress the transcription of VCAM-1 and E-selectine (Kapoor *et al.* 2010).

Additionally, changes in PPARβ/δ activity leads to changes in the induction of gene expression of three important anti-oxidative stress enzymes: superoxide dismutase 1 (SOD1), catalase, and thioredoxin, which are key in the elimination of ROS from the cell (Fan *et al.* 2008). An induction/trans-repression mechanism for the anti-inflammatory effects of PPARβ/δ in endothelial cells has been proposed, namely that the activation of PPARβ/δ leads to the activation of the target genes, including the antioxidative enzymes SOD1, catalase and thioredoxin (induction), and releases Bcl6, which represses the transcription of pro-inflammatory genes such as VCAM-1 and E-selectin (trans-repression) (Figure 1.3-5). Such a synergistic action leads to a potent inhibition of endothelial activation and therefore to the vascular protection (Fan *et al.* 2008).

On the contrary, other studies have shown no effect or pro-inflammatory effects after PPARβ/δ-ligand activation. In a murine model of asthma, PPARβ/δ failed to inhibit the allergen-induced airway inflammation (Trifilieff *et al.* 2003). Similarly, other studies shown that PPARβ/δ agonist did not protect against colitis (Hollingshead *et al.* 2007) or even promoted the colonic inflammation (Wang *et al.* 2014). In the same line, it has been shown that PPARβ/δ is over expressed in psoriasis and its activation in a murine model of psoriasis triggers the inflammatory response (Romanowska *et al.* 2010), and also the treatment with an agonist of PPARβ/δ in pigs with organ-induced dysfunction did not attenuate histological damage nor improved inflammation parameters (Wepler *et al.* 2013).

1.4.2 Lung inflammation and PPARβ/δ

Acute lung injury (ALI) is a frequent complication in critical ill ICU patients that led to the development of multiple organ failure and ultimately the death of the patients (Bellani *et al.* 2016). ALI is characterised by an intense inflammatory parenchymal process that includes lung tissue destruction, neutrophil accumulation, and diffuse

lung inflammation, resulting in the release of pro-inflammatory cytokines (Ware and Matthay 2000). In this scenario, the regulation of lung inflammation by PPARβ/δ is becoming a very interesting pharmacological target.

A number of murine models for ALI and septic shock have been developed and used to study the regulation of lung inflammation by PPARβ/δ *in vivo* (Galuppo *et al.* 2010, Bao *et al.* 2014, Nullens *et al.* 2018, Song *et al.* 2018). Most of the studies showed anti-inflammatory effects after ligand-activation of PPARβ/δ, however the mechanism underlying these beneficial effects are more controversial.

In a model of hyperbaric oxygen (HBO_2)-induced ALI in rats, the treatment with the PPARβ/δ agonist GW0742 led to a significant decrease in the overall lung injury by inhibiting the activation of NF-κB and increasing the activity of antioxidant enzymes (Bao *et al.* 2014). In the same line, Di Paola *et al.* (2010) used carrageenan-induced pleurisy mice treated with GW0742 which also showed to have anti-inflammatory effects by inhibiting the degradation of IκB-α and inhibiting the translocation of NF-κB into the nucleus. Similarly, Zymosan-induced multiple organ inflammation in mice was reduced after treatment with GW0742 by inhibiting the degradation of IκB-α and the translocation of NF-κB into the nucleus (Galuppo *et al.* 2010).

Cecal ligation and puncture (CLP) operation is a widely used model for experimental sepsis in rodents (Nullens *et al.* 2018, Song *et al.* 2018), which was also used to study the regulation of inflammation by PPARβ/δ in rats. GW501516, another PPARβ/δ agonist, showed to reduce the mortality of the animals as well as alleviate lung injury during sepsis. Interestingly, in this model the anti-inflammatory effects were independent of the NF-κb pathway. Alternatively, GW501516 showed to inhibit the phosphorylation of STAT3 and the inhibition of

the STAT3/JAK kinases cascade was proposed as the anti-inflammatory mechanism instead (Wang *et al.* 2014).

Same CLP-induced sepsis was used in mice, which were treated with GW0742, showing higher survival rate and reduced inflammation (Kapoor *et al.* 2010). In this study, the beneficial effects of PPARβ/δ-activation were associated with the activation of the PI3K/Akt pathway and inhibition of the MAPK-ERK1/2 pathway, which together could suppress NF-kB activity. In parallel, the authors showed that PPARβ/δ-activation is also associated with the suppression of the pro-inflammatory transcription factor STAT-3 (Kapoor *et al.* 2010).

In a model of LPS-stimulated lungs in mice, GW0742 attenuates pulmonary inflammation by decreasing the inflammatory cell influx as well as pro-inflammatory cytokines IL-1β, TNFα and IL-6 in the bronchial alveolar lavage fluid. Interestingly, the transcription of these cytokines on post-lavage lung tissue showed increased levels after administration of LPS but did not demonstrate a reduction in GW0742-treated animals. The authors hypothesised that these results may be due to an insufficient number of PPARβ/δ receptors in lung tissue and the anti-inflammatory effects of GW0742 are due to the regulation of the immune reaction to LPS that alters the quality and quantity of the cellular infiltrate into the lung (Haskova *et al.* 2008).

As shown, there are great discrepancies in the literature, which may be due to differences in experimental variables (Nandhikonda *et al.* 2013). PPARβ/δ receptor appears to be a sensitive molecular switch that has both endogenous and exogenous ligands which controls cellular function through changes in very small concentration range. Added to this, in any cell or tissue, the activity of PPARβ/δ may also depend on its promoter activity and relative expression, as well as presence and activity of co-repressor and co-activator proteins. It is clear though

that PPARβ/δ has a dual effect in the cell and indeed acts as a molecular switch having both pro- and anti- effects in inflammation (Di Paola *et al.* 2010, Wang *et al.* 2014), cell proliferation (Zhang *et al.* 2002, Wang *et al.* 2006) and migration (Lim *et al.* 2009, Ham *et al.* 2014). It has been shown that GW0742 is capable of behaving as an agonist activating the transcription pathway at lower concentrations (nM) and antagonist inhibiting this effect at higher concentrations (µM) (Nandhikonda *et al.* 2013). In the same line, a study done in a model of systematic inflammation on mice showed that higher doses of GW0742 (0.3 mg/kg) triggered a pro-inflammatory response, whereas lower concentration (0.03 mg/kg) showed an anti-inflammatory trend, although without a significant difference (Yin *et al.* 2018). The mechanism by which GW0742 inhibits activity is not clear, but it has been suggested that GW0742 inhibits PPARβ/δ by competing with the co-activators (Nandhikonda *et al.* 2013). Alternatively, the large ligand binding pocket of the receptor can accommodate more than one ligand and high GW0742 concentrations could result in unusual PPAR:ligand stoichiometries that could trigger inactive receptor conformations (Nandhikonda *et al.* 2013), an issue that requires further investigation. In the same line, Adhikary *et al.* (2015) suggests that the pro- or anti-inflammatory response of the ligand activated PPARβ/δ is stimulus-dependent.

1.4.3   Transcriptomics of PPARβ/δ

A key insight into the complexity of induction and trans-repression has been provided through microarray analysis of mouse keratinocytes, where GW0742 was used as the principle agonist in PPARβ/δ$^{+/+}$ and PPARβ/δ$^{-/-}$ mice. Khozoie *et al.* (2012) organised the genes regulated by PPARβ/δ into four main groups plus a further 4 minor groups (constituting 5% of responses collectively). This model compares well with a study in human myofibroblasts, where Adhikary *et al.* (2011) used gene silencing to parallel the use of knockouts by Khozoie *et al.* (2012). By

exposing cells to GW501516 and comparing the results from siPPARβ/δ to normal untreated cells, they developed a three mode of action model for PPARβ/δ: Group I: Trans-repression no exogenous ligand; Group II: induction or repression with exogenous ligand; and Group III: induction no exogenous ligand (Adhikary *et al.* 2011). Strikingly, both studies indicate that PPARβ/δ induces gene transcription when there is no exogenous ligand, Khozoie *et al.* (2012) argues that gene induction occurs due to endogenous ligands found within the cell; however, few studies have shown to which extent these endogenous ligands produce cellular effects by binding and activating PPARβ/δ.

The models so far proposed to explain the different modes of action of PPARβ/δ may be further complicated by endogenous ligands, which may account for induction with no exogenous ligand, suggesting that signalling by different ligands would have a large impact on the functional outcome for the cell (Khozoie *et al.* 2012, Nandhikonda *et al.* 2013). While this is a novel concept to explain the diverse range of effects of PPARβ/δ in the control of cellular function, a parallel argument has been made on the cause of the side effects of glucocorticoids. It has been argued that subtle changes to transcriptional activity of glucocorticoid receptors would alter the related side effects of these drugs as opposed to the traditional view that the benefits of glucocorticoids are due to the inhibition of transcription and the side effects due to activation of transcription by the glucocorticoid receptor (Clark and Belvisi 2012). Implications for drug design for PPARβ/δ therefore needs to take this difference into account. It is tempting to think that direct control of the PPARβ/δ molecular switch would be possible by tipping the balance between endogenous-like ligands and exogenous ligands.

1.5   Non-genomic regulation of the vascular tone by PPARβ/δ

Surprisingly, PPARβ/δ also have non-genomic effects. It has been shown that the activated PPARβ/δ receptor binds directly to PKCα in platelets to inhibit aggregation (Ali *et al.* 2006, Ali *et al.* 2009) and also induces vasodilatation in arteries (Harrington *et al.* 2010, Jimenez *et al.* 2010, Li *et al.* 2012).

Vascular tone, or the state of contractile tension in the vessel walls, is determined by the smooth muscle contractility, which depends on the phosphorylated state of myosin (Figure 1.4). The phosphorylation/dephosphorylation of myosin and hence the contraction/relaxation of the vessels is mainly regulated by three pathways: potassium channels (Li *et al.* 2012, Morales-Cano *et al.* 2015, Perez-Diaz *et al.* 2016), RhoA/ROCK (Harrington *et al.* 2010, Rao *et al.* 2013, Perez-Diaz *et al.* 2016) and PI3K/Akt/eNOS (Jimenez *et al.* 2010, Gu *et al.* 2016). These pathways have shown to be impaired in diabetic vessels (Rao *et al.* 2013, Morales-Cano *et al.* 2015, Sun *et al.* 2015, Perez-Diaz *et al.* 2016) resulting in a significantly increased contractile response and/or decrease vasodilator response to stimuli, which might contribute to the development of diabetes-associated vascular complications.

Cardiovascular diseases, including hypertension, stroke, myocardial infarction and heart failure are the major causes of mortality and morbidity in diabetic patients. Moreover, hypertension is three times more common in diabetic patients than non-diabetic, and it is found in up to 60-65% of type 2 diabetic patients (Dai *et al.* 2010, Reboldi *et al.* 2012). The resistance of target cells to insulin is the main mechanism underlying the development of T2DM (Saini 2010), resulting in an impaired glucose up-take by the tissues and therefore high levels of glucose in blood. The insulin-resistance of vascular tissues along with high blood glucose levels are related to

the dysfunction of the vascular reactivity, contributing to the diabetes-related hypertension (Xie *et al.* 2010, Oelze *et al.* 2011).

The reduction in vascular dysfunction after PPARβ/δ activation has been largely documented (Jimenez *et al.* 2010, Quintela *et al.* 2012, Tian *et al.* 2012, Quintela *et al.* 2014). Most of these studies show this protection after several hours or days of treatment, involving the transcription or inhibition of target genes - as it would be expected from a nuclear receptor. However, PPARβ/δ agonists can also induce full vasodilation of aorta, pulmonary artery and mesenteric artery in a non-genomic manner. As an example, in one study done with rat aortic rings pre-contracted with phenylephrine (PE), a selective α_1-adrenergic receptor agonist, the vessels were relaxed using the two PPARβ/δ agonists GW0742 and L-165041, both at μM levels. The maximal vasodilator response was reached after 15 min incubation, indicating that this effect is genome-independent, and was also blocked by the PPARβ/δ antagonist GSK0660, indicating that it is mediated by PPARβ/δ (Jimenez *et al.* 2010). Similarly, in pulmonary arteries from rat pre-contracted with U46619, a thromboxane A_2 receptor agonist, the prostacyclin-like drugs iloprost and treprostinil provoked the relaxation of the vessels, which was blocked with GSK0660 and mimicked by GW0742, suggesting that PPARβ/δ regulates the dilation of the pulmonary artery (Li *et al.* 2012).

It has been shown that the PPARβ/δ mediated relaxation of vessels involves the three pathways mentioned above: PI3K/Akt/eNOS pathway (Jimenez *et al.* 2010), RhoA/ROCK pathway (Harrington *et al.* 2010) and K^+ channels (Li *et al.* 2012), but how exactly these pathways are regulated by PPARβ/δ remains unclear.

1.5.1 PPARβ/δ-regulation of potassium channels

Membrane voltage is largely determined by potassium (K^+) channel activity (Stott *et al.* 2014). Among the different types of potassium channels, the Kv7 family (voltage-dependent potassium channels) seem to play a central role in the control of vascular tone. At resting membrane potential Kv7 channels are open, letting the outflux of K^+ and contributing to the hyperpolarization of the membrane, making the contraction less likely (Archer *et al.* 1998). When the membrane is depolarized, the voltage-dependent calcium channels (VDCC) are opened and the Ca^{2+} enters in the cell, increasing the concentration of intracellular Ca^{2+}. Calmodulin binds to this Ca^{2+} now available in the cytosol and together activate the myosin light chain kinase (MLCK), which then phosphorylate myosin promoting the contraction of the vessel (Figure 1.4) (Yuan *et al.* 1998, Cole and Welsh 2011). It has been shown that the hyperglycaemia in diabetic rats reduces Kv7 channel activity, expression and vasodilatory function contributing to the vascular pathology in diabetes (Morales-Cano *et al.* 2015).

Human pulmonary artery smooth muscle cells (PASMCs) treated with GW0742 was associated with an acute and significant decrease in $[Ca^{2+}]$, and the treatment with either ITX, a selective inhibitor of calcium-activated K^+ channel, or calcium-activated K^+ channel-siRNA abolished the effect. Similarly, iloprost and treprostinil induced the activation of calcium-activated K^+ channel, which was blocked by GSK0660, and the treatment with PPARβ/δ-siRNA abolished the prostacyclin-induced activation of calcium-activated K^+ channels. Taken all together, the relaxation of pulmonary artery by prostacyclin-like drugs is PPARβ/δ dependent and through the activation of calcium-activated K^+ channels. (Li *et al.* 2012).
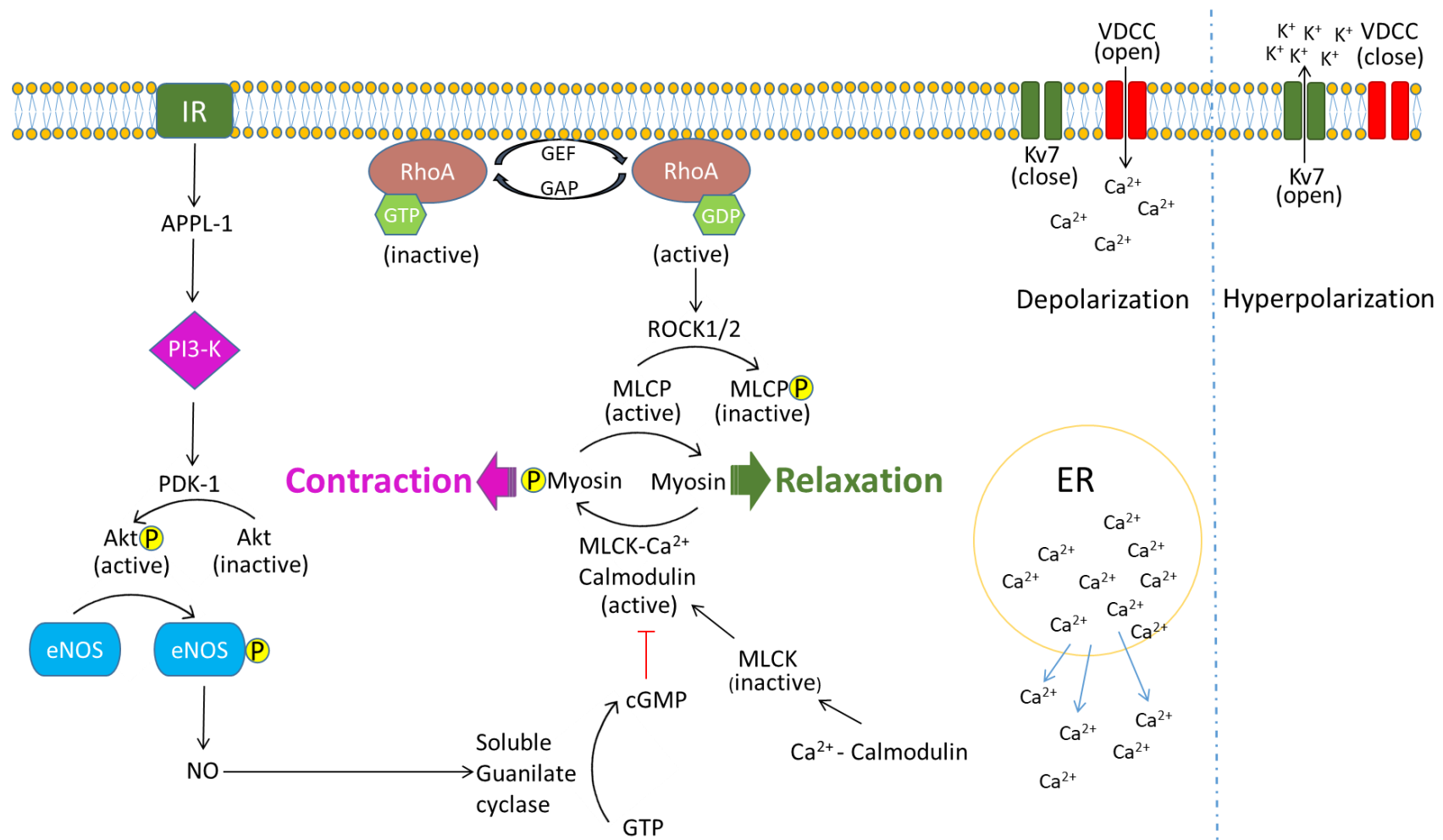
Figure 1.4 Mechanisms of VSMC contractility. The contraction of the vessels is ultimately controlled by the phosphorylation/dephosphorylation of the myosin in the smooth muscle cells, which is mainly regulated by three pathways: 1- potassium channels, 2- Rho/ROCK and 3- PI3K/Akt/eNOS. 1- At resting membrane potential Kv7 channels are open, letting the outflux of K+ and contributing to the hyperpolarization of the membrane, making the contraction less likely. When the membrane is depolarized, the VDCC channels are opened and the Ca2+ enters in the cell, increasing the concentration of intracellular Ca2+ and promoting the contraction of the vessel. 2- RhoA is converted from the inactive GDP-bound to the active GTP-bound form in response to stimuli. GTP-RhoA activates ROCK, which phosphorylates and inactivates MLCP, allowing an increase of phosphorylated myosin and causing the contraction of the vessel. 3- The activation of IR results in the autophosphorylation of multiple tyrosine residues, which then activates PI3K, leading to phosphorylation and activation of Akt and its multiple downstream target, including eNOS, and increasing the production of NO. NO activates soluble guanylate cyclase converting GTP into cGMP, which inhibits MLCK-Ca2+-Calmodulin, preventing the phosphorylation of myosin and causing the relaxation of the vessel. Akt: protein kinaseB. APPL-1: adaptor protein, phosphotyrosine interacting with PH domain and leucine zipper 1. cGMP: cyclic guanosine monophosphate. eNOS: endothelial nitric oxide synthase. ER: endoplasmic reticulum. GAP: GTPase activation protein. GDP: guanosine diphosphate. GEF: guanine nucleotide exchange. GTP: guanosine triphosphate. IR: insulin receptor. Kv7: voltage-dependent potassium channel 7. MLCK: myosin light chain kinase. MLCP: myosin light chain phosphatase. NO: nitric oxide. PDK-1: phosphoinositide-dependent protein kinase-1. PI3K: phosphatidylinositol 3-kinase. RhoA: ras homolog gene family, member A. ROCK: Rho-associated protein kinase. VDCC: voltage-dependent calcium channels.

1.5.2 PPARβ/δ-regulation of RhoA/ROCK pathway

RhoA is a small G-protein which is converted from the inactive GDP-bound to the active GTP-bound form in response to stimuli such as PE (Budzyn *et al.* 2006), thrombin (Walsh *et al.* 2008) or high glucose (Xie *et al.* 2006). GTP-RhoA activates Rho kinase (ROCK), a serine/threonine kinase, which phosphorylates and inactivates the myosin light chain phosphorylase protein (MLCP), allowing an increase of phosphorylated myosin and causing the contraction of the vessel (Figure 1.4).

In diabetic tissue, the RhoA/ROCK signalling pathway is impaired and it has been largely linked to hypertension (Sandu *et al.* 2001, Xie *et al.* 2006, Rao *et al.* 2013, Soliman *et al.* 2015). In a model of type 2 diabetic mice, RhoA was activated in aorta and mesenteric arteries, which contributed to the artery contractile hyperreactivity of the vasculature (Xie *et al.* 2006). In the same line, a study done using Goto-Kakizaki rats, a non-obese model of type 2 diabetes that also develop mild hypertension, the inhibition of ROCK normalized the blood pressure similar to that of control rats; besides, it had no effect in control animals (Rao *et al.* 2013). This suggests that the RhoA/ROCK pathway contributes to the development of diabetes-associated hypertension.

A very interesting study done with PPARβ/δ$^{-/-}$ mice showed that the GW0742-induced vasodilation of pulmonary and mesenteric arteries was PPARβ/δ-independent, since there was no difference on dilation between control and knockout. However, the dilation of aorta from PPARβ/δ$^{-/-}$ mice was significantly reduced compared to control, suggesting an involvement of PPARβ/δ on aorta dilation and indicating that vessels of different anatomical locations can utilize different signalling pathways (Harrington *et al.* 2010). In a further experiment, the authors performed a RhoA activation assay on mouse aortic rings, and the

treatment with GW0742 inhibited the GTP-bound RhoA to a similar extent to that of the classic RhoA inhibitor Y27632, suggesting that the dilatory effect of GW0742 is through the inhibition of the RhoA/ROCK pathway (Harrington *et al.* 2010).

1.5.3 PPARβ/δ-regulation of PI3K/Akt/eNOS pathway

Under normal physiological conditions, insulin receptor (IR) activation results in the autophosphorylation of multiple tyrosine residues, which then activates phosphatidylinositol 3 kinase (PI3K), leading to phosphorylation and activation of Akt and its multiple downstream targets, which finally phosphorylates and activates eNOS, increasing the production of nitric oxide (NO) (Jiang *et al.* 1999). NO activates soluble guanylate cyclase converting GTP into cGMP, which inhibits myosin light chain kinase (MLCK)-Ca^{2+}-Calmodulin, preventing the phosphorylation of myosin and causing the relaxation of the vessel (Figure 1.4) (Kitazawa *et al.* 2009).

It has been shown that this pathway is also impaired in diabetes, probably because a failure of the activation of IR and subsequent interaction with PI3K (Soliman *et al.* 2015), leading to an inactivation of the rest of the pathway and contributing to the diabetes-associated hypertension. A number of studies have shown an improvement in hypertension of diabetic animals by recovering this pathway (Gu *et al.* 2016, Li *et al.* 2016, Zheng *et al.* 2017).

The PPARβ/δ agonists GW0742 and L-165041 induced the relaxation of rat aorta rings, which was significantly reduced with the incubation with the PI3K inhibitor, indicating that PPARβ/δ relaxes rat aorta rings through PI3K/Akt/eNOS pathway. Furthermore, human umbilical vascular endothelium cells (HUVECs) were incubated with either GW0742 or L-165041 for 15 min and some of them were co-incubated with either LY294002 or GSK0660, inhibitors of PI3K and PPARβ/δ respectively, which significantly blocked the phosphorylation of Akt and eNOS,

providing stronger evidence of the regulation of PI3K/Akt/eNOS pathway through PPARβ/δ (Jimenez *et al.* 2010).

In the same line, in another study done on human mononuclear cells, the treatment with another PPARβ/δ agonist GW501516 showed the highest phosphorylation of Akt 10 min after the treatment. This phosphorylation was blocked by both, the PPARβ/δ antisense oligodeoxynucleotide transfection and incubation with LY294002, adding more evidence at the regulation of the PI3K/Akt/eNOS pathway by PPARβ/δ (Han *et al.* 2008).

Additionally, the authors co-immunoprecipitated PPARβ/δ and the PI3K subunit p85α, showing a direct interaction of PPARβ/δ and PI3K which would trigger the PI3K/Akt/eNOS cascade causing the relaxation of the vessel in a genome independent manner (Han *et al.* 2008).

Interestingly, the RhoA/ROCK and PI3K/Akt/eNOS pathways are not independent to each other and a few studies have linked them together. In vascular smooth muscle cells (VSMCs), insulin inhibits the activation of RhoA through the NO/cGMP pathway (Sandu *et al.* 2001). Also, the ROCK inhibitor Y27632 is able to increase the Akt activity in bone marrow endothelium cells. Moreover, the inhibition of ROCK or the enhancing Akt activity improves the diabetes-induced dysfunction of marrow endothelium cells (Mangialardi *et al.* 2013).

Taken all together, it can be affirmed that the non-genomic effects of PPARβ/δ are yet not fully understood and more research is needed.

1.6   Aims and objectives

The aim of this thesis is to expand the knowledge on PPARβ/δ combining a number of pharmacological, molecular and *in silico* methods. A brief outline of the different approaches employed is as follows:

- Chapter 3: Study of the non-genomic effects of PPARβ/δ activation on vascular contractility comparing healthy with diabetic vessels using organ bath and myography pharmacological based experiments.

- Chapter 4: Study of the genomic effects of PPARβ/δ activation on the regulation of inflammation in lung using molecular based experiments including ELISA, Griess assay and qRT-PCR.

- Chapter 5: Study of the molecular interaction of PPARβ/δ with different agonists and antagonists using docking *in silico* modelling methods.

Chapter 2: Methods

2.1 Material

Table 2.1 List of materials used in this thesis.

Chemical	Supplier	Product Number
1400W	Sigma	W4262
Acrylamide:Bis-acrylamide 30%	Fisher Scientific	J61505.K2
Agarose	Fisher Scientific	BP1356-100
Anti-NF-κB p65 antibody	Abcam	ab16502
Anti-PPARβ/δ monoclonal antibody	Santa Cruz Biotechnology	sc-74517
Anti-PPARβ/δ policlonal antibody	Santa Cruz Biotechnology	sc-7197
Anti-PPARβ/δ policlonal antibody	Abcam	ab23673
Anti-Retinoid X receptor alpha antibody	Abcam	ab125001
Biotinylated protein ladder detection pack	Cell Signaling Technology	7727
Bovine serum albumin (BSA)	Sigma	A7906
Calcium chloride (CaCl2)	Fisher Scientific	10171800
Citric acid	Fisher Scientific	10345410
Collagenase	Sigma	C7657
Complete Mini EDTA-free protease inhibitor cocktail tablets	Roche	11 836 170 001

Dithiothreitol (DTT)	Fisher Scientific	10592945
DMSO	Fisher Scientific	D/4121/PB08
Dubecco's modified Eagle medium (DMEM)	Gibco	41965-039
Elastase	Sigma	E-1250
Fasudil	Sigma	CDS021620
Foetal bovine serum (FBS)	Gibco	10500-064
Formaldehyde	Fisher Scientific	BP531-25
Glucose	Fisher Scientific	10385940
Glutaraldehyde	Fisher Scientific	G/0518/PB08
Goat anti-mouse antibody	Invitrogen	32430
Goat anti-rabbit antibody	Abcam	ab97051
Goat Anti-Rabbit IgG	Abcam	ab97051
GSK0660	Sigma	G5795
GSK3787	Sigma	G7423
GW0742	Sigma	G3295
Hank's	Sigma	H8264
HEPES solution	Sigma	H0887
Immobilon-P PVDF membrane	Merk Millipore	IPVH00010
Immunoprecipitation kit	Abcam	ab206996
Insulin	Sigma	I6634
iScript cDNA synthesis kit	Bio-Rad	170-8891
L-165041	Sigma	L2167
LPS O55:B5	Sigma	L2880
LY294002	Tocris	1130
Magnesium sulfate (MgSO4)	Fisher Scientific	M/1000/62
Methanol	Fisher Scientific	11976961

Naphthylethylenediamine dihydrochloride	Sigma	N9125
Non-essential aminoacids	Sigma	M7145
Orthophsphoric acid	Fisher Scientific	O/0500/PB17
Penicillin/Streptomycin	Sigma	P0781
Phenilephryne	Sigma	P6126
Pierce BCA Protein Assay kit	ThermoFisher	23225
Pierce Co-immunoprecipitation kit	ThermoFisher	26149
Pierce ECL western blotting substrate	ThermoFisher	32106
Potassium chloride (KCl)	Fisher Scientific	10375810
Potassium dihydrogen phosphate (KH2PO4)	Fisher Scientific	10783611
Purelink Genomic DNA minikit	Invitrogen	K1820-00
Rat IL-6 Duo Set ELISA kit	R&D Systems	DY506
Rat PPARβ/δ ELISA kit	Abbkine	KTE100973
Restore Plus western blot stripping buffer	ThermoFisher	SJ257621
Rneasy Fibrous Tissue Minikit	Quiagen	74704
Sodium carbonate	Fisher Scientific	10264540
Sodium chloride (NaCl)	Fisher Scientific	10735921
Sodium dodecylsulfate polyacrylamide (SDS)	Fisher Scientific	1281-1680
Sodium nitrate	Fisher Scientific	10696842
Stabilized goat anti-mouse IgG peroxidase conjugated	ThermoFisher	32430
Streptozotocin	Sigma	S0130
Sulfanilamide	Sigma	S2951
SupersignalWest Femto Masimum Sensitivity Substrate	ThermoFisher	34094

SYBER Green Master Mix	Applied Biosystem	A25741
Tac DNA polymerase	Invitrogen	10342-020
Tapman PCR Master Mix	Applied Biosystem	4304437
TEMED	Fisher Scientific	10689543
Tris-base	Fisher Scientific	10785341
Trypsin	Sigma	T-4174
Tween-20	Sigma	P7949
U46619	Tocris	1932
Y27632 dihydrochloride	Sigma	Y0503

2.2 Animals and environmental conditions

Male Wistar rats (350-450 g) were sourced from Charles River (UK) and housed in pairs in standard cages (Techniplast 2000P) with sawdust (Datesand grade 7 substrate) and shredded paper wool bedding with water and food (5LF2 10% protein LabDiet) freely available in the Biological Services Unit, University of Hertfordshire. The housing room was maintained at a constant temperature of 22 ± 2 °C, under a 12 h light/dark cycle (lights on: 07:00 to 19:00 h). All testing was conducted under the light phase of the animals' light/dark cycle, and care was taken to randomise treatment sequences to control for possible order effects.

All studies were approved by the University of Hertfordshire Animal Welfare and Ethics review committee and conducted in accordance with the guidelines established by the Animals (Scientific Procedures) Act, 1986 and European directive 2010/63/EU and diabetes experiments were carried out under project licence PPL70/7732.

2.3 Induction and maintenance of Streptozotocin (STZ) induced diabetes (carried out by licenced researchers and animal technicians)

Groups of rats were randomly selected and administered a single injection of 55 mg/kg Streptozotocin (STZ; dissolved in 20 mM citrate buffer at pH 4.5) intraperitoneally (i.p., DV 10 mL/kg) or vehicle control (20 mM citrate buffer at pH 4.5, i.p., DV 10 mL/kg) or untreated (Naïve group) by a licenced researcher. For 48 hours following STZ or control injection an additional choice of 2% sucrose solution was provided to avoid the initial hypoglycaemia that is seen following STZ. After 48 hours all STZ-diabetic rats were supplied with extra unmodified drinking water to compensate for diabetic polydipsia. Home cages were changed more frequently due to polyuria. Moreover, food was also changed from 10% protein (LabDiet 5LF2, EURodent Diet 10%) into protein rich diet 22% protein (LabDiet 5LF5, EURodent Diet 14%) after injection to compensate possible diabetes-induced protein loss. Sunflower seeds and wheatgerm seeds were provided to enrich dietary fats and protein post STZ. To minimise discomfort of spontaneous pain (allodynia, guarding) animals were placed on suitable bedding throughout the study.

Blood glucose was measured before the intraperitoneal injection (baseline), at day 7 after intraperitoneal injection to confirm hyperglycaemia and finally on the day of sacrifice (terminal). Blood glucose was measured from a single drop of tail vein blood obtained by a needle prick of conscious rats, using an Accu-check blood glucose monitor (Roche). Blood glucose concentrations above 16mmol/L (≥300 mg/dL) were considered diabetic (hyperglycaemic) and included in the diabetes study. All experiments were powered to take into consideration the loss of animals of 10% weight i.e. those that do not develop diabetes following the intraperitoneal

injection or develop acute toxicity following STZ despite welfare provisions of sucrose, high protein diet and frequent home changes.

2.4 Tissue dissection and preparation

Rats (Naïve, control and STZ-diabetic) were euthanised according to schedule 1 procedure by CO_2 asphyxiation followed by cervical dislocation. Lungs, aortas and mesenteric arteries were removed and immediately placed in a black background dissection plate containing physiological saline solution (PSS) buffer (118 mM NaCl, 4.7 mM KCl, 2.5 mM $CaCl_2$, 1.17 mM $MgSO_4$, 1 mM KH_2PO_4, 5.5 mM glucose and 25 mM $NaHCO_3$).

The connective tissue surrounding the aortas from Naïve, control and STZ-diabetic rats was gently removed using spring scissors. The thoracic upper half of the aorta was cut into approximately 2-3 mm long rings and used for the organ bath experiments (Section 2.5). The abdominal half of the aorta was cut into approximately 1.5 mm long rings and used for the subsequent experiments in the myograph (Section 2.6).

The mesentery from Naïve, control and STZ-diabetic rats was placed on the dissection plate with the duodenum upward endowing the whole tissue as a C shape to yield the vein toward the objective lens of the microscope while the artery underneath proximal to the tray surface. The vein and the tissue surrounding the mesenteric arteries were gently removed under DMT 2000 stereomicroscope (magnification 4-40x) using spring scissors and once the artery was completely clean it was cut from the mesentery and loaded in the myograph (Section 2.6).

The lungs from Naïve rats were removed and immediately placed in a dissection plate for the dissection of pulmonary artery, bronchi and parenchyma. Each lung was dissected individually. Using a DMT 2000 stereomicroscope (magnification 4-

40x) and spring scissors the primary vein was cut longitudinally. The vein was very carefully removed without damaging the bronchi, which is immediately underneath. The bronchi was then removed without damaging the principal artery, which is also very closely attached underneath the bronchi. Then, the principal pulmonary artery was removed from the lung and finally pieces of lung parenchyma from each lung were also cut. Once the pulmonary arteries and bronchi were isolated from the lung, they were placed again in the dissection plate with fresh PSS and completely cleaned from the surrounding connective tissue and cut into rings. The tissues from four rats (n=4) were immediately used to quantify the expression of PPARβ/δ (Section 2.9). The rest of the tissues were immediately placed in the required treatment detailed in Chapter 4 Section 4.3.1. After 24 h incubation, the culture medium was removed and kept at -20 $^{\circ}$C until needed for the detection of NO (Section 2.10) and IL-6 (Section 2.11), and the tissues were kept at -80 $^{\circ}$C until needed for PPARβ/δ co-immunoprecipitation (Section 2.12) or qRT-PCR (Section 2.17).

2.5   Organ bath

Freshly isolated thoracic aorta rings were threaded by superior and inferior loops where the inferior thread loop was attached to a fixed hook and kept suspended in the Bennet isolated tissue vessel organ bath of 95% O_2 / 5% CO_2 Kreb's buffer (pH 7.4, 118 mM NaCl, 4.7 mM KCl, 1.2 mM $MgSO_4$, 1.2 mM KH_2PO_4, 2.5 mM $CaCl_2$, 25.0 mM $NaHCO_3$ and 11.0 mM glucose) at 37 ± 1°C. The superior loop was attached through long terminal thread to FT-100 force transducer under 2 g tension force immediately after the Labscribe software was calibrated with a standard 2 g weight. FT-100 force transducer transmitted the tissue responses to iWORKS amplifier that generated electrical signals to be recorded through Labscribe software from iWORKS version 1.817.

Rings were then left to equilibrate for 20 min and the viability of the tissue was tested by adding 1 µM of phenylephrine. The tissue was washed three times until the tension was stable at the baseline. The tissue was then ready to perform the required experiment, the experimental design is explained in detail in the Methods section of Chapter 3.

2.6 Myography

Mesenteric arteries and abdominal aorta rings were mounted in a four channel Mulvany-Halpern wire myograph (Model 610 M, Danish Myo Technology) using 2 tungsten wires of 40 µm diameter. The tissues were normalized, and the tension was set to 100 mmHg using the Labchart software. Rings were left to equilibrate for 30 min in PSS and the viability of the tissue was tested by adding high potassium physiological saline solution (KPSS) (4.7 mM NaCl, 118 mM KCl, 1.17 mM $MgSO_4$, 1 mM KH_2PO_4, 2.5 mM $CaCl_2$, 25 mM $NaHCO_3$, and 5.5 mM glucose), which induces vasoconstriction in a viable tissue. The rings were washed three times until the tension was stable at the baseline. The tissue was then ready to perform the required experiment, the experimental design is explained in detail in the Methods section of Chapter 3.

2.7 Cell culture of pulmonary smooth muscle cells (PSMCs)

Pulmonary arteries from Naïve rats were dissected and carefully washed in filtered HEPES (4-(2-hydroxyethyl)-1-piperazineethanesulfonic acid) Ca^{2+}-free solution (pH 7.3, 130 mM NaCl, 5mM KCl, 10 mM HEPES, 1.2 mM $MgCl_2$, 10 mM glucose) and treated with an enzymatic solution (1.125 mg/mL collagenase, 2.5% vol/vol elastase, 1 mg/mL albumin in filtered HEPES Ca^{2+}-free solution) for 4 min at 4 °C followed by 1 min at 37 °C. After incubation, the enzymatic treatment was removed and substituted for HEPES Ca^{2+}-free solution; pulmonary artery rings were shaken

vigorously with a glass Pasteur pipette and then transferred to a Petri dish. Rings were opened and the endothelium was mechanically removed. Strips were cut into small pieces and stuck on the Petri dish with the luminal side facing down. Carefully, culture medium was added (20% fetal bovine serum (FBS), 1% penicillin/streptomycin, 1% no essential amino acids) and incubated under 5% CO_2 at 37 °C. When cells started to grow the explants were removed and the cells were left to grow (passage 0); after 7-8 days the cells were transferred into a T25 flask (passage 1). When the cells were confluent they were trypsinized; briefly, the medium was removed and the cells were washed twice with 5 mL of Hank's solution. Then, 4.5 mL of fresh Hank's solution and 0.5 mL of 10x trypsin were added into the flask and incubated at 37 °C for 1 min. The flask was then hit on the sides to detach the cells, which was verified under the microscope. At that point 2.5 mL of culture medium was added into the flask and vigorously shaken to dissolve any remaining lump of cells. The content of the flask was then transferred into a 15 mL Falcom tube and centrifuged at 1500 rpm for 10 min. The supernatant was discarded and the cells were resuspended in 2-3 mL of fresh culture medium. The cells were then counted using a Neubauer chamber and plated into 6 well-plates in a density of 500,000 cells/well (passage 2). Next day the medium was removed and substituted for the required treatments in triplicate. After 24 h incubation the supernatant was removed and kept at -20 °C until needed for IL-6 detection (Section 2.11), and cells were lysed and kept at -20 °C until needed to analyse protein expression by Western blot (Section 2.15).

2.8   Quantification of proteins by BCA assay

The quantification of total protein is a pre-step required for the quantification of PPARβ/δ expression in pulmonary artery, bronchi and lung parenchyma (Section 2.9) as well as PPARβ/δ immune precipitation of whole lung homogenate and PSMCs lysate (Section 2.12).

The total protein concentration of the tissue/cell homogenates mentioned above was measured by the bicinchoninic acid (BCA) protein assay, which is a 2-step colorimetric assay. In the first step the Cu^{+2} present in the peptide bonds are reduced to Cu^+ in an alkaline medium forming a light blue colour. In the second step, two molecules of BCA chelate with one Cu^+, forming a purple complex that absorbs light at 562nm in a linear relationship. The amount of Cu^+ produced and purple colour is proportional to the amount of protein present in the sample, which can be quantified by comparison to a standard curve of bovine serum albumin (BSA) (0-10 mg/mL).

Pierce™ BCA Protein Assay Kit (ThermoFisher) was used for protein quantification. The protocol was modified from that supplied for the manufacturer. Briefly, 5 µL of each standard diluted on lysis buffer was added into a 96 microtate-plate in triplicate. Then, 5 µL of sample (either tissue homogenate or cell lysate) was added into wells also in triplicate. BCA reagent A was mixed with the BCA reagent B in a ratio 50:1, and 100 µL of the mixture was added to both, samples and standards. The plate was incubated at 37 °C for 30 min and the absorbance measured at 562 nm.

2.9 Quantification of PPARβ/δ expression in pulmonary artery, bronchi and parenchyma by enzyme-linked immunosorbent assay (ELISA)

The expression of PPARβ/δ on pulmonary artery, bronchi and parenchyma from Naïve rat was measured using Rat PPARβ/δ ELISA kit (Abbkine) according to the manufacturer's instructions. Briefly, the tissues were dissected (Section 2.4) and homogenized with liquid N_2 using a mortar and a pestle. The powder was transferred to a micro fudge tube containing ice-cold phosphate buffered saline (PBS) with proteinase inhibitor cocktail in a ratio 9 mL PBS (NaCl 137 mM, KCl 2.7 mM, Na_2HPO_4 10 mM, KH_2PO_4 1.8 mM, pH 7.4) per g tissue. The samples were sonicated 3x30 seconds and then centrifuged for 5 min at 5000 g. The supernatant was collected, and the protein concentration was quantified by BCA assay (Section 2.8). Then, 50 µL of standards and samples were added in duplicate to the plate containing pre-coated anti-PPARβ/δ and incubated 45 min at 37 °C. The wells were washed and incubated with 50 µL of the horseradish peroxidase (HRP)-conjugated detection antibody for another 30 min at 37 °C. The wells were washed again and incubated in dark with the chromogen solution for 15 min at 37 °C. Finally, the reaction was stopped by adding 50 µL of Stop solution and the plate was immediately measured in a microplate reader at 450 nm. The concentrations of PPARβ/δ were determined by comparison with the standard curve (0-8 ng/mL).

2.10 Quantification of nitric oxide released by pulmonary artery, bronchi and parenchyma by Griess assay

The NO produced by pulmonary artery, bronchi and parenchyma (Section 2.4) and accumulated in the culture medium after 24 h of incubation under different treatments (specified in Chapter 4) was measured by Griess reaction. Briefly, the NO released by tissues is very unstable and is stoichiometrically converted to nitrite (NO_2^-) very quickly. An aliquot of the culture medium (50 µL) previously thaw in ice was mixed with an equal volume of Griess reagent (mixture of equal volumes Griess reagent 1 and Griess reagent 2 containing sulfanilamide 1% w/v + orthophosphoric acid 5% v/v and naphthylethylenediamine dihydrochloride 0.5% w/v respectively). Sulfanilamide forms a diazonium salt with the nitrites, as shown in the reaction below (Figure 2.1). When the azo dye agent (N-alpha-naphthylethylenediamine) is added, a pink colour develops.

This second compound is proportional to the NO initially present in the culture medium and the concentration was determined by comparison of the OD_{540} to a standard curve of solutions of sodium nitrite (0-1 mM) dissolved in Dulbecco's modified Eagle medium (DMEM), the same culture medium used for the incubation of the tissues.
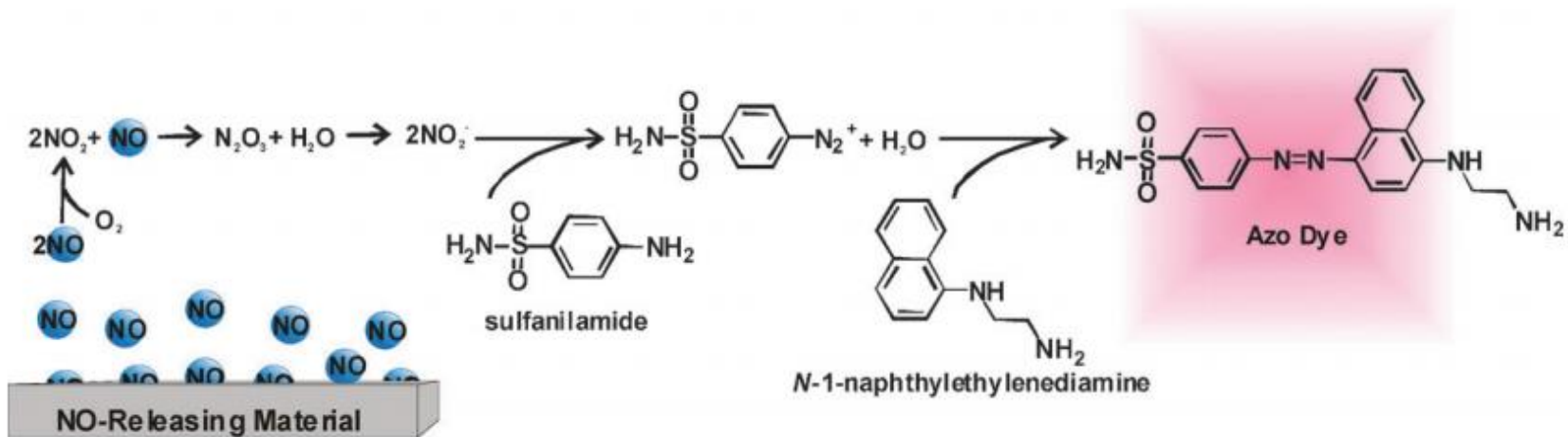
Figure 2.1 Griess reaction. The NO released by cells/tissues is very unstable and is stoichiometrically converted to NO^{2-} very quickly. Under acidic conditions one molecule of nitrite reacts with one molecule of sulphanilamide forming the diazonium ion, which is then coupled to one molecule of naphthylethylenediamine forming the Azo dye, seen as pink colour. This dye strongly absorbs at 540 nm and its concentration is proportional to the NO initially present in the medium (Coneski and Schoenfisch 2012).

2.11 Quantification of IL-6 released by PSMCs and lung tissues by ELISA

The release of IL-6 by PSMCs (Section 2.7) and lung tissues (Section 2.4) was measured using Rat IL-6 DuoSet ELISA kit (R&D Systems) according to the manufacturer's instructions. Briefly, the samples previously thawed in ice and standards were added in duplicate to a microtiter plate containing the capture antibody. After two hours of incubation the wells were washed and incubated with the detection antibody for another two hours. The wells were washed again and incubated in dark with Streptavidin-HRP for 20 min. The wells were washed once more and incubated in dark with Substrate Solution. After 20 min the stop solution was added and immediately measured in a microplate reader. The readings at 540 nm were subtracted from the readings at 450 nm and the concentrations of samples were determined by comparison with the standard curve (0-8 ng/mL).

2.12 Co-immunoprecipitation of PPARβ/δ from lung and PSMCs

There are different methods to immunoprecipitate proteins; among them two were tried out in this thesis: covalent antibody immobilization in agarose beads and antibody binding protein A/G sepharose beads

2.12.1 Covalent antibody immobilization in agarose beads

PSMCs and a piece of lung from Naïve rat were homogenised with lysis buffer provided by the Pierce Co-Immunoprecipitation kit (ThermoScientific) and supplemented with Complete Mini EDTA-free protease inhibitor cocktail tablets (Roche). PSMCs were lysed on ice using a cell scrapper and the lung was homogenised with liquid N_2 using a mortar and pestle. The lysates were incubated in ice for 30 min vortexing every 10 min and centrifuged at 10,000 rpm for 15 min

at 4 °C, the pellet was discarded. Protein concentration of the supernatant was quantified by BCA assay (Section 2.8) and used for the subsequent co-immunoprecipitation of proteins.

PPARβ/δ was isolated with the Pierce Co-Immunoprecipitation kit (ThermoScientific) following the manufacturer's instructions (Figure 2.2). Briefly, 75 µg of antibody anti-PPARβ/δ was immobilized in a column by incubating the antibody with the resin overnight at 4 °C with end-over-end mixing. In parallel, 1 mg of sample lysate was pre-cleared by incubating the sample in a column containing control agarose resin for 30 min with end-over-end mixing. The column was centrifuged and the flow-through containing the clear sample was diluted to a final volume of 500 µL. These 500 µL were added to the column containing the immobilised anti-PPARβ/δ and left incubating overnight at 4 °C with end-over-end mixing. The column was centrifuged and the flow-through was kept (FT). The resin was washed three times with IP Lysis Buffer (W1, W2, W3) to remove any protein that non-specifically bound the column. The specifically bound protein was eluted with 60 µL of Elution buffer (E1), and any remaining protein was removed by adding 50 µL of Elution buffer twice more (E2, E3). All the centrifugation steps were done at 1,000 g for 1 min at room temperature. All the fractions were further analysed by silver staining (Section 2.14) and Western blot (Section 2.15).
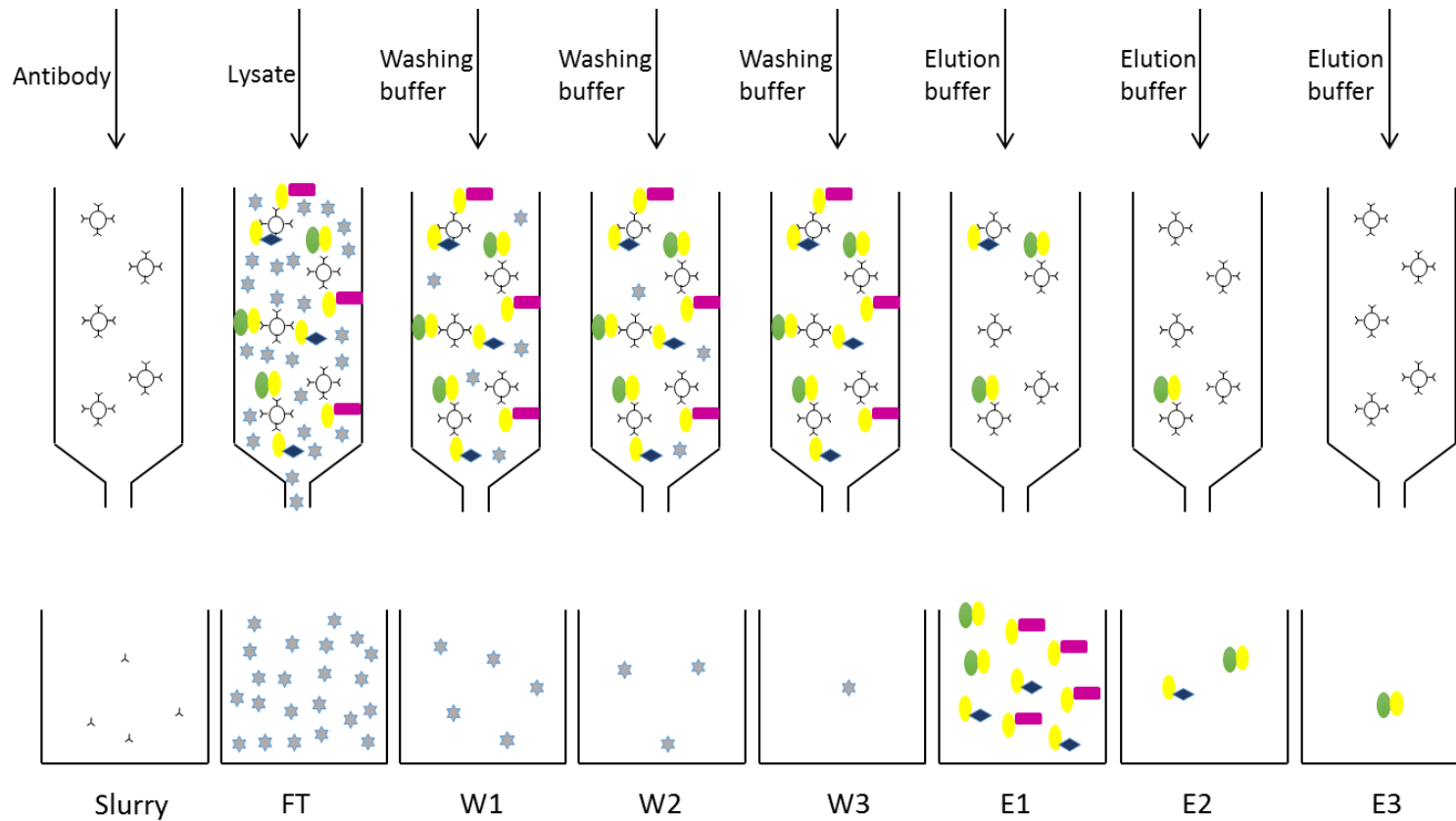
Figure 2.2 Diagram of the covalent antibody immobilization Co-IP. The antibody was added to a column containing the pre-activated resin. After incubation, the column was centrifuged, and the slurry was collected for further analysis. The lysate was then added to the column containing the immobilised antibody. After incubation, the column was centrifuged and the flow through (FT) was collected in a new tube. The column was then washed three times with washing solution to remove any protein that non-specifically bound the column (W1, W2, W3). The specifically bound protein was eluted with elution buffer and collected in a new fraction (E1). Any remained protein was removed in following elution steps (E2, E3).

2.12.2 Antibody binding protein A/G sepharose beads

PPARβ/δ was isolated with the Immunoprecipitation kit ab206996 (Abcam) following the manufacturer's instructions (Figure 2.3). Briefly, a piece of lung from Naïve rat was homogenized in a mortar and pestle using liquid nitrogen and transferred to a tube containing ice-cold lysis buffer (300 µL of buffer per 5 mg of tissue). The tube was mixed on a rocker at 4 °C for 1h. The tissue was centrifuged at 10,000 g for 5 min at 4 °C and supernatant was transferred to a new tube. The protein was quantified. The primary antibody was added to the sample at the recommended concentration by the antibody's manufacturer and mixed overnight at 4 °C on a rocker. In the meantime, the protein A/G sepharose was washed twice with washing buffer, centrifuged at 2,000 g for 2 min and removing the supernatant between washes. Then it was suspended as 50% slurry in wash buffer. After antibody binding, the sample and the protein A/G sepharose beads were mixed and incubated for 1 h at 4 °C. The complex Protein A/G sepharose beads-antibody-protein was collected by low speed centrifugation at 2,000 g for 2 min at 4 °C. The complex was washed three times with 1 mL of wash buffer and the supernatant was removed after centrifuging at 2,000 g for 2 min at 4 °C. Finally, 40 µL of SDS-PAGE loading buffer was added to the beads and boiled for 5 min. Then it was centrifuged to collect the eluent and stored at -80 °C until use for SDS-PAGE electrophoresis (Section 2.13).
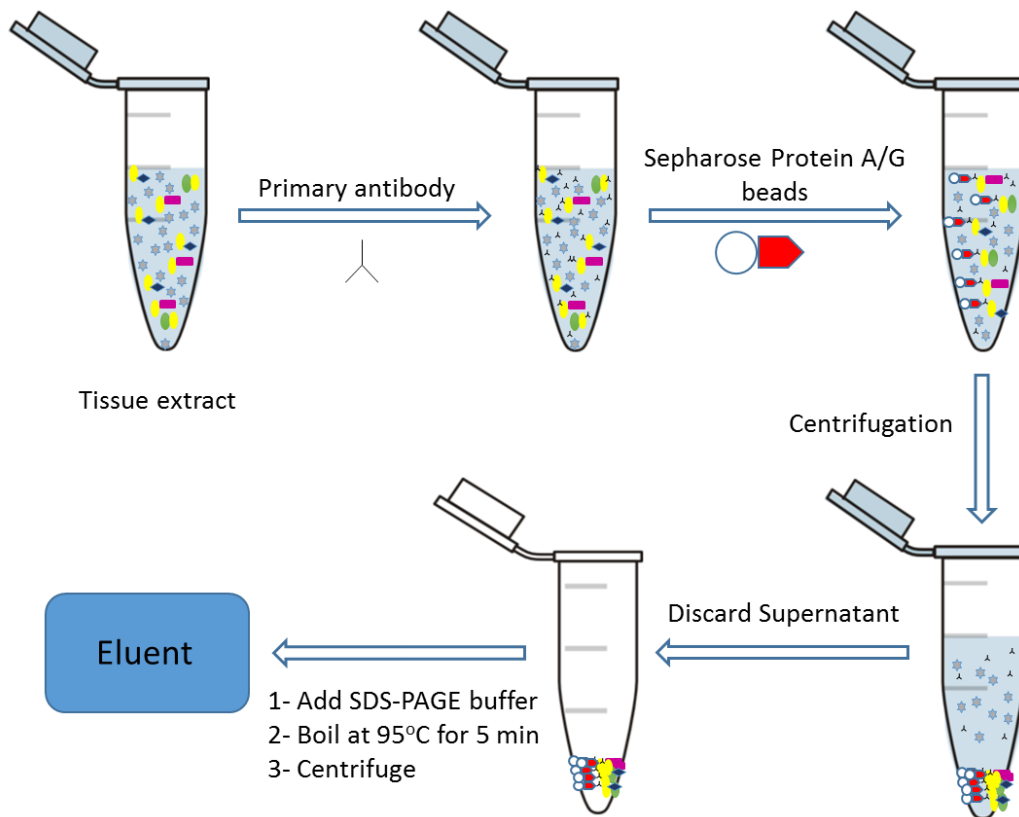
Figure 2.3 Diagram of the protein A/G sepharose Co-IP. The tissue lysate was mixed with the anti- PPARβ/δ antibody. After the incubation, the Protein A/G beads were added in the mixture and incubated again. The mixture was then centrifuged and the pellet containing the precipitated protein was boiled in SDS-PAGE loading buffer at 95 °C for 5 min. Finally, the sample was centrifuged, and the supernatant loaded in an SDS-PAGE gel.

2.13 SDS-PAGE electrophoresis

Electrophoresis of the fractions resulted from the co-immunoprecipitation of PPARβ/δ (Section 2.12) was performed using the Mini-protean system (Bio-Rad). A total of 20 μL of sample was heated at 95 °C for 5 min to denature the protein. Samples and molecular weight markers were loaded into the sample wells and proteins were separated in a 7.5% sodium dodecylsulfate polyacrylamide gels (SDS-PAGE) at a current of 200 mV supplied by a PowerPac 300 (Bio-Rad) unit for approximately 40 min, until the dye front was near the bottom of the gel. The gels were used for either silver staining or Western blot.

2.14 Silver staining

SDS-PAGE gels were silver stained as a check point of the purification of PPARβ/δ. After electrophoresis, gels were washed in washing solution (5% methanol, 7% acetic acid, in water) for 30 min and incubated with 10% glutaraldehyde for 30 min. Any remaining glutaraldehyde was removed by washing with continuous changes of distilled water for 4 h. Gels were then treated with dithiothreitol (DTT) 5 μg/mL for 30 min followed by 0.01% silver nitrate treatment for another 30 min. Gels were finally incubated with the developer (3% sodium carbonate and add 0.02% formaldehyde) until they were stained, and the reaction was stopped with 5 mL of 2.3 M citric acid.

2.15 Western blot

The proteins contained in an SDS-PAGE gel were transferred to a polyvinylidene difluoride (PVDF) membrane (GE Healthcare Life Science) using the Mini-protean system (Bio-Rad) at a current of 400 mA supplied by a PowerPac 300 (Bio-Rad) unit for 105 min. After transference, Tris-buffered saline with Tween 20 (TBST) plus 5% non-fat milk was used to block the membrane at room temperature for 1 h (TBST buffer: 5 M NaCl, 2 M Trys pH 7.6 and 0.1% Tween-20). Membranes were incubated with the target primary antibodies at 4 °C overnight (PPARβ/δ 1:200 in 3% milk; RXR 1:1000 in 3% milk; p-65 1:1000 in 5% BSA; NOS2 1:500 in 5% milk; β-actin 1:5000 in 5% milk) followed by four washes with TBST every 8 min. Bound antibodies were detected by HRP-conjugated secondary antibodies at a dilution of 1:10000 in TBST-1% non-fat milk powder for 1 h at room temperature. Protein signal intensities were determined by chemiluminescence using the enhanced chemiluminescence (ECL) Prime Western Blotting Detection Reagent (GE Healthcare Life Science) or SuperSignal™ West Femto Maximum Sensitivity

Substrate (ThermoFisher). When needed, relative signal intensities were normalized to β-Actin and quantified.

2.16 Stripping of membranes

The stripping of the membranes was done using Re-Blot Plus Strong Solution (Millipore) following the manufacturer's instructions. Briefly, the membranes were incubated in Re-Blot Plus Solution for 30 min, washed with TBS-T and blocked in blocking solution for 30 min.

2.17 Quantitative real time-polymerase chain reaction (qRT-PCR)

2.17.1 RNA extraction

Total RNA was extracted from pulmonary artery, bronchi and parenchyma (Section 2.4) using RNeasy Fibrous Tissue Mini Kit (Quiagen). The tissues were first pulverized in a pestle with liquid N_2 and the RNA was then extracted following the manufacturer's instruction. Briefly, the tissue (<20 mg) was transferred into a 1.5 mL tube containing 300 µL of Buffer RLT. Then, 590 µL of RNase-free water was added followed by 10 µL of proteinase K. The mixture was incubated at 55 °C for 10 min and centrifuged at 10,000 g for 3 min. The supernatant was transferred into a new tube and 0.5 volumes of 100% ethanol was added. After mixing, 700 µL was transferred to a RNeasy Minicolumn and centrifuged at 8,000 g for 30 s. This last step was repeated with the rest of the sample and flow-through was discarded. Then, 350 µL Buffer RW1 was added and centrifuged at 8,000 g for 30 s, flow-through was discarded. A mixture of 10 µL of DNase + 70 µL Buffer RDD was added into the column and incubated for 15 min at room temperature. After, 350 µL Buffer RW1 was added and centrifuged at 8,000 g for 30 s. The columns were washed with 500 µL of Buffer RPE and centrifuged at 8,000 g for 2 min. Finally, 30

µL of RNase-free water was added to the column and incubated for 5 min at room temperature. After, the columns were centrifuged, and the last step was repeated using the same 30 µL of RNase-free water. After the last centrifugation the samples were kept at -80 °C until use.

The quality and concentration of the RNA was measured using Nanodrop (SimpliNano, GE Healthcare Life Science) at wavelength of 260 nm. Further to that, the degradation of RNA was also checked in a 1% agarose gel, and the DNA contamination of RNA was checked by PCR (Polymerase chain reaction), using genomic DNA (gDNA) as a positive control. Two primers for the housekeeping gene *β-actin* were design (forward CTGGTCGTACCACTGGCATT, reverse AATGCCTGGGTACATGGTGG) and used to perform a PCR of the RNA samples together with the positive control. The termociclator Mastercycler Nexus gradient (Eppendorf) was set with the following PCR protocol: 95 °C for 10 min, 40 cycles of 95 °C for 30 s, 56 °C for 30 s and 72 °C for 30 s, 72 °C for 10 min and hold at 4 °C.

2.17.2 Genomic DNA extraction

Genomic DNA was extracted from pulmonary artery, bronchi and parenchyma to use as a positive control of PCR. PureLink Genomic DNA mini kit from Invitrogen was used following the manufacturer's instructions. Briefly, up to 25 mg of tissue was incubated at 55 °C in a 1.5 mL tube containing 180 µL of PureLink Genomic Digestion Buffer and 20 µL of Proteinase K until the tissue was completely digested. Then, the tube was centrifuged at maximum speed for 3 min and the supernatant was transferred into a new sterile tube. 20 µL of RNase A was added, mixed and incubated at room temperature for 2 min. After, 200 µL of PureLink Genomic Lysis Buffer was added and mixed until the solution was homogeneous, and 200 µL of absolute ethanol was added and mixed. The sample was then

transferred into a PureLink Spin Column and centrifuged at 10,000 g for 1 min at room temperature. The flow through was discarded and 500 µL of wash buffer was added, centrifuged at 10,000 g for 1 min at room temperature and the flow through was discarded. Finally, 100 µL of PureLink genomic Elution Buffer was added to the column, incubated at room temperature for 1min and centrifuged at max speed for 1 min at room temperature. The flow through was collected and kept at -20 ºC until use.

2.17.3 Quantitative real time polymerase chain reaction (qRT-PCR)

cDNA was obtained by reverse transcription (RT) using iScript cDNA synthesis kit (Bio-rad) following the manufacturer's instructions. Briefly, 300 ng of RNA was diluted to a final volume of 15 µL, and 4 µL of iScript reaction mix and 1 µL of iScript reverse transcriptase were added. The RT was performed using a thermociclator Stratagene Mx3005P (Agilent Technologies) with the following steps: 5 min at 25 ºC, 20 min at 46 ºC, 5 min at 95 ºC, and hold at 4 ºC.

2.17.3.1 SYBR GREEN

qRT-PCR was performed to analyse mRNA expression using SYBR GREEN system. Briefly, 20 µL of reaction mix containing the primers was incubated in a 96 well-plate following the cycle conditions: 94 °C for 2.5 min, 40 cycles of 94 °C for 30 s 60 °C for 30 s 72 °C for 15 s, and a final dissociation curve consisting on 72 °C for 5 min. The primers used for the amplification were design using the Roche ProbeFinder Assay Design Software available online at https://qpcr.probefinder.com/organism.jsp and are as follows: *Pdk-4* (forward cgcttagtgaacaccccttc, reverse tccactaaatccatcaggctct), *Angplt-4* (forward tccgaggggaccttaactgt, reverse attggaatggctgcaggt), *NOS2* (forward accatggagcatcccaagt, reverse cagcgcataccacttcagc), *Serpine-1* (forward agagccaatcacaaggcact, reverse gaggcaagtgagggctga), *Timp-1* (forward

cagcaaaaggccttcgtaaa, reverse tggctgaacagggaaacact), *Sema7a* (forward ctatggcgttttctccaacc, reverse gtcaatgtcaccaagcgaatac), *Ppfibp1* (forward acaaggagtccctcgttgag, reverse ttcaagttagagatctcagccatc), *β-actin* (forward gccctagacttcgagcaaga, reverse tcaggcagctcatagctcttc). Relative quantification of the different transcripts was determined with the ΔΔCt method using β-actin as an endogenous control and normalized to control group.

2.17.3.2 Taqman

qRT-PCR was performed to analyse mRNA expression using a Taqman System (TaqMan PCR Master mix, Applied biosystem). Briefly, 10 µL of reaction mix containing the primers and cDNA was incubated in a 96 well-plate following the cycle conditions: 95 °C for 10 min, 40 cycles of 95 °C for 15 s and 60 °C for 1min. The primers used for amplification are *Pdk-4, Angplt-4, NOS2, Serpine-1, Timp-1, Sema7a, Ppfibp1, β-actin* (Applied biosystem). Relative quantification of these different transcripts was determined with the ΔΔCt method using β-actin as an endogenous control and normalized to control group.

2.18 Docking

Molecular docking is a computational-based procedure to predict non-covalent interactions of a receptor and a ligand, as well as determine binding affinities of ligands. The ability of drugs to bind into protein active sites was investigated using AutoDock/Vina with Pymol and and Ligplot+ as a graphical user interface

2.18.1 Protein preparation

For the docking simulations, the PPARβ/δ crystal structure 3TKM was selected for having one of the highest resolutions (1.95 Å). The PDB file was downloaded from Protein Data Bank. Water molecules, ligands and other hetero atoms were removed from the protein structure, and the addition of hydrogen atoms to the

protein was performed using AutoDock Tools version 1.5.6. The grid was set manually to cover the active site. The file was saved as pdbqt file.

2.18.2 Ligand preparation

The ligand molecule structures were drawn in ChemSketch, the energy was minimized and saved in PDB and MOL-2 format. Same file was opened in AutoDock Tools version 1.5.6 and saved as pdbqt file.

2.18.3 Docking

Molecular docking was performed with the software AutoDock Vina and all parameters set as default. Results with minor calculated free energy variations (the best theoretical binding energy) were analysed using Pymol version 1.7.4 and LigPlot+ version1.4.5 softwares.

For the docking of two molecules, the 3TKM PDB file without hetero atoms was combined with the best docking result of each ligand in one single PDB file, one PDB file per ligand. These files were opened in Autodock Tools, H_2 were added, the grid was set manually and saved in a new pdbqt file. This file was used for the docking with the second molecule.

2.19 Statistical analysis

The number of different experiments conducted from different animals is referred as the studies group size (n). Data subjected to statistical analysis had at least n=3 and showed consistency and robust reproducibility.

Statistical comparisons were performed on GraphPad Prism 5.0 software using one-way or two-way ANOVA with Bonferroni's procedure for post hoc analysis, the values are expressed as mean ± SEM.

One-way ANOVA was conducted to examine the effect of a single independent variable on more than 2 groups. The experiments analysed by one-way ANOVA are Griess assay, ELISA, and qRT-PCR (Chapter 4). Data was normalized previously to the statistical analysis. In short, data from Griess assay and ELISA for IL-6 detection was normalised against the group treatment LPS and expressed as a fold change. Data from ELISA for the expression of PPARβ/δ in tissues was normalized against total protein. The relative quantification of genes analysed by qRT-PCR was calculated with the comparative CtΔΔ method, β-actin was used as endogenous control and data was normalized against control group.

Two-way ANOVA analysis was conducted to examine the effect of two independent variables in the experiments performed in the organ bath and myograph, where the effect of treatments (or STZ-induced diabetes condition) in addition to the effect of the applied drug concentration (x-axis) was studied (Chapter 3). Two-way ANOVA was also use for the analysis of NO production by lung tissues (variable 1) over time (variable 2) (Chapter 4).

Values of $p < 0.05$ were considered statistically significant. When the level of probability (P) is less than 0.05 (*), less than 0.01 (**) or less than 0.001 (***), the effect of the difference was regarded as significance.

Chapter 3: Non-genomic effects of PPARβ/δ on vascular tone

3.1 Introduction

As explained in Chapter 1 (1.5), hypertension is a side effect of diabetes due to the impairment of the mechanisms that regulate vascular tone (PI3K/Akt/eNOS pathway, RhoA/ROCK pathway and K^+ channels). Additionally, diabetes is characterized by the dysregulation of blood glucose levels, which is abnormally high, especially in untreated patients, and can also contribute to hypertension. It makes it interesting to study the effects of new drugs for the treatment of hypertension in normal and high glucose conditions, especially in diabetic tissues.

Another factor to take into account when studying a potential new treatment for hypertension is its effect on different types of vessels, since several studies showed different responses from different arteries under same conditions. For example, Budzyn *et al.* (2006) found differences on PE and U46619 mediated contraction between rat aorta and mesenteric arteries, and MacKenzie *et al.* (2008) found different effects of high glucose exposure between human mesenteric and subcutaneous arteries relaxations. In this thesis two main type of arteries with different functions are differentiated: systemic (aorta) and resistance arteries (mesenteric arteries).

Systemic arteries, such as aorta, are large conducting vessels with thick and elastic walls that expand and recoil during systole and diastole, thereby allowing the heart to function at an optimal rate and stroke volume.

Resistance arteries, such as mesenteric arteries, are smaller vessels with lumen diameters measuring <400 µm when relaxed, which constitute the major site of generation of vascular resistance. Peripheral resistance, and hence blood pressure, is primarily determined by small resistance arteries.

3.1.1 Factors affecting vascular reactivity

The lack of insulin or the lack of tissue response to insulin as well as the high glucose levels in plasma are the main features in diabetes, which can also affect the vascular reactivity.

3.1.1.1 Insulin

As well as its function as endocrine hormone to increase the uptake of glucose in skeletal muscle, insulin is also a vasodilator factor (Steinberg *et al.* 1994, Iida *et al.* 2001, Qu *et al.* 2014). It has been shown that mesenteric and posterior tibial arteries from mice pre-contracted with 1 µM PE relaxed after a single dose of 0.3 µM insulin. This dilation was blocked with a 30 min pre-incubation of the artery with the PI3K inhibitor LY294002 (5 µM) and NOS inhibitor L-NAME (100 µM), which suggests the activation of the PI3K/Akt/eNOS pathway, the classical downstream cascade of the insulin receptor (IR) (Qu *et al.* 2014).

Interestingly, the addition of 10 and 100 µU/mL insulin to a PE pre-contracted mesenteric arteries from rat significantly dilated the arteries, but in this case it was not inhibited by the presence of 100 µM L-NAME, indicating that the vasorelaxation effect of insulin is NO-independent (Iida *et al.* 2001). To find out the molecular mechanism, the authors examined the effects of a number of K^+ channel blockers: 30 nM charybdotoxin (blocker of large-conductance Ca^{2+}-activated K^+ channels), 1 µM apamin (blocker of small-conductance Ca^{2+}-activated K^+ channels) and 10 µM glibenclamide (ATP-sensitive K^+ channels blocker). They found that charybdotoxin was the only blocker that significantly inhibited insulin-induced

vasorelaxation, which indicates that large-conductance Ca^{2+}-activated K^{+} channels have an important role on insulin-induced relaxation of rat mesenteric arteries (Iida *et al.* 2001).

However, another study has linked insulin to the RhoA/ROCK pathway (Sandu *et al.* 2001). VSMCs isolated from rats exposed to 100 nM insulin for 10 min prevented the thrombin induced RhoA translocation to the membrane, which is indicative of RhoA inactivation. Furthermore, the exposure of VSMCs to insulin for 10 min decreased the phosphorylation of MLCP and increased its activity by 30%. The results indicate that insulin induces smooth muscle relaxation by preventing the translocation of RhoA to the membrane, which leads to the inhibition of RhoA kinase activity decreasing MLCP phosphorylation and therefore causing its activation (Sandu *et al.* 2001). This study provides an alternative molecular mechanism by which insulin can induce vasodilation, however further experiments involving the measurement of contraction/relaxation of arteries are needed in order to test the hypothesis.

3.1.1.2 Glucose

High glucose levels have been proved to contribute to the damage of the vessels (Xie *et al.* 2006, Brouwers *et al.* 2010, Liu *et al.* 2016) and to cause hypertension by reducing NO production and preventing the phosphorylation of Akt and eNOS (Quintela *et al.* 2014). Some studies were designed to investigate the effects of high glucose *per se*, without the effect of any additional disease, showing that high glucose leads to endothelial dysfunction in several ways such as reducing the Kv channel activity (Li *et al.* 2003), reducing eNOS activity through the PI3K/Akt/eNOS pathway (Liu *et al.* 2016) or activating RhoA/ROCK pathway (Xie *et al.* 2006). Most of these dysfunctions are a consequence of a long-term exposure to high glucose,

however there are a few studies arguing that short-term exposure also has a negative impact on the vasculature.

One of the first studies done in this line showed that the exposure of rat mesenteric arteries to 20 mM and 45 mM glucose for 2 h lead to a reduced acetylcholine (Ach)-induced relaxation and enhanced contraction to noradrenalin of the vessels (Taylor and Poston 1994). In the same line, another study using also rat mesenteric arteries incubated with 22.2 mM glucose for 6 h showed an inhibition on Ach-induced relaxation, but in this case the high glucose did not increase the contractility induced by PE (Ozkan and Uma 2005).

More recently, the exposure of mesenteric and femoral rat arteries to 23 mM glucose for 30 min was enough to enhance the PE-induced contraction (Vorn and Yoo 2017). However, different effects were observed on rat aortic rings incubated at 44 mM glucose for 3 h, where PE-induced contraction was reduced, although the Ach-induced relaxation was also decreased (El-Awady *et al.* 2014).

Human mesenteric and subcutaneous arteries were exposed to 20 mM glucose for periods of 2 or 6 h. The results from these experiments are a bit more surprising, since Ach-induced relaxation was enhanced in mesenteric arteries but had no change in subcutaneous arteries; however, longer incubation for 6 h improved the Ach-induced relaxation on subcutaneous arteries and had no significant effects on mesenteric arteries (MacKenzie *et al.* 2008).

Unfortunately, these studies failed to explain the molecular mechanism underlying the effects of the acute high glucose exposure. Some of them argue that is a result of a contribution of a number of pathways (Taylor and Poston 1994). Others do some further experiments providing evidence that the endothelial function is not affected (Vorn and Yoo 2017) and the ability of NO to induce relaxation is not affected (MacKenzie *et al.* 2008); also, it has been suggested that an increased

level of reactive oxygen species like O_2^- and H_2O_2 could be responsible (Ozkan and Uma 2005).

In conclusion, all these studies indicate that glucose influences vascular contractility, although there are great discrepancies on how exactly. One reason is the different experimental conditions such as different times of exposure, different concentrations of glucose or the use of different species. However, it is also important to consider the types of vessels used, because different vessels might have different molecular mechanisms.

As well as studying the potential adversary effect of high glucose on vessels, another reason of using high glucose in this thesis is because it is also a good control for STZ-diabetic tissues, because it is more representative of what non-treated diabetic tissues are exposed to.

3.1.2 Animal models of diabetes mellitus

There are two main types of diabetes mellitus: Type 1 diabetes mellitus (T1DM) is characterized by a specific destruction of the insulin-producing pancreatic β cells, commonly associated with immune-mediate damage. T1DM is most commonly diagnosed in children and young adults (2005).

Type 2 diabetes mellitus (T2DM) is characterized by insulin resistance and impaired insulin secretion and defined by a raised fasting or post-challenge blood glucose. T2DM is most commonly diagnosed in middle-aged adults and can be improved by weight reduction and exercise (2005).

A number of different animal models have been developed for the study of type 1 and 2 diabetes, some of the most commonly used are listed below.

3.1.2.1 Animal models for T1DM

Diabetes inducers (diabetogenics) are experimental toxins including alloxan and streptozotocin (Lenzen 2008). Alloxan was firstly discovered by Wohler and Liebig in 1838, and afterward it was applied as a diabetogenic in 1943 (Lenzen 2008). Twenty years later, Rackeiten and colleagues found the naturally occurring *Streptomyces achromogenes* – derived streptozotocin (STZ) antibiotic, 2-deoxy-2-(3methyl-3-nitrosureido)-D-glucopyranose that enters in the pancreatic β cells and causes alkylation and thus fragmentation of DNA. STZ is a source of free radicals that can contribute to DNA damage and subsequent cell death. STZ can be administered as a single dose to animals, which leads to a rapid destruction of β cells and hyperglycaemia, or as multiple low doses over 5 days to induce insulitis and has been widely applied experimentally (Lenzen 2008). Numerous differences shift the favour toward STZ rather than alloxan, since alloxan is less stable at physiological conditions; pH 7.4 and 37 $^{\circ}$C where it decomposes into alloxanic acid with a 90 seconds short half-life, while STZ is more stable with approximately 1 hour short half-life (Szkudelski 2001). Moreover, alloxan is highly hydrophilic and therefore less stable in aqueous solutions where it decomposes into another lipophilic derivative, butyl-alloxan (Lenzen 2008). In contrast, STZ is highly stable in aqueous media and induces diabetes according to its selective N-methyl-N-nitrosurea (MNU) moiety which renders STZ to act on glucose transporter 2 (GLUT-2) expressing tissues only such as pancreatic β cells (Elsner *et al.* 2000).

Numerous diabetic transgenic models are utilised in diabetes research to help decipher pathophysiological pathways. Transgenic or highly inbred animal strains have been developed that spontaneously or conditionally develop diabetes (eg ob/ob, Zucker).

The non-obese diabetic (NOD) mouse spontaneously develop autoimmune diseases similar to human T1DM. These animals have been inbred in laboratories for many generations and, as a result, many genes and phenotypes will have been enriched, but not all will be relevant to the pathophysiology of diabetes. NOD mice are potentially suitable for testing therapies for the modulation of the autoimmune response (Makino *et al.* 1980, Atkinson and Leiter 1999) .

Biobreeding (BB) rats were derived from outbred Wistar rats. The diabetic phenotype is quite severe, and the rats require insulin therapy for survival. The model has been valuable in elucidating more about the genetics of the T1DM and it is the preferable model for islet transplantation tolerance induction (Nakhooda *et al.* 1977, Mordes *et al.* 2004).

AKITA mouse is derived from a spontaneous mutation in the *insulin 2* gene preventing correct processing of pro-insulin and resulting in a severe insulin-dependent diabetes. It has been used as a model of T1DM to study islet transplantation (Mathews *et al.* 2002).

3.1.2.2   *Animal models for T2DM*

The KK mouse produced by Prof Kyoji Kondo and Prof. Masahiko Nishimura is a mildly obese strain that develop severe hyperinsulinemia and hyperglycemia, and demonstrate insulin resistance in both muscle and adipose tissue as well as hypertrophic pancreatic islets (Nakamura and Yamada 1967, Reddi and Camerini-Davalos 1988).

The Nagoya-Shibata-Yasuda (NSY) mouse spontaneously develop diabetes in an age-dependent manner. They develop an impaired insulin secretion and mild insulin resistance. Obesity is not a major feature of these animals and there is a marked gender difference with almost all males developing hyperglycaemia, but less than a third of females being affected (Ueda *et al.* 1995).

Psammomys obesus (the Israeli sand rat) has an essential vegetarian diet. However, when fed laboratory chow, the animals become obese, insulin resistant and hyperglycaemic. This model is particularly useful when studying the effects of diet and exercise of the development of type 2 diabetes (Ziv *et al.* 1999).

The Otsuka Long-Evans Tokoshima fatty (OLETF) rat originates from an outbred colony of Long-Evans rats selectively bred for glucose intolerance. The rats are mildly obese and males are more likely to develop diabetes in adult life than females (Kawano *et al.* 1992).

The Goto Kakizaki (GK) rat was developed by the selective breeding of Wistar rats with the highest blood glucose over many generations. The rats develop relatively stable hyperglycaemia in adult life. Both insulin resistance and impaired insulin secretion are present. The GK rat develops deseases that can be compared with the complications of diabetes seen in humans (Goto *et al.* 1976, Liepinsh *et al.* 2009).

The use of these genetic T1DM and T2DM models can be restricted by their cost and the fact that diabetes is highly genetically determined unlike the heterogeneity seen in humans (Rees and Alcolado 2005). Furthermore, genetic models can show a variety of alterations, for instance, suppressed GLUT-1 mice are associated with reduced protein kinase C (PKC) activity and fibronectin, which can trigger further complications in organ function since fibronectin is involved in regulating cellular differentiation and organogenesis (Mosesson and Amrani 1980).

Among all these models, the Streptozotocin-induced experimental diabetes rat model is validated as a predictive T1DM related complications model, and several reports on STZ-induced vascular dysfunctions have been published (Chang and Stevens 1992, Taylor *et al.* 1994). It also has the advantage that is a cheaper and more robust model compared to others - in our laboratory over 90% of rats treated

with a single dose of STZ become diabetic. Therefore, this model was selected in this thesis for the assessment of diabetes-derived cardiovascular complications and its potential treatment with PPARβ/δ agonists.

3.1.3 Aims and objectives

This chapter aims to identify the molecular mechanisms underneath the vascular reactivity of Naive and STZ-diabetic aorta vs mesenteric arteries as a model of systemic and resistance arteries respectively, and how they can be regulated by PPARβ/δ in a non-genomic manner, which may lead to new therapeutic approaches for the treatment of hypertension. Objectives:

1- Investigate the non-genomic effects of PPARβ/δ in normal and STZ-diabetic vessels focusing on RhoA/ROCK and PI3K/Akt/eNOS pathways using the PPARβ/δ ligands GW0742 and GSK3787, the ROCK inhibitors Fasudil and Y27632 and the PI3K inhibitor LY294002.

2- Investigate the effects of high glucose (20 mM glucose) on PI3K/Akt/eNOS pathway and whether they can be reverted by PPARβ/δ and/or insulin in normal and STZ-diabetic vessels.

3.2 Methods

3.2.1 Organ bath

Thoracic aorta rings 2-3 mm long from Naïve and STZ-diabetic rats were used in an organ bath of 15 mL capacity. The design of the experiments performed are detailed below and the cumulative concentration response and treatments of the organ bath experiments are detailed in Table 3.1 below. For a full description of the method refer to Chapter 2 Section 2.5.

3.2.1.1 Thoracic aorta rings

Experiment 1: Aorta rings were incubated with GW0742 (1 nM, 10 nM or 100 nM) or vehicle (0.01% dimethyl sulfoxide (DMSO)) for 30 min followed by a response to increasing concentrations of PE (10 nM to 30 μM) or U46619 (1 nM to 300 nM).

Experiment 4: Aorta rings were incubated with the RhoA/ROCK inhibitors 10 μM Fasudil or 10 μM Y27632 as well as vehicle (0.01% DMSO) for 30 min followed by a response to increasing concentrations of PE (10 nM to 30 μM) or U46619 (1 nM to 300 nM).

Experiment 5: Aorta rings were incubated with 10 μM Fasudil or vehicle (0.01% DMSO) for 30 min, pre-contracted with 100 nM U46619 and exposed to increasing concentrations of GW0742 (1 μM to 30 μM).

Experiment 6: Aorta rings were pre-contracted with high potassium physiological saline solution (KPSS) followed by increasing concentrations of GW0742 (1 μM to 30 μM).

Table 3.1 Treatments and cumulative concentrations response dose schedules used in a 15 mL capacity organ bath.

Final concentration	Stock	Amount (µL)
Treatments		
Vehicle 0.01% DMSO	10% DMSO	15
1 nM GW0742	1 µM GW0742	15
10 nM GW0742	10 µM GW0742	15
100 nM GW0742	100 µM GW0742	15
10 µM Fasudil	10 mM Fasudil	15
10 µM Y27632	10 mM Y27632	15
PE response-dose schedule		
10 nM PE	10 µM PE	15
30 nM PE	10 µM PE	30
100 nM PE	100 µM PE	15
300 nM PE	100 µM PE	30
1 µM PE	1 mM PE	15
3 µM PE	1 mM PE	30
10 µM PE	10 mM PE	15
30 µM PE	10 mM PE	30
U46619 response-dose schedule		
1 nM U46619	1 µM U46619	15
3 nM U46619	1 µM U46619	30
10 nM U46619	10 µM U46619	15
30 nM U46619	10 µM U46619	30
100 nM U46619	100 µM U46619	15
300 nM U46619	100 µM U46619	30
GW0742 response-dose schedule		
1 µM GW0742	1 mM GW0742	15
3 µM GW0742	1 mM GW0742	30
10 µM GW0742	10 mM GW0742	15
30 µM GW0742	10 mM GW0742	30

3.2.2 Myography

Abdominal aorta rings and mesenteric artery rings 1.5 mm long from Naïve and STZ-diabetic rats were used in an myograph with a final volume of 5 mL per chamber. The design of the experiments performed are detailed below and the cumulative concentration response and treatments of the myograph experiments are detailed in Table 3.2 below. For a full description of the method refer to Chapter 2 Section 2.6.

3.2.2.1 *Abdominal aorta rings*

Experiment 2: Abdominal aortic rings were incubated with 100 nM GW0742, 1 µM GSK3787, 100 nM GW0742 + 1 µM GSK3787 or vehicle control (0.01% DMSO) for 30 min followed by a response to increasing concentrations of PE (10 nM to 30 µM).

Experiment 3: Abdominal aortic rings were incubated with 1 U/mL insulin, 100 nM GW0742, 1 U/mL insulin + 100 nM GW0742, 1 U/mL insulin + 1 µM LY294002, 100 nM GW0742 + 1 µM LY294002, 1 U/mL insulin + 100 nM GW0742 + 1 µM LY294002 or vehicle control (0.01% DMSO), and then were subjected to increasing concentrations of PE (10 nM to 30 µM). After reaching the maximum contraction, the rings were washed three times until the tension was stable at baseline. The tissues were then expose to 20 mM glucose PSS for 10 min and incubated with the same treatments as before for extra 20 min; at that point increasing concentrations of PE (10 nM to 30 µM) were added.

3.2.2.2 *Mesenteric arteries*

Experiment 1: Mesenteric rings were incubated with GW0742 (1 nM, 10 nM or 100 nM) or vehicle control (0.01% DMSO) for 30 min followed by a response to increasing concentrations of PE (10 nM to 30 µM) or U46619 (1 nM to 300 nM).

Experiment 2: Mesenteric rings were incubated with 100 nM GW0742, 1 μM GSK3787, 100 nM GW0742 + 1 μM GSK3787 or vehicle control (0.01% DMSO) for 30 min followed by a response to increasing concentrations of PE (10 nM to 30 μM).

Experiment 3: Mesenteric rings were incubated with 1 U/mL insulin, 100 nM GW0742, 1 μM LY294002, 1 U/mL insulin + 100 nM GW0742, 1 U/mL insulin + 1 μM LY294002, 100 nM GW0742 + 1 μM LY294002, 1 U/mL insulin + 100 nM GW0742 + 1 μM LY294002 or vehicle control (0.01% DMSO), and then were subjected to increasing concentrations of PE (10 nM to 30 μM). After reaching the maximum contraction, the rings were washed three times until the tension was stable at baseline. The tissues were then expose to 20 mM glucose PSS for 10 min and incubated with the same treatments as before for extra 20 min, at that point increasing concentrations of PE (10 nM to 30 μM) were added.

Experiment 4: Mesenteric rings were incubated with the RhoA/ROCK inhibitors 10 μM Fasudil or 10 μM Y27632 as well as vehicle (0.01% DMSO) for 30 min followed by a response to increasing concentrations of PE (10 nM to 30 μM) or U46619 (1 nM to 30 nM).

Experiment 5: Mesentery rings were incubated with 10 μM Fasudil, 1 μM GSK3787 or vehicle (0.01% DMSO) for 30 min, pre-contracted with 10^{-5} M PE and exposed to increasing concentrations of GW0742 (1 μM to 30 μM).

Experiment 6: Mesenteric rings were incubated with 1 μM GSK3787 or vehicle (0.01% DMSO) for 30 min, pre-contracted with KPSS, and exposed to increasing concentrations of GW0742 (1 μM to 30 μM).

Table 3.2 Treatments and cumulative concentrations response dose schedules used in the myograph with a final volume of 5 mL per chamber.

Final concentration	Stock	Amount (μL)
Treatments		
Vehicle 0.01% DMSO	10% DMSO	5
1 nM GW0742	1 μM GW0742	5
10 nM GW0742	10 μM GW0742	5
100 nM GW0742	100 μM GW0742	5
1 μM GSK3787	1 mM GSK3787	5
10 μM Fasudil	10 mM Fasudil	5
10 μM Y27632	10 mM Y27632	5
1 U/mL Insulin	1000 U/mL Insulin	5
1 μM LY294002	1 mM LY294002	5
PE response-dose schedule		
10 nM PE	10 μM PE	5
30 nM PE	10 μM PE	10
100 nM PE	100 μM PE	5
300 nM PE	100 μM PE	10
1 μM PE	1 mM PE	5
3 μM PE	1 mM PE	10
10 μM PE	10 mM PE	5
30 μM PE	10 mM PE	10
U46619 response-dose schedule		
1 nM U46619	1 μM U46619	5
3 nM U46619	1 μM U46619	10
10 nM U46619	10 μM U46619	5
30 nM U46619	10 μM U46619	10
100 nM U46619	100 μM U46619	5
300 nM U46619	100 μM U46619	10
GW0742 response-dose schedule		
1 μM GW0742	1 mM GW0742	5
3 μM GW0742	1 mM GW0742	10
10 μM GW0742	10 mM GW0742	5
30 μM GW0742	10 mM GW0742	10

Table 3.3 Overview of the experiments of Chapter 3.

	Aorta			Mesenteric arteries		
	Method	**Treatments**	**Figure**	**Method**	**Treatments**	**Figure**
Exp 1	Organ bath	0.01% DMSO 1 nM GW0742 10 nM GW0742 100 nM GW0742	Figure 3.2 Figure 3.3	Myograph	0.01% DMSO 1 nM GW0742 10 nM GW0742 100 nM GW0742	Figure 3.5 Figure 3.6
Exp 2	Myograph	0.01% DMSO 100 nM GW0742 1 µM GSK3787 100 nM GW0742 + 1 µM GSK3787	Figure 3.4	Myograph	0.01% DMSO 100 nM GW0742 1 µM GSK3787 100 nM GW0742 + 1 µM GSK3787	Figure 3.7
Exp 3	Myograph	0.01% DMSO 1 U/mL insulin 100 nM GW0742 1 U/mL insulin + 100 nM GW0742 1 U/mL insulin + 1 µM LY294002 100 nM GW0742 + 1 µM LY294002 1 U/mL insulin + 100 nM GW0742 + 1 µM LY294002	Figure 3.10 Figure 3.11	Myograph	0.01% DMSO 1 U/mL insulin 100 nM GW0742 1 U/mL insulin + 100 nM GW0742 1 U/mL insulin + 1 µM LY294002 100 nM GW0742 + 1 µM LY294002 1 U/mL insulin + 100 nM GW0742 + 1 µM LY294002	Figure 3.12 Figure 3.13
Exp 4	Organ bath	0.01% DMSO 10 µM Fasudil 10 µM Y27632	Figure 3.14	Myograph	0.01% DMSO 10 µM Fasudil 10 µM Y27632	Figure 3.16
Exp 5	Organ bath	0.01% DMSO 10 µM Fasudil	Figure 3.15	Myograph	0.01% DMSO 10 µM Fasudil 1 µM GSK3787	Figure 3.17
Exp 6	Organ bath	0.01% DMSO	Figure 3.18	Myograph	0.01% DMSO	Figure 3.19

GW0742 is a PPARβ/δ agonist ; GSK3787 is a PPARβ/δ antagonist; LY294002 is a PI3K inhibitor; Fasudil is a ROCK inhibitor; Y27632 is a ROCK inhibitor

3.3 Results

3.3.1 Animals became diabetic after a single dose of STZ (55 mg/kg i.p)

Plasma glucose levels and body weight of all rats were monitored from the day they were dosed with 55 mg/kg STZ day 0, day 7 and the day they were sacrificed (day 10-27). As shown in Table 3.4, all rats became hyperglycaemic (blood glucose>16 mmol/L) after seven days following a single dose of STZ with an increase in weight of 23.6 g over the time. There was a significant increase in blood glucose on day 7 and terminal day compared with day 0 (***$p<0.001$) and no significant change in body weight at day 7 ($p>0.05$) but significantly different at terminal day (***$p<0.001$). 55 mg/kg STZ induced diabetes in rats without compromising the wellbeing of the animal. Tissues from STZ-diabetic rats were harvested on terminal day for vasoactive organ bath and myograph studies.

Table 3.4 Plasma glucose levels and body weight of rats dosed with 55 mg/kg STZ on day 0, 7 and terminal day. Significant difference on plasma glucose level and body weight at Day 7 and Terminal day compared with Day 0 was analysed by a repeated measures one-way ANOVA followed by Bonferroni post-hoc test. The data are presented as mean ± standard error of the mean. ***$p < 0.001$ vs Day 0.

Animal	Plasma glucose level (mmol/L)			Body weight (g)		
	Day 0	Day 7	Terminal day (D10-27)	Day 0	Day 7	Terminal day (D10-27)
S1	6.2	27.1	28.0	380	382	378
S2	6.8	31.7	26.1	394	383	382
S3	8.4	29.5	28.2	398	399	397
S4	7.5	33.3	24.4	387	381	390
S5	6.5	33.3	28.7	418	407	406
S6	6.1	33.3	28.1	384	391	396
S7	6.7	33.3	25.7	392	380	414
S8	6.0	33.3	30.8	392	372	409
S9	6.3	26.0	23.8	398	395	440
S10	7.2	23.6	26.7	399	376	410
S11	6.0	19.5	20.7	407	423	446
S12	6.8	21.8	23.6	402	389	410
S13	7.2	25.3	29.2	383	386	399
S14	6.7	26.6	33.3	387	380	400
S15	6.7	18.8	28.6	389	390	408
S16	6.4	31.6	26.4	382	397	423
S17	6.7	33.3	30.1	393	407	445
S18	5.3	24.5	30.8	389	411	455
S19	7.3	22.8	33.3	394	407	466
S20	5.4	25.5	33.3	389	410	455
Mean	6.61	27.71***	27.99***	392.85	393.30	416.45***
Stdev	0.72	4.97	3.43	9.13	13.89	25.93
Sem	0.24	1.66	1.14	3.04	4.63	8.64

3.3.2 Aorta and mesenteric arteries are dysfunctional in STZ-diabetic rat and improved by GW0742 via PPARβ/δ

PE-induced contraction of aorta and mesenteric arteries is significantly increased in STZ-diabetic tissues compared to Naïve (Figure 3.1 A, C); however, U46619 mediated contraction shows no significant difference on aorta (Figure 3.1 B) or it is significantly decreased on STZ-diabetic mesenteric arteries (Figure 3.1 D). U46619 was only tested until a concentration of 300 nM since any further addition induces an irreversible contraction.
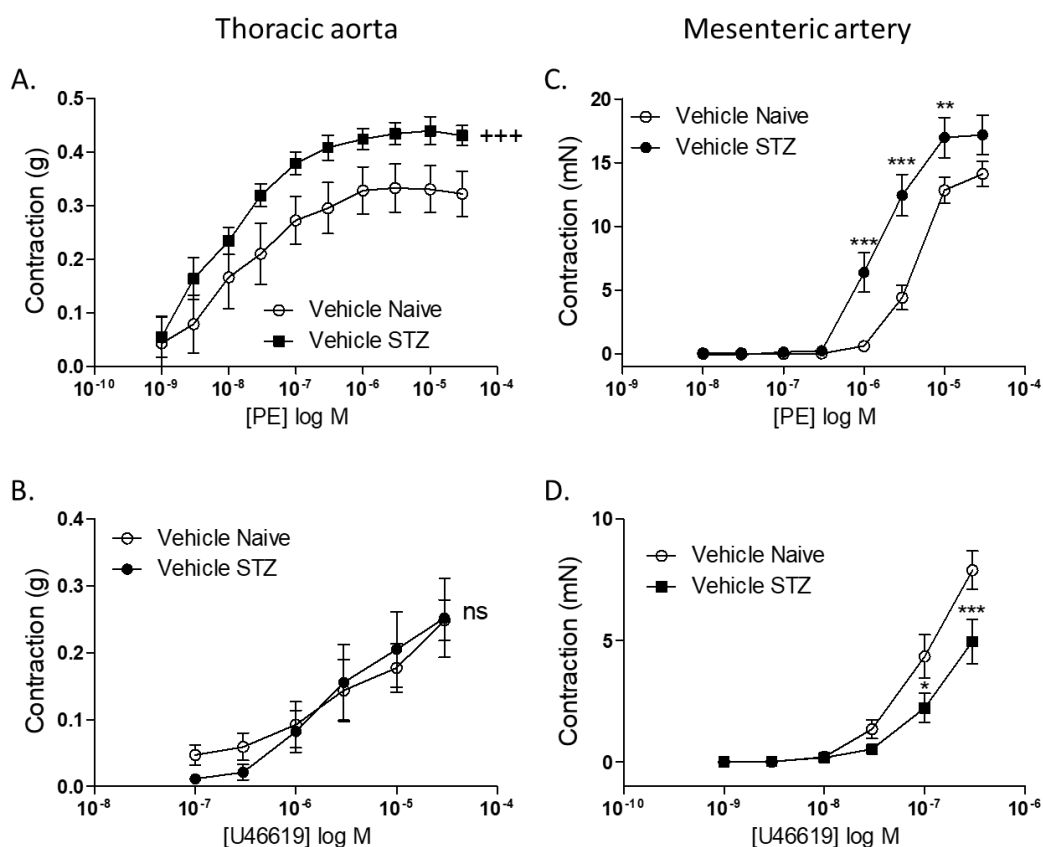
Figure 3.1 Change in tension in thoracic aorta and mesenteric arteries induced by A-C) PE and B-D) U46619 in Naïve and STZ-diabetic rat vessels. Data are represented as mean ± SEM (n=4-13). Significant difference compared to Vehicle controls was analysed by two-away ANOVA denoted by +++=p<0.001; and followed by Bonferroni's post hoc test denoted by ***=p<0.001, **=p<0.01, ns= non-significance.

3.3.2.1 Aorta

Aorta rings from STZ-diabetic and Naïve rats were incubated with increasing concentrations of GW0742 to observe the effect of this drug on PE and U46619 mediated contraction. In both cases, low concentration of GW0742 (1 nM and 10 nM) had no effect on aorta contraction (Figure 3.2 A, B, D, E; Figure 3.3 A, B, D, E). However, 100 nM GW0742 significantly decreases both PE and U46619 mediated contraction in Naïve and STZ-diabetic tissues (Figure 3.2 C, E; Figure 3.3 C, E).

Table 3.5 E_{max} and EC_{50} of thoracic aorta and mesenteric artery from Naïve and STZ-diabetic rats contracted with PE and U46619. E_{max} is represented as mean ± SEM (n=4-13). Significant difference compared to Vehicle Naïve controls was analysed by two-way ANOVA and followed by Bonferroni's post hoc test denoted by ** = $p<0.01$, ***= $p<0.001$.

		Thoracic aorta		Mesenteric arteries	
	Treatment	E_{max}	EC_{50}	E_{max}	EC_{50}
PE	**Vehicle Naive**	0.33 ± 0.04 g	16.1 nM	14.11 ± 1.0 mN	6.7 µM
	Vehicle STZ	0.44 ± 0.02 g***	10.3 nM	17.18 ± 1.6 mN**	1.8 µM
U46619	**Vehicle Naive**	0.25 ± 0.05 g	4.8 µM	7.90 ± 0.8 mN	214.3 nM
	Vehicle STZ	0.25 ± 0.05 g	2.2 µM	4.96 ± 0.9 mN***	517.4 nM

Thoracic aorta

Figure 3.2 Change in tension induced by PE in Naïve and STZ-diabetic rat thoracic aorta incubated with 1 nM, 10 nM or 100 nM GW0742. Naïve and STZ-diabetic rat aorta rings were treated with 0.01% DMSO (Vehicle), 1 nM, 10nM or 100 nM GW0742. After 30 min incubation a PE dose-response curve was performed. Data are represented as mean ±SEM (n=4-6). Significant difference compared to vehicle controls was analysed by two-way ANOVA denoted by +++=$p<0.001$; and followed Bonferroni's post hoc test denoted by **=$p<0.01$, *=$p<0.05$, ns= non-significance.

Thoracic aorta
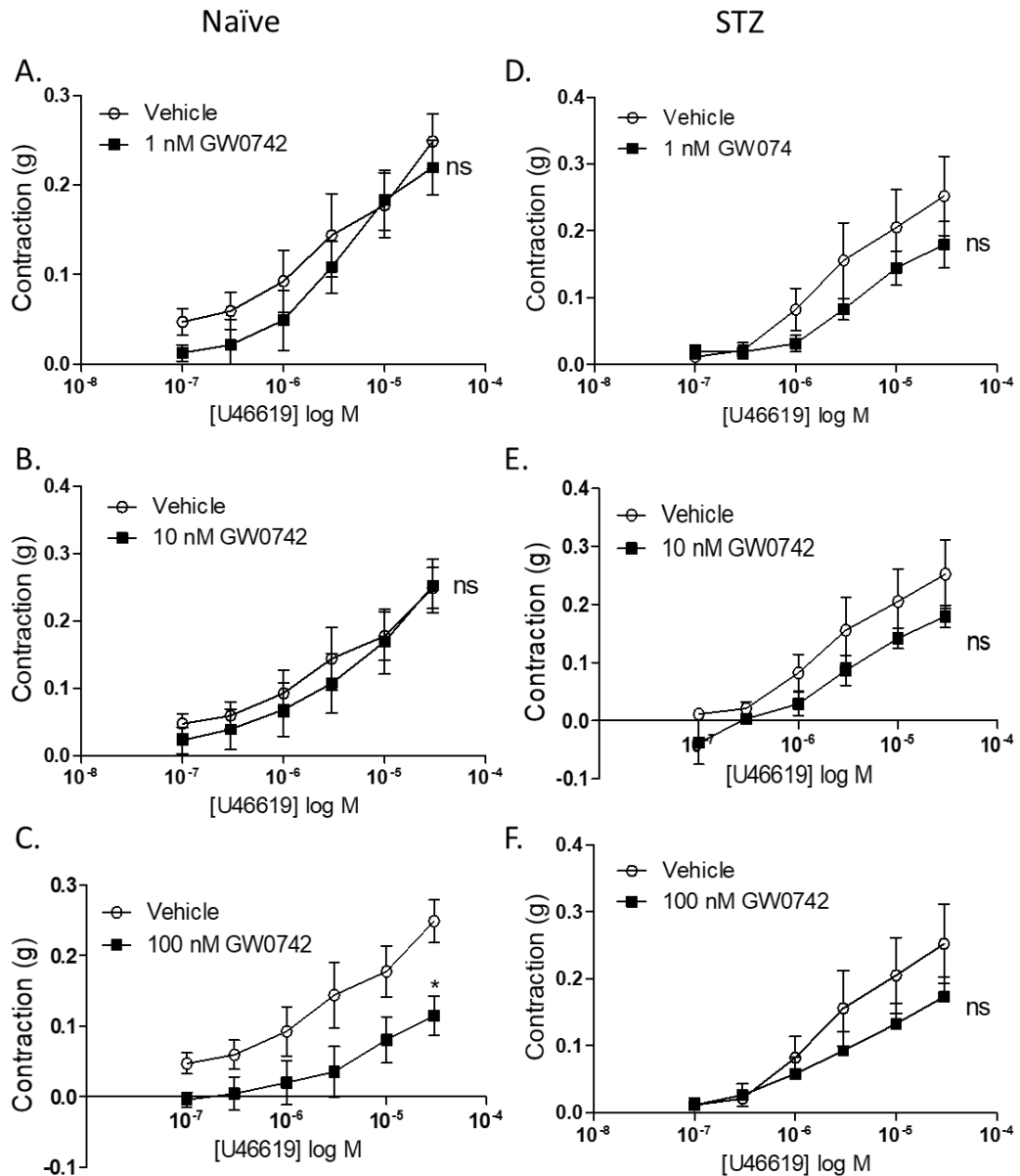
Figure 3.3 Change in tension induced by U46619 in Naïve and STZ-diabetic rat thoracic aorta incubated with 1 nM, 10 nM or 100 nM GW0742. Naïve and STZ-diabetic rat aorta rings were treated with 0.01% DMSO (Vehicle), 1 nM, 10 nM or 100 nM GW0742. After 30 min incubation a U46619 dose-response curve was performed. Data are represented as mean ±SEM (n=4-6). Significant difference compared to vehicle controls was analysed by two-way ANOVA followed by Bonferroni's post hoc test denoted by *=p<0.05, ns=non-significance.

Table 3.6 E_{max} and EC_{50} of thoracic aorta from Naïve and STZ-diabetic rats incubated with 1 nM, 10 nM or 100 nM GW0742 and contracted with PE and U46619. E_{max} is represented as mean ± SEM (n=4-6). Significant difference compared to Vehicle controls was analysed by two-way ANOVA and followed by Bonferroni's post hoc test denoted by * = $p<0.05$, *** = $p<0.001$.

		Thoracic aorta			
		Naïve		STZ	
	Treatment	E_{max} (g)	EC_{50}	E_{max} (g)	EC_{50}
PE	Vehicle	0.33 ± 0.04	16.1 nM	0.44 ± 0.02	10.3 nM
	1 nM GW0742	0.35 ± 0.05	29.4 nM	0.47 ± 0.04	9.5 nM
	10 nM GW0742	0.28 ± 0.04	18.1 nM	0.44 ± 0.06	6.3 nM
	100 nM GW0742	0.15 ± 0.04*	36.9 nM	0.31 ± 0.08***	28.3 nM
U46619	Vehicle	0.25 ± 0.03	10.3 μM	0.25 ± 0.06	2.2 μM
	1 nM GW0742	0.22 ± 0.03	9.5 μM	0.17 ± 0.03	5.6 μM
	10 nM GW0742	0.25 ± 0.04	6.3 μM	0.18 ± 0.02	2.6 μM
	100 nM GW0742	0.11 ± 0.03*	2.8 μM	0.17 ± 0.03	3.4 μM

Although 100 nM GW0742 is a concentration selective for PPARβ/δ (Sznaidman *et al.* 2003), a further experiment was performed to confirm that the effect of GW0742 is PPARβ/δ-dependent. Aorta rings were incubated with either 0.01% DMSO (Vehicle), 100 nM GW0742, the PPARβ/δ antagonist GSK3787 (1 μM), or GW0742 together with GSK3787. The Figure 3.4 F shows how GSK3787 blocks the effect of GW0742, verifying that the action of GW0742 is mediated by PPARβ/δ.
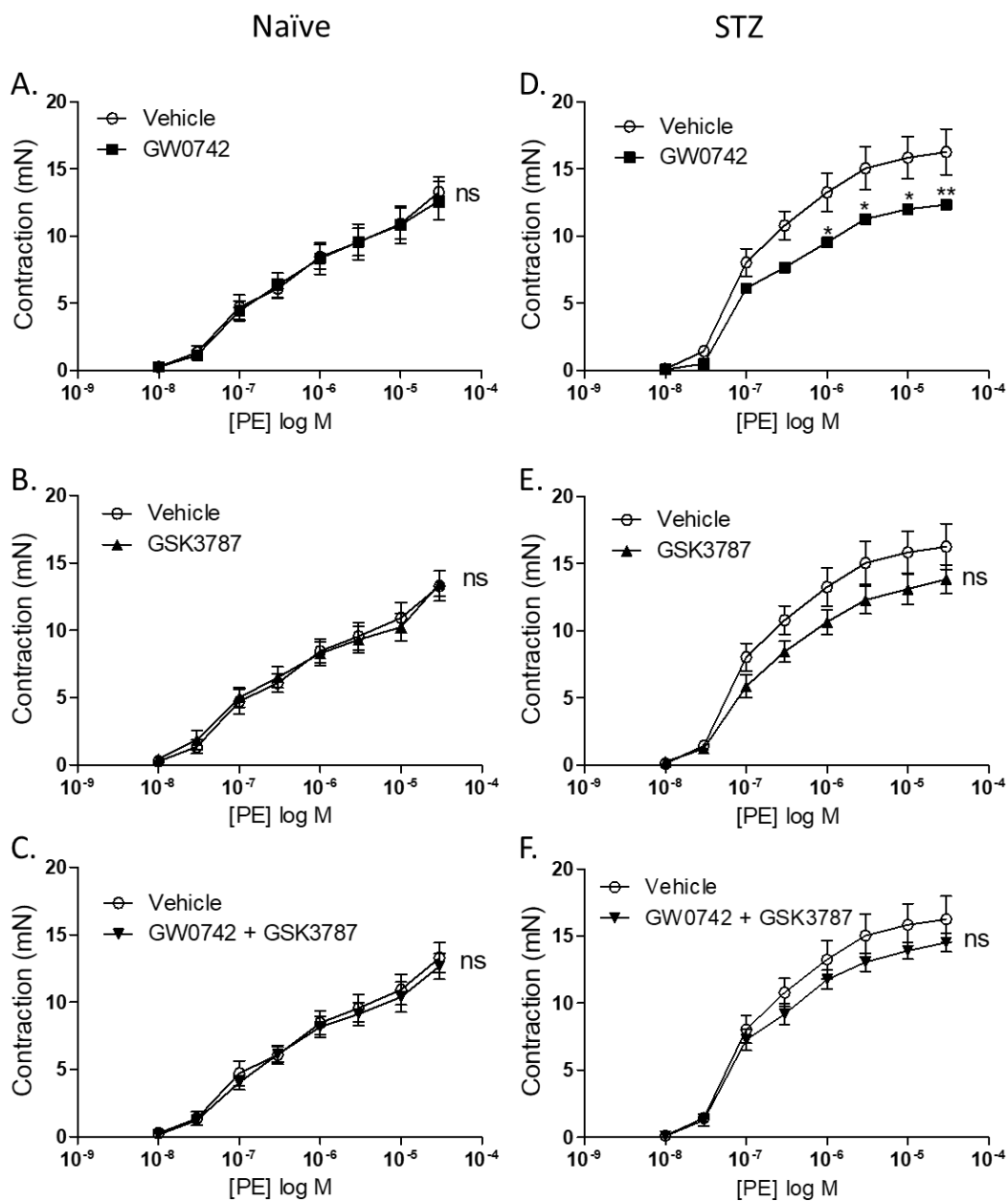
Abdominal aorta

Figure 3.4 The effect of GW0742 on PE-induced abdominal aorta contraction is reversed by the PPARβ/δ antagonist GSK3787. Four aorta rings from Naïve and STZ-diabetic rats were incubated in four different treatments: 0.01% DMSO (Vehicle), 100 nM GW0742, 1 μM GSK3787 and 100 nM GW0742 + 1 μM GSK3787. After 30 min incubation a PE dose-response curve was performed. Data are represented as mean ±SEM (n=6-7). Significant difference compared to vehicle controls was analysed by two-way ANOVA followed by Bonferroni's post hoc test denoted by **=$p<0.01$, *=$p<0.05$, ns=non-significance.

Table 3.7 E_{max} and EC_{50} of abdominal aorta from Naïve and STZ-diabetic rats incubated with 100 nM GW0742, 1 μM GSK3787 or 100 nM GW0742 + 1 μM GSK3787 and contracted with PE. E_{max} is represented as mean ± SEM (n=6-7). Significant difference compared to Vehicle controls was analysed by two-way ANOVA and followed by Bonferroni's post hoc test denoted by ** = $p<0.01$.

	Abdominal aorta			
	Naïve		STZ	
Treatment	**E_{max} (mN)**	**EC_{50}**	**E_{max} (mN)**	**EC_{50}**
Vehicle	13.3 ± 1.3	290.7 nM	16.26 ± 1.7	102.8 nM
100 nM GW0742	12.62 ± 1.4	240.0 nM	12.34 ± 0.4**	114.6 nM
GSK3787	13.45 ± 0.9	238.1 nM	13.85 ± 1.1	143.6 nM
100 nM GW0742 + GSK3787	12.65 ± 1.0	264.2 nM	14.52 ± 0.7	103.8 nM

3.3.2.2 *Mesenteric arteries*

The same protocols were conducted in parallel on mesenteric arteries with similar results, 100 nM GW0742 significantly reduce PE- and U46619-induced contraction both in Naïve and STZ-diabetic vessels (Figure 3.5 C, F and Figure 3.6 C, F). Moreover, 10 nM GW0742 also significantly reduced PE-induced contraction from 10 μM PE in Naïve tissue (Figure 3.5 B), but 100 nM was maintained for the following experiments to keep the same concentration through-out the study.

To verify that this reduction on vascular contractility in the mesentery is also mediated by PPARβ/δ, mesenteric artery rings were co-incubated with GW0742 and GSK3787. Figure 3.7 C, F shows that GSK3787 prevented the inhibition of contraction caused by GW0742 providing the evidence that GW0742 acts through PPARβ/δ in mesenteric arteries.

Mesenteric arteries
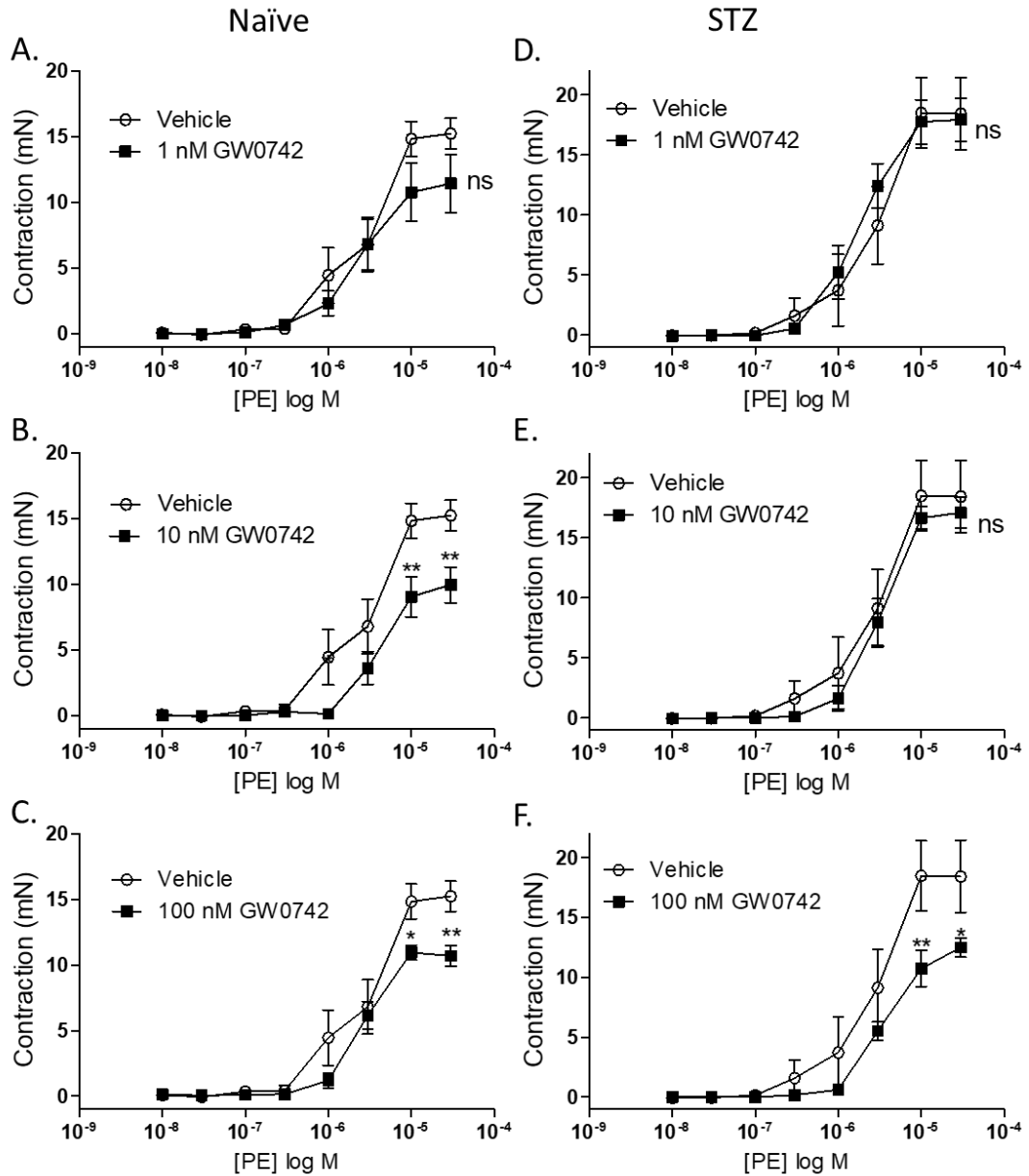
Figure 3.5 Change in tension induced by PE in Naïve and STZ-diabetic mesenteric arteries incubated with 1 nM, 10 nM or 100 nM GW0742. Naïve and STZ-diabetic rat mesenteric artery rings were treated with 0.01% DMSO (Vehicle), 1 nM, 10 nM or 100 nM GW0742. After 30 min incubation a PE dose-response curve was performed. Data are represented as mean ±SEM (n=5-6). Significant difference compared to vehicle controls was analysed by two-way ANOVA denoted and followed by Bonferroni's post hoc test denoted by **=$p<0.01$, *=$p<0.05$, ns= non-significance.
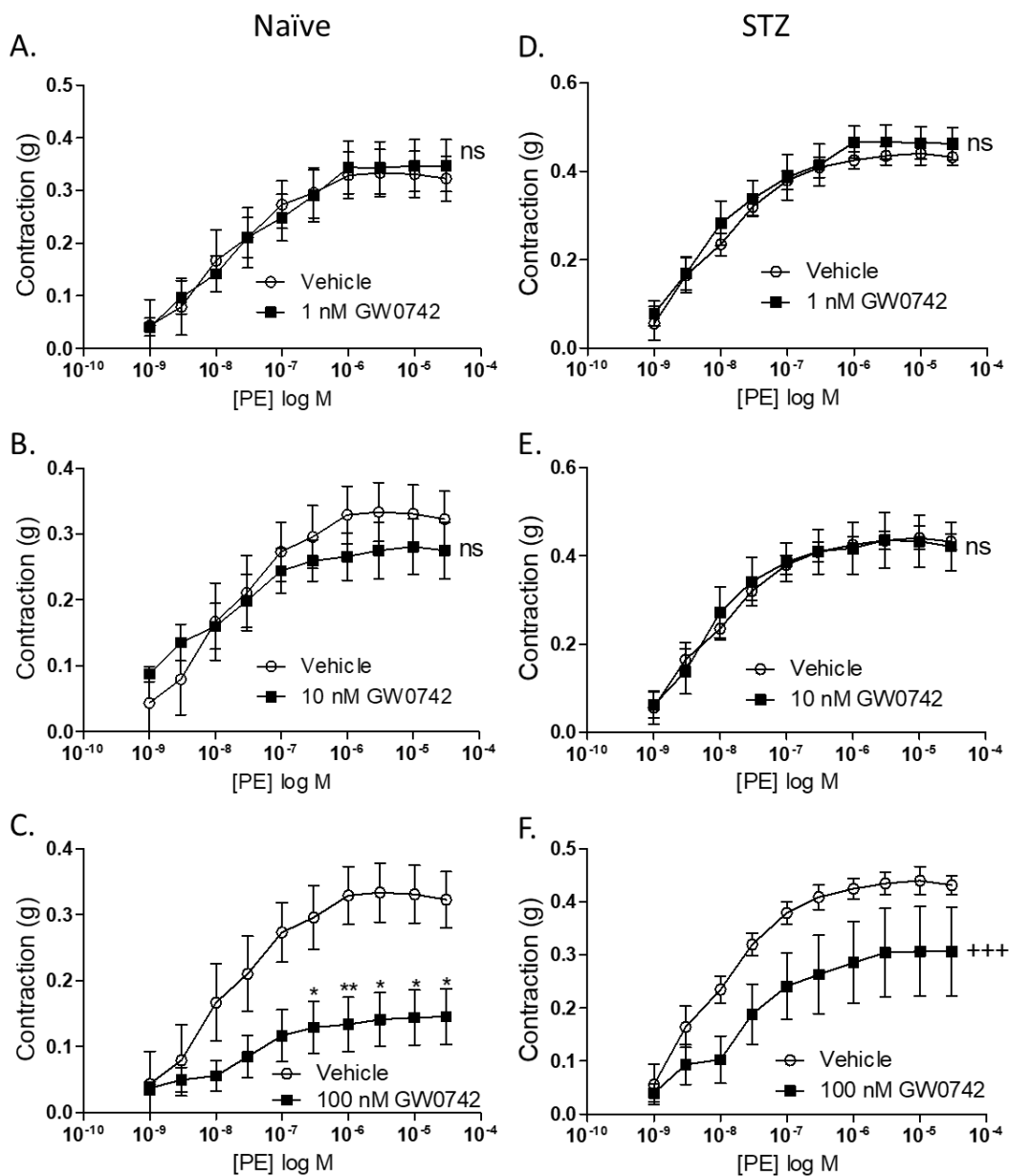
Mesenteric arteries
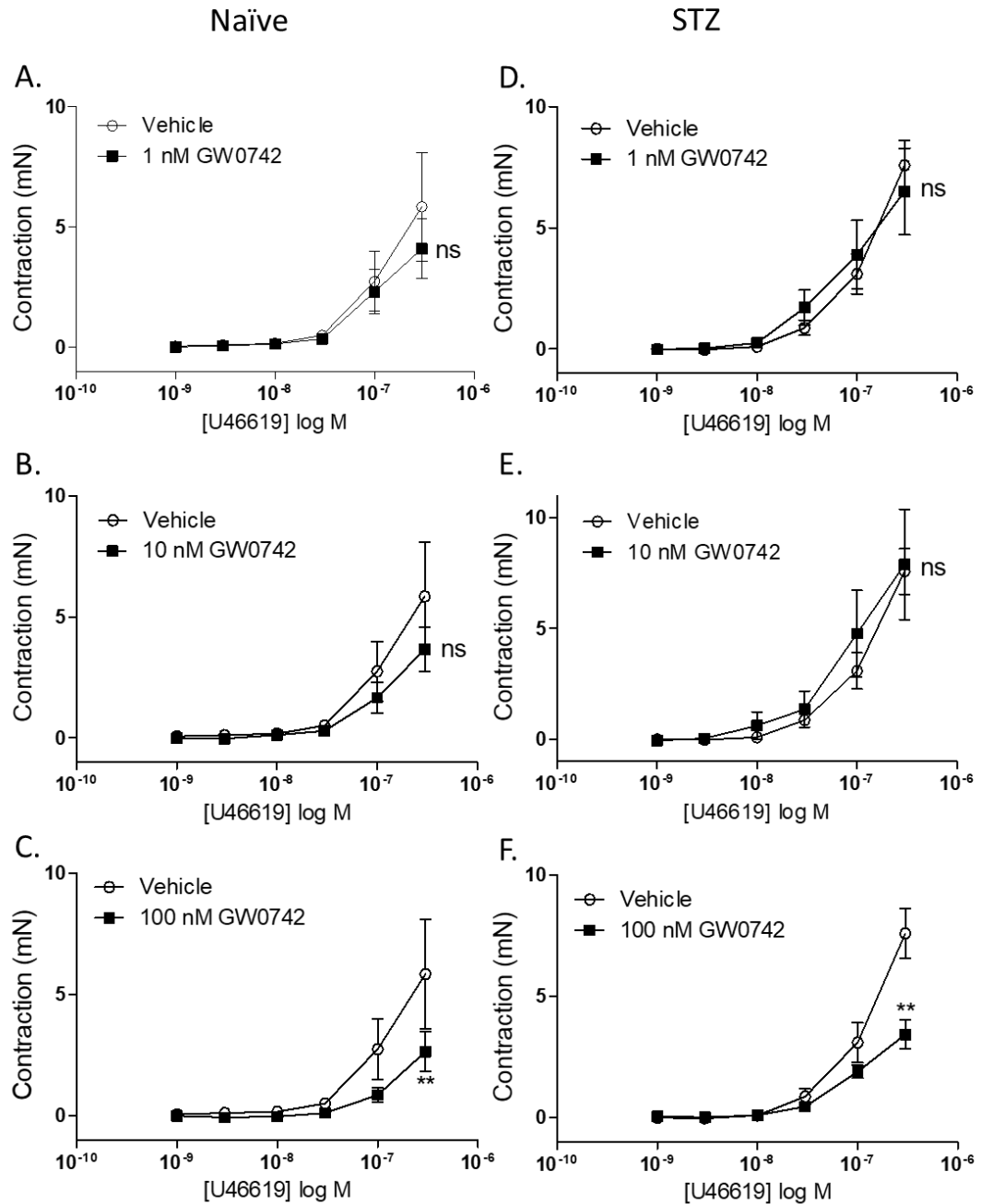
Figure 3.6 Change in tension induced by U46619 in Naïve and STZ-diabetic mesenteric arteries incubated with 1 nM, 10 nM or 100 nM GW0742. Naïve and STZ-diabetic rat mesenteric artery rings were treated with 0.01% DMSO (Vehicle), 1 nM, 10 nM or 100 nM GW0742. After 30 min incubation a U46619 dose-response curve was performed. Data are represented as mean ±SEM (4-6). Significant difference compared to vehicle controls was analysed by two-way ANOVA denoted and followed by Bonferroni's post hoc test denoted by **=p<0.01, *=p<0.05, ns= non-significance.

Table 3.8 E_{max} and EC_{50} of mesenteric arteries from Naïve and STZ-diabetic rats incubated with 1 nM, 10 nM or 100 nM GW0742 and contracted with PE and U46619. E_{max} is represented as mean ± SEM (n=4-6). Significant difference compared to Vehicle controls was analysed by two-way ANOVA and followed by Bonferroni's post hoc test denoted by * = $p<0.05$, **= $p<0.01$.

		Mesenteric arteries			
		Naïve		STZ	
	Treatment	E_{max} (mN)	EC_{50}	E_{max} (mN)	EC_{50}
PE	**Vehicle**	15.23 ± 1.2	3.6 µM	18.47 ± 2.9	3.6 µM
	1 nM GW0742	11.43 ± 2.2	3.0 µM	17.93 ± 1.8	2.1 µM
	10 nM GW0742	10.00 ± 1.4**	6.2 µM	17.09 ± 1.3	4.4 µM
	100 nM GW0742	10.90 ± 0.6**	3.5 µM	12.50 ± 0.8*	5.4 µM
U46619	**Vehicle**	5.84 ± 2.3	478.2 nM	7.58 ± 1.0	723.4 nM
	1 nM GW0742	4.10 ± 1.2	255.2 nM	6.50 ± 1.8	135.3 nM
	10 nM GW0742	3.65 ± 0.9	168.1 nM	7.89 ± 2.5	168.1 nM
	100 nM GW0742	2.64 ± 0.8**	-	3.43 ± 0.6**	243.9 nM

Mesenteric arteries
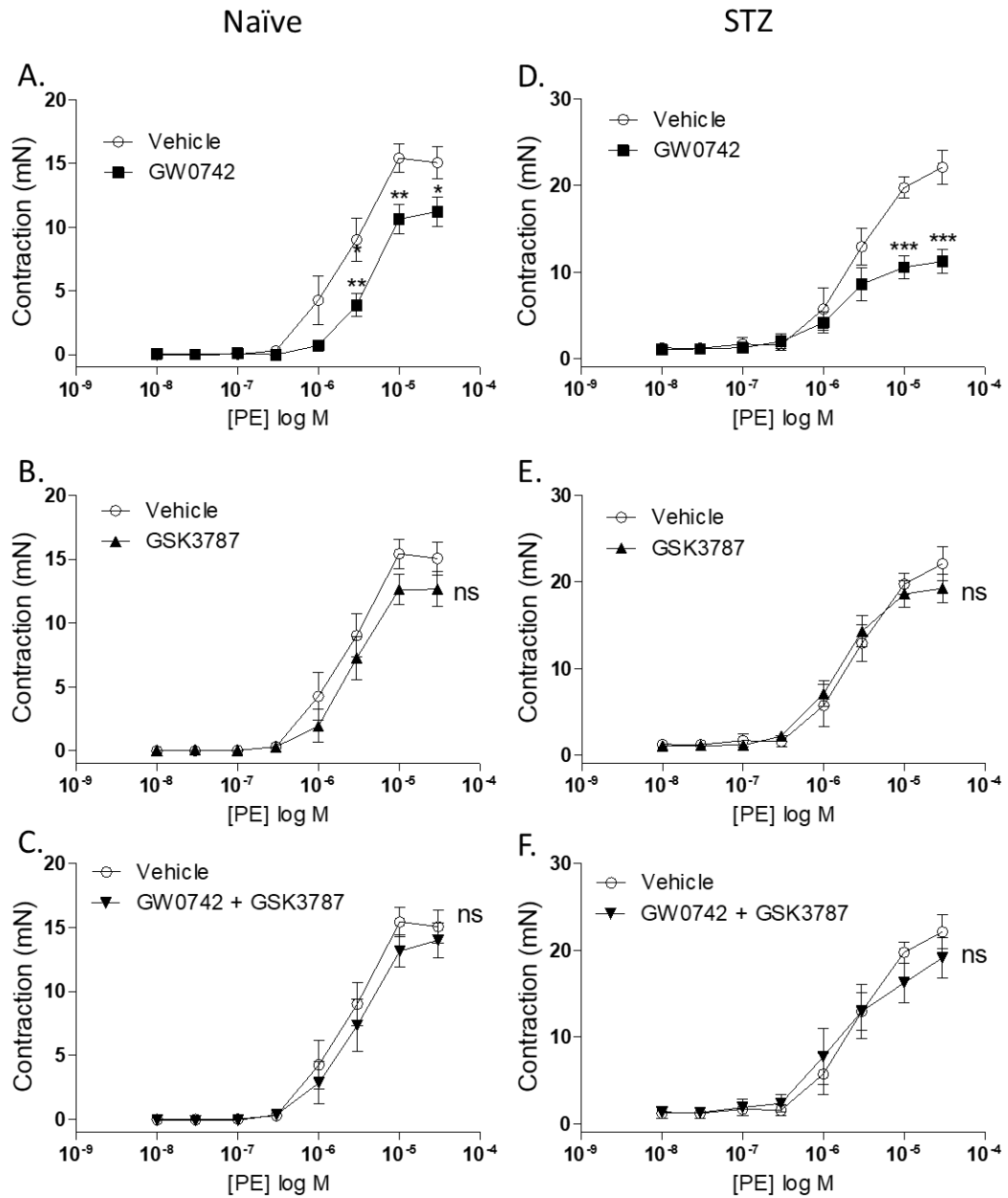
Figure 3.7 The effect of GW0742 on PE-induced mesenteric arteries contraction is reversed by the PPARβ/δ antagonist GSK3787. Four mesenteric artery rings from both Naïve and STZ-diabetic rats were incubated in four different treatments: 0.01% DMSO (Vehicle), 100 nM GW0742, 1 µM GSK3787 and 100 nM GW0742 + 1 µM GSK3787. After 30 min incubation a PE dose-response curve was performed. Data are represented as mean ±SEM (n=4-6). Significant difference compared to vehicle controls was analysed by two-way ANOVA followed by Bonferroni's post hoc test denoted by ***=$p<0.001$, **=$p<0.01$, *=$p<0.05$, ns=non-significance.

Table 3.9 E_{max} and EC_{50} of mesenteric arteries from Naïve and STZ-diabetic rats incubated with 100 nM GW0742, 1 µM GSK3787 or 100 nM GW0742 + 1 µM GSK3787 and contracted with PE. E_{max} is represented as mean ± SEM (n=4-6). Significant difference compared to Vehicle controls was analysed by two-way ANOVA and followed by Bonferroni's post hoc test denoted by *=$p<0.05$, *** = $p<0.001$.

Treatment	Mesenteric arteries			
	Naïve		STZ	
	E_{max} (mN)	EC_{50}	E_{max} (mN)	EC_{50}
Vehicle	15.42 ± 1.3	2.6 µM	22.12 ± 2.0	3.2 µM
100 nM GW0742	11.22 ± 1.2*	6.0 µM	11.2 ± 1.4***	1.9 µM
GSK3787	12.65 ± 1.4	3.3 µM	19.25 ± 1.7	1.9 µM
100 nM GW0742 + GSK3787	14.01 ± 1.3	3.4 µM	19.10 ± 2.3	1.9 µM

3.3.3 Acute exposure to high concentrations of glucose does not influence vascular contractility

3.3.3.1 Aorta

The exposure to 20 mM glucose concentration for 30 min does not influence the vascular contractility on aorta neither in Naïve or STZ-diabetic tissues as shown on Figure 3.8 below.
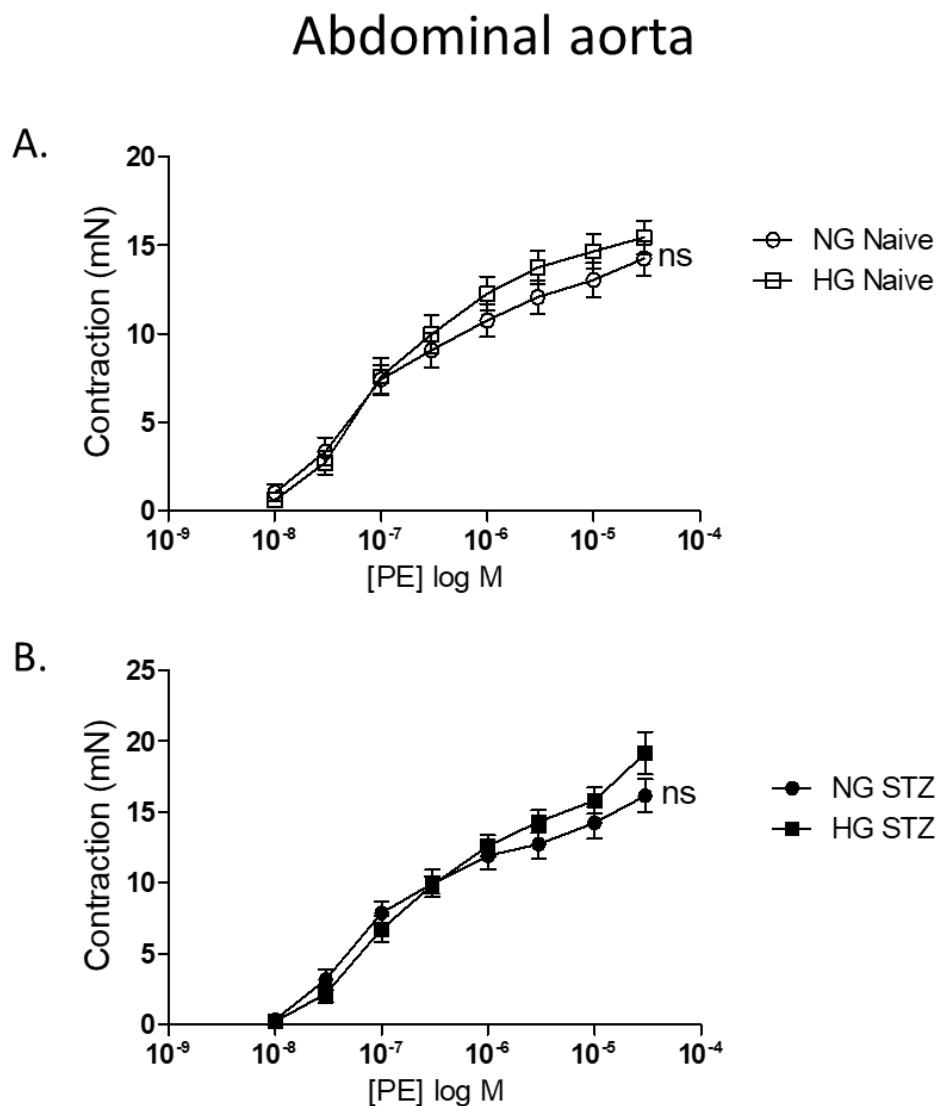
Figure 3.8 Effects of acute exposure to high glucose on abdominal aorta contraction. Aorta rings from Naïve (A) and STZ-diabetic rats (B) were exposed to normal levels of glucose (NG=5 mM) or high levels of glucose (HG=20 mM). After 30 min incubation a PE dose-response curve was performed. Data are represented as mean ±SEM (n=9-13). Significant difference compared to NG was analysed by two-way ANOVA followed by Bonferroni's post hoc test denoted by ns=non-significance.

3.3.3.2   Mesenteric arteries

Similarly, mesenteric arteries are not influenced by acute high concentrations of glucose either in Naïve or STZ-diabetic tissues, as shown on Figure 3.9 below.

Mesenteric arteries
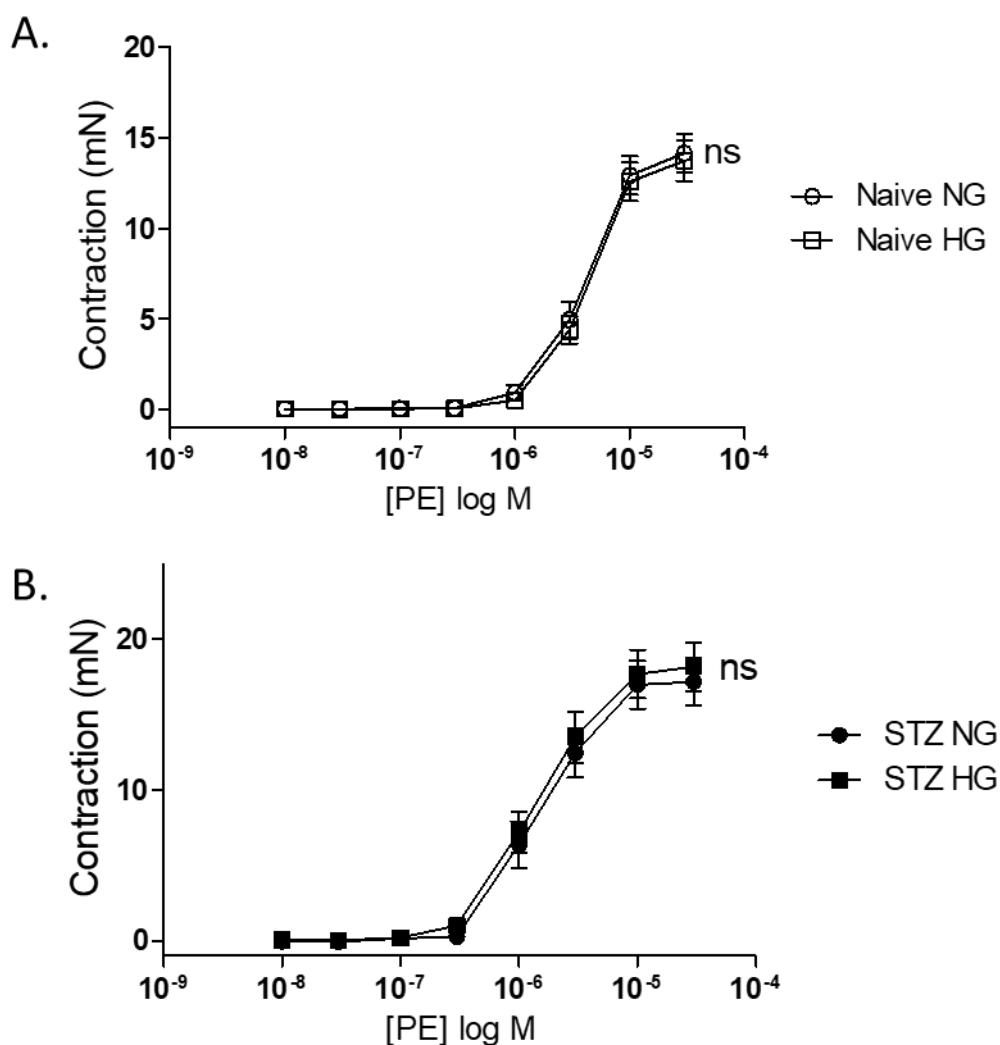
Figure 3.9 Effects of acute exposure to high glucose on mesenteric arteries contraction. Mesenteric artery rings from Naïve (A) and STZ-diabetic rats (B) were exposed to normal levels of glucose (NG=5 mM) or high levels of glucose (HG=20 mM). After 30 min incubation a PE dose-response curve was performed. Data are represented as mean ±SEM (n=9-13). Significant difference compared to NG analysed by two-way ANOVA followed by Bonferroni's post hoc test denoted by ns=non-significance.

Table 3.10 E_{max} and EC_{50} of abdominal aorta and mesenteric arteries from Naïve and STZ-diabetic rats exposed to normal levels of glucose (NG= 5 mM) high levels of glucose (HG= 20 mM) and contracted with PE. E_{max} is represented as mean ± SEM (n=9-13). Significant difference compared to NG was analysed by two-way ANOVA and followed by Bonferroni's post hoc test.

		Vehicle Naïve		Vehicle STZ	
	Treatment	**E_{max} (mN)**	**EC_{50}**	**E_{max} (mN)**	**EC_{50}**
Abdominal aorta	**NG**	14.26 ± 1.0	102.2 nM	16.6 ± 1.2	84.4 nM
	HG	15.44 ± 1.0	110.1 nM	19.15± 1.5	212.1 nM
Mesenteric arteries	**NG**	14.14 ± 1.1	6.1 µM	17.18 ± 1.5	1.8 µM
	HG	13.73 ± 1.1	6.6 µM	18.17 ± 1.1	1.6 µM

3.3.4   Role of PPARβ/δ on PI3K/Akt/eNOS pathway

Previous results showed that the activation of PPARβ/δ reduces vascular contraction both in aorta and mesenteric arteries (Figure 3.2, Figure 3.3, Figure 3.5, Figure 3.6). Next interest was understanding the molecular mechanism underlying this regulation and the differences, if any, between Naïve vs diabetic tissue as well as aorta vs mesenteric arteries. The regulation of the PI3K/Akt/eNOS pathway and the effects of high glucose concentrations were studied first. With that aim, aorta and mesenteric artery rings from Naïve and STZ-diabetic rats were incubated with different combinations of Insulin, LY29002 (PI3K inhibitor), and GW0742 at normal and high glucose concentrations.

3.3.4.1 Aorta

Insulin significantly decreases the PE-induced contraction from 1 µM PE on Naïve aorta rings (Figure 3.10 A, D), while GW0742 does not have a significant effect (Figure 3.10 B, E); however, GW0742 reverses the effect of the Insulin when they are incubated together (Figure 3.10 C, D). Surprisingly, the PI3K inhibitor LY294002 enhances the effect of Insulin and GW0742 blocking the contraction of the artery (Figure 3.10), which is the opposite of the expected response where LY294002 inhibits dilation via PI3K/Akt/eNOS.

Although the acute exposure to high glucose did not have an effect on aorta contraction *per se* (Figure 3.8) it enhaces the effect of the treatments in Naïve aorta rings (Figure 3.10).

Naïve abdominal aorta

NG   HG
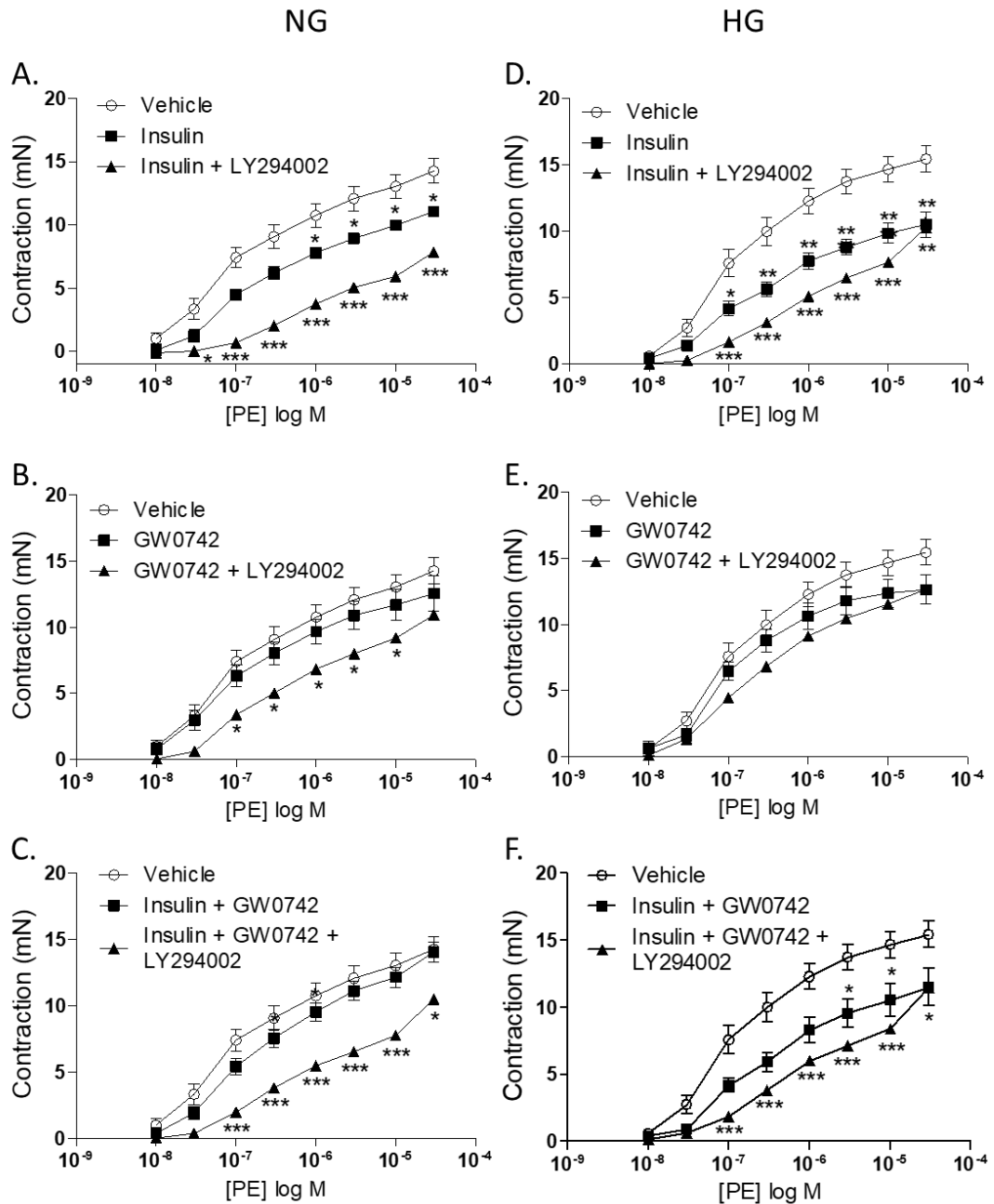
Figure 3.10 PI3K/Akt/eNOS pathway in Naïve rat aorta. Naïve abdominal aorta rings were exposed to one of the following treatments: 0.01% DMSO (Vehicle); 1 U/mL Insulin; 1 µM LY29002; 1 U/mL Insulin + 1 µM LY29002, 100 nM GW0742; 100 nM GW0742 + 1 µM LY29002; 1 U/mL Insulin + 100 nM GW0742; 1 U/mL Insulin + 100 nM GW0742 + 1 µM LY29002. Same treatments were performed in normal glucose (NG) concentration of 5 mM and high glucose (HG) concentration of 20 mM. After 30 min incubation a PE dose-response curve was performed. Data are represented as mean ±SEM (n=5-13). Significant difference compared to vehicle controls was analysed by two-way ANOVA followed by Bonferroni's post hoc test denoted by ***=$p<0.001$, **=$p<0.01$, *=$p<0.05$, ns=non-significance.

Interestingly, insulin does not have an effect on PE-induced contraction of STZ-diabetic aortic rings (Figure 3.11 A, D), however, it is significantly reduced by GW0742 (Figure 3.11 B-E). Similar to Naïve aorta rings, the co-incubation of insulin and GW0742 reverses any loss of contraction produced by GW0742 (Figure 3.11 C, F). LY294002 reverses the effect of the GW072 to levels similar to control, as predicted (Figure 3.11 B, E), and alike in Naïve tissues, high glucose intensifies the effect of GW0742 (Figure 3.11. B, D, E, F).

STZ abdominal aorta
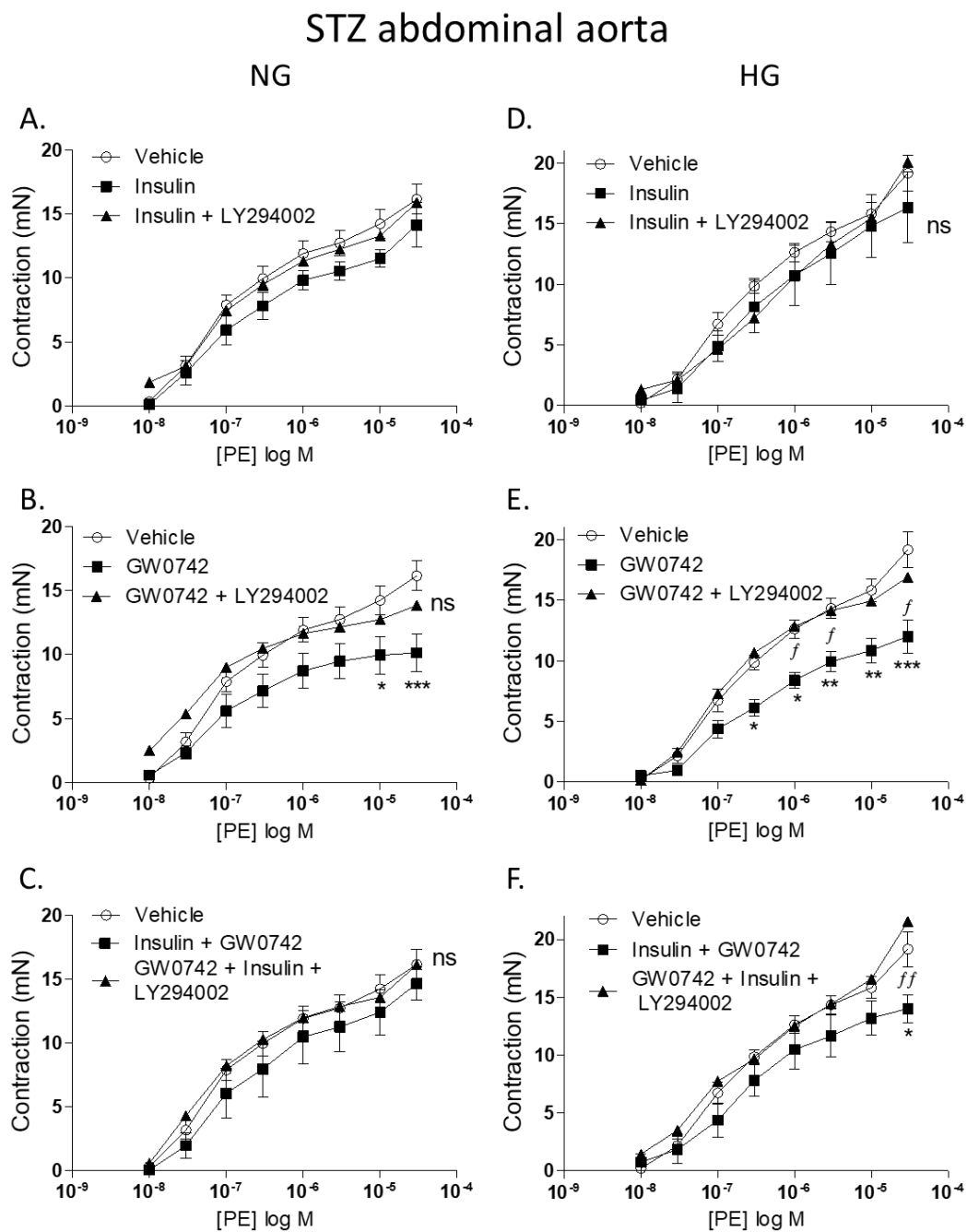
Figure 3.11 PI3K/Akt/eNOS pathway in STZ-diabetic rat aorta. STZ-diabetic abdominal aorta rings were exposed to one of the following treatments: 0.01% DMSO (Vehicle); 1 U/mL Insulin; 1 μM LY29002; 1 U/mL Insulin + 1 μM LY29002, 100 nM GW0742; 100 nM GW0742 + 1 μM LY29002; 1 U/mL Insulin + 100 nM GW0742; 1 U/mL Insulin + 100 nM GW0742 + 1 μM LY29002. Same treatments were performed in normal glucose (NG) concentration of 5 mM and high glucose (HG) concentration of 20 mM. After 30 min incubation a PE dose-response curve was performed. Data are represented as mean ±SEM (n=4-9). Significant difference compared to vehicle controls was analysed by two-way ANOVA followed by Bonferroni's post hoc test denoted by ***=p<0.001, **=p<0.01, *=p<0.05, ns=non-significance. Significant difference GW0742 vs GW0742 + LY294002 and Insulin + GW0742 vs Insulin + GW0742 + LY294002 was analysed by Bonferroni's post hoc test denoted by *ff*=p<0.01, *f*=p<0.05.

Table 3.11 E_{max} and EC_{50} of abdominal aorta from Naïve and STZ-diabetic rats incubated with 1 U/mL Insulin; 1 µM LY29002; 1 U/mL Insulin + 1 µM LY29002, 100 nM GW0742; 100 nM GW0742 + 1 µM LY29002; 1 U/mL Insulin + 100 nM GW0742; 1 U/mL Insulin + 100 nM GW0742 + 1 µM LY29002 in conditions of NG (5 mM) or HG (20 mM) and contracted with PE. E_{max} is represented as mean ± SEM (n=4-13). Significant difference compared to Vehicle controls was analysed by two-way ANOVA and followed by Bonferroni's post hoc test denoted by * = p<0.05, **=P<0.01, ***= p<0.001.

		Abdominal aorta			
		NG		HG	
	Treatment	E_{max} (mN)	EC_{50} (nM)	E_{max} (mN)	EC_{50} (nM)
Naïve	Vehicle	14.26 ± 1.0	102.2	15.44 ± 1.0	110.1
	Insulin	11.05 ± 0.3*	163.7	10.51 ± 1.0**	214.5
	Insulin + LY294002	7.85 ± 0.5***	1023.0	10.27 ± 1.9**	945.1
	GW0742	12.55 ± 1.3	109.9	12.62 ± 1.1	100.8
	GW0742 + LY294002	10.93 ± 0.7	300.9	12.66 ± 1.0	208.3
	Insulin + GW0742	14.05 ± 0.7	200.0	11.51 ± 1.4*	146.3
	Insulin + GW0742 + LY294002	10.50 ± 0.9*	686.7	11.50 ± 2.2*	825.6
STZ	Vehicle	16.16 ± 1.2	94.4	19.15 ± 1.5	212.1
	Insulin	14.16 ± 1.7	134.5	16.33 ± 2.9	306.0
	Insulin + LY294002	15.89 ± 3.3	144.2	20.07 ± 3.6	937.8
	GW0742	10.15 ± 1.5***	83.0	12.02 ± 1.4***	250.1
	GW0742 + LY294002	13.84 ± 1.4	50.0	16.89 ± 1.8	115.0
	Insulin + GW0742	14.66 ± 1.3	235.9	14.02 ± 1.2*	247.8
	Insulin + GW0742 + LY294002	16.12 ± 3.1	74.4	21.54 ± 3.4	486.0

3.3.4.2   Mesenteric arteries

Insulin and GW0742 significantly reduce PE-induced contraction on Naïve mesenteric artery, which is partially blocked in the presence of LY294002 (Figure 3.12 A, B, D, E). Surprisingly, the incubation of insulin and GW0742 together inhibit each other's effect resulting in contractions similar to that of the Vehicle (Figure 3.12 C, F). Strangely, the presence of LY294002 together with insulin and GW0742 leads to a loss of contraction compared to Vehicle (Figure 3.12 C, F).

Insulin but not GW0742 significantly reduces PE-induced contraction on STZ-diabetic mesenteric artery, which again, is partially blocked by the presence of LY294002 at low glucose (Figure 3.13 A, B, D, E). Similar to Naïve mesenteric arteries, the presence of insulin and GW0742 together inhibit any effect of the insulin and leads to a contraction similar to Vehicle (Figure 3.13 C, F).

High glucose does not affect the contraction of the mesenteric arteries from Naïve or STZ-diabetic tissues compared to normal glucose incubations, as shown in Figure 3.12 and Figure 3.13.

Mesenteric arteries Naïve
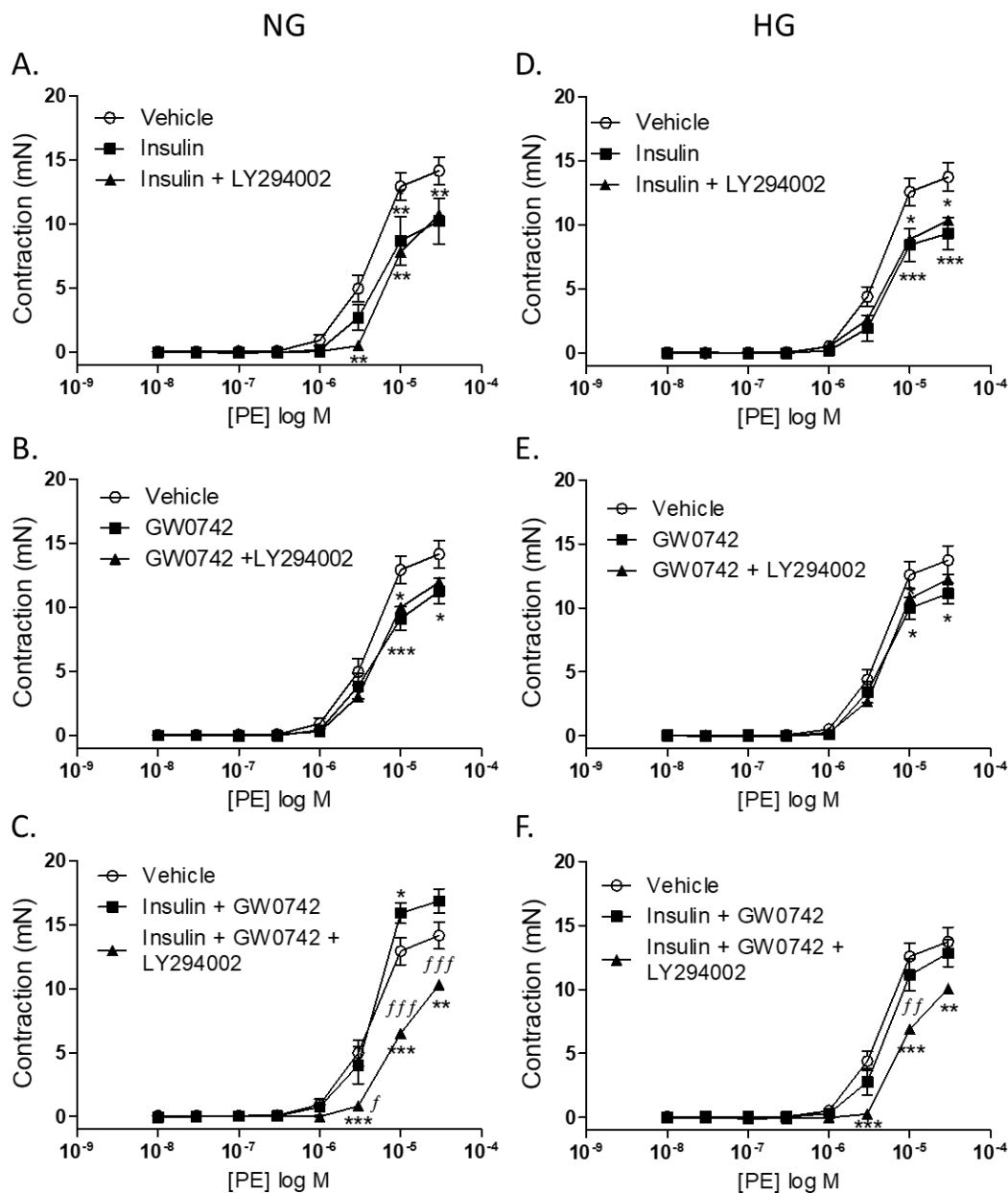
Figure 3.12 PI3K/Akt/eNOS pathway in Naïve rat mesenteric arteries. Naïve mesenteric artery rings were exposed to one of the following treatments: 0.01% DMSO (Vehicle); 1 U/mL Insulin; 1 μM LY29002; 1 U/mL Insulin + 1 μM LY29002, 100 nM GW0742; 100 nM GW0742 + 1 μM LY29002; 1 U/mL Insulin + 100 nM GW0742; 1 U/mL Insulin + 100 nM GW0742 + 1 μM LY29002. Same treatments were performed in normal glucose (NG) concentration of 5 mM and high glucose (HG) concentration of 20 mM. After 30 min incubation a PE dose-response curve was performed. Data are represented as mean ±SEM (n=4-13). Significant difference compared to vehicle controls was analysed by two-way ANOVA followed by Bonferroni's post hoc test denoted by ***=p<0.001, **=p<0.01, *=p<0.05, ns=non-significance. Significant difference Insulin + GW0742 vs Insulin + GW0742 + LY294002 was analysed by Bonferroni's post hoc test denoted by *fff*=p<0.001, *ff*=p<0.01, *f*=p<0.05.

Mesenteric arteries STZ
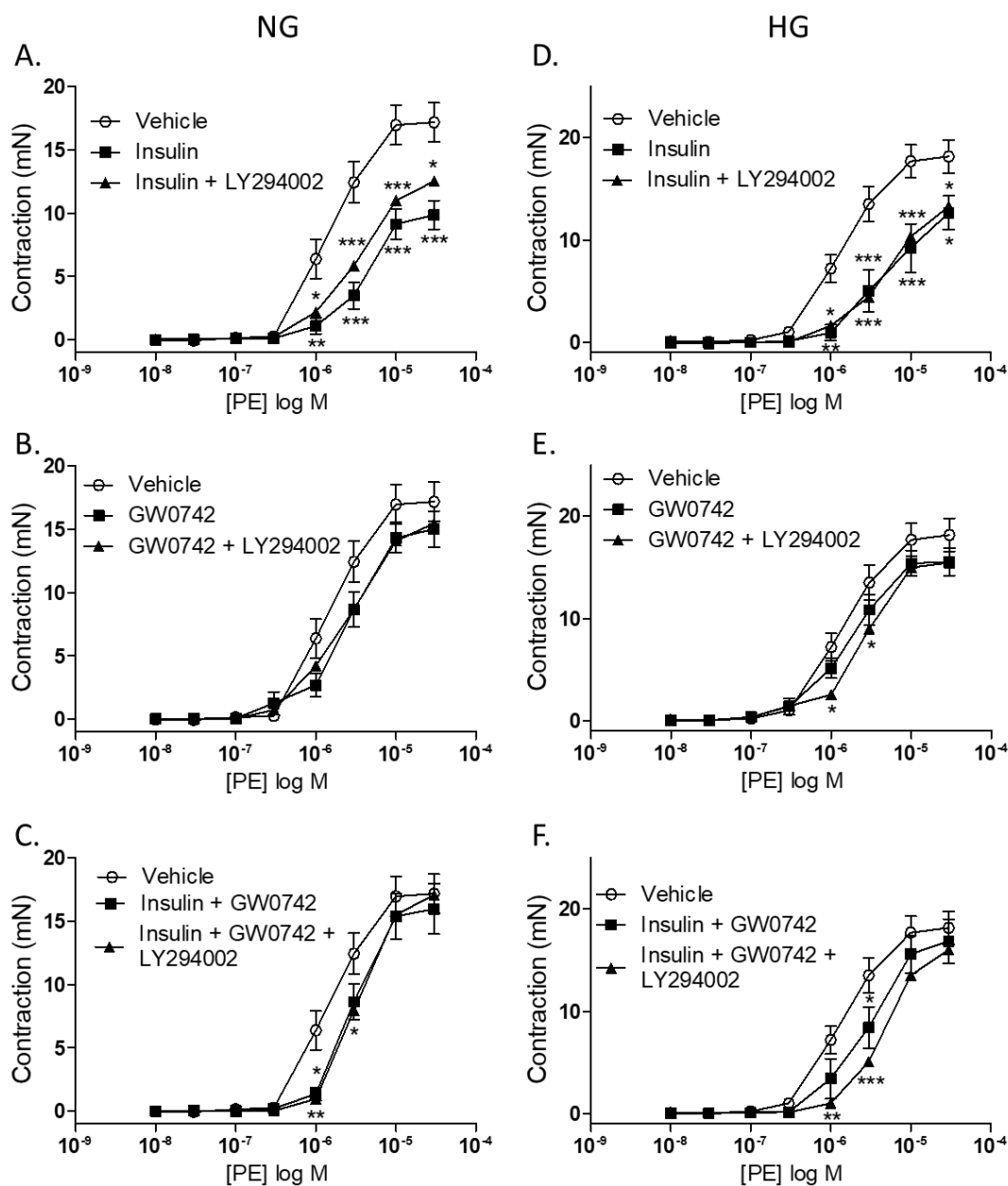
Figure 3.13 PI3K/Akt/eNOS pathway in STZ-diabetic rat mesenteric arteries. STZ-diabetic mesenteric artery rings were exposed to one of the following treatments: 0.01% DMSO (Vehicle); 1 U/mL Insulin; 1 µM LY29002; 1 U/mL Insulin + 1 µM LY29002, 100 nM GW0742; 100 nM GW0742 + 1µM LY29002; 1 U/mL Insulin + 100 nM GW0742; 1 U/mL Insulin + 100 nM GW0742 + 1 µM LY29002. Same treatments were performed in normal glucose (NG) concentration of 5 mM and high glucose (HG) concentration of 20 mM. After 30 min incubation a PE dose-response curve was performed. Data are represented as mean ±SEM (n=4-9). Significant difference compared to vehicle controls was analysed by two-way ANOVA followed by Bonferroni's post hoc test denoted by ***=p<0.001, **=p<0.01, *=p<0.05, ns=non-significance.

Table 3.12 E_{max} and EC_{50} of mesenteric arteries from Naïve and STZ-diabetic rats incubated with 1 U/mL Insulin; 1 µM LY29002; 1 U/mL Insulin + 1 µM LY29002, 100 nM GW0742; 100 nM GW0742 + 1 µM LY29002; 1 U/mL Insulin + 100 nM GW0742; 1 U/mL Insulin + 100 nM GW0742 + 1 µM LY29002 in conditions of NG (5 mM) or HG (20 mM) and contracted with PE. E_{max} is represented as mean ± SEM (n=4-13). Significant difference compared to Vehicle controls was analysed by two-way ANOVA and followed by Bonferroni's post hoc test denoted by * = p<0.05, **=P<0.01, ***= p<0.001.

		Mesenteric arteries			
		NG		HG	
	Treatment	E_{max} (mN)	EC_{50} (µM)	E_{max} (mN)	EC_{50} (µM)
Naïve	Vehicle	14.14 ±1.1	6.1	13.73 ± 1.1	6.6
	Insulin	10.23 ± 1.8**	8.2	9.34 ± 1.2***	8.4
	Insulin + LY294002	10.73 ± 1.6	16.6	10.35 ± 1.3*	8.1
	GW0742	11.26 ± 1.0*	7.2	11.12 ± 0.8*	7.1
	GW0742 + LY294002	11.96 ± 1.2	8.5	12.23 ± 1.8	8.5
	Insulin + GW0742	16.84 ± 0.9	7.4	12.83 ± 1.0	8.8
	Insulin + GW0742 + LY294002	10.31 ± 1.5**	21.5	10.07 ± 1.5**	19.6
STZ	Vehicle	17.18 ± 1.5	1.8	18.17 ± 1.6	1.6
	Insulin	9.87 ± 1.1***	5.7	12.64 ± 1.7*	6.8
	Insulin + LY294002	12.51 ± 1.7*	4.3	13.26 ± 1.6*	7.0
	GW0742	15.01 ± 1.4	3.2	15.53 ±1.4	1.9
	GW0742 + LY294002	15.46 ± 1.4	2.8	15.45 ± 1.3	3.2
	Insulin + GW0742	15.97 ± 2.0	3.9	16.86 ± 2.2	3.7
	Insulin + GW0742 + LY294002	17.05 ± 2.2	4.8	16.02 ± 1.7	7.2

3.3.5   Role of PPARβ/δ on RhoA/ROCK pathway

The inhibition of the RhoA/ROCK pathway by PPARβ/δ was studied next. The drawback of using ROCK inhibitors is the lack of contraction of the vessels, making the investigation of a ROCK inhibitor difficult to determine directly. The approach taken here was to use a contractile agent that induced a non-RhoA mediated contractile response and measure the effects of GW0742 on tone. To achieve this, the tissues were incubated with the ROCK inhibitors Fasudil and Y27632 first and then contracted with U46619 or phenylephrine.

3.3.5.1   Aorta

The ROCK inhibitors Y27632 and Fasudil led to a loss of PE-mediated contraction in Naïve rat aorta (Figure 3.14 A). In contrast, ROCK inhibitors reduced U46619-mediated contraction in Naïve rat aorta when incubated with Y27632 and Fasudil (Figure 3.14 B). STZ-diabetic rat aorta contraction in response to U46619 was significantly reduced by Fasudil and completely inhibited by Y27632 (Figure 3.14 C).

Essentially, the Figure 3.11 (B, C) shows that Fasudil significantly reduces the U46619-induced contraction both in Naïve and STZ-diabetic aorta rings, but leads to enough vascular tone to study the vasodilator effect of GW0742, therefore Fasudil was used for further experiments.

Thoracic aorta
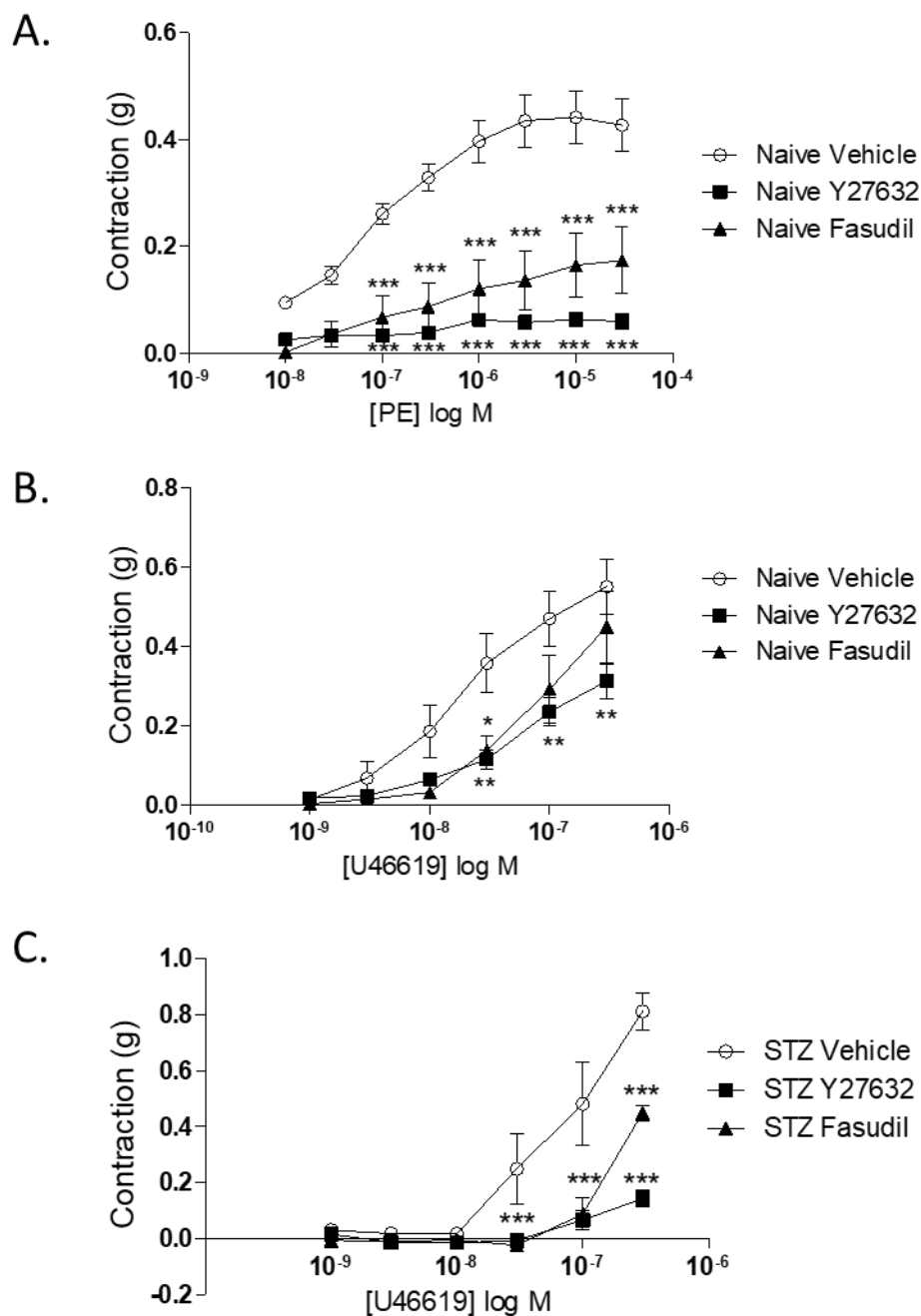
Figure 3.14 Change in tension induced by A) phenylephrine, B) U46619 in naïve rat aorta, C) U46619 in STZ-diabetic rat thoracic aorta after incubation with 10 µM Y27632 and 10 µM Fasudil. Aorta rings were incubated with 0.01% DMSO (Vehicle), 10 µM Y27632 or 10 µM Fasudil for 30 min and a PE or U46619 dose-response curve was performed. Data are represented as mean ± SEM (n=4-6). Significant difference compared to vehicle controls was analysed by two-way ANOVA followed by Bonferroni's post hoc test and denoted by ***=$p<0.001$, **=$p<0.01$, *=$p<0.05$, ns = non-significance.

Table 3.13 E_{max} and EC_{50} of thoracic aorta from Naïve and STZ-diabetic rats incubated with 10 μM Y27632 or 10 μM Fasudil and contracted with PE and U46619. E_{max} is represented as mean ± SEM (n=4-6). Significant difference compared to Vehicle controls was analysed by two-way ANOVA and followed by Bonferroni's post hoc test denoted by **=p<0.01, *** = p<0.001.

		Thoracic aorta			
		Naïve		STZ	
	Treatment	E_{max} (g)	EC_{50} (nM)	E_{max} (g)	EC_{50} (nM)
PE	**Vehicle**	0.44 ± 0.05	101.5	-	-
	Y27632	0.06 ± 0.01***	310.7	-	-
	Fasudil	0.17 ± 0.06***	276.4	-	-
U46619	**Vehicle**	0.55 ± 0.07	19.0	0.81 ± 0.07	137.0
	Y27632	0.31 ± 0.04**	71.0	0.14 ± 0.03***	644.6
	Fasudil	0.45 ± 0.09	105.1	0.45 ± 0.03***	-

Aorta pre-contracted with EC_{80} U46619 was exposed to increasing concentrations of GW0742 resulting in a full relaxation of the vessel, which is significantly reduced in STZ-diabetic rat aorta (Figure 3.15 A). Fasudil significantly reduced the GW0742 mediated dilation in naïve rat aorta (Figure 3.15 B), but not in STZ-diabetic rat aorta (Figure 3.15 C).
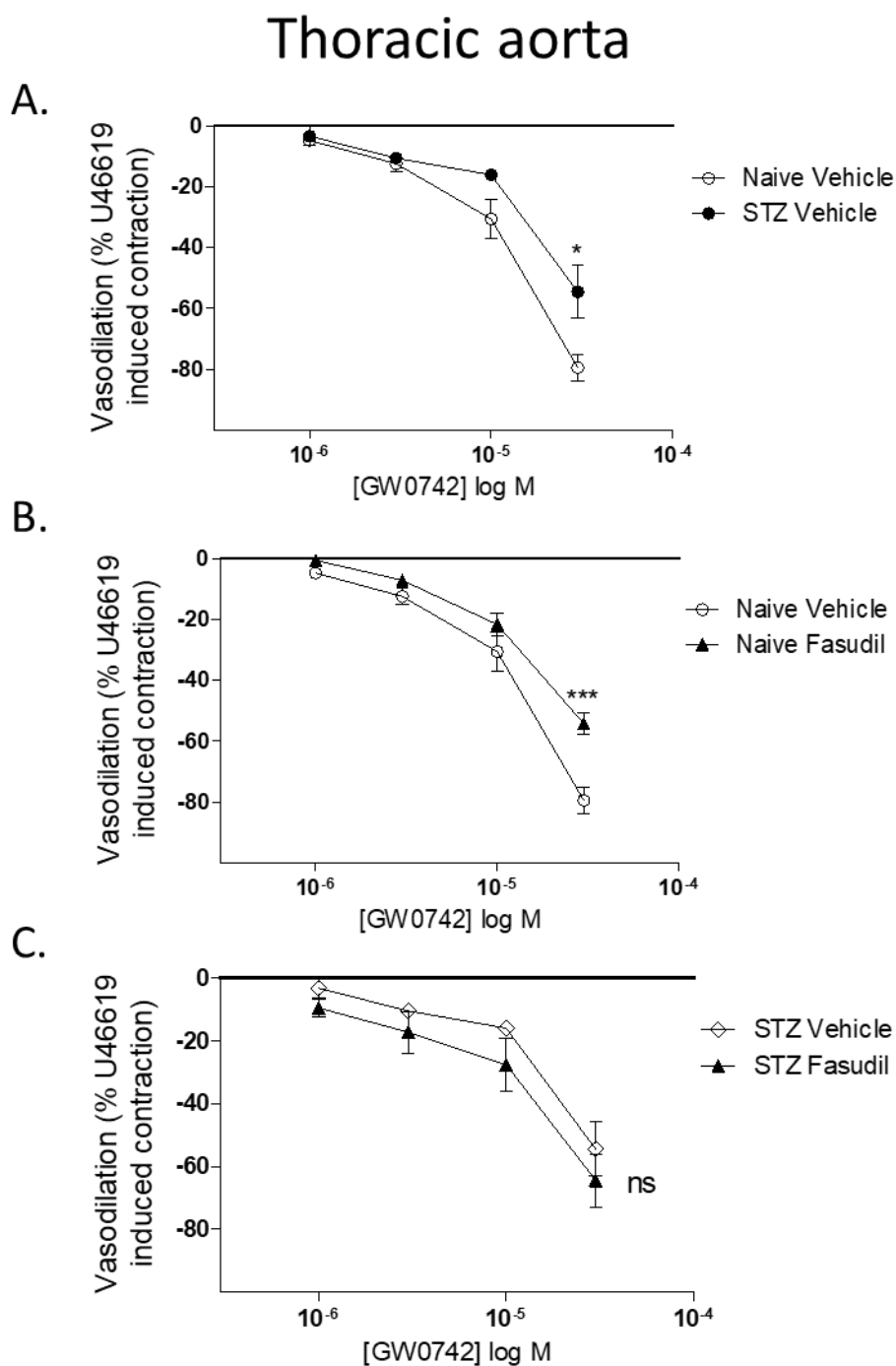
Figure 3.15 Dilation of Naïve and STZ-diabetic rat thoracic aorta to GW0742 following pre-contraction to U46619. Rat aorta rings were incubated with 0.01% DMSO (Vehicle) or 10 µM Fasudil of 30 min, pre-contracted with EC_{80} U46619 and exposed to increasing concentrations of GW0742. Data are represented as mean ± SEM (n=4-13). Significant difference compared to vehicle controls was analysed by two-way ANOVA and followed by Bonferroni's post hoc denoted by ***=p<0.001, *=p<0.05, ns= non-significance.

Table 3.14 I$_{max}$ and IC$_{50}$ of thoracic aorta from Naïve and STZ-diabetic rats incubated with 10 μM Fasudil, pre-contracted with U46619 and relaxed with GW0742. I$_{max}$ is represented as mean ± SEM (n=4-13). Significant difference compared to Vehicle controls was analysed by two-way ANOVA and followed by Bonferroni's post hoc test denoted by *=$p<0.05$, *** = $p<0.001$.

	Thoracic aorta			
	Naïve		STZ	
Treatment	**I$_{max}$ (%)**	**IC$_{50}$**	**I$_{max}$ (%)**	**IC$_{50}$**
Vehicle	-79.44 ± 4.5	17.2 μM	-54.45 ± 8.6	-
Fasudil	-54.21 ± 3.7***	65.9 μM	-64.37 ± 8.4*	-

3.3.5.2 Mesenteric arteries

Fasudil and Y22763 led to a loss of the U46619-induced contraction (Figure 3.16 B, D), but only partially inhibited the PE-induced contraction (Figure 3.16 A, C). Same effects were observed on Naïve and STZ-diabetic mesenteric arteries.

To be consistent with the experiments done in aorta, Fasudil was used to perform further experiments. However, since the ROCK inhibitors completely abolished any contraction produced by U46619 in mesenteric arteries, PE was used to contract the mesenteric arteries instead. It is worth pointing out that the minimum concentration of GW0742 used for the dilation of the vessels is 100-fold higher than the concentrations used in previous experiments, which might produce off target effects. To find out if the GW0742-induced dilation is an effect independent of PPARβ/δ activation one extra treatment with GSK3787 was included. Therefore, mesenteric arteries were incubated with Vehicle, Fasudil or GSK3787, pre-contracted with EC$_{80}$ PE and relaxed with increasing concentrations of GW0742. The Figure 3.17 A shows that GW0742 induces vascular dilation on Naïve and STZ-diabetic mesenteric arteries with no significant difference between them. This dilation is significantly reduced by Fasudil on STZ-diabetic tissues but not on Naïve

(Figure 3.17 B, C), and GSK3787 does not have any effect on GW0742-induced

dilation (Figure 3.17 B, C).

Mesenteric arteries
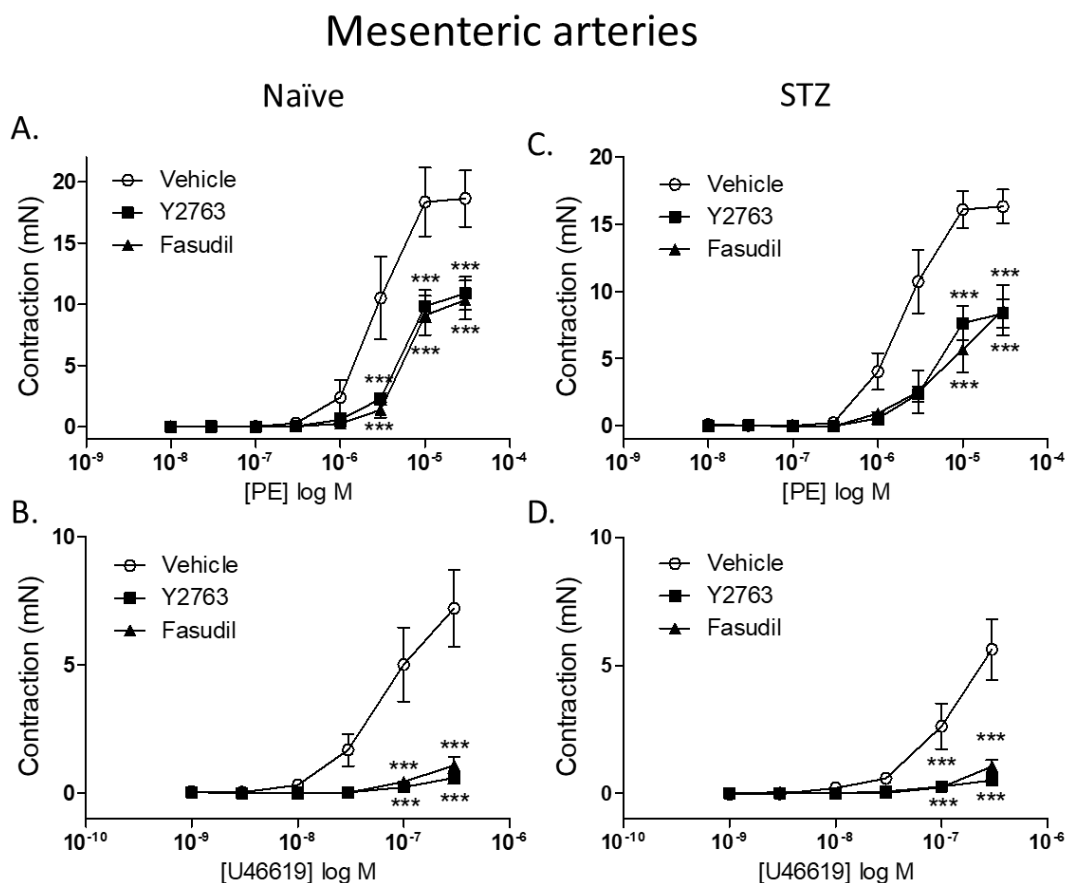
Figure 3.16 Change in tension induced by A) phenylephrine, B) U46619 in naïve rat mesenteric artery, C) U46619 in STZ-diabetic rat mesenteric artery after incubation with 10 µM Y27632 and 10 µM Fasudil. Mesenteric rings were incubated with 0.01% DMSO (Vehicle), 10 µM Y27632 or 10 µM Fasudil for 30 min and a PE or U46619 dose-response curve was performed. Data are represented as mean ± SEM (n=5-6). Significant difference compared to vehicle controls was analysed by two-way ANOVA followed by Bonferroni's post hoc test and denoted by ***=$p<0.001$, **=$p<0.01$, *=$p<0.05$, ns = non-significance.

Table 3.15 E_{max} and EC_{50} of mesenteric arteries from Naïve and STZ-diabetic rats incubated with 10 µM Y27632 or 10 µM Fasudil and contracted with PE and U46619. E_{max} is represented as mean ± SEM (n=5-6). Significant difference compared to Vehicle controls was analysed by two-way ANOVA and followed by Bonferroni's post hoc test denoted by *** = p<0.001

| | | Mesenteric arteries | | | |
| | | Naïve | | STZ | |
	Treatment	E_{max} (mN)	EC_{50}	E_{max} (mN)	EC_{50}
PE	**Vehicle**	18.33 ± 2.8	3.5 µM	16.32 ± 1.2	2.5 µM
	Y27632	10.88 ± 1.4***	8.2 µM	8.36 ± 1.1***	6.9 µM
	Fasudil	10.34 ± 1.6***	10.1 µM	8.60 ± 1.9***	10.4 µM
U46619	**Vehicle**	7.21 ± 1.5	109.2 nM	5.63 ± 1.5	425.7 nM
	Y27632	0.60 ± 0.6***	2.3 µM	0.52 ± 0.2***	335.3 nM
	Fasudil	1.09 ± 0.3***	1.3 µM	1.06 ± 0.2***	-

Mesenteric arteries
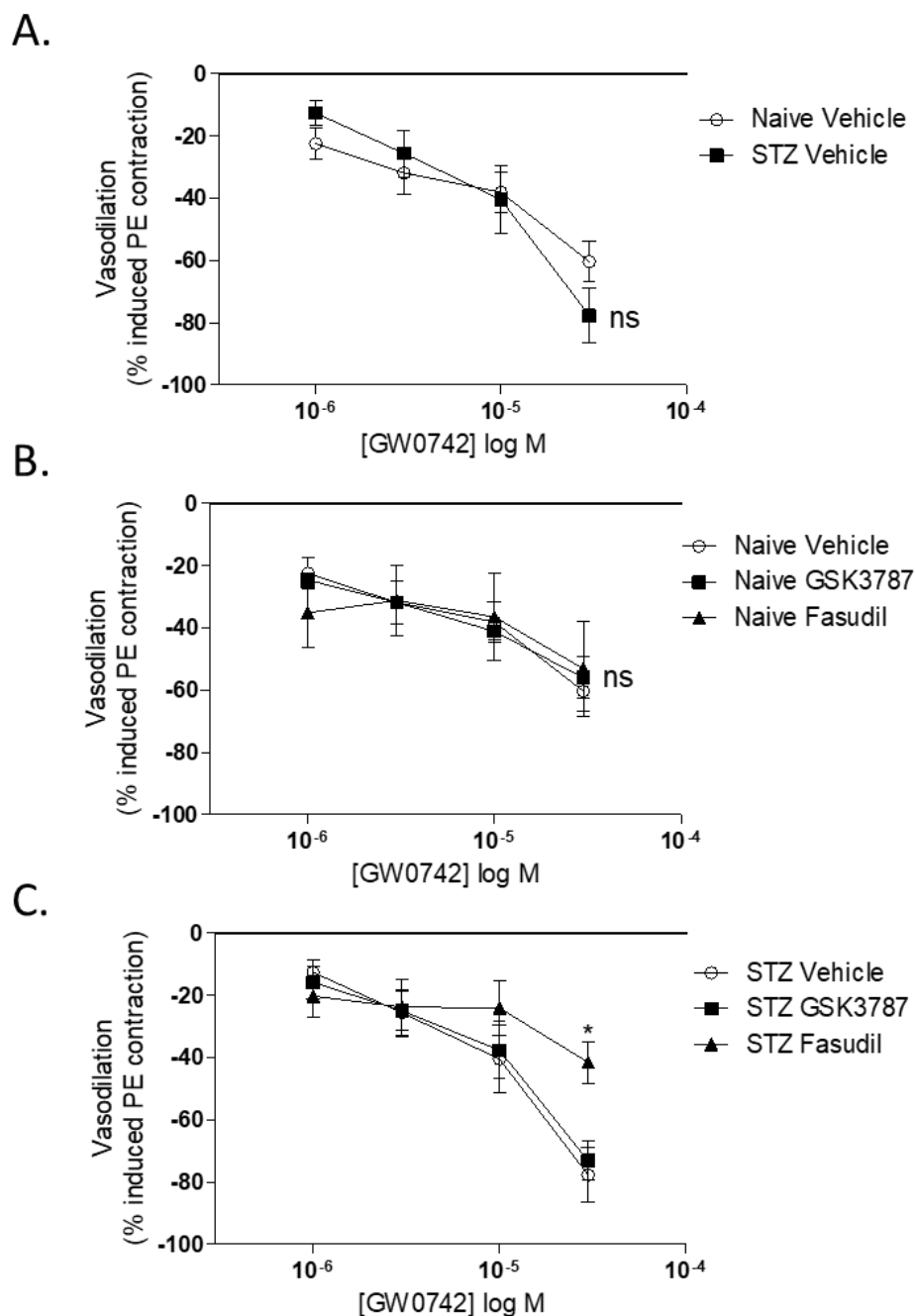
Figure 3.17 Dilation of Naïve and STZ-diabetic mesenteric arteries to GW0742 following pre-contraction to PE. Rat mesenteric artery rings were incubated with 0.01% DMSO (Vehicle), 1 µM GSK3787 or 10 µM Fasudil of 30 min, pre-contracted with EC_{80} PE and exposed to increasing concentrations of GW0742. Data are represented as mean ± SEM (n=4). Significant difference compared to vehicle controls was analysed by two-way ANOVA and followed by Bonferroni's post hoc denoted by *=p<0.05, ns= non-significance.

Table 3.16 I_{max} and IC_{50} of mesenteric arteries from Naïve and STZ-diabetic rats incubated with 10 µM Fasudil or 1 µM GSK3787, pre-contracted with PE and relaxed with GW0742. I_{max} is represented as mean ± SEM (n=4). Significant difference compared to Vehicle controls was analysed by two-way ANOVA and followed by Bonferroni's post hoc test denoted by *=p<0.05.

	Mesenteric arteries			
	Naïve		STZ	
Treatment	**I_{max} (%)**	**IC_{50}**	**I_{max} (%)**	**IC_{50}**
Vehicle	-60.28 ± 6.6	49.7 µM	-77.59 ± 8.8	41.5 µM
GSK3787	-56.00 ± 6.7	17.0 µM	-73.06 ± 6.2	82.9 µM
Fasudil	-53.07 ± 15.3	-	-41.47 ± 6.7*	-

3.3.6 Potassium channels

In an attempt to do a brief study of the regulation of potassium channels by PPARβ/δ, aorta and mesenteric artery rings were pre-contracted with KPSS and then relaxed with increasing concentrations of GW0742.

3.3.6.1 Aorta

The relaxation in response to GW0742 in STZ-diabetic rat aorta was significantly reduced compared to Naïve control rat aorta, as shown on Figure 3.18 below.

Thoracic Aorta
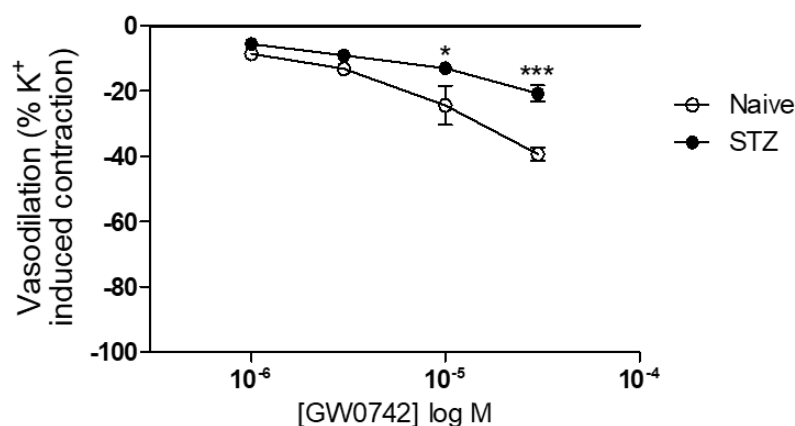
Figure 3.18 Dilation of Naïve and STZ-diabetic rat thoracic aorta to GW0742 following pre-contraction to high potassium solution (KPSS). Rat aorta rings pre-contracted with KPSS and exposed to increasing concentrations of GW0742. Data are represented as mean ± SEM (n=3). Significant difference compared to Naïve vehicle control was analysed by two-way ANOVA and followed by Bonferroni's post hoc denoted by ***=$p < 0.001$, *=$p < 0.05$.

3.3.6.2 Mesenteric arteries

On the contrary to aorta, GW0742-induced dilation on Naïve mesenteric artery was significantly reduced compared to STZ-diabetic mesenteric arteries (Figure 3.19).

Mesenteric arteries
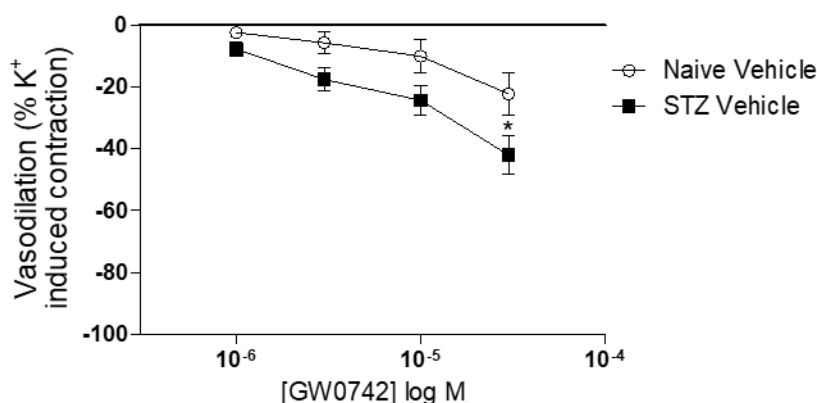
Figure 3.19 Dilation of Naïve and STZ-diabetic rat mesenteric arteries to GW0742 following pre-contraction to high potassium solution (KPSS). Rat mesenteric artery rings were pre-contracted with KPSS and exposed to increasing concentrations of GW0742. Data are represented as mean ± SEM (n=4). Significant difference compared to Naïve vehicle control was analysed by two-way ANOVA and followed by Bonferroni's post hoc denoted by *=$p < 0.05$.

Table 3.17 I$_{max}$ and IC$_{50}$ of thoracic aorta and mesenteric arteries from Naïve and STZ-diabetic rats pre-contracted with KPSS and relaxed with GW0742. I$_{max}$ is represented as mean ± SEM (n=3-4). Significant difference compared to Vehicle controls was analysed by two-way ANOVA and followed by Bonferroni's post hoc test denoted by *=$p<0.05$, ***=$p<0.001$.

|	Thoracic aorta		Mesenteric artery	
Treatment	I$_{max}$ (%)	IC$_{50}$	I$_{max}$ (%)	IC$_{50}$
Vehicle Naive	-39.32 ± 2.0	20.3 μM	-22.18 ± 6.9	75.6 μM
Vehicle STZ	-20.69 ± 2.5***	21.4 μM	-41.92 ± 6.3*	21.7 μM

3.4   Discussion

In this chapter further evidence that aorta and mesenteric arteries contraction is dysfunctional in STZ-diabetic rat model was provided, and it was shown that GW0742 significantly improves PE and U46619 mediated contraction. While similar results have previously been noted (Harrington *et al.* 2010, Jimenez *et al.* 2010, Li *et al.* 2012), to our knowledge this is the first time to determine and publish that 100 nM GW0742 is the minimum concentration needed to perceive these beneficial results (Perez-Diaz *et al.* 2018).

The effects of 100 nM GW0742 are non-genomic and PPARβ/δ-dependent, which has been proved by three facts: 1) the incubations were 30 min long, a time frame that is too short to allow for new genes to be induced, 2) the use of a concentration that is selective for PPARβ/δ (100 nM) (Sznaidman *et al.* 2003); 3) the selective PPARβ/δ antagonist GSK3787 blocked the effect of 100 nM GW0742.

The incubation of aorta and mesenteric arteries in high glucose for 30 min did not have any effect in vascular contractility. The lack of effect of high glucose in STZ-diabetic tissues is expected because the vessels from these animals were exposed to high glucose levels for over 14 days (see Table 3.4), therefore during the experiment the tissues were not exposed to an acute high glucose concentration but to an acute normal glucose concentration instead. All together suggests that the influence of high glucose to the impairment of contraction of STZ-diabetic vessels is the result of a prolonged exposure rather than punctual peaks of elevated glucose levels.

There is also new evidence of the different mechanistic pathways used by different contraction agents that change with the type of vessel and health condition. PE-induced contraction pathway is impaired in diabetic tissues, while U46619-induced

contraction is only affected in STZ-diabetic mesenteric arteries and not in aorta (Figure 3.1). On the other hand, PE induces contraction through the RhoA/ROCK pathway in aorta, since this contraction is abolished by the ROCK inhibitors, as shown in Figure 3.14 A and supported by previous studies (Budzyn *et al.* 2006, Hamblin *et al.* 2009). Same inhibitors prevent the U46619-induced contraction but only to some extent, confirming previous data showing that U46619 contracts using partially different contractile machinery to PE (Budzyn *et al.* 2006). Therefore, if the PE-contraction is dysfunctional in aorta STZ-diabetic tissue and this contraction is mainly mediated by the RhoA/ROCK pathway, it suggests that the impairment of the RhoA/ROCK pathway contributes the most to the dysfunction of the aorta contraction in diabetes. Same conclusion was achieved using a different approach in another *in vivo* study using insulin resistance obese rats, where the authors demonstrate that RhoA/ROCK pathway is activated in aorta and is involved in the increased systemic vascular resistance in hypertension (Kanda *et al.* 2006).

On the contrary, and according to the results from this study, U46619 mainly signals via the RhoA/ROCK pathway to contract mesenteric arteries, while PE only partially utilizes this pathway to contract. Therefore, and following the same rationalising as before, if PE-contraction is dysfunctional in STZ-diabetic mesenteric arteries and it is only partially mediated by the RhoA/ROCK pathway, this suggest that other pathways such as PI3K/Akt/eNOS or potassium channels might have more relevance in the dysfunction of the mesenteric arteries in diabetes. The same hypothesis was suggested in a previous study where Y2763, the antagonist of ROCK1/2, partially inhibited the hyperreactivity of mesenteric mice arteries (Xie *et al.* 2006). However, RhoA/ROCK showed to be the main pathway contributing to the development of diabetes-associate hypertension in Goto-kakizaki rats, a model of diabetes type 2 (Rao *et al.* 2013). It is possible that different types of diabetes develop hypertension involving different pathways,

suggesting different treatments depending on the type of diabetes. More research is needed to answer this question.

In a previous study Budzyn *et al.* (2006) described very similar findings where the RhoA/ROCK pathway contributes to contractile responses more in aorta than in mesenteric arteries from rat. Furthermore, responses of the aorta to PE were abolished by Rho-kinase inhibition and relatively reduced in mesenteric arteries and caused relatively weak attenuation of contractile responses to U46619 in aorta and mesenteric arteries. Equally, the authors concluded that RhoA/ROCK pathway has a major role in mediating contractile responses of larger conductance vessels, whereas its contribution is greatly diminished in small resistance vessels.

After these findings, next step was to find out how insulin and PPARβ/δ regulates the different contraction pathways in every possible scenario, signifying health vs disease and aorta vs mesenteric arteries.

3.4.1   Aorta

3.4.1.1   PI3K/Akt/eNOS pathway

This study shows that insulin has a relaxation effect on Naïve rat aorta, but not in STZ-diabetic rat aorta. Interestingly, the relaxation of Naïve rat aorta is not inhibited by the PI3K inhibitor LY294002, indicating that insulin is relaxing the vessel through another pathway, possibly via RhoA/ROCK. In the same line, Sandu *et al.* (2001) showed that insulin inhibits the RhoA/ROCK pathway in aorta SMCs from rats. Since this pathway is impaired in diabetic aorta, that can explain the loss of insulin-induced vascular relaxation in diabetic tissue; however, more research is needed to confirm this hypothesis.

PPARβ/δ significantly reduces aorta contraction in STZ-diabetic tissues and possibly Naïve tissues. Whereas the incubation with 100 nM GW0742 of Naïve

thoracic aorta rings mounted in an organ bath significantly reduce the contraction of the vessel, as shown in Figure 3.2 C, this effect is lost when the same treatment is used in abdominal aorta rings mounted in the myograph (Figure 3.4 A and Figure 3.10 B). One study done with two different hypertension murine models showed region-specific differences between thoracic and abdominal aortic expression of several genes, including metalloproteinases and cathepsins (Ruddy *et al.* 2017). Although any study showing differences on the expression of PPARβ/δ between thoracic and abdominal aorta was found, Ruddy *et al.* (2017) showed a decrease on the expression of *Timp1* on abdominal aorta, a gene that was reported to be regulated by PPARβ/δ (Adhikary *et al.* 2011, Khozoie *et al.* 2012). Another study showed a decrease on PPARγ expression on the perivascular adipose tissue surrounding abdominal rat aorta compared to perivascular adipose tissue from thoracic rat aorta (Padilla *et al.* 2013). All together suggests the possibility of a lower expression of PPARβ/δ in Naïve abdominal aorta which could explain the loss of dilation with GW0742, although further studies need to be done to confirm this hypothesis.

However, the inhibition of STZ-diabetic aorta contraction by 100 nM GW0742 is consistent throughout all the experiments regardless the region of the aorta used. Therefore, it can safely be concluded that PPARβ/δ improves vascular dilation of at least STZ-diabetic aorta. Interestingly, the effect of PPARβ/δ on STZ-diabetic aorta is blocked by LY294002, an inhibitor of PI3K, indicating that in STZ-diabetic rat aorta PPARβ/δ causes vascular relaxation through the PI3K/Akt/eNOS, which agrees with previous studies (Jimenez *et al.* 2010).

Surprisingly, the incubation of the vessel with insulin and GW0742 together reverse any beneficial effect that these drugs can have independently. Since they trigger two different pathways, it is possible that some sort of downstream interference

occurs that cannot be explained with the present data. Further experiments need to be done in order to further understand this phenomenon.

The insulin-induced relaxation effect is lost on STZ-diabetic aorta; thus, it is tempting to consider the use of GW0742 for the treatment of hypertension in diabetes. However, the fact that the effect of GW072 is inhibited in the presence of insulin makes it infeasible as a therapy for type 1 diabetes. It would be interesting to find out if the same phenomenon is seen in a model of diabetes type 2, a type of diabetes that is not responsive to insulin, in which case PPARβ/δ might be good target for the treatment of T2DM-induced hypertension.

Another observation that was very surprising is that LY294002 inhibits the contraction of the aorta on Naïve tissue. This is puzzling, since the initial hypothesis is that LY294002 inhibits PI3K blocking the downstream pathway and preventing the dilation of the vessel, therefore the opposite effect was expected. It has been described previously a dilatory effect of LY294002 both in aorta (Northcott *et al.* 2002) and mesenteric arteries (Northcott *et al.* 2004) in a rat model of spontaneous hypertension. The authors found that PI3K is overexpressed in the vessels of hypertensive rats, and they also associated PI3K with the activation of Ca^{2+} channels which would increase the intracellular concentration of Ca^{2+} in the vascular smooth muscle cells and contribute to the contraction of the vessel. In this scenario, the inhibition of PI3K by LY294002 would correct the enhanced contraction and relax the artery. However, in the model used in this study the dilatory effect of LY294002 is observed in the Naïve tissue, which does not fit with this explanation, and further investigations need to be done to fully explain this finding.

3.4.1.2 RhoA/ROCK pathway

Direct pharmacological evidence of the effects of PPARβ/δ on inhibiting RhoA/ROCK mediated contraction has so far not been demonstrated possibly due to the complication of RhoA inhibition inducing a lack of contractile tone. Here a novel protocol was developed, which allowed the measurement of this response using a non-RhoA mediated contractile response.

The vasodilatory response of U46619 pre-contracted aorta elicited by GW0742 was significantly inhibited by Fasudil in Naïve but not in STZ-diabetic aorta rings, providing direct pharmacological evidence that GW0742 induces vasodilation mediated in part by the inhibition of RhoA/ROCK activity in Naïve rat contracted arteries but not in STZ. Additionally, because the presence of Fasudil in STZ-diabetic aorta does not have any significant effect on GW0742-induced dilation, that provides further evidence that the RhoA/ROCK pathway is impaired in diabetes and explains why although GW0742 still dilates STZ-diabetic aorta, it is significantly reduced compared to Naïve tissues.

It is worth noting that the maximum concentrations used in the GW0742-induced vasodilation are 300-fold higher than 100 nM, which might have off-target effects as reported in previous studies. Harrington *et al.* (2010) showed that the GW0742-induced dilation of aorta using 30 μM GW0742 are partially regulated by PPARβ/δ, since they observed a decrease on the dilatory effect of GW0742 on PPARβ/δ$^{-/-}$ aorta. Unfortunately, from the experiments performed here it is not clear if the effects of GW0742 are exclusively PPARβ/δ-dependent and further experiments need to be done to clarify this point.

3.4.1.3 Potassium channels

To investigate the contribution of potassium channels to GW0742-mediated dilation, the depolarization of the SMCs of the aorta was induced with high KPSS, which inhibited GW0742-induced depolarization. While GW0742-mediated dilation was inhibited in Naïve rat aorta pre-contracted with high KPSS, it was abolished in STZ-diabetic rat aorta, which indicates that GW0742-mediated dilation of aorta involves potassium channels more in the diabetic state.

Again, from this experiment it is not clear whether the effect of GW0742 is mediated by PPARβ/δ or it is off-target, and extra experiments need to be done to clarify this question.

3.4.2   Mesenteric arteries

3.4.2.1 PI3K/Akt/eNOS pathway

Insulin significantly decrease mesenteric arteries contraction both in health and disease. This contraction is only partially inhibited by LY294002, suggesting that insulin inhibits contraction not only through the PI3K/Akt/eNOS pathway but involving other mechanisms of action. Supporting this finding, it has been shown that insulin relaxes rat mesenteric arteries mediated by large-conductance Ca^{2+}-activated K^+ channels (Iida *et al.* 2001).

Similarly, PPARβ/δ also significantly reduces contraction in Naïve and STZ-diabetic mesenteric arteries. It is worth noting that Figure 3.13 B does not show this inhibitory effect on STZ-diabetic artery and, although it was not possible to confirm the reason for this lack of effect, there is a high possibility that the GW0742 used in this batch of experiments was off. Nevertheless, because most of the data show the inhibition of STZ-diabetic mesenteric artery contraction by GW0742 which also agrees with the majority of the literature published, it was concluded that this result is an isolated phenomenon and that PPARβ/δ inhibits contraction

on STZ-diabetic mesenteric arteries. It was also found that PPARβ/δ inhibits mesenteric artery contraction in a PI3K/Akt/eNOS dependent manner, since it is inhibited by LY294002; however, the pathway used on STZ-diabetic mesenteric arteries remains unclear.

Similar to the results obtained in aorta, the presence of GW0742 and Insulin at same time inhibit each other's effects, which again, is a very surprising finding and cannot be explained with the current data shown in this study, further research is needed to explain this result.

3.4.2.2 *RhoA/ROCK pathway*

GW0742 induces dilation of PE pre-contracted Naïve and STZ-diabetic rat mesenteric arteries. This dilation is inhibited by Fasudil on STZ-diabetic tissues but not in Naïve rat tissues, suggesting that GW0742 induces dilation mediated by the RhoA/ROCK pathway more in STZ-diabetic than in Naïve rat mesenteric arteries.

Interestingly, the GW0742 dilatory effect is not blocked in the presence of GSK3787, suggesting that this beneficial effect is PPARβ/δ-independent. This agrees with a previous study done by Harrington *et al.* (2010), where they did not find any significant difference on the dilatory effect of GW0742 on mesenteric arteries of wild control mice compared to PPARβ/δ$^{-/-}$ animals.

3.4.2.3 *Potassium channels*

The depolarization of the SMCs of the mesenteric arteries was induced with high KPSS which inhibited GW0742 induced depolarization. GW0742-mediated dilation was abolished in Naïve rat mesenteric arteries pre-contracted with high KPSS, but it was inhibited in STZ-diabetic rat aorta, which indicates that GW0742-mediated dilation of mesenteric artery involves potassium channels more in Naïve rat tissue.

3.4.3 Conclusion

The evidence provided shows that PPARβ/δ inhibits contraction of aorta and mesenteric arteries from Naïve and Type 1 diabetic rat model. The impairment of the RhoA/ROCK pathway contributes the most to the dysfunctional contraction in aorta, while other pathways such as PI3K/Akt/eNOS or potassium channels have a more relevant role in the dysfunction of STZ-diabetic rat mesenteric arteries.

In large systemic arteries such as aorta, GW0742 activates PPARβ/δ which will act through the PI3K/Akt/eNOS pathway to improve the dilation on STZ-diabetic vessel. GW0742 also improves the dilation through the RhoA/ROCK pathway in Naïve aorta and through potassium channels in STZ-diabetic aorta, whether this GW0742-dependent dilation is PPARβ/δ-mediated or it is an off target effect is still to be determined (Figure 3.20).

In resistance arteries such as mesenteric arteries, GW0742 activates PPARβ/δ which inhibits the contraction through the PI3K/Akt/eNOS pathway in Naïve and possibly STZ-diabetic tissues. Additionally, GW0742 inhibits the RhoA/ROCK pathway on STZ-induced diabetes in a PPARβ/δ-independent manner and regulates the potassium channels in Naïve mesenteric arteries, although it is not known if the regulation of potassium channels is PPARβ/δ-dependent or an off-target effect (Figure 3.21).
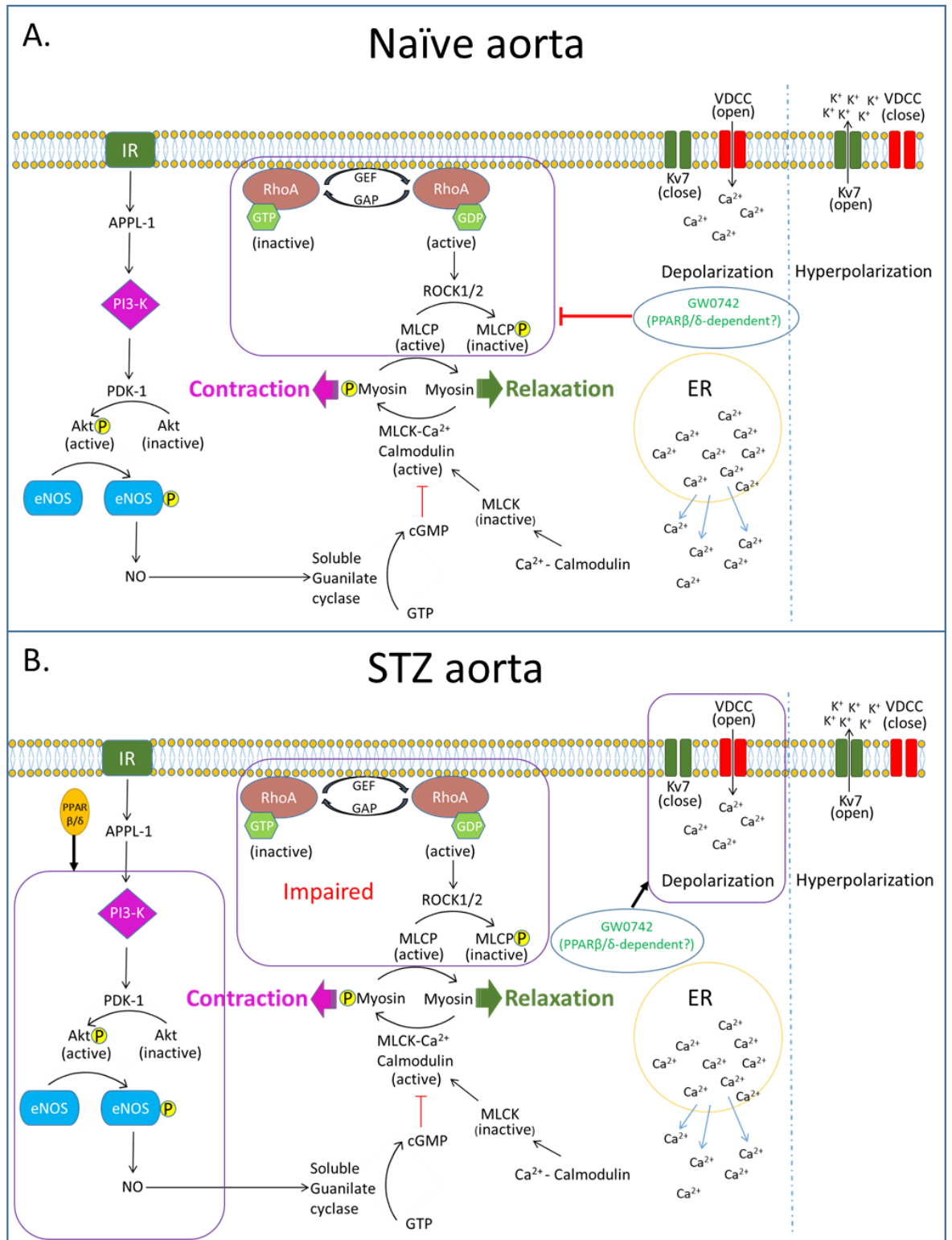
Figure 3.20 Main findings on GW0742-induced dilation of Naïve and STZ-diabetic aorta. A) GW0742 induces Naïve aorta dilation by inhibiting the RhoA/ROCK pathway. Whether this inhibition is PPARβ/δ-dependent or not is still to be confirmed. B) The RhoA/ROCK pathway is impaired in STZ-diabetic aorta. The activation of PPARβ/δ induces dilation through the PI3K/Akt/eNOS pathway. GW0742 also induces dilation through the regulation of K$^+$ channels, whether PPARβ/δ is involved or not is to be confirmed.
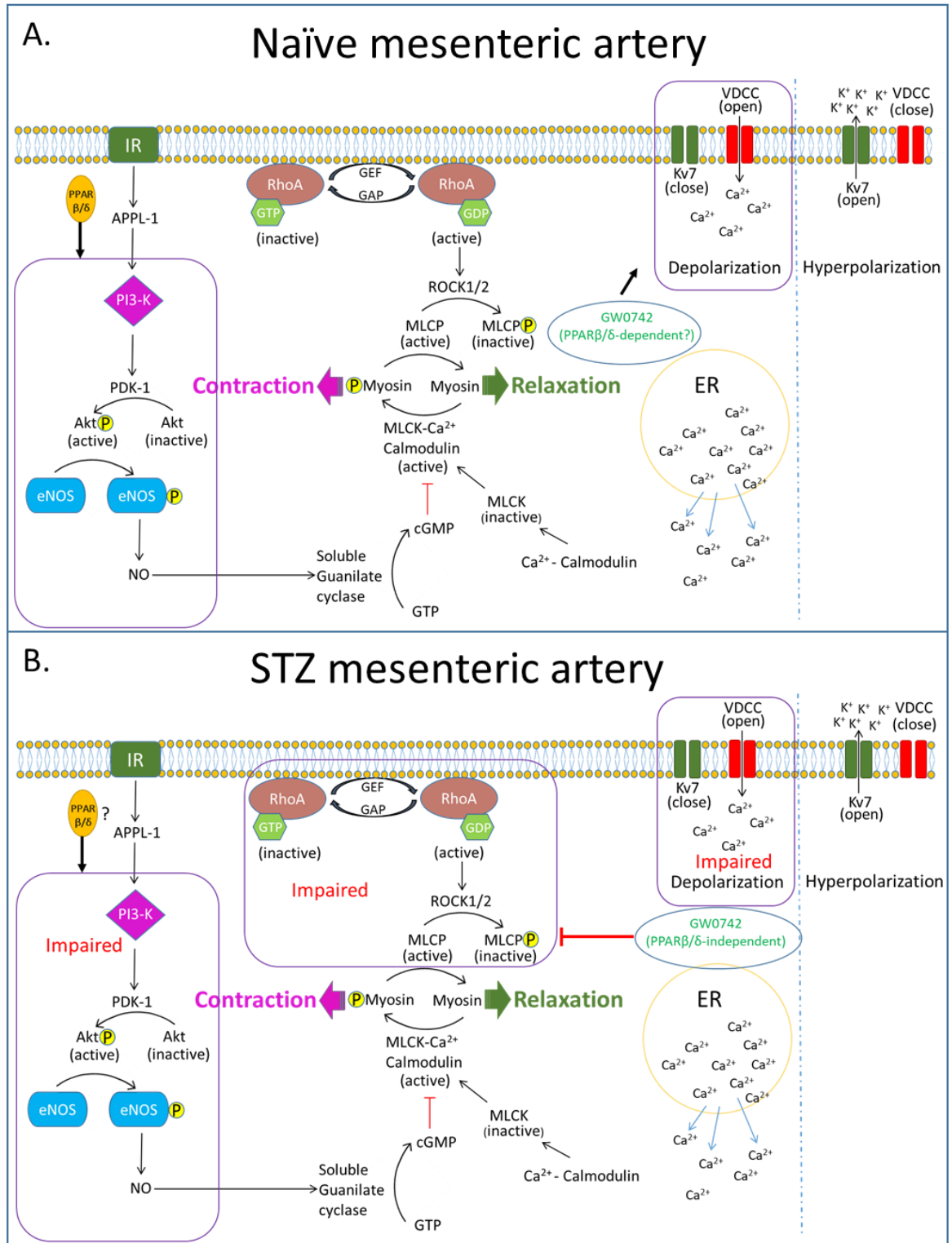
Figure 3.21 Main findings on GW0742-induced dilation of Naïve and STZ-diabetic mesenteric arteries. A) PPARβ/δ induces Naïve mesenteric arteries dilation through PI3K/Akt/eNOS. GW0742 induces dilation through K⁺ channels, not confirmed whether it is PPARβ/δ-dependent or not. B) The RhoA/ROCK pathway, PI3K/Akt/eNOS pathway and K⁺ channels are impaired in STZ-diabetic mesenteric arteries. The activation of PPARβ/δ possibly induces dilation through the PI3K/Akt/eNOS pathway, and GW0742 inhibits RhoA/ROCK pathway in a PPARβ/δ-independent manner.

In conclusion, this chapter provides with some clues of the mechanism underlying the beneficial effects of PPARβ/δ-activation as well as GW0742 off- target effects, and a deeper understanding of dilatory mechanism involved in diabetes, which can help in developing a better strategy for treating diabetes-induced hypertension.

Chapter 4: PPARβ/δ molecular switch.

4.1   Introduction

Understanding how PPARβ/δ switches between induction and trans-repression mode of action and how this determines cellular function is of great interest and may provide new molecular targets for treating a variety of inflammation-dependent diseases, including atherosclerosis, diabetes, and cancer. Whether differences in endogenous and exogenous ligands induce slightly different genes in different cells is a great possibility, and one that has not been so far explored. The question that needs to be addressed is not whether activation leads to proliferation and cancer, but whether the type of agonist activation and the subsequent molecular control can be adjusted to place the cell into a non-proliferative and non-inflammatory state of gene expression. A parallel argument has been made on the cause of the side effects of glucocorticoids; the type of ligand determines whether the glucocorticoid receptor forms a homodimer, and the subsequent type of trans-repression and transcriptional control exerted leads to change in cellular function (Clark and Belvisi 2012).

4.1.1 Hypothesis and objectives

It is hypothesised that PPARβ/δ acts as a molecular switch between induction and trans-repression (Figure 4.1) and depending on which mechanism is triggered it will have pro- or anti-effects.

To test this hypothesis the following will be done:

1- Validate an experimental model where the PPARβ/δ molecular switch is active. This will be identified by the detection of pro- and anti-inflammatory effects after activation and/or blocking of PPARβ/δ.

2- Characterize the PPARβ/δ molecular switch linking the induction and trans-repression mode of action with the pro- or anti-inflammatory response of PPARβ/δ.
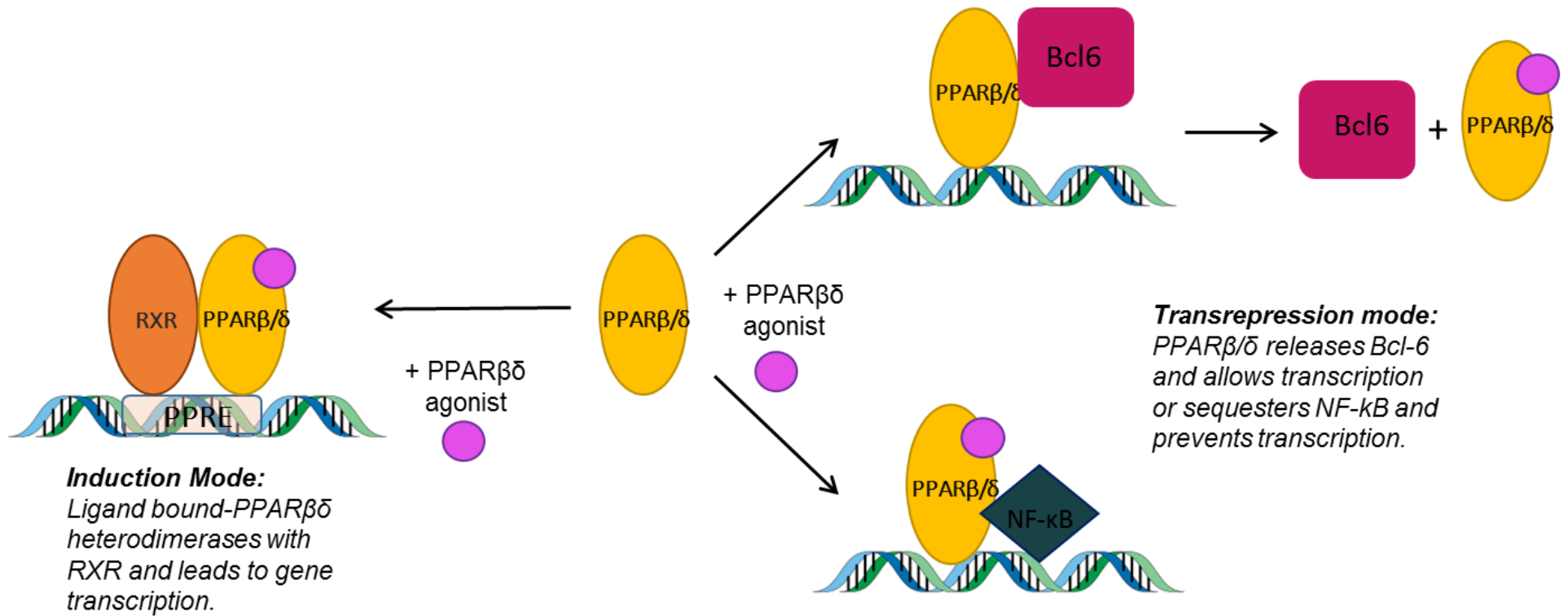
Figure 4.1 Switch between induction and trans-repression mode of PPARβ/δ. The ligand activated response of PPARβ/δ can be either via induction or trans-repression depending on the pre-state of the receptor.

4.2   Validation of drug concentrations

In pharmacology, the concentration of the drug used is preferably based on a dose-response curve previously done in the same system as the actual experiment. However, considering the number of different drugs used and the small amount of tissue obtained per animal (especially pulmonary artery and bronchi), it was not feasible or moral to do one dose-response curve per tissue and per drug because of the large number of animals needed. Instead, a deep research in the literature was done to carefully choose an appropriate concentration.

4.2.1   GW0742.

GW0742 was used to study the regulation of inflammation by PPARβ/α in different human, murine and rat cell types. Treatment with 100 nM GW0742 supresses IFN-γ and IL-12 family cytokines in human immune cells (Dunn *et al.* 2010). The same treatment in the LPS-stimulated murine cell line J44.A1 inhibited the production of TNF-α by direct inhibition of NF-κB transactivation (Zingarelli *et al.* 2010); similarly, primary hepatocytes from mice stimulated with IL-1β showed a significantly reduced transcription of TNF-α after treatment with 100 nM GW0742 (Shan *et al.* 2008).

Moreover, rat cardiomyocytes were activated with LPS and treated with different concentrations of GW0742 (0 to 100 nM), which inhibited the transcription of TNF-α and the proteolysis of IκBα and IκBβ, preventing the translocation of NF-κB to the nucleus (Ding *et al.* 2006). In another study, the treatment with 50 nM GW0742 protected rat cardiac myocytes cells from H_2O_2 oxidative stress, increasing the cell viability and inhibiting apoptosis (Barlaka *et al.* 2015). On the other side it was also shown that the treatment of IL-6 activated rat skeletal muscle cells with 100 nM

GW0742 increases the expression of the genes F*OXO1, atrogin-1, MuRF1* involved in the muscle wasting and responsible for atrophy (Castillero *et al.* 2013).

4.2.2 L-165041

L-165041 is another PPARβ/δ agonist widely used in research that uses human, murine and rat models. For example, it has been reported that high glucose produces adversary effects on endothelial cells (Quintela *et al.* 2014). ROS production by HUVEC incubated in high glucose (30 mM) is significantly reduced by PPARβ/α activation using 1 μM L-165041 (Quintela *et al.* 2014). Similarly, human embryonic kidney 293 (HEK293) cells incubated in high glucose significantly increased the IL-6 production, which was significantly attenuated by treatment with 1 μM L-165041 (Liang *et al.* 2011).

The expression of IL-6 by H9c2 cells, a cell line of rat cardiomyoblasts, was induced with C-reactive protein. This production was again attenuated with the treatment of 1 μM L-165041 which also abolished the translocation of NF-κB to the nucleus (Liang *et al.* 2010). Furthermore, the incubation of rat VSMCs with 1 μM L-165041 significantly inhibited PDGF-induced cellular proliferation and migration (Lim *et al.* 2009). Additionally, the treatment LPS-stimulated rat astrocytes with 1 μM L-165041 significantly decreases the expression of Cox2 (Astakhova *et al.* 2015).

4.2.3 GSK0660

GSK0660, a PPARβ/δ antagonist, was extensively used on human, mouse and rat cells as well. Human skeletal muscle cells incubated with GW0742 increased the transcription of the PPARβ/δ target genes *Pdk-4, Angptl-4* and *Cpt-1*, which was significantly repressed by the coincubation with 1 μM GSK0660 (Shearer *et al.* 2008). Similarly, HUVECs treated with GW0742 showed an increment of *Pdk-4*

levels, which was again abolished by co-incubation with 1 μM GSK0660 (Quintela *et al.* 2014).

C2C12 mouse myotubes treated with palmitate increase the synthesis of TNF-α, which is repressed by GW501516. The protective effect of GW501516 is abolished in the presence of 1 μM GSK0660 (Coll *et al.* 2010). Likewise, GW0742 prevents LPS-induced endothelial dysfunction as well as NO and ROS production in mouse aortic endothelial cells. These protective effects are inhibited by the co-incubation with 1 μM GSK0660. Additionally, the expression of the gene *Ucp2* is increased in the presence of GW0742, which is repressed when these same endothelial cells are co-incubated with 1 μM GSK0660 (Toral *et al.* 2016).

Same antagonist behaviour of GSK0660 was found in rats. The mRNA ppET-1 and p47[phox] upregulation induced by high glucose in rat aortic rings was supressed by GW0742, whose protective effects were inhibited by co-incubation with 1 μM GSK0660 (Quintela *et al.* 2012). In rat cardiac myocytes, the protective effect of GW0742 to H_2O_2 oxidative stress was abolished by 0.5 μM GW0660 (Barlaka *et al.* 2015).

4.2.4   GSK3787

Treatment with 1 μM GSK3787, another PPARβ/δ antagonist, effectively antagonized the GW0742-induced expression of the PPARβ/δ target genes *Pdk-4* and *Ctp1* in human skeletal muscle cells (Shearer *et al.* 2010). Additionally, in another study using cancer cell lines treated with GW0742, the authors showed that 1 μM GSK3787 antagonizes the expression of the PPARβ/δ target genes *Angptl-4* and *Adrp* (Palkar *et al.* 2010).

An *in vivo* model of corneal damage in adult Sprague-Dawley rats showed an improvement on corneal scars after PPARβ/δ activation with GW501516, which was reversed by 1 μM GSK3787 (Gu *et al.* 2014).

4.2.5   1400W

1400W is a potent and selective inhibitor of inducible nitric oxide synthase (iNOS). Left ventricular myocardium from senescence rats was induced by isoproterenol *in vitro* and nitric oxide was measured, which was significantly decreased by treatment with 100 µM 1400W (Birenbaum *et al.* 2008).

In another study, alveolar macrophages (AM) were co-cultured with pulmonary microvascular endothelial cells (PMVEC) at an AM:PMVEC ratio of 3:1. The albumin leak under 3 ng/mL cytomix stimulation was measured and it was found to be inhibited by 100 µM 1400W (Farley *et al.* 2008).

Based on the studies mentioned above, the concentrations chosen for the experiments in this study are the ones shown in the Table 4.1 below.

Table 4.1 Concentrations of drugs used in Chapter 4 and publications using same concentrations

Drug	Concentration (µM)	Publications
GW0742	0.1	(Sznaidman *et al.* 2003, Ding *et al.* 2006, Shan *et al.* 2008, Dunn *et al.* 2010, Zingarelli *et al.* 2010, Castillero *et al.* 2013, Barlaka *et al.* 2015)
L-165041	1	(Berger *et al.* 1999, Lim *et al.* 2009, Liang *et al.* 2010, Liang *et al.* 2011, Quintela *et al.* 2014, Astakhova *et al.* 2015)
GSK3787	1	(Palkar *et al.* 2010, Shearer *et al.* 2010)
GSK0660	1	(Shearer *et al.* 2008, Coll *et al.* 2010, Quintela *et al.* 2012, Quintela *et al.* 2014, Barlaka *et al.* 2015, Toral *et al.* 2016)
1400W	100	(Birenbaum *et al.* 2008, Farley *et al.* 2008)

4.3 Methods

4.3.1 Samples and treatments used

Since PPARβ/δ is expressed and highly active in the lung (Di Paola *et al.* 2010, Li *et al.* 2012) and it is involved in the inflammatory response (Barish *et al.* 2008, Fan *et al.* 2008), pulmonary smooth muscle cells (PSMCs) as well as different lung tissues from rat (pulmonary artery, bronchi and parenchyma) were used as an experimental system.

PSMCs were grown from Naïve rat pulmonary artery extracts, as explained in Chapter 2 Section 2.7, and incubated for 24 h under 5% CO_2 at 37 °C with one of the treatments shown in the Table 4.2 below. The markers of inflammation IL-6 and NO were measured after 24 h incubation as explained in Chapter 2.

Pulmonary artery, bronchi and lung parenchyma from Naïve rats were dissected as explained in Chapter 2 Section 2.4, and immediately placed in a final volume of 500 µL of DMEM containing 1% penicillin/streptomycin and one of the treatments shown in Table 4.2 below. Tissues were incubated in 5% CO_2 at 37 °C, the inflammation biomarker NO was measured at 8 h, 20 h and 24 h in order to monitor the evolution of the inflammation on time, and IL-6 at 24 h incubation, as explained in Chapter 2 Sections 2.10 and 2.11 respectively.

Table 4.2 Treatments of tissues. Two different combinations of agonists and antagonists were used to confirm the results.

	Combination 1	**Combination 2**
Vehicle	0.01% DMSO	0.01% DMSO
LPS	1 µg/mL LPS	1 µg/mL LPS
LPS + agonist	1 µg/mL LPS + 0.1 µM GW0742	1 µg/mL LPS + 1 µM L-165041
LPS + antagonist	1 µg/mL LPS + 1 µM GSK3787	1 µg/mL LPS + 1 µM GSK0660
LPS + agonist + antagonist	1 µg/mL LPS + 0.1 µM GW0742 + 1 µM GSK3787	1 µg/mL LPS + 1 µM L-165041 + 1 µM GSK0660
LPS + 1400W	1 µg/mL LPS + 100 µM 1400W	1 µg/mL LPS + 100 µM 1400W

4.4   Results.

131

4.4.1   Inflammatory response regulated by PPARβ/δ in rat PSMCs

LPS increased IL-6 production after 24h incubation, GW0742 does not have an effect and GSK0660 significantly decreases IL-6 production (Figure 4.2 A). The expression of iNOS, an enzyme that is induced in inflammation, was analysed by Western blot; however, as shown in Figure 4.2 B, the iNOS polyclonal antibody detects several bands. According to the manufacturer, the molecular weight of iNOS is 132 kDa (indicated with an arrow), but this information is not enough to conclude that this band corresponds to iNOS.
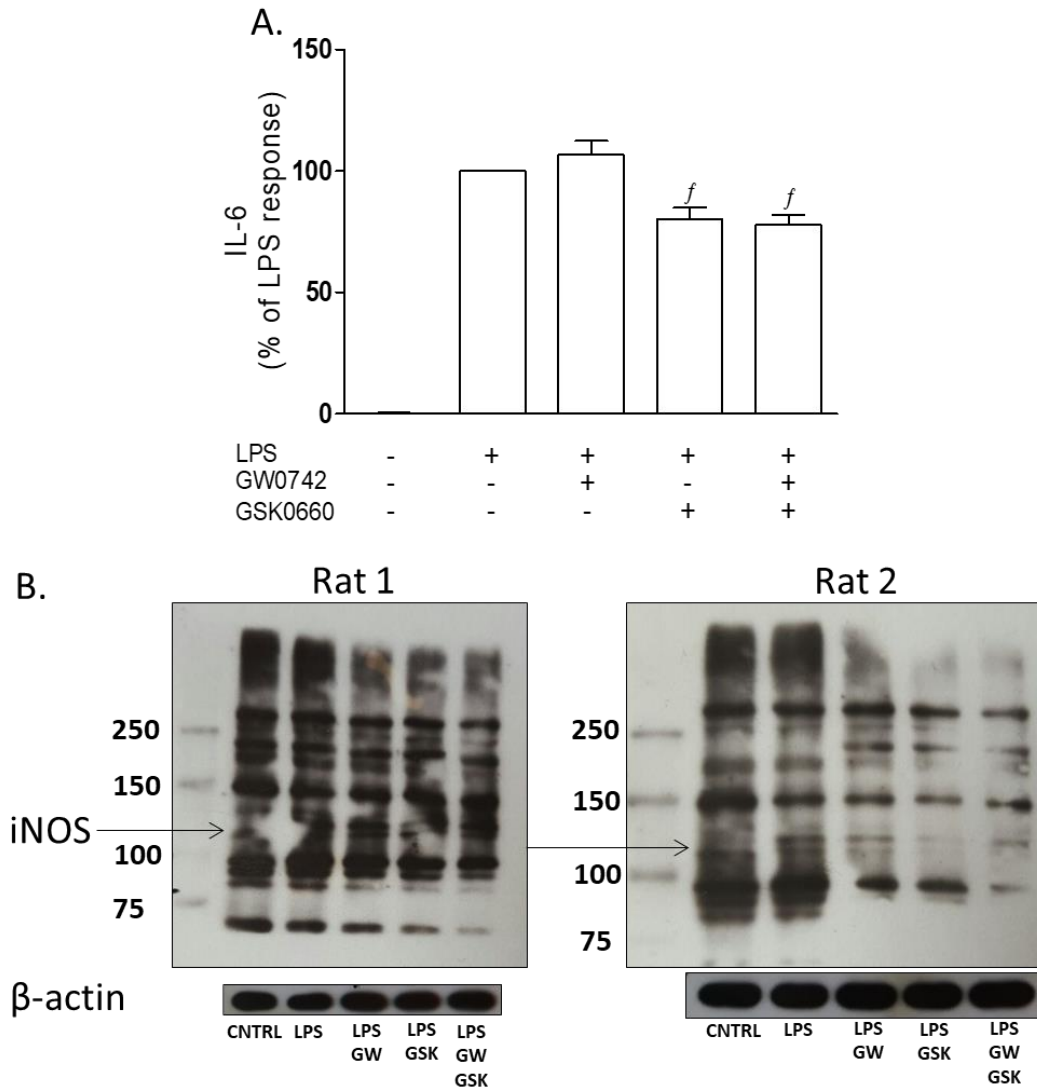
Figure 4.2 Regulation of the inflammatory response by PPARβ/δ in rat PSMCs. A) IL-6 released by rat PSMCs incubated for 24 h with different combinations of 1 µg/mL LPS, 100 nM GW0742 and 1 µM GSK0660. Each experiment (n=3) was normalized with LPS treatment and the results are expressed as a fold change vs LPS. The significant difference between treatments was analysed by one-way ANOVA followed by Bonferroni post-hoc test and the data are presented as mean ± standard error of the mean. f=P<0.05 shows difference compared to LPS. B) Differences in iNOS expression after 24 h incubation (n=2) with the same treatments as before. The protein was not quantified and analysed because the uncertainty of knowing which band corresponds to iNOS.

4.4.2 Expression of PPARβ/δ in rat lung

The expression of PPARβ/δ was measured in pulmonary artery (PA), bronchi and parenchyma. Among them, bronchi shows the lowest expression of PPARβ/δ and parenchyma shows an expression two-fold higher than PA (Figure 4.3).
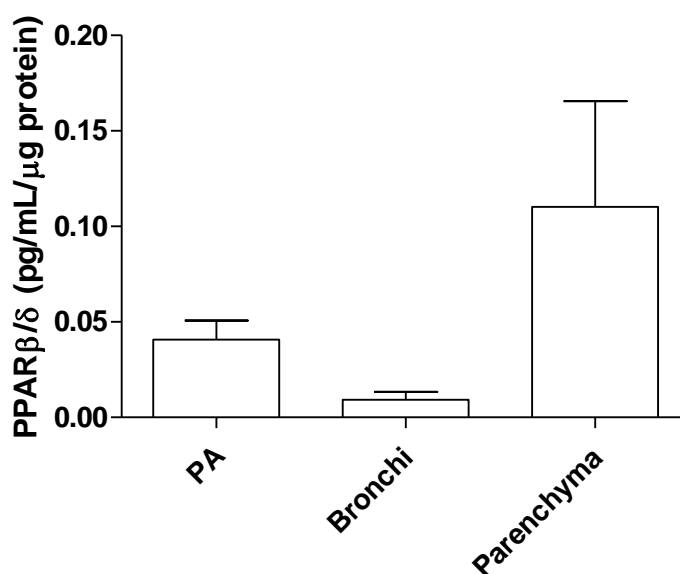
Figure 4.3 Expression of PPARβ/δ in pulmonary artery, bronchi and parenchyma. PPARβ/δ expression in three different tissues from rat lung was quantified by ELISA and normalized by the concentration of protein extracted (n=4)**.** The data are presented as mean ± standard error of the mean.

4.4.3   Inflammatory response regulated by PPARβ/δ in rat lung

The NO produced by pulmonary artery, bronchi and lung parenchyma was measured after 8 h, 20 h and 24 h of incubation. The Figure 4.4 shows that the effects of the treatments for all the tissues tested are greater after 24 h of incubation. An additional experiment was performed to compare 24 h with 48 h of incubation, but the vehicle showed high inflammation after 48 h indicating that another source of inflammation was affecting the tissues at this time point (data not shown). For the reasons exposed above, 24 h of incubation was selected for the subsequent experiments.
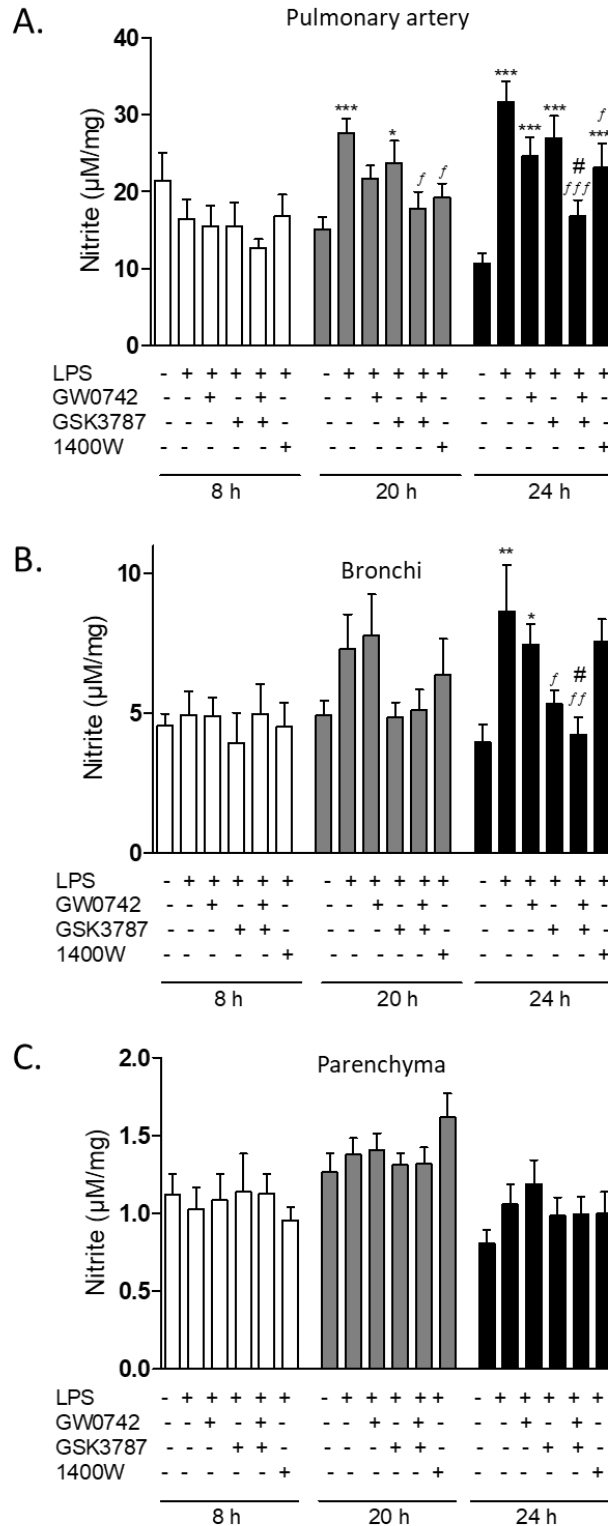
Figure 4.4 NO production by lung tissues over the time. A) Pulmonary artery (n=13), B) bronchi (n=9) and parenchyma (n=14) were dissected, cut into six pieces and incubated under six different treatments of different combinations of 1 µg/mL LPS, 100 nM GW0742, 1 µM GSK3787, 10 µM 1400W; the NO production was measured at 8 h, 20 h and 24 h of incubation. Significant difference between treatments was analysed by two-way ANOVA followed by Bonferroni post-hoc test and the data are presented as mean ± standard error of the mean. *=P<0.05, **=P<0.01, ***=P<0.001 compared with vehicle; *f*=P<0.05, *ff*=P<0.01, *fff*=P<0.001 compared with LPS; #=P<0.05 compared with LPS+GW0742.

4.4.3.1   Pulmonary artery.

The pulmonary artery rings used for the time-line incubations were found to be very small to use for further experiments, for that reason the same experiment was repeated using bigger rings. However, since the amount of pulmonary artery is limited there was only enough tissue to obtain three rings per animal, which means that only two treatments plus vehicle can be performed per animal. NO production was measured after 24 h as shown in Figure 4.5 A. LPS, as expected, significantly increased NO production by 4-fold, the PPARβ/δ ligands GW0742 and GSK3787 on their own do not have a significant effect on LPS-induced NO; surprisingly, the combination of GW0742 and GSK3787 significantly reduces NO production.

In order to confirm this unexpected result, same experiment was repeated using L-165041 as agonist and GSK0660 as antagonist with similar result (Figure 4.5 B), the co-incubation with the agonist-antagonist attenuates the LPS-induced NO production more effectively.

Additionally, IL-6 was also measured as another inflammatory biomarker (Figure 4.6). LPS increases IL-6 production by 10-fold, and the PPARβδ ligands GW0742, L-165041 and GSK0660 do not have a significant effect on their own. However, the antagonist GSK3787 significantly decreases IL-6 production by half, as well as the co-incubation with GW0742-GSK3787 or L-165041-GSK0660.
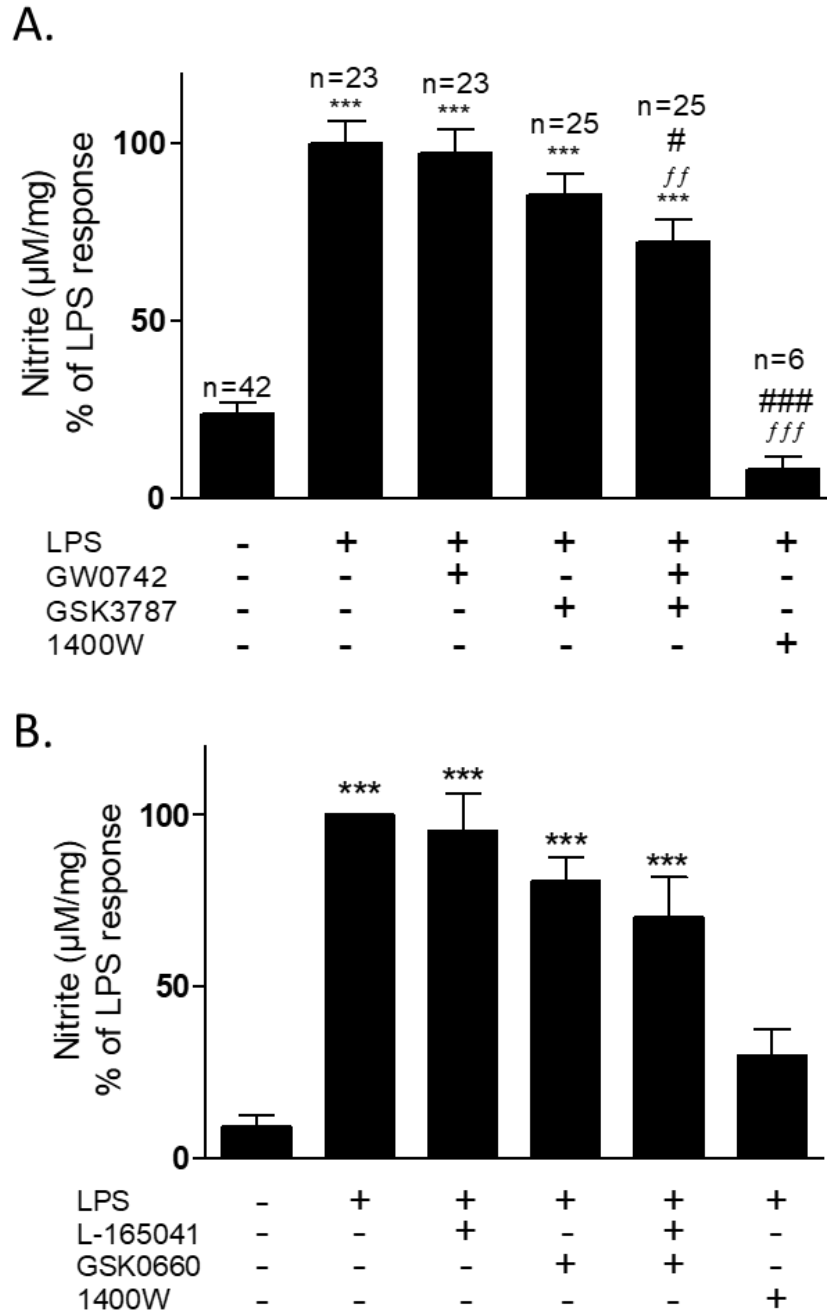
Figure 4.5 NO production by pulmonary artery. Rat pulmonary artery rings were treated with two combinations of PPARβ/δ agonist-antagonist and iNOS inhibitor 1400W: A) 100 nM GW0742 – 1 μM GSK3787 – 100 μM 1400W B) 1 μM L-165041 – 1 μM GSK0660 – 100 μM 1400W. NO production was measured after 24 h and normalized with LPS: A) The average of NO production in LPS was used for the normalization of the data and the number of samples per treatment is written at the top of the bar; B) each experiment was normalized with its own LPS treatment (n=9). Significant difference between treatments was analysed by one-way ANOVA followed by Bonferroni post-hoc test and the data are presented as mean ± standard error of the mean. ***=P<0.001 compared with vehicle; *ff*=P<0.01, *fff*=P<0.001 compared with LPS; #=P<0.05, ###=P<0.001 compared with LPS+GW0742.
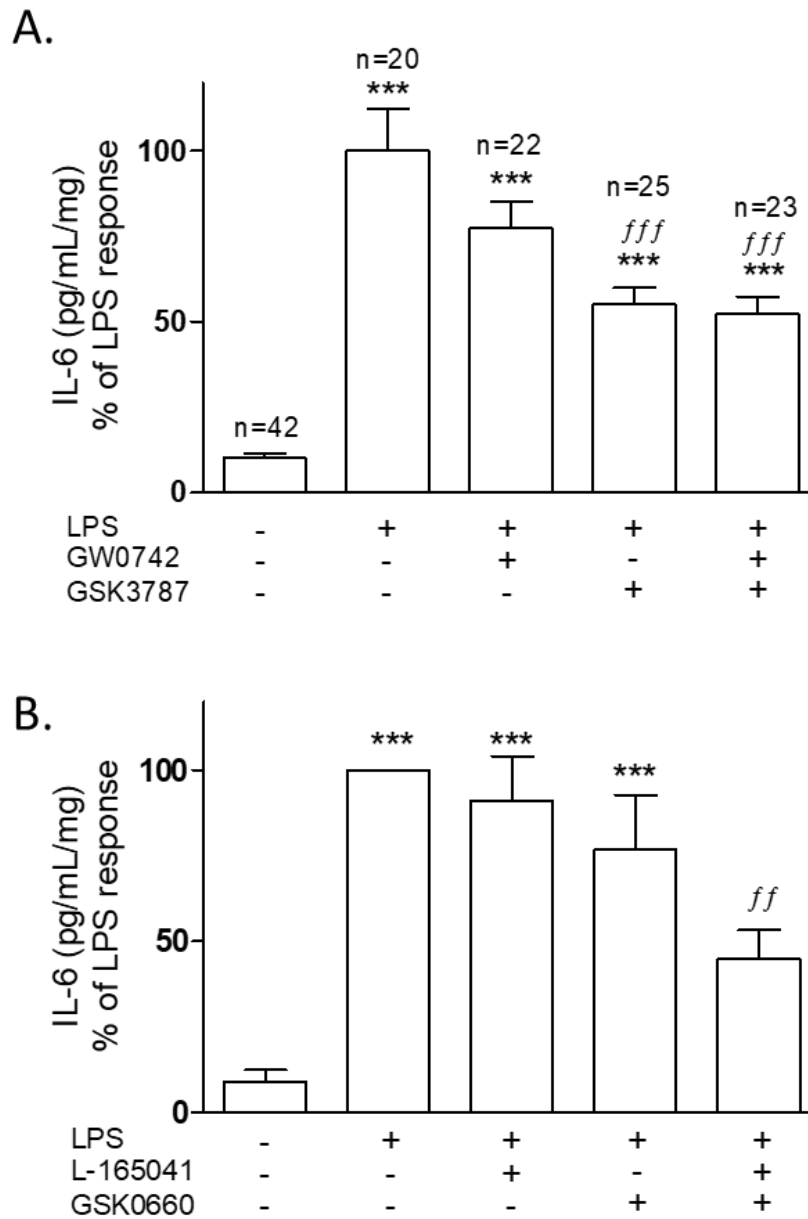
Figure 4.6 IL-6 production by pulmonary artery. Rat pulmonary artery rings were treated with two combinations of PPARβ/δ agonist-antagonist and iNOS inhibitor 1400W: A) 100 nM GW0742 – 1 µM GSK3787 – 100 µM 1400W B) 1 µM L-165041 – 1 µM GSK0660– 100 µM 1400W. IL-6 production was measured after 24 h and normalized with LPS: A) The average of IL-6 production with LPS treatment was used for the normalization of the data and the number of samples per treatment is written at the top of the bar; B) each experiment was normalized with its own LPS treatment (n=9). Significant difference between treatments was analysed by one-way ANOVA followed by Bonferroni post-hoc test and the data are presented as mean ± standard error of the mean. ***=P<0.001 compared with vehicle; *ff*=P<0.01, *fff*=P<0.001 compared with LPS.

4.4.3.2   Bronchi.

NO production in bronchi shows a similar profile to pulmonary artery (Figure 4.7). LPS increases the production of NO 2- to 4-fold with LPS, which is decreased in the presence of the co-incubation with PAPRβ/δ agonist and antagonist, although this reduction showed not to be statistically significant.

Similarly, LPS increases IL-6 production by 2 to 4-fold, but this increment is not significantly affected by the PAPRβ/δ ligands used (Figure 4.8).
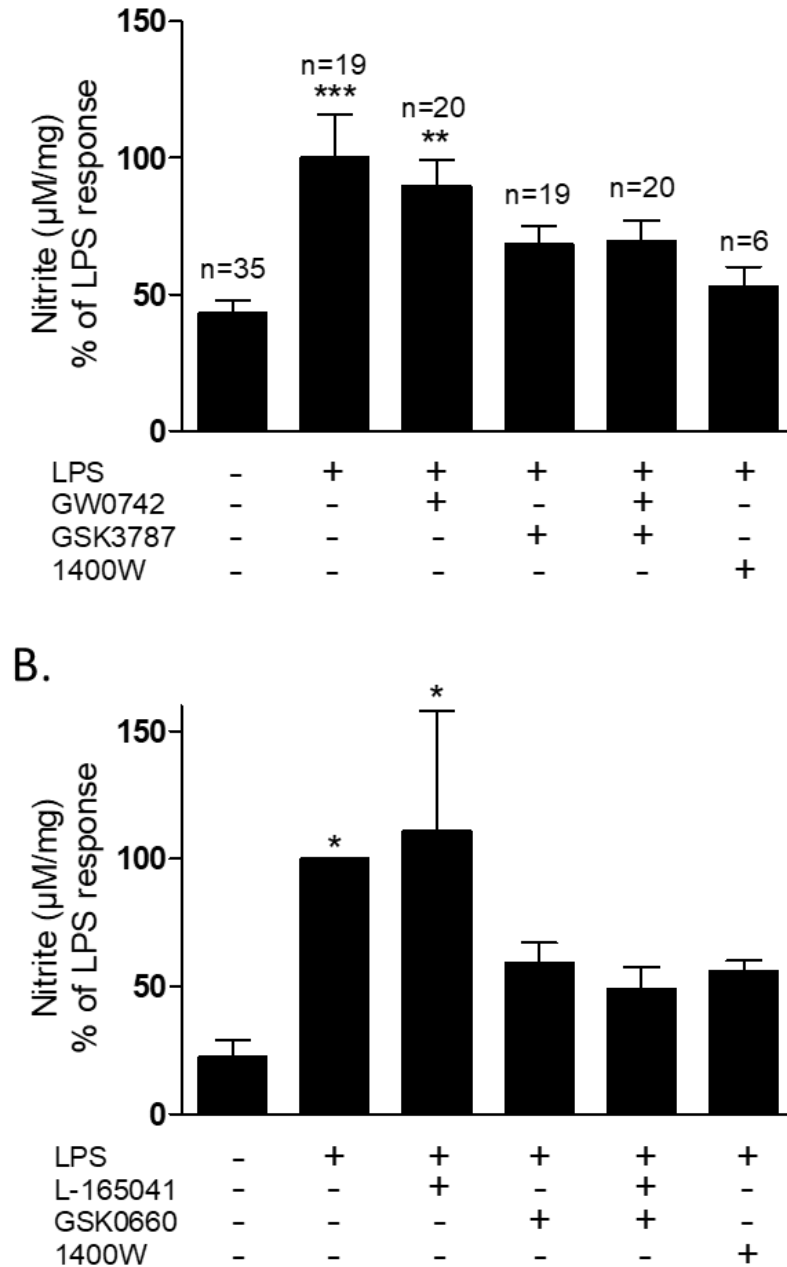
Figure 4.7 NO production by bronchi. Rat bronchi rings were treated with two combinations of PPARβ/δ agonist-antagonist and iNOS inhibitor 1400W: A) 100 nM GW0742 – 1 μM GSK3787 – 100 μM 1400W B) 1 μM L-165041 – 1 μM GSK0660– 100 μM 1400W. NO production was measured after 24 h and normalized with LPS: A) The average of NO production in LPS was used for the normalization of the data and the number of samples per treatment is written at the top of the bar; B) each experiment was normalized with its own LPS treatment (n=5). Significant difference between treatments was analysed by one-way ANOVA followed by Bonferroni post-hoc test and the data are presented as mean ± standard error of the mean. *=P<0.05, **=P<0.01, ***=P<0.001 compared with vehicle.

Figure 4.8 IL-6 production by bronchi. Rat bronchi rings were treated with two combinations of PPARβ/δ agonist-antagonist and iNOS inhibitor 1400W: A) 100 nM GW0742 – 1 µM GSK3787 – 100 µM 1400W B) 1 µM L-165041 – 1 µM GSK0660 – 100 µM 1400W. IL-6 production was measured after 24 h and normalized with LPS: A) The average of IL-6 production with LPS treatment was used for the normalization of the data and the number of samples per treatment is written at the top of the bar; B) each experiment was normalized with its own LPS treatment (n=5). Significant difference between treatments was analysed by one-way ANOVA followed by Bonferroni post-hoc test and the data are presented as mean ± standard error of the mean. *=P<0.05, **=P<0.01, ***=P<0.001 compared with vehicle.

4.4.3.3   Parenchyma.

LPS increases NO production in parenchyma as well by 2-fold, as seen in Figure 4.9. The PPARβ/δ ligands do not have any significantly effect on LPS-induced NO, although the same pattern of NO reduction when agonist and antagonist are present at the same time is followed.

IL-6 is also increased in the presence of LPS by 3 to 4-fold. The PPARβ/δ ligands on their own do not have an effect, however the co-incubation with GW0742 and GSK3787 significantly reduces the LPS-induced IL-6 production by 1-fold.
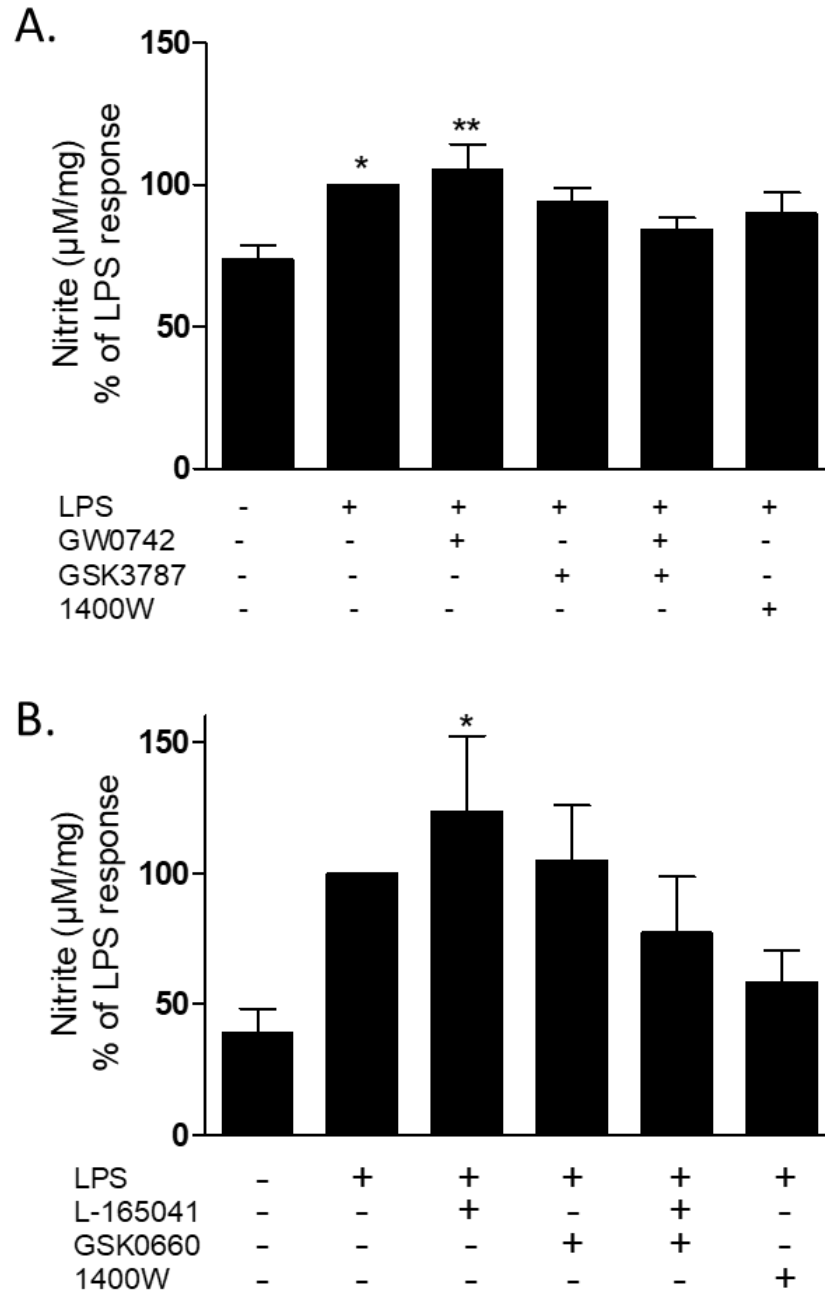
Figure 4.9 NO production by parenchyma. Rat pieces of parenchyma were treated with two combinations of PPARβ/δ agonist-antagonist and iNOS inhibitor 1400W: A) 100 nM GW0742 – 1 μM GSK3787 – 100 μM 1400W (n=10) B) 1 μM L-165041 – 1 μM GSK0660 – 100 μM 1400W (n=7). NO production was measured after 24 h and each experiment was with its own LPS. Significant difference between treatments was analysed by one-way ANOVA followed by Bonferroni post-hoc test and the data are presented as mean ± standard error of the mean. *=P<0.05, **=P<0.01 compared with vehicle.
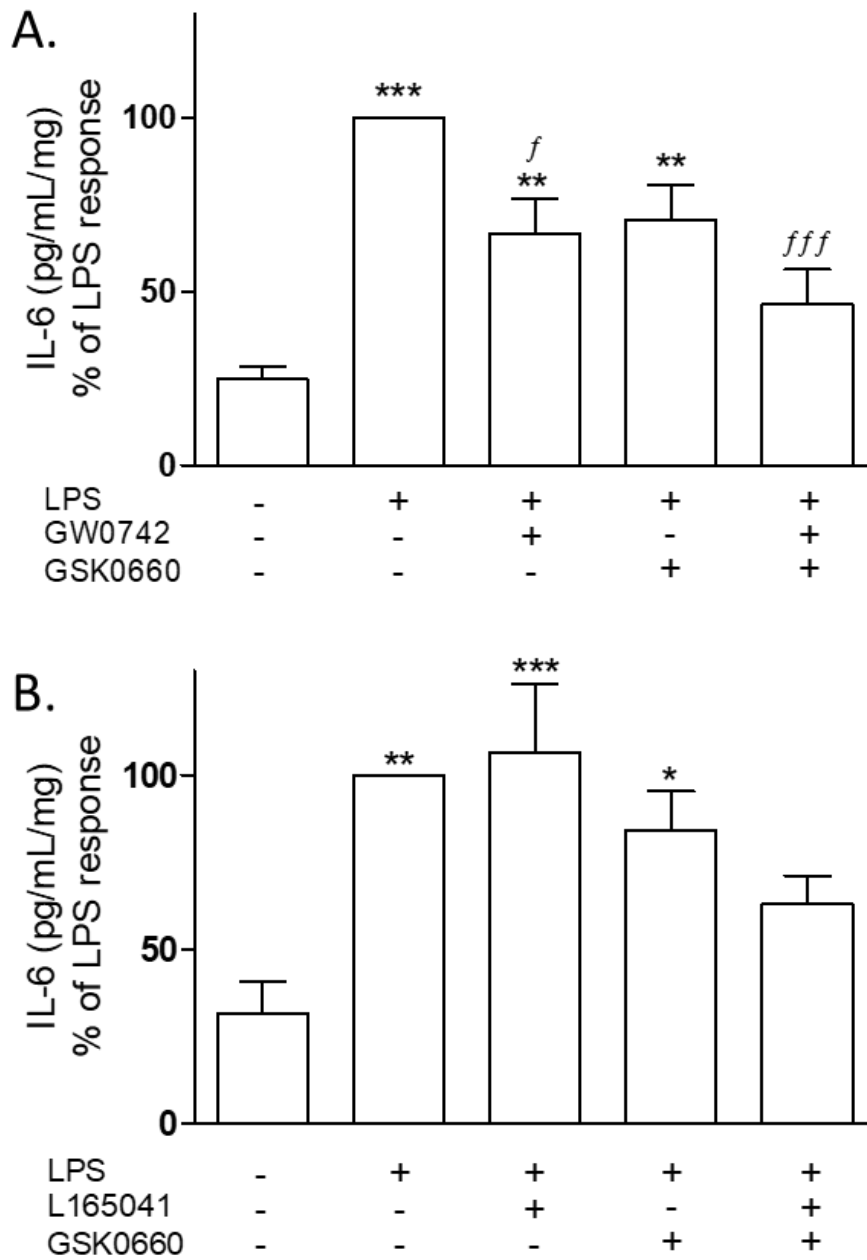
Figure 4.10 IL-6 production by parenchyma. Rat parenchyma pieces were treated with two combinations of PPARβ/δ agonist-antagonist and iNOS inhibitor 1400W: A) 100 nM GW0742 – 1 µM GSK3787 – 100 µM 1400W B) 1 µM L-165041 – 1 µM GSK0660 – 100 µM 1400W. IL-6 production was measured after 24 h and normalized with LPS (n=8). Significant difference between treatments was analysed by one-way ANOVA followed by Bonferroni post-hoc test and the data are presented as mean ± standard error of the mean. *=P<0.05, **=P<0.01, ***=P<0.001 compared with vehicle; *f*=P<0.05, *fff*=P<0.001 compared with LPS.

4.4.4 Verification of the functioning PPARβ/δ molecular switch by co-immunoprecipitation

To confirm that the PPARβ/δ switch is working in this specific model, the immune-precipitation of PPARβ/δ together with the protein bound to it was attempted. The idea is to quantify RXR and NF-κB as markers of the induction and trans-repression mode of action respectively and observe how the ratio RXR:NF-κB changes with the treatment. If the hypothesis is true, there will be a shift of the ratio depending on the pro-inflammatory or anti-inflammatory state of PPARβ/δ.

4.1.1.1 *Covalent antibody immobilization in agarose beads*

The co-immunoprecipitation and relative quantification of the proteins bound to PPARβ/δ is a new approach that needs to be optimised. Two lysates of rat lung where loaded in a column containing the immobilized polyclonal anti-PPARβ/δ from Abcam. All the fractions obtained were run in a SDS-PAGE gel and silver stained to check for any immunoprecipitated protein (Figure 4.11 A). The profiles of the elution and wash fractions are clearly different, indicating that some proteins have been retained in the columns. The molecular weight of PPARβ/δ and RXR is 50 kDa, and the strongest band in the elution fraction is slightly less than 50 kDa, which suggests that PPARβ/δ was successfully retained in the column and the eluted sample is enriched with PPARβ/δ and RXR.

Next step was to identify and quantify PPARβ/δ, RXR and NF-kB by Western blot. Using the same anti-PPARβ/δ used in the column, one clear band of ~30 kDa and one faint band ~75 kDa were identified in the lysates L1 and L2 (Figure 4.11 B-1 indicated with an arrow), both bands very different to the expected 50 kDa. To confirm this result, another polyclonal anti-PPARβ/δ was used (from Santacruz), which detected the same two bands, but this time the one at ~75 kDa appeared stronger (Figure 4.11 B-2 indicated with an arrow).

RXR and p-65 (the NF-κB subunit that physically binds to PPARβ/δ) were also identified. Figure 4.11 B-3 shows a band in the elution fraction E1 of ~50 kDa, as it would be expected if the PPARβ/δ co-immunoprecipitation had been successful, but no band was detected in the lysates L1 or L2. However, it is worth noting that the membrane was exposed to the super-signal ECL substrate for long time and it could be a random blot. On the other hand, p-65 appears in the flow-through and in the lysates (Figure 4.11 B-4), but not in the elution fractions.
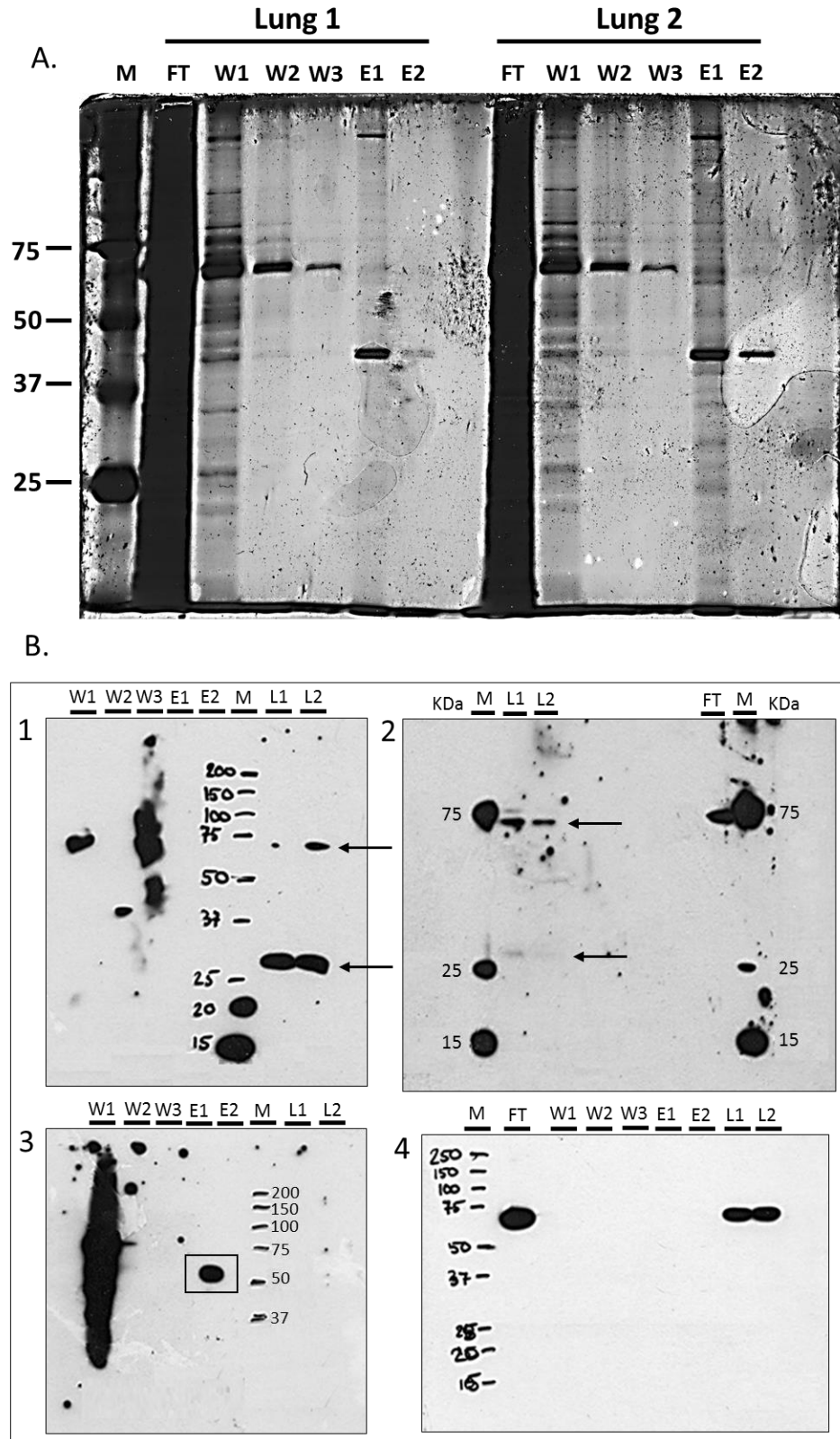
Figure 4.11 Co-immunoprecipitation of PPARβ/δ using polyclonal anti-PPARβ/δ from Abcam in agarose beads. A) Silver stained SDS-PAGE gel of the fractions from the co-immunoprecipitation of two lung lysates from rat. M: marker, FT: flow-through, W1-2-3: washes 1-2-3, E1-2: elution 1-2; L1: lysate from lung 1; L2: lysate from lung 2. B) Immunodetection by Western blot of (1) PPARβ/δ using anti-PPARβ/δ from Abcam; (2) PPARβ/δ using anti-PPARβ/δ from Santacruz, (3) RXR and (4) p-65.

Same experiment was repeated using another immobilized polyclonal anti-PPARβ/δ (from Santacruz). Lung lysate was loaded into the column and all the fractions were run in a SDS-PAGE gel for silver staining (Figure 4.12 A), which showed that the elution fraction profiles are again different from the washing fractions. The Western blot using the same anti-PPARβ/δ from Santacruz revealed one band in the flow-through and one band in the elution fraction of ~50 kDa (Figure 4.12 B), and the detection of PPARβ/δ using anti- PPARβ/δ from Abcam in the same membrane detected same band of ~50 KDa in the flow-through (Figure 4.12 C), but none of them identified any protein in the lysate.
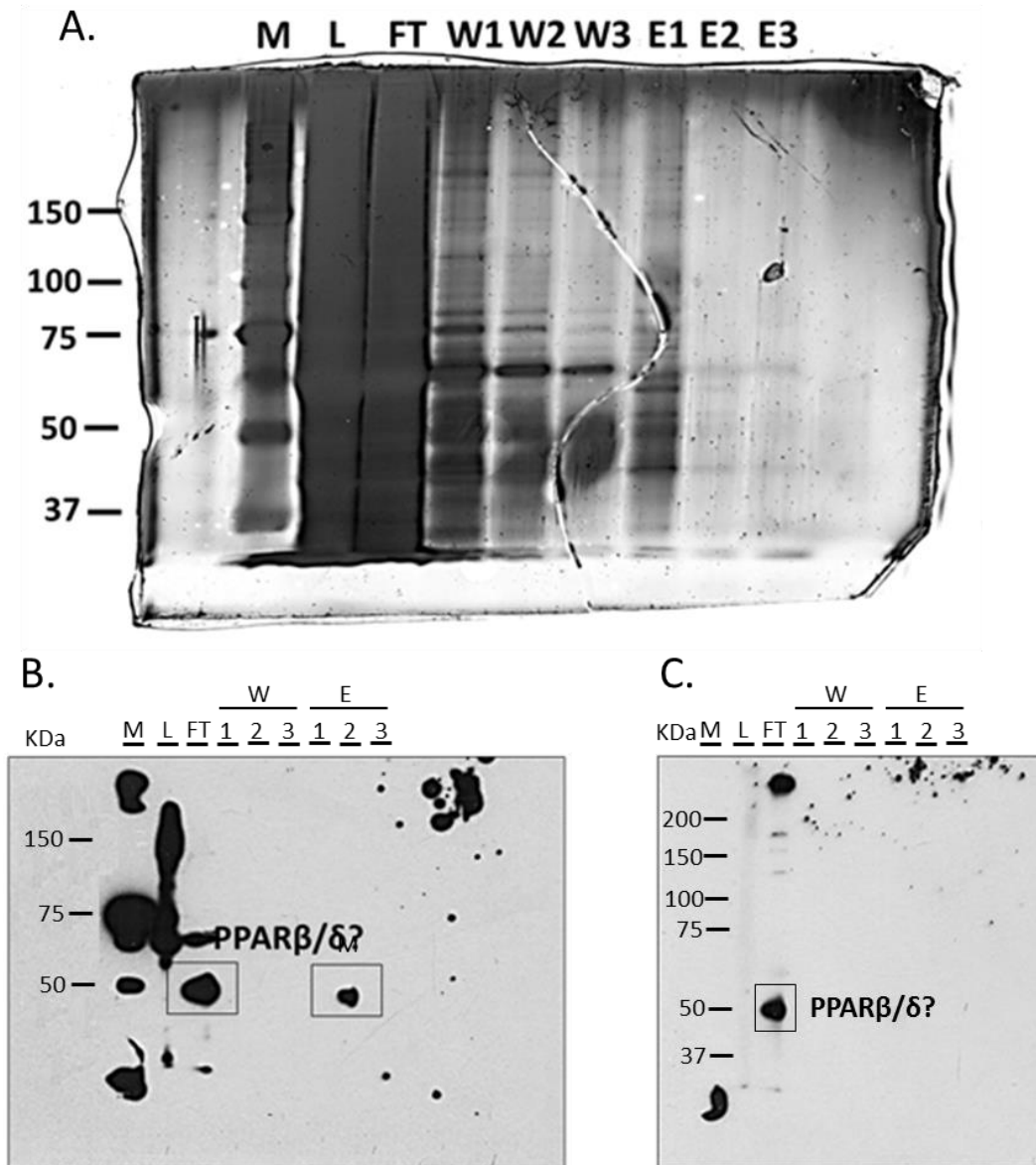
Figure 4.12 Co-immunoprecipitation of PPARβ/δ using polyclonal anti-PPARβ/δ from Santacruz in agarose beads. A) Silver stained SDS-PAGE gel of the fractions from the co-immunoprecipitation of one lung lysate from rat. M: marker, L: lysate, FT: flow-through, W1-2-3: washes 1-2-3, E1-2-3: elution 1-2-3. B) Immunodetection by Western blot of PPARβ/δ using anti-PPARβ/δ from Santacruz and C) using anti- PPARβ/δ from Abcam.

Using the same column with the immobilized anti-PPARβ/δ from Santacruz, two rat PSMCs lysates samples of different treatments were compared, control vs LPS. Figure 4.13 A shows an increase of p-65 after 24 h incubation with LPS, as expected. Because the signal was very intense in the FT, it was possible that it was hiding a weaker signal in the elution fractions, so the FT fraction was physically removed. By doing this, two bands in the elution fractions were detected (Figure 4.13 B), however the molecular weight of these bands are not the same as the one detected in the FT. The membrane was stripped and incubated with polyclonal anti-PPARβ/δ, again excluding the FT (Figure 4.13 C) and same two bands appeared.
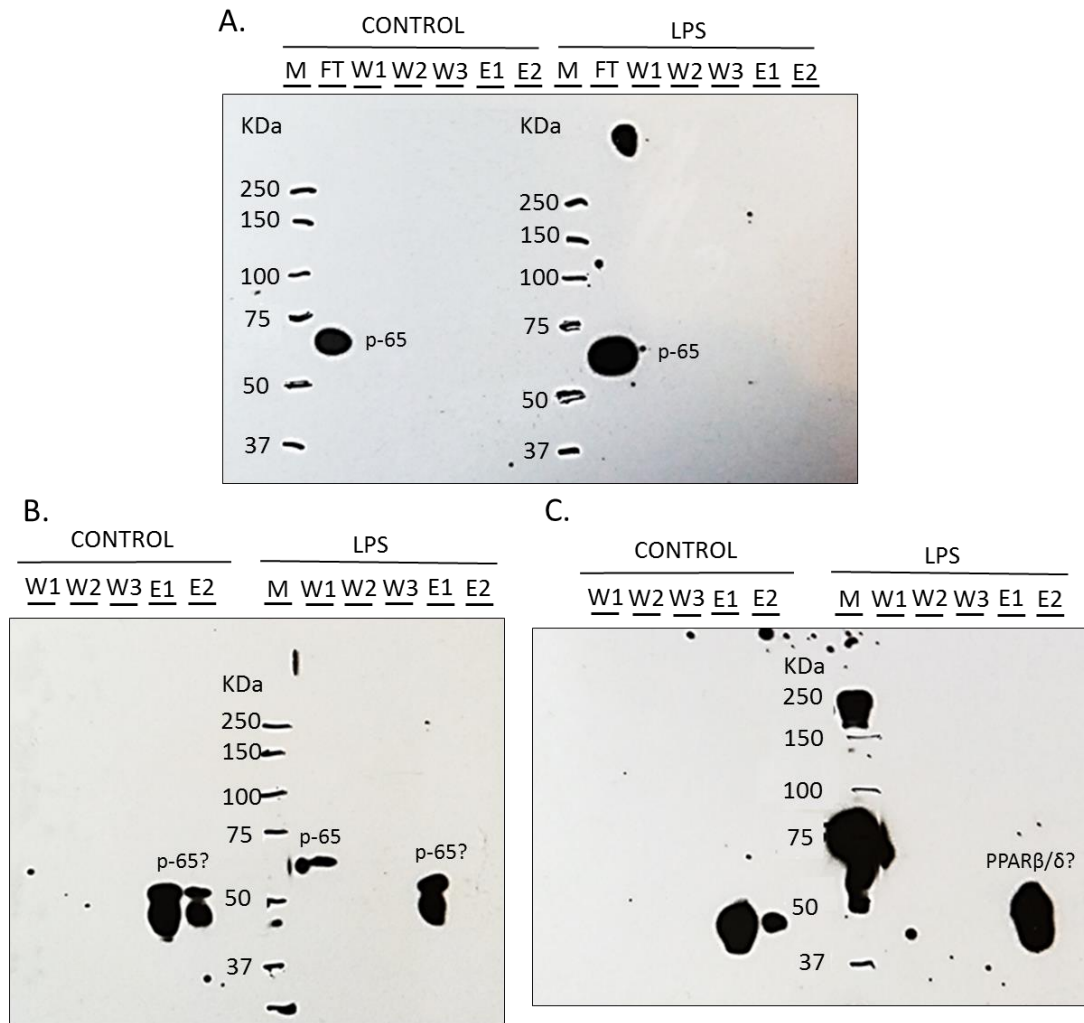
Figure 4.13 Co-immunoprecipitation of PPARβ/δ from rat PSMCs using polyclonal anti-PPARβ/δ from Santacruz in agarose beads. Rat PSMCs were incubated for 24 h with DMEM (control) or with LPS, and the lysates were immunoprecipitated. A) Immunodetection of p-65 in all the fractions, B) Immunodetection of p-65 in Elution and Washing fractions. C) Immunodetection of PPARβ/δ in Elution and Washing fractions.

Two new columns were done using fresh polyclonal anti-PPARβ/δ antibody from Santacruz. The two slurries obtained after the incubation of the antibody with the activated resin were compared to an aliquot of the antibody in an SDS-PAGE gel to check the efficiency of the immobilization of the antibody in the columns (Figure 4.14 A). Also, Western blot conditions for immunodetection of PPARβ/δ, RXRα and p-65 were optimised (Figure 4.14 B, C).
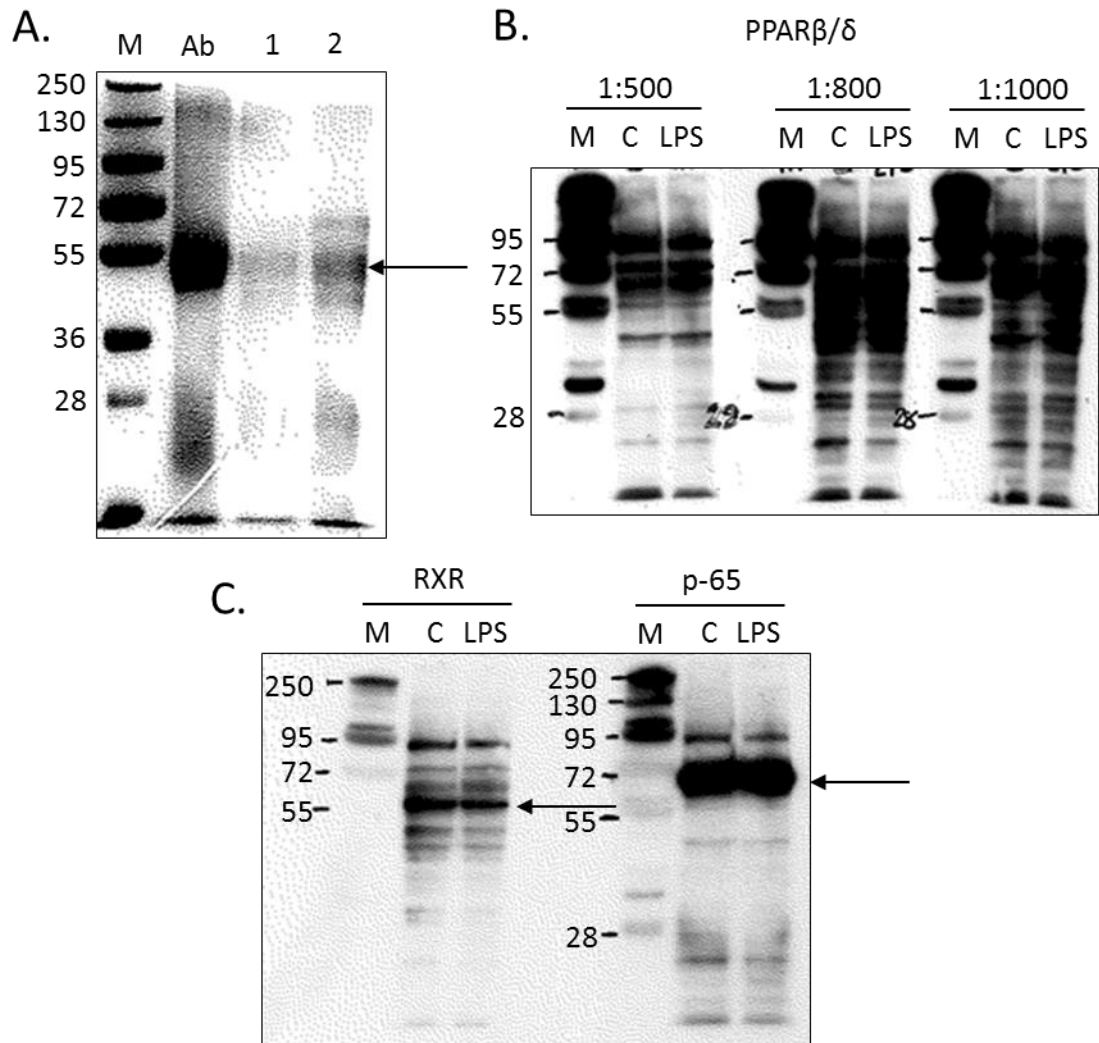
Figure 4.14 Validation of columns and antibodies. A) Verification of the efficiency of the immobilization of the polyclonal anti-PPARβ/δ in the columns. B) Optimization of the conditions of the immunodetection of PPARβ/δ, C) RXRα and p-65 in Western blot. The samples used were lysates of PSMCs control and treated with LPS.

Once it was verified that the anti-PPARβ/δ has successfully bound to the column and the conditions of the antibodies have been optimised for Western blot, a new attempt of Co-IP was done. Two cell lysates treated with LPS or LPS+GW0742 were loaded into these two columns, and the fractions E1 and FT were compared in a SDS-PAGE gel. The membrane was used for the detection of p-65 (Figure 4.15 A), PPARβ/δ (Figure 4.15 B) and RXR (Figure 4.15 C). In all cases two bands of ~50 kDa and ~65 kDa were detected in the E1 fraction. It is worth saying that after each stripping step the membrane was incubated with ECL substrate to make sure that all the protein has been removed from the membrane before adding a new primary antibody. Since all three antibodies detect the same two bands in the E1 fraction, the membrane was stripped once more, blocked and incubated only with the secondary antibody to check for non-specific bindings (Figure 4.15 D), and the same two bands appeared.
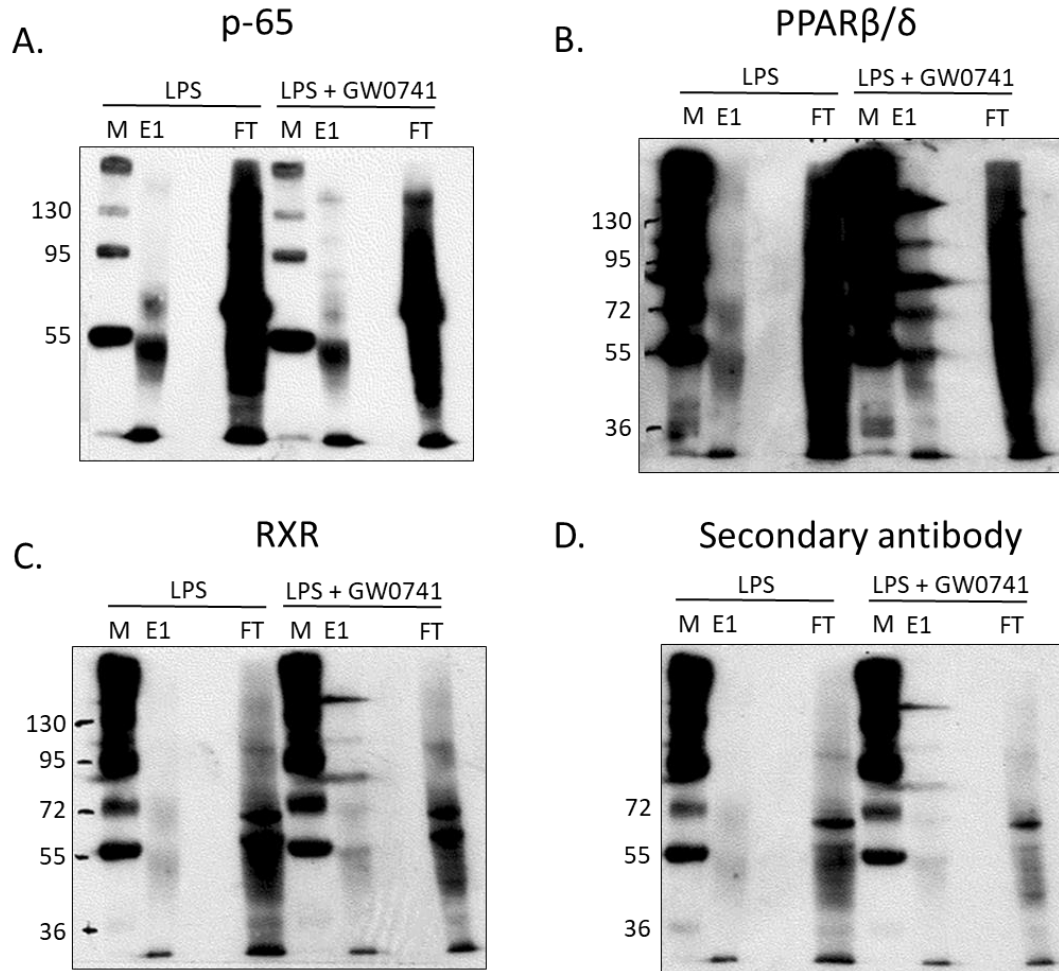
Figure 4.15 Co-immunoprecipitation in agarose beads of PPARβ/δ from lysates of PSMCs treated with LPS and LPS+GW0742. Fractions E1 and FT were run in a SDS-GEL followed by immunodetection of p-65 (A), PPARβ/δ (B) and RXR (C). D is the same membrane incubated only with the secondary antibody. M: marker, E1: elution fraction 1, FT: flow through.

One more attempt was done using lysates of cells incubated with all different treatments (vehicle, LPS, LPS+GW0742, LPS+GSK0660, LPS+GW0742+GSK0660). E1 fractions of each lysate were compared in a SDS-PAGE gel, together with the marker and a positive control, which is one aliquot of the lysate (Figure 4.16). Additionally, the W3 fractions were run in parallel in another SDS-PAGE. As before, the membrane was used for the immunodetection of PPARβ/δ, p-65 and RXR, and the same two bands of ~50 kDa and ~65 kDa were detected in all E1 fractions, which do not match with the band detected in the positive control of each antibody. It is worth noting that the positive control of the membrane incubated with anti-PPARβ/δ detects one single band at ~80 kDa (Figure 4.16 C).

A.

PPARβ/δ

B.

p-65

C.

RXR
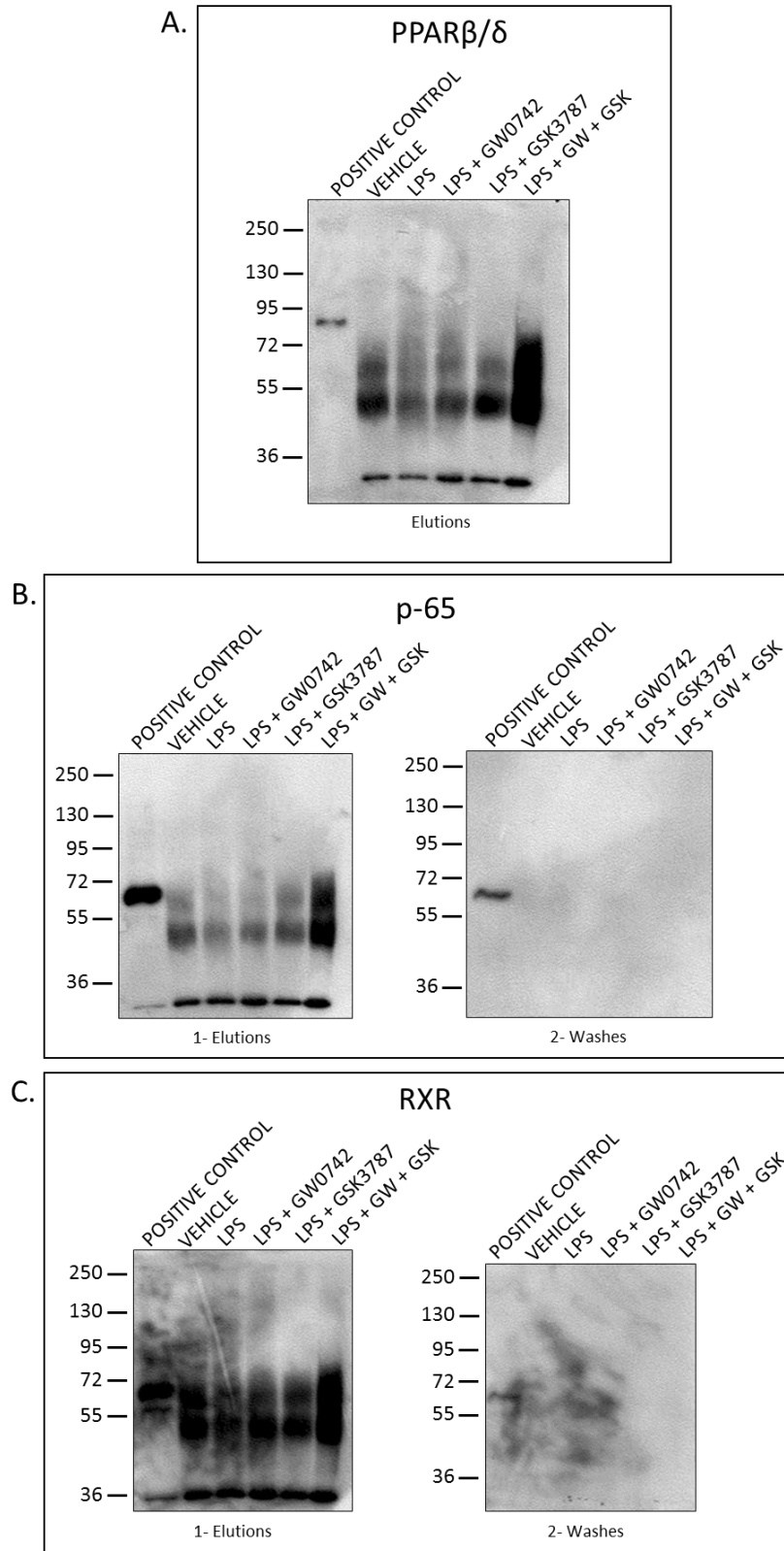
Figure 4.16 Co-immunoprecipitation of PPARβ/δ from lysates of PSMCs in agarose beads.
PSMCs were incubated for 24 h with different treatments (Vehicle, LPS, LPS+GW0742,
LPS+GSK0660, LPS+GW0742+GSK0660), lysed and used for the co-immunoprecipitation of
PPARβ/δ. The elutions and washes of each lysate were run in parallel gels together with the positive
control (an aliquot of the lysate) and a marker. Membranes containing the elutions (1) and washes
(2) of the samples were used for the immunodetection of PPARβ/δ (A), p-65 (B) and RXR (C).

An additional experiment was conducted to find out whether the two bands detected in the elution fractions are anti-PPARβ/δ antibodies that eluted from the column or something else. A new monoclonal anti-PPARβ/δ raised in mouse was immobilized in the column, which cannot be detected by the anti-rabbit antibody used for the detection of RXR, PPARβ/δ and p-65. As before, it was verified that the monoclonal antibody was successfully bound to the column (Figure 4.17 A); then, a lysate of rat PA treated with LPS+GSK3787 was loaded into the column. The three elutions, three washes, and flow-through fractions were run in a SDS-PAGE gel, together with the marker and an aliquot of the cell lysate as a positive control. The membrane was incubated with anti-p-65, which was detected in the positive control and FT (Figure 4.17 B). The membrane was stripped and incubated with RXR, identifying two bands again in the positive control and FT (Figure 4.17 C). To check whether the band at ~65 kDa was detected by anti-RXR antibody or is the result of an unsuccessful stripping, the membrane was stripped again and incubated only with the secondary antibody (Figure 4.17 D). Same band at ~65 kDa appears, indicating that anti-p-65 cannot be removed with the mild stripping protocol used. Finally, the same membrane was incubated with anti-PPARβ/δ, detecting a new band at ~90 kDa again, in the positive control and FT (Figure 4.17 E).

None of the proteins of interest are detected in the elution fractions, indicating that the PPARβ/δ is not being retained in the column and this method was discarded.
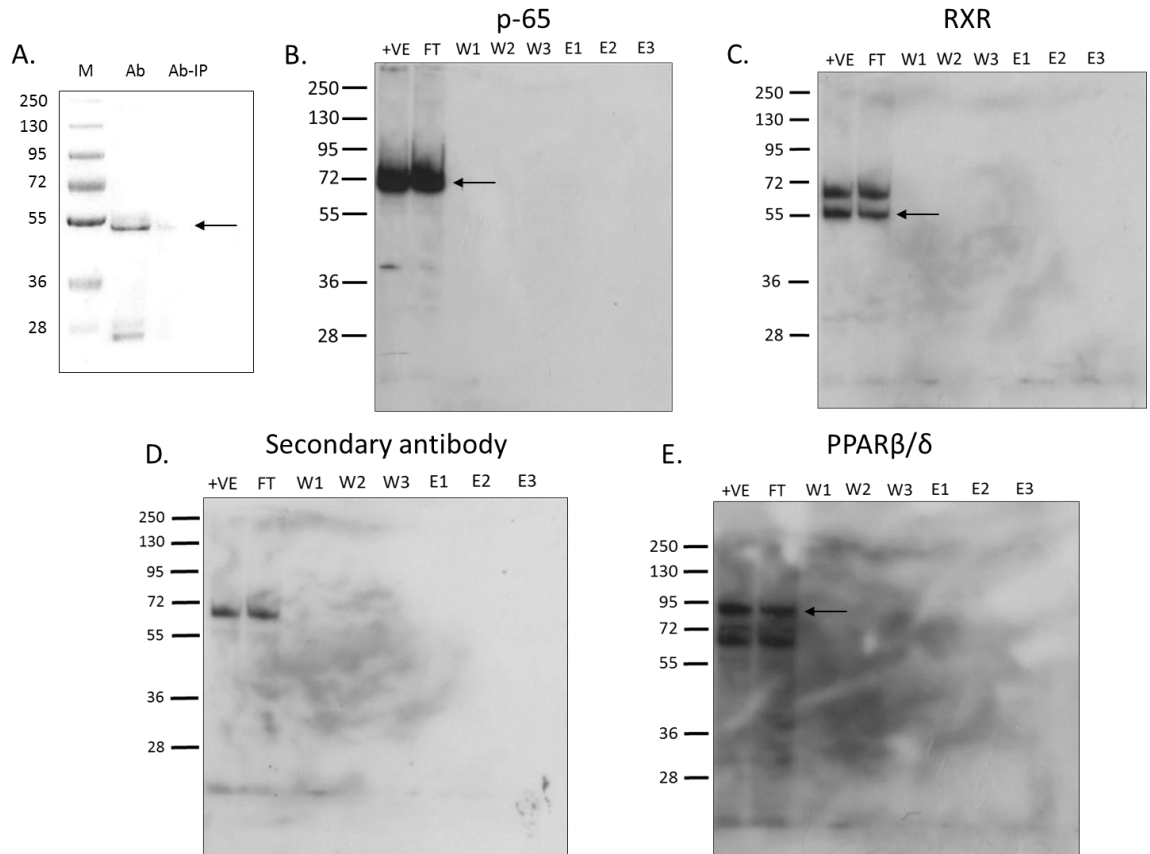
Figure 4.17 Co-immunoprecipitation of PPARβ/δ from pulmonary artery using monoclonal anti-PPARβ/δ antibody in agarose beads. A) Verification of the efficiency of the immobilization of the monoclonal anti-PPARβ/δ in the columns. B) Immunodetection by Western blot of p-65, C) RXR, E) PPARβ/δ of the fractions of the immunoprecipitation. D) Membrane incubated with secondary antibody to test how well the primary antibodies have been removed from the membrane after stripping. +VE: positive control, FT: flow-through, W1-2-3: washing fractions, E1-2-3: elution fractions.

4.4.4.1   Antibody binding protein A/G sepharose beads.

Three ring lysates of pulmonary artery treated as vehicle, LPS+GW0742 and LPS+GSK3787 were used for the co-immunoprecipitation of PPARβ/δ using protein A/G sepharose beads. The flow through and elutions resulted were run in an SDS-PAGE gel together with the marker, one positive control (an aliquot of pulmonary artery lysate) and one negative control (elution of the lysate buffer without sample). The anti-RXR antibody detects one band of ~60 kDa in the positive control and FT, and a higher band of ~70 kDa in all the elutions (Figure 4.18 A). The anti-p65 antibody detects a band of ~70 kDa in the positive control, elutions and FT fractions (Figure 4.18 B). It is worth noting that both antibodies used detect the same band in the elution fractions, including the elution of the negative control, indicating that the antibodies are detecting something coming from the column rather than from the sample.

A.

RXR

B.

p-65
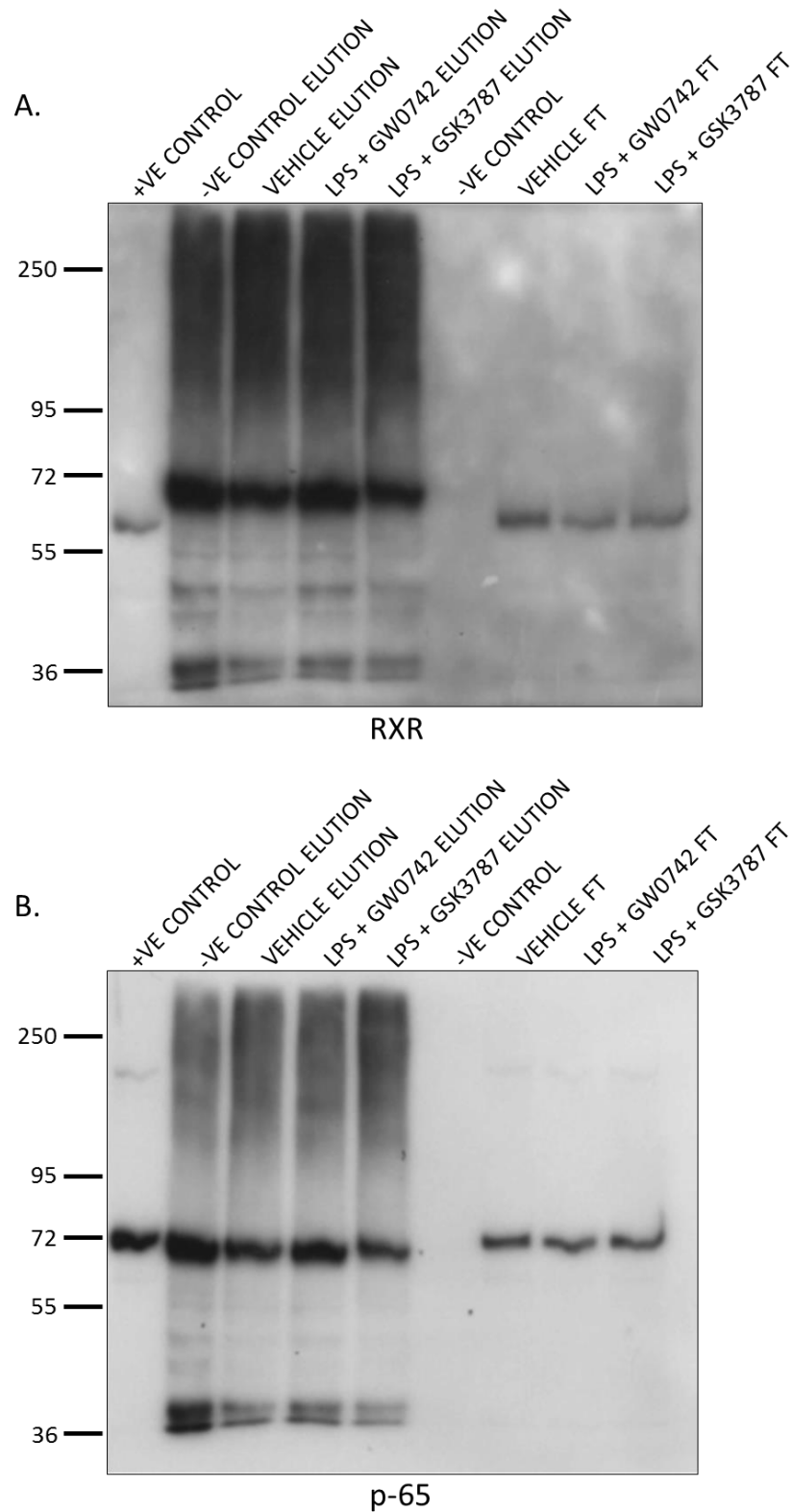
Figure 4.18 Co-immunoprecipitation of PPARβ/δ from pulmonary artery using monoclonal anti-PPARβ/δ antibody and protein A/G sepharose beads. Rat PA rings were treated with vehicle, LPS+GW0742 or LPS+GSK3787 for 24 h and lysed. The lysates were used for the co-immunoprecipitation of PPARβ/δ using protein A/G sepharose beads. The elution fractions, flow through fractions, positive control (PA lysate) and negative controls (lysate buffer) were run in an SDS-PAGE gel and the membrane was use for the immunodetection of A) RXR and B) p-65.

In order to check if the pulmonary artery lysate is somehow incompatible or is affected by the buffers used in this method, a commercial nuclear extract suggested by the manufacturer as a positive control of the monoclonal anti-PPARβ/δ was used for the co-immunoprecipitation of PPARβ/δ. Additionally, a commercial cell lysate as a positive control for Western blot was also used. The elution and flow through fractions resulted from the co-immunoprecipitation of the nuclear extract, an aliquot of the nuclear extract, and an aliquot of the cell lysate were run in a SDS-PAGE gel. The incubation of the membrane with polyclonal anti-PPARβ/δ showed a band in the elution fraction of ~70 kDa, but no bands in the FT or positive controls (Figure 4.19 A). Anti-RXR shows same band of ~70 kDa in the elution fraction and a band of ~60 kDa in the flow through and the nuclear extract, but nothing was detected in the cell lysate (Figure 4.19 B). Similarly, anti-p65 shows a band of ~70 kDa in the elution and flow through fraction, as well as the nuclear extract.
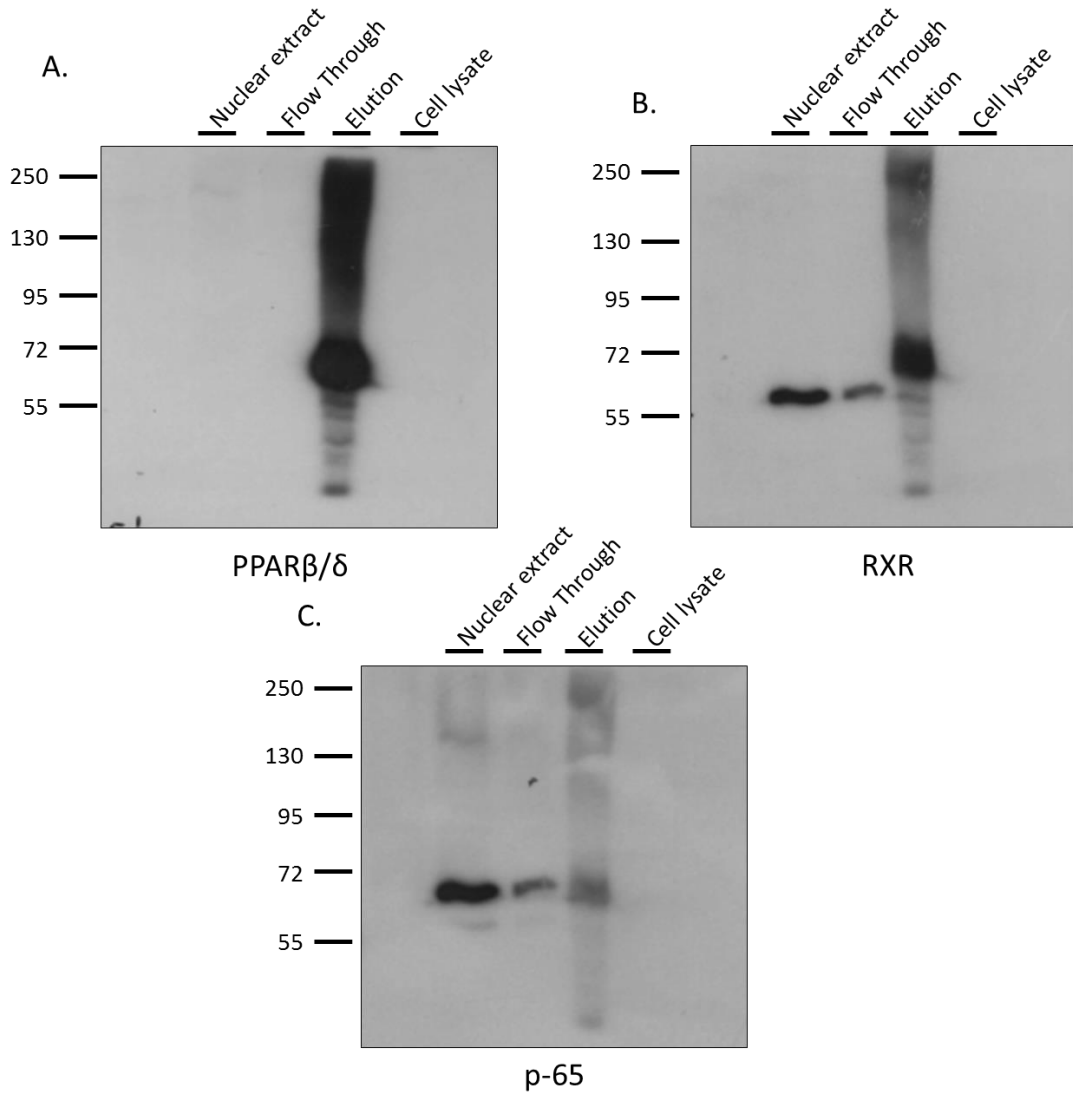
Figure 4.19 Co-immunoprecipitation of PPARβ/δ from the nuclear extract positive control using monoclonal anti-PPARβ/δ antibody and protein A/G sepharose beads. The commercial monoclonal anti-PPARβ/δ positive control was used to co-immunoprecipitate PPARβ/δ. The elution and flow through fractions were loaded into an SDS-PAGE gel together with an aliquot of the nuclear extract as a positive control, and an aliquot of a commercial cell lysate as another positive control. The membrane was incubated with A) polyclonal PPARβ/δ, B) anti-RXR and C) p-65, and the proteins were detected by ECL detection.

Because PPARβ/δ was not detected in any of the positive controls, the monoclonal anti-PPARβ/δ was used to detect the protein. This antibody is the same used in the column, consequently the secondary antibody will detect the anti-PPARβ/δ antibody eluted from the beads. For that reason, the membrane was stripped and incubated with secondary antibody first, showing a band in the eluted fraction of ~50 kDa, which corresponds to the eluted monoclonal anti-PPARβ/δ (Figure 4.20 A). The membrane was stripped once more and incubated with monoclonal anti-PPARβ/δ (Figure 4.20 B). The idea is to identify and remove the signal of the secondary antibody incubation which corresponds to the eluted antibody from the beads from the signal of the monoclonal anti-PPARβ/δ, which corresponds to the actual PPARβ/δ protein. However, as seen in Figure 4.20, there are no differences between them, and PPARβ/δ was still not detected in any of the positive controls or FT.
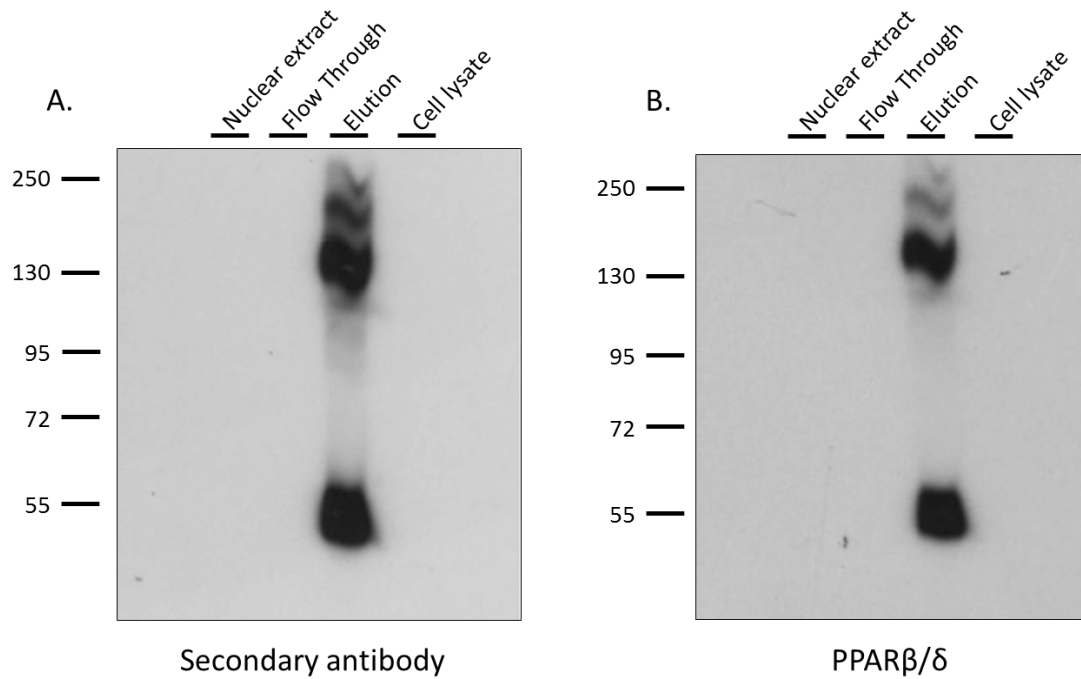
Figure 4.20 Immunodetection of PPARβ/δ in the nuclear extract using polyclonal anti-PPARβ/δ antibody. A) The same membrane was stripped and incubated with A) Anti-mouse secondary antibody. B) The membrane was stripped once more and incubated with polyclonal anti-PPAR

As last attempt, two different amounts of the positive controls nuclear extract and cell lysate were run in two SDS-PAGE gels (25 µg and 50 µg). Each membrane was treated with two different dilutions of the anti-PPARβ/δ antibody, and no band was detected in any membrane (data not shown). As a result, it was concluded that the anti-PPARβ/δ antibodies are not suitable antibodies for this type of experiments.

4.4.5 Verification of the functioning PPARβ/δ molecular switch by RT-qPCR

A different approach was design for the detection of the PPARβ/δ molecular switch. Instead of identifying which protein is bound to PPARβ/δ, marker genes for the induction and trans-repression mode of action were chosen and its transcription or repression was linked with the pro- and anti-inflammatory responses of the tissues tested.

To do that, RNA was extracted from tissues and converted to cDNA as described in Chapter 2.13. Standard curves of the target genes comparing SYBER GREEN and Taqman qRT-PCR were conducted to check the performance of the assay - a slope of the standard curve of -3.3 and an efficiency of 90-110% is considered optimal. The Table 4.3 below shows the slope and efficiency for each gene using SYBR GREEN reagents, and Table 4.4 shows the same data for Taqman in pulmonary artery, bronchi and parenchyma. *Ppfia-1* and *Sema7a* did not amplify with SYBR GREEN and therefore these genes were not tested with Taqman.

The standard curves performed with Taqman are closer to the optimum values than SYBER GREEN, thus all the subsequent qRT-PCR experiments were run using Taqman.

Table 4.3 Primers used for SYBR GREEN qRT-PCR. Standard curves were run with cDNA obtained from pulmonary artery to check for gene amplification and performance.

Gene	Primers sequence	RSq	Slope	Efficiency (%)
β-actin	S (5' to 3'): GCCCTAGACTTCGAGCAAGA AS (5' to 3'): TCAGGCAGCTCATAGCTCTTC	0.970	-2.669	137.0
Pdk-4	S (5' to 3'): CGCTTAGTGAACACCCCTTC AS (5' to 3'): TCCACTAAATCCATCAGGCTCT	0.995	-3.431	95.6
Angptl-4	S (5' to 3'): TCCGAGGGGACCTTAACTGT AS (5' to 3'): ATTGGAATGGCTGCAGGT	0.984	-2.862	123.6
Nos2	S (5' to 3'): ACCATGGAGCATCCCAAGT AS (5' to 3'): CAGCGCATACCACTTCAGC	0.939	-1.803	258.6
Serpine-1	S (5' to 3'): AGAGCCAATCACAAGGCACT AS (5' to 3'): GAGGCAAGTGAGGGCTGA	0.997	-2.561	145.7
Timp-1	S (5' to 3'): CAGCAAAAGGCCTTCGTAAA AS (5' to 3'): TGGCTGAACAGGGAAACACT	0.990	-2.834	125.4
Ppfia-1	S (5' to 3'): ACAAGGAGTCCCTCGTTGAG AS (5' to 3'): TCAAGTTAGAGATCTCAGCCATC	N/A	N/A	N/A
Sema7a	S (5' to 3'): CTATGGCGTTTTCTCCAACC AS (5' to 3'): GTCAATGTCACCAAGCGAATAC	N/A	N/A	N/A

Table 4.4 Primers used for Taqman qRT-PCR. Standard curves were run with cDNA obtained from pulmonary artery, bronchi and parenchyma to check for gene amplification and performance.

Gene	Assay ID	Tissue	RSq	Slope	Efficiency (%)
β-actin	Rn00667869_m1	Pulmonary artery	0.994	-3.304	100.8
		Bronchi	0.984	-3.999	77.9
		Parenchyma	0.998	-3.440	95.3
Pdk-4	Rn00585577_m1	Pulmonary artery	0.983	-3.039	113.3
		Bronchi	0.966	-1.964	223.0
		Parenchyma	0.991	-3.850	81.9
Angptl-4	Rn015228817_m1	Pulmonary artery	0.998	-3.997	77.9
		Bronchi	N/A	N/A	N/A
		Parenchyma	0.988	-3.303	100.8
Nos2	Rn00561646_m1	Pulmonary artery	0.997	-3.763	84.4
		Bronchi	0.990	-3.402	96.8
		Parenchyma	0.995	-3.436	95.5
Serpine-1	Rn01481341_m1	Pulmonary artery	0.943	-3.399	96.9
		Bronchi	0.984	-3.480	93.8
		Parenchyma	0.995	-3.434	95.5
Timp-1	Rn01430873_m1	Pulmonary artery	0.990	-4.155	74.0
		Bronchi	0.923	-3.144	108.0
		Parenchyma	0.994	-3.268	102.3
Id2	Rn01495280_m1	Pulmonary artery	0.877	-3.466	94.3
		Bronchi	0.803	-2.416	159.4
		Parenchyma	0.983	-3.407	96.6

4.4.5.1   qRT-PCR pulmonary artery

Pdk-4 and *Angptl-4* are genes known to be expressed in the induction mode of action of PPARβ/δ (Khozoie *et al.* 2012, Adhikary *et al.* 2015, Klingler *et al.* 2016), therefore they were chosen as markers for this mechanism of action. Figure 4.21 A and B shows a 6-fold significant increase of the transcription of *Pdk-4* and *Angptl-4* in the presence of GW0742, which is inhibited by the antagonist GSK3787.

Timp-1 and *Serpine-1* are two target genes of NF-κB whose expression is activated by LPS (Schreiber *et al.* 2006) and also showed to be regulated by PPARβ/δ (Khozoie *et al.* 2012), therefore they were chosen as marker genes of the PPARβ/δ trans-repression mode of action through NF-κB.

As expected, the transcription of *Timp-1* is increased 1-fold by LPS in pulmonary artery, (Figure 4.21 C), and the agonist-activation of PPARβ/δ blocks the transcription by 4-fold compared to LPS. Interestingly, the treatment with LPS+GW0742+GSK3787 decreases the transcription of *Timp-1* to the same level as the treatment with LPS+GW0742. The one-way ANOVA statistical analysis showed significant differences between treatments, and the post-hoc test showed a borderline significant difference between LPS vs LPS+GW with a p-value=0.0556 and LPS vs LPS+GW+GSK p-value=0.0617.

Serpine-1 shows the same transcription profile as *Timp-1*, LPS increases the transcription and GW0742 inhibits the transcription by 3-fold compared to LPS, although the differences between treatments are not significantly different (Figure 4.21 D).

Pulmonary artery
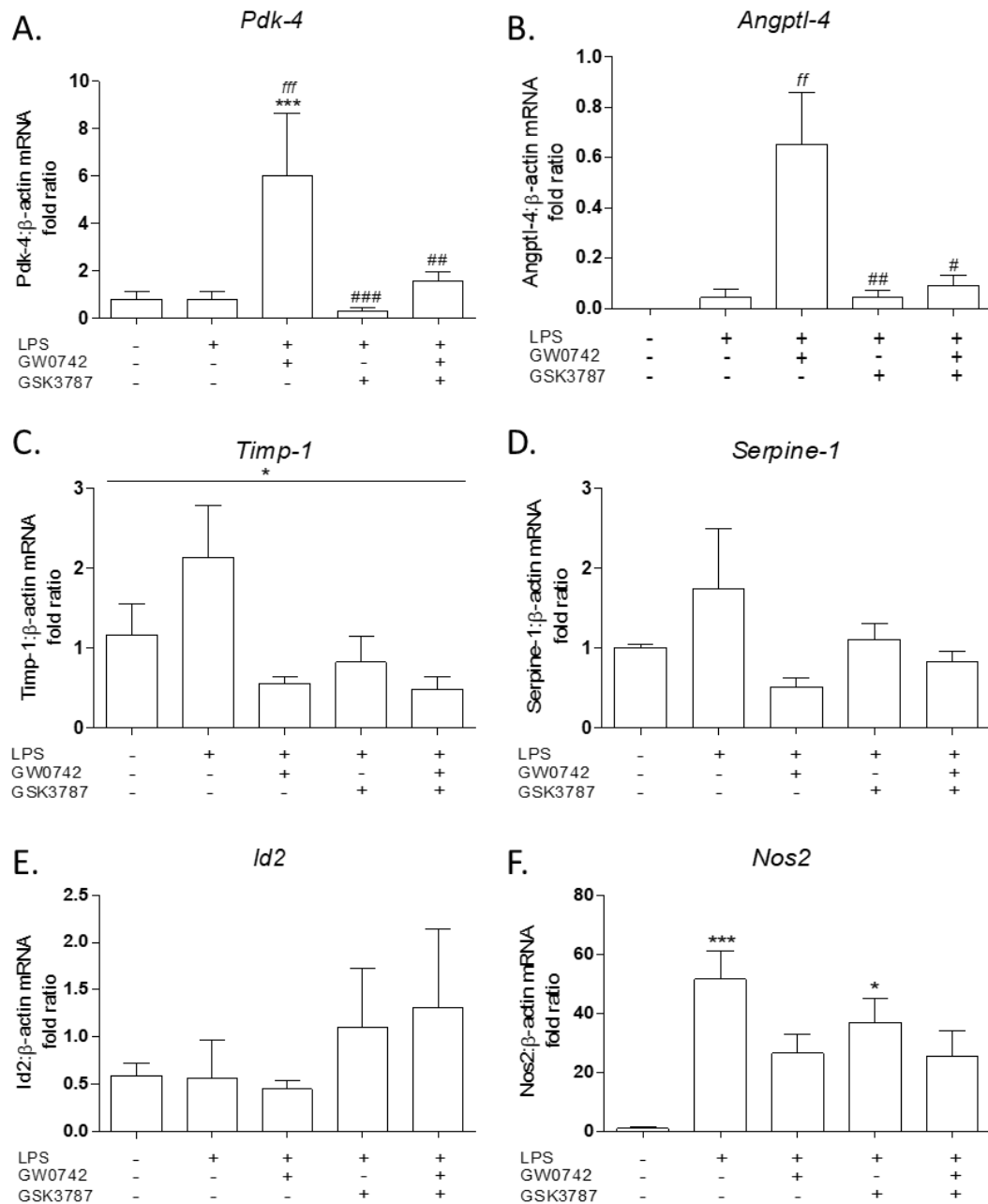
Figure 4.21 Expression of genes regulated by PPARβ/δ in pulmonary artery. The expression of different PPARβ/δ target genes was measured after 24 h incubation under five different treatments: vehicle (0.01% DMSO); 1 µg/mL LPS; 1 µg/mL LPS + 100 nM GW0742; 1 µg/mL LPS + 1 µM GSK3787; and 1 µg/mL LPS + 100 nM GW0742 + 1 µM GSK3787 (n=4-5). Relative quantitation was calculated with the comparative CtΔΔ method and normalized against β-actin as an endogenous control. Significant difference between treatments was analysed by one-way ANOVA followed by Bonferroni post-hoc test and the data are presented as mean ± standard error of the mean. ***=P<0.001 and *=P<0.05 compared with vehicle; *fff*=P<0.001 and *ff*=P<0.01 compared with LPS; ###=P<0.001, ##=P<0.01 and #=P<0.05 compared with LPS+GW0742.

Id2 is a target gene of Bcl-6 (Sandhu *et al.* 2012) which is induced by LPS (Wang *et al.* 2011) and is also regulated by PPARβ/δ (Khozoie *et al.* 2012), therefore it was chosen as a marker of the PPARβ/δ trans-repression mode of action trough Bcl-6. The Figure 4.21 E shows that LPS does not induced the expression of *Id2* in pulmonary artery, and similarly its expression is not affected by the PPARβ/δ ligands.

The expression of *Nos2,* the gene that encodes for iNOS, is significantly increased by LPS, and its expression is inhibited by GW0742 (Figure 4.21 F). Surprisingly, the treatment LPS+GW0742+GSK3787 reduces the expression of *Nos2* to levels similar to the treatment LPS+GW0742.

4.4.5.2   qRT-PCR bronchi

Similar to pulmonary artery samples, GW0742 significantly increased the expression of *Pdk-4* by ~2.5-fold and the presence of GSK3787 inhibited its expression (Figure 4.22 A). Interestingly, *Angptl-4* did not amplify in bronchi samples and the expression of *Timp-1*, *Serpine-1* and *Id2* showed not to be regulated by the treatments (Figure 4.22 B, C and D).

The transcription of *Nos2* is significantly increased by LPS, as expected. Surprisingly, GW0742 significantly increases *Nos2* expression compared to LPS, and the presence of GSK3787 significantly reduces the transcription of *Nos2* compared to LPS+GW0742, although it is still significantly higher than control (Figure 4.22 E).

Bronchi
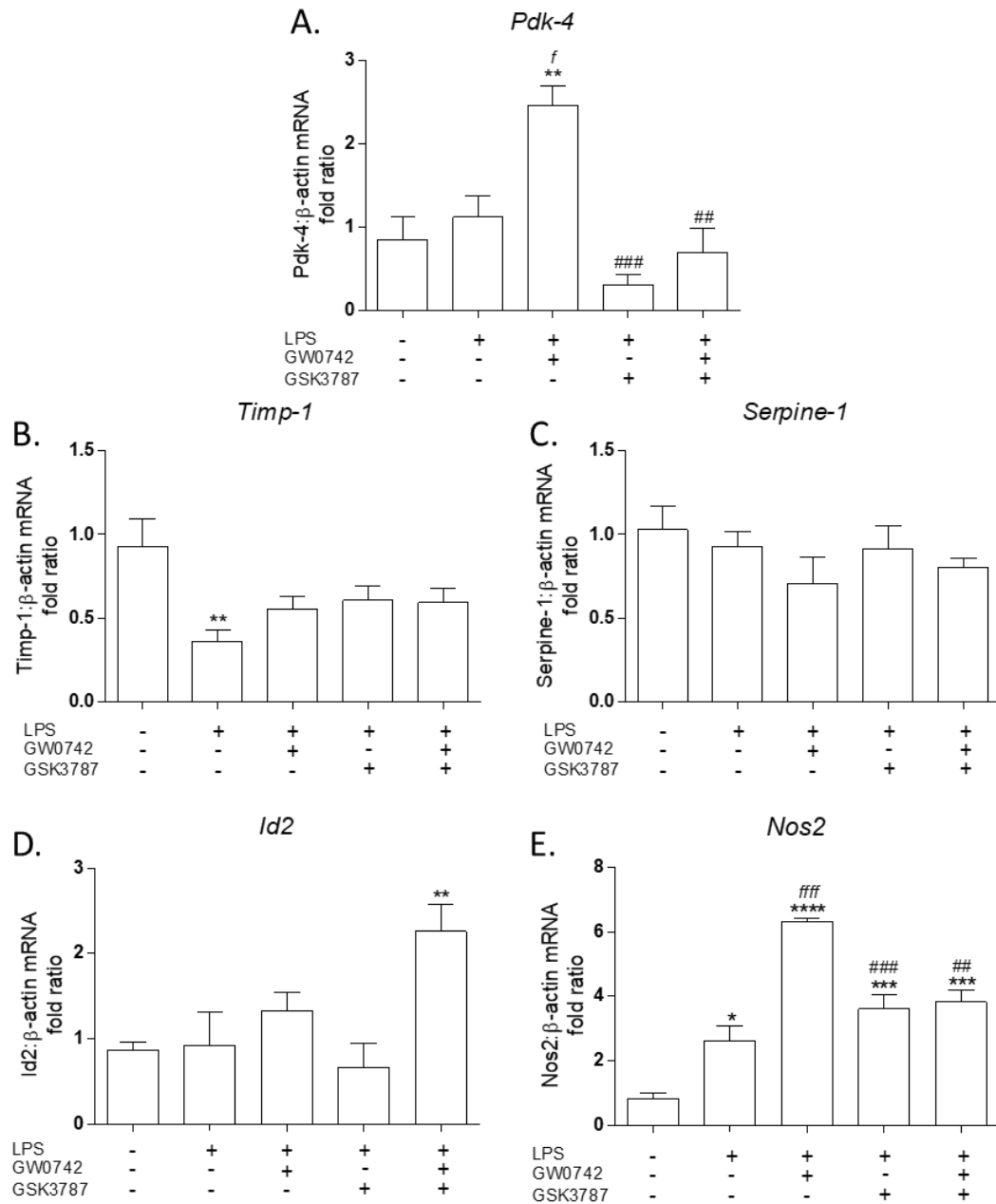
Figure 4.22 Expression of genes regulated by PPARβ/δ in bronchi. The expression of different PPARβ/δ target genes was measured after 24 h incubation under five different treatments: vehicle (0.01% DMSO); 1 μg/mL LPS; 1 μg/mL LPS + 100 nM GW0742; 1 μg/mL LPS + 1 μM GSK3787; and 1 μg/mL LPS + 100 nM GW0742 + 1 μM GSK3787 (n=4-5). Relative quantitation was calculated with the comparative CtΔΔ method and normalized against β-actin as an endogenous control. Significant difference between treatments was analysed by one-way ANOVA followed by Bonferroni post-hoc test and the data are presented as mean ± standard error of the mean. ****=P<0.0001, ***=P<0.001, **=P<0.01, *=P<0.05 compared with vehicle; *ffff*=P<0.0001, *f*=P<0.05 compared with LPS; ###=P<0.001, ##=P<0.01 and #=P<0.05 compared with LPS+GW0742.

4.4.5.3   qRT-PCR parenchyma

Interestingly, the expression of the marker genes tested are affected by the PPARβ/δ ligands in lung parenchyma (Figure 4.23 A).

The expression of *Nos2* is significantly increased by LPS, but again, it is not regulated by PPARβ/δ ligands (Figure 4.23 E).

Parenchyma
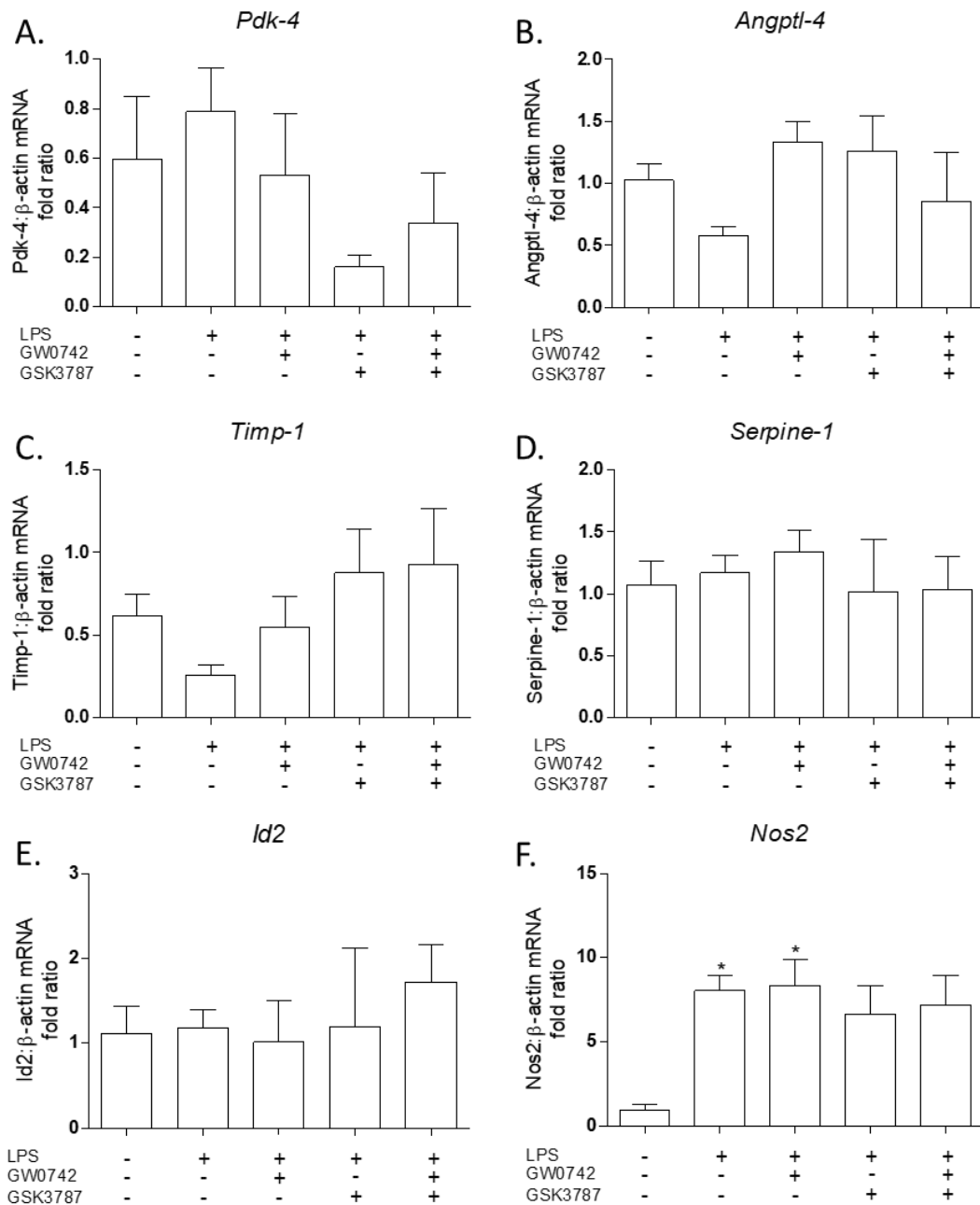
Figure 4.23 Expression of genes regulated by PPARβ/δ in parenchyma. The expression of different PPARβ/δ target genes was measured after 24 h incubation under five different treatments: vehicle (0.01% DMSO); 1 μg/mL LPS; 1 μg/mL LPS + 100 nM GW0742; 1 μg/mL LPS + 1 μM GSK3787; and 1 μg/mL LPS + 100 nM GW0742 + 1 μM GSK3787 (n=4-5). Relative quantitation was calculated with the comparative CtΔΔ method and normalized against β-actin as an endogenous control. Significant difference between treatments was analysed by one-way ANOVA followed by Bonferroni post-hoc test and the data are presented as mean ± standard error of the mean. *=P<0.05 compared with vehicle.

4.5 Discussion.

This chapter was designed to further understand the PPARβ/δ molecular switch between induction and trans-repression, so the first thing to do was to establish a model where this induction/trans-repression switch is occurring.

The first attempt was using PSMCs, since these cells are known to express PPARβ/δ (Li *et al.* 2012, Liu *et al.* 2013). The inflammation of the cells was induced by LPS, however PPARβ/δ did not show any regulation of the inflammation and therefore PSMCs were discarded as a suitable model.

Next focus was on lungs because it has been shown that PPARβ/δ is highly expressed in this organ (Huang *et al.* 2007, Girroir *et al.* 2008, Bao *et al.* 2014). However, the lung is a complex structure composed of different tissues and cell types whose expression of PPARβ/δ might vary and therefore respond differently under same conditions. Three main tissues were identified in the lung, pulmonary artery, bronchi and parenchyma, and it was shown that all three tissues express PPARβ/δ although at different concentrations.

The expression of PPARβ/δ in pulmonary artery agrees with previous results where PPARβ/δ was shown to be expressed in endothelial cells (Bishop-Bailey and Hla 1999). Bronchi express the lowest concentration of PPARβ/δ, which also agrees with the weak PPARβ/δ immunostaining of bronchial epithelial cells of mice (Higashiyama *et al.* 2007), and parenchyma shows the highest expression of PPARβ/δ, which differs to the expression profile in mice, where the expression of PPARβ/δ is also week in alveolar type II cells (Higashiyama *et al.* 2007).

The inflammation of the tissues was induced by LPS, and the PPARβ/δ-regulation of the inflammation was studied by incubating the tissues with different agonists (GW0742 and L-165041) and antagonists (GSK3787 and GSK0660), which

showed similar regulatory profile in all tissues. In general terms, LPS induces the release of NO and IL-6, and the incubation with one of the agonists or antagonists individually does not reduce the production of these inflammation markers. However, when the agonist and antagonist are present at the same time the inflammation is significantly reduced. This result is very surprising and has never being described before, which raises the possibility that the compounds were impure or unstable. A further analysis on the ligands by mass spectrometry (Appendix A) and nuclear magnetic resonance (NMR) (Appendix B) confirmed that the agonists and antagonists used in the experiments are pure and have not been degraded. This analysis together with the fact that same response is replicated when using two chemically different agonists such as GW0742 and L-165041 and the high n number used indicates that the result is consistent and is not an isolated phenomenon.

However, it cannot be ignored the fact that these results disagree with a large number of studies where the treatment with GW0742 attenuated the lung inflammation in murine models, the effects of GW0742 were abolished or significantly reduced by GSK0660, and the PPARβ/δ deletion exacerbates the lung inflammation (Haskova *et al.* 2008, Kapoor *et al.* 2010, Bao *et al.* 2014). The difference is that these studies are *in vivo* and, although the inflammation is monitored in the lung, the whole organism is fighting the infection, the immune system is being activated and immune cells such as neutrophils and macrophages are infiltrated into the alveolar cavity. This means that there is a synergic response composed of different tissues and cells that makes the anti-inflammatory response more effective. In the model used in this thesis, the tissues were separated from each other and the LPS-induced regulation of inflammation by PPARβ/δ was analysed in isolated tissues. Under these conditions, PPARβ/δ seems to play a

more important role in the regulation of inflammation in the pulmonary artery than in bronchi and lung parenchyma.

The initial hypothesis was that PPARβ/δ acts as a molecular switch between induction and trans-repression and depending on which mechanism is triggered it will have pro- or anti-inflammatory effects. If the hypothesis is true, the results would indicate that the incubation with an agonist led to a pro-inflammatory state of PPARβ/δ and the incubation with the agonist and antagonist together switches PPARβ/δ to an anti-inflammatory state. However, the data do not provide enough information to know if the pro- and anti-inflammatory states regulate genes in the induction or trans-repression mode of action. To find this out a qRT-PCR was performed for the expression of marker genes for each mechanism of action in all treatments and all tissues.

The appropriate marker genes were selected to represent the induction and trans-repression modes of action. Khozoie *et al.* (2012) performed a genomewide analysis of genes regulated by PPARβ/δ in mouse keratinocytes. They found that a total of 612 genes are regulated by PPARβ/δ and, furthermore, the analysis of ChIP-seq data demonstrated a PPARβ/δ promoter occupancy of 203 genes out of these 612. Similarly, Adhikary *et al.* (2011) did another genomewide study in human myofibroblasts, where they found a total of 3704 genes regulated PPARβ/δ. Khozoie *et al.* (2012) crosslinked the two lists of genes regulated by PPARβ/δ and created a new list of 103 genes regulated by PPARβ/δ in both human and mouse models. This list of genes was used because if they are regulated by PPARβ/δ in mouse and human then it is more likely that they are also regulated by PPARβ/δ in rat.

It is very tempting to accept that those genes found with PPARβ/δ bound to its promoter are regulated through the induction mode of action and those without PPARβ/δ bound to the promoter are regulated through the trans-repression mode

of action, however this assumption can lead to a big mistake. For example, *Angptl-4* is well known to be regulated by induction mode (Inoue *et al.* 2014, Adhikary *et al.* 2015, Klingler *et al.* 2016), which agrees with Khozoie *et al.* (2012) results, where they found PPARβ/δ bound to the promoter of *Angptl-4.* However, *Pdk-4* is another well-known gene regulated in the induction mode (Degenhardt *et al.* 2007, Adhikary *et al.* 2015, Klingler *et al.* 2016), but Khozoie *et al.* (2012) did not identified PPARβ/δ bound to the promoter of the gene. Consequently, it can be presumed that the genes with PPARβ/δ bound to the promoter are regulated through the induction mode of action, but it cannot be ruled out that genes without PPARβ/δ in their promoter are regulated in the trans-repression mode. Therefore, other ways of identifying potential markers for the trans-repression mode of action are needed.

A separate study was used to identify the genes regulated by NF-κB after LPS activation of human cells (Schreiber *et al.* 2006) and crosslinked with the list of 103 genes regulated by PPARβ/δ in mouse and human. After LPS-activation, NF-κB was found in the promoter of four genes common in the two lists, whose transcription was also increased (Schreiber *et al.* 2006), therefore they were selected as potential markers for the trans-repression mode of action of PPARβ/δ: *Ppfia-1*, *Sema7a*, *Timp-1* and *Serpine-1*. The idea is that when PPARβ/δ is activated and functioning in the trans-repression mode of action it will sequester NF-κB and inhibit the transcription of the selected genes.

Bcl-6 has shown to be another important trans-repression mechanism of action of PPARβ/δ, for that reason another marker gene for this pathway was identified. One study showed that LPS increases the transcription of *Id2* in some tissues, like the brain (Wang *et al.* 2011), and another study showed that *Id2* is regulated by Bcl-6 (Sandhu *et al.* 2012), therefore *Id2* was chosen as a marker gene of the PPARβ/δ trans-repression mode of action through Bcl-6. The idea is that when PPARβ/δ is not activated it sequesters Bcl-6, which will allow the transcription of *Id2* in the

presence of LPS. If PPARβ/δ is activated it will release Bcl-6 which will then repress the expression of *Id2*.

The qRT-PCR of pulmonary artery showed that the activation of PPARβ/δ with GW0742 increases the transcription of *Pdk-4* and *Angptl-4* and represses the transcription of *Timp-1* and *Serpine-1*, indicating that agonist activation of PPARβ/δ triggers both, induction and trans-repression. However, the presence of GW0742 and GSK3787 together does not induce the transcription of *Pdk-4* or *Angptl-4* but it still represses the transcription of *Timp-1* and *Serpine-1*, indicating that the trans-repression but not induction is occurring. The transcription of *Id2* seems not to be affected by any of the treatments used in this study and therefore it can be concluded that *Id2* is not regulated by PPARβ/δ in pulmonary artery.

By combining these findings with the inflammatory response, it can be deduced that in pulmonary artery GW0742 triggers both, induction and trans-repression, resulting in a pro-inflammatory state of PPARβ/δ. Interestingly, the presence of GW0742 and GSK3787 together inhibits the induction mode of action but activates the trans-repression mode of action through NF-κB, which is the treatment that produces the strongest anti-inflammatory effect. Taken together, it suggests that GW0742 triggers the induction mechanism, which is pro-inflammatory, and GW0742 plus GSK3787 switches PPARβ/δ to the trans-repression mechanism through NF-κB which is responsible for the anti-inflammatory effects of PPARβ/δ in LPS-induced inflamed pulmonary artery.

This finding fits well with the conclusions of Adhikary *et al.* (2015), where they describe a fatty acid oxidation and lipid metabolism function related of the genes regulated by induction, and genes regulated by trans-repression were associated with pro- or anti-inflammatory functions. Hence, they suggest that the response to PPARβ/δ agonists is mainly anti-inflammatory through trans-repression.

In bronchi, *Angptl-4* is not expressed but *Pdk-4* is significantly increased by GW0742, suggesting that the induction mechanism of action of PPARβ/δ is occurring. On the other side, the transcription of *Timp-1*, *Serpine-1* and *Id2* does not vary with the treatments, indicating that trans-repression mode is not a major mechanism of action of PPARβ/δ in bronchi, which can explain the weaker inhibition of the inflammatory response in bronchi.

The PPARβ/δ marker genes used in this study seem not to be regulated by PPARβ/δ in lung parenchyma, indicating that PPARβ/δ is not being activated either in the induction nor in the trans-repression mode of action, which agrees with previous results where NO production showed not to be regulated by PPARβ/δ. However, IL-6 production showed to be reduced when GW0742 and GSK3787 are present, which suggests that, although not as strong, some anti-inflammatory effect of PPARβ/δ is happening. There is the possibility that the marker genes selected in this study are not the right markers to detect the trans-repression mechanism in parenchyma.

It has been shown in several studies that *Nos2* is regulated by PPARβ/δ (Kapoor *et al.* 2010, Di Paola *et al.* 2011, Bojic *et al.* 2014), although it has not been described whether this regulation is via induction or trans-repression. To find this out, the expression of *Nos2* was measured in all tissues under the same conditions. As expected, LPS increases *Nos2* expression in all tissues, however the regulation of its expression by PPARβ/δ is different dependent on the tissue. In pulmonary artery, GW0742 and GW0742+GSK3787 represses the expression of *Nos2*, suggesting that PPARβ/δ is inhibiting *Nos2* through the trans-repression mode of action. Surprisingly, in bronchi GW0742 significantly increases the transcription of *Nos2* compared to LPS, but this increment does not occur with the treatment LPS+GW0742+GSK3787, suggesting that PPARβ/δ enhances the expression of *Nos2* through the induction mode of action. This observation fits well with the

previous conclusion that the induction-activation of PPARβ/δ is pro-inflammatory and trans-repression activation of PPARβ/δ is anti-inflammatory.

In parenchyma, LPS increases the expression of *Nos2*, but its expression is not regulated by PPARβ/δ, which fits well with previous results where PPARβ/δ is not a major player in the regulation of inflammation.

4.5.1 Conclusion

In summary, it is clear that PPARβ/δ ligands can have pro- and anti-inflammatory effects. Conformational changes of PPARβ/δ caused by different agonists, antagonists and partial agonists can cause differential recruitment of co-regulators resulting in alteration of the dynamics of transcriptional complexes and interactions with DNA binding sites. The cell/tissue type is another important co-determinant of the type of response of PPARβ/δ target genes. Thus, there are multiple levels of regulation by which PPARβ/δ can influence the expression of target genes.

In the model used in this thesis, the presence of agonist and antagonist at same time switches the PPARβ/δ mode of action from induction to trans-repression, and the trans-repression mode of action was linked with anti-inflammatory effects. Among the tissues tested, PPARβ/δ seems to play a more important role on the regulation of inflammation in pulmonary artery, however it is not as important in lung parenchyma.

Chapter 5: *In silico* modelling of PPARβ/δ

5.1   Introduction

Molecular docking is a computational method that predicts the preferred and most stable orientation binding of one molecule to a second, being protein-protein or protein-ligand. The docking algorithms and programs rank the predicted ligand poses according to their "binding affinity", which is an indicator on how well the ligand binds to the receptor at that specific orientation. These studies are very useful for providing deep information on the interaction between the two molecules docked, and it is widely used in drug discovery to predict the most stable drug interactions between a drug and a target receptor molecule, where the most suitable ones are selected for further research.

The best option when doing docking is to use the crystal structure of the receptor. Fortunately, there is a number of X-ray crystal structures of all three PPAR-LBD subtypes complexed with ligands, which provides an insight into the binding and activation of PPARs by ligands. A comparison of the crystal structure of the three PPARs showed a 60-70% homology with a large Y-shaped ligand binding pocket of ~1300 $Å^3$ composed of 13 α-helix and four stranded β-sheets (Figure 5.1) (Kahremany *et al.* 2015) organized in three arms (I, II and III) (Xu *et al.* 2001). Arm I is predominantly polar, well conserved and includes the activation helix 12 (AF-2 helix). Arms II and III are predominantly hydrophobic and less well conserved among PPARs (Maltarollo *et al.* 2015, Laghezza *et al.* 2019). The pocket is sealed on the left side by the C-terminal helix that contains the AF-2 (helix 12) and on the right side by helix 1 and small β-sheet (Xu *et al.* 1999).
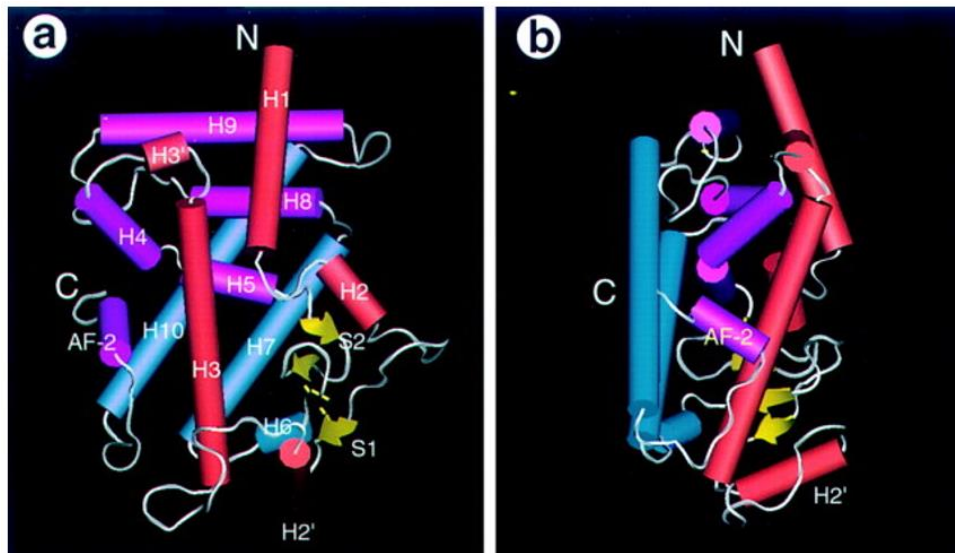
Figure 5.1 Structure of the ligand binding domain (LBD) of PPARβ/δ (Xu *et al.* 1999).

Most known synthesized PPAR ligands share the same structure: a hydrophilic head group, a central hydrophobic part, and a flexible hydrophobic tail. The binding mode of these compounds in the binding pocket is very similar, with the head group interacting with the AF-2 helix, which is crucial for PPAR activation and successful coactivator binding, the central part forming hydrophobic interactions, and the tail toward the lower or upper distal cavity binding Arm II and/or Arm III (Cronet *et al.* 2001, Laghezza *et al.* 2019).

Although the overall size of the binding pocket is similar, there are some differences among the PPARs. The PPARβ/δ-LBD cavity is significantly narrower in the region adjacent to the AF-2 helix (Xu *et al.* 2001). Therefore, PPARβ/δ hardly accommodates bulky polar heads or substituents, which could explain why large headed TZDs agonists show little or no binding to PPARβ/δ (Xu *et al.* 2001).

It is now widely accepted the mechanism of activation of PPARs in response to the ligand binding. When a ligand is present in the LBD, the AF-2 helix H12 closes the binding pocket resulting in the active form of the receptor which triggers the binding of the co-activators (Renaud *et al.* 1995). This model was proposed based on the observation that in the unliganded RXR structure, the AF-2 helix adopts an alpha-

helical structure that extends away from the LBD, while the AF-2 helix in the agonist-bound RAR, thyroid hormone receptor and oestrogen receptor structures is folded against the LBD (Renaud *et al.* 1995).

Due to the large binding pocket of PPARβ/δ a number of researchers suggested the possibility of accommodating more than one ligand at the time, which could result in unusual PPARβ/δ:ligand stoichiometries (Nandhikonda *et al.* 2013, Adhikary *et al.* 2015). This situation could cause the receptor to adopt different conformations that might result in the recruitment of different co-regulators, resulting in the alteration of the dynamics of transcriptional complexes and interactions with DNA binding sites and ultimately alterations in the responses of PPARβ/δ. To our knowledge, this possibility has so far not been explored, and could explain the surprising results from Chapter 4.

5.1.1 Aims and objectives

This chapter will explore how PPARβ/δ is activated/repressed after ligand binding as well as the possibility of binding more than one ligand into the binding pocket simultaneously using *in silico* methods. This approach aims to give a new light to the PPARβ/δ molecular switch theory.

Objectives:

1- Dock and analyse the synthesised agonists and antagonists used in this thesis (GW0742, L-165042, GSK3787 and GSK0660) into the PPARβ/δ binding pocket.

2- Explore the possibility of accommodating more than one ligand into the PPARβ/δ binding pocket mimicking the conditions of the experiments performed in this thesis.

5.2 Results

The PPARβ/δ-LBD crystal structure 3TKM was chosen for the docking experiments for several reasons. The X-ray resolution is 1.95 Å, a good enough resolution to distinguish the atoms from each other. Also, PPARβ/δ was co-crystallised with GW0742, same agonist that was used during the development of this project. And finally, this structure only contains 5 missing residues: Lys229, Gln230, Leu231, Val232 and Asn233.

The PDB file for 3TKM was downloaded from Protein Data Bank, and the protein and ligands were prepared as previously explained in Chapter 2.

5.2.1 Docking of PPARβ/δ ligands

The two PPARβ/δ agonists used in the experiments of the present study GW0742 and L-165041 as well as the two antagonists GSK3787 and GSK0660 were docked into the crystal structure of the LBD of PPARβ/δ. The best eight hits were analysed by Pymol to identify the residues that form polar interactions with each of the different poses of the ligands; the results are summarised in Table 5.1 below.

Table 5.1 Best eight docking hits of four ligands into PPARβ/δ (PBD: 3TKM). In green are the residues more likely to bind agonists and in red the residues more likely to bind antagonists.

Best fit	Agonists				Antagonists			
	GW0742		L-165041		GSK3787		GSK0660	
	Affinity (Kcal/mol)	Aa with polar interactions	Affinity (Kcal/mol)	Aa with polar interactions	Affinity (Kcal/mol)	Aa with polar interactions	Affinity (Kcal/mol)	Aa with polar interactions
1	-11.1	His287 His413 Tyr437	-8.7	His287 His413 Tyr437	-9.1	Thr252 Asn307	-8.6	Arg248 Thr252 Ala306 Asn307
2	-10.8	Thr253 His287 His413 Tyr437	-8	Met192 Thr252 Thr256 Ile290 Ala306	-8.9	Thr252	-8.3	Arg248 Thr252 Ala306
3	-9.9	Thr253 His413	-7.6	Thr252 Arg258 Glu259	-8.6	Thr252	-8.1	Thr256 Asn307
4	-9.6	Thr256	-7.5	Thr252 Thr253 Ala306	-8.5	Thr256	-8.1	Asn307
5	-9.3	No bonds	-7.5	Trp228 Thr252 Thr256 Ile290	-8.4	No bonds	-7.9	Thr256 Ala306 Asn307
6	-8.8	Thr253	-7.1	Thr252 Thr256 Ala306	-8.3	Thr252 Thr253	-7.6	Asn307
7	-8.7	Thr252	-6.9	Tyr284 Arg361	-8.3	Thr252	-7.5	Ala306 Asn307
8	-8.4	Arg258	-6.8	Glu255 Asn307	-8.2	Met192	-7.4	Thr256 Asn307

The best orientation of each ligand was selected for further analysis using Pymol and Ligplot+.

5.2.1.1 Docking of GW0742

The Figure 5.2 A shows the most stable orientation of GW0742 within the PPARβ/δ binding pocket predicted by Autodock Vina (green) vs the real GW0742 present in the crystal structure (pink). Figure 5.2 B is a more detailed image showing the residues that form polar interactions with GW0742 (His247, His413 and Tyr437) according to Pymol and Figure 5.2 C is a 2D image showing both polar and hydrophobic interactions of the residues with GW0742 according to Ligplot+. This last image shows very clearly how the head of GW0742 forms the polar bindings and how the tail is surrounded by the hydrophobic amino acids.
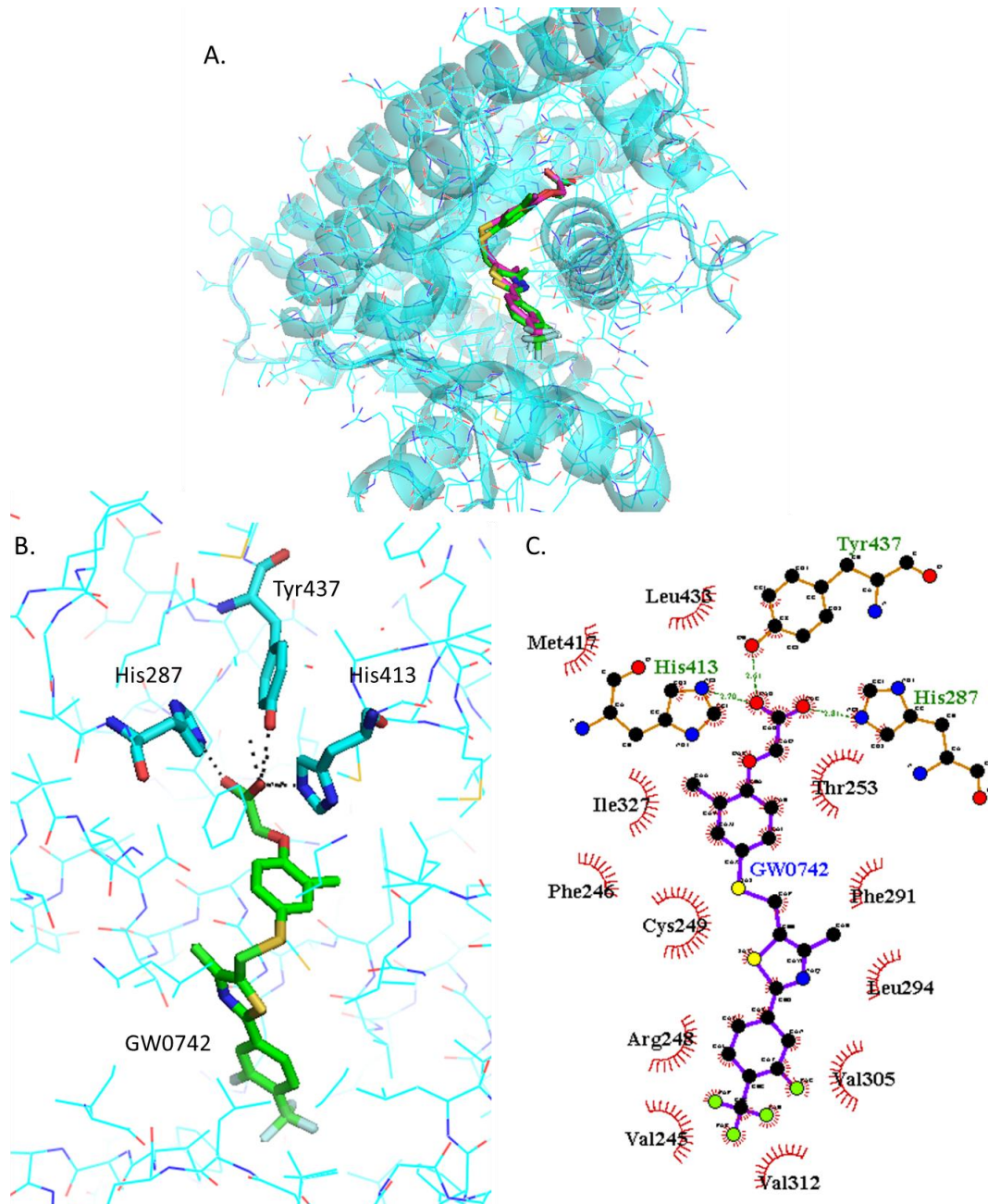
Figure 5.2 Analysis of GW0742 docked into PPARβ/δ (PBD:3TKM). A) Representation of the most stable GW0742 docking conformation (green) compared to the GW0742 of the crystal structure (pink). B) 3D detail of the amino acids forming polar bindings with GW0742 calculated by Pymol. C) Schematic 2D representation of the interaction between PPARβ/δ LBD and GW0742 calculated using Ligplot+. The green dashed lines indicate polar interactions and the red spoked arcs indicate hydrophobic interactions. Color coding of atoms: red O, Blue N, mustard S, pink C of GW0742 from the crystal structure, green C of GW0742 docked into the crystal structure, cyan C from PPARβ/δ.

5.2.1.2   Docking of L-165042

The most stable L-165041 orientation predicted by Autodock Vina binds in the same physical place as GW0742 (Figure 5.4 A), and the same three amino acids (His287, His413, Tyr437) form polar interactions with the head of L-165041, as shown in Figure 5.4 B. The tail of L-165041 also forms hydrophobic interactions with a number of residues in common with GW0742, such as Val245, Arg248, Cys249, Thr253, Phe291, Leu294, Val305, Val312, Met417, Leu433, as shown in Figure 5.4 C.
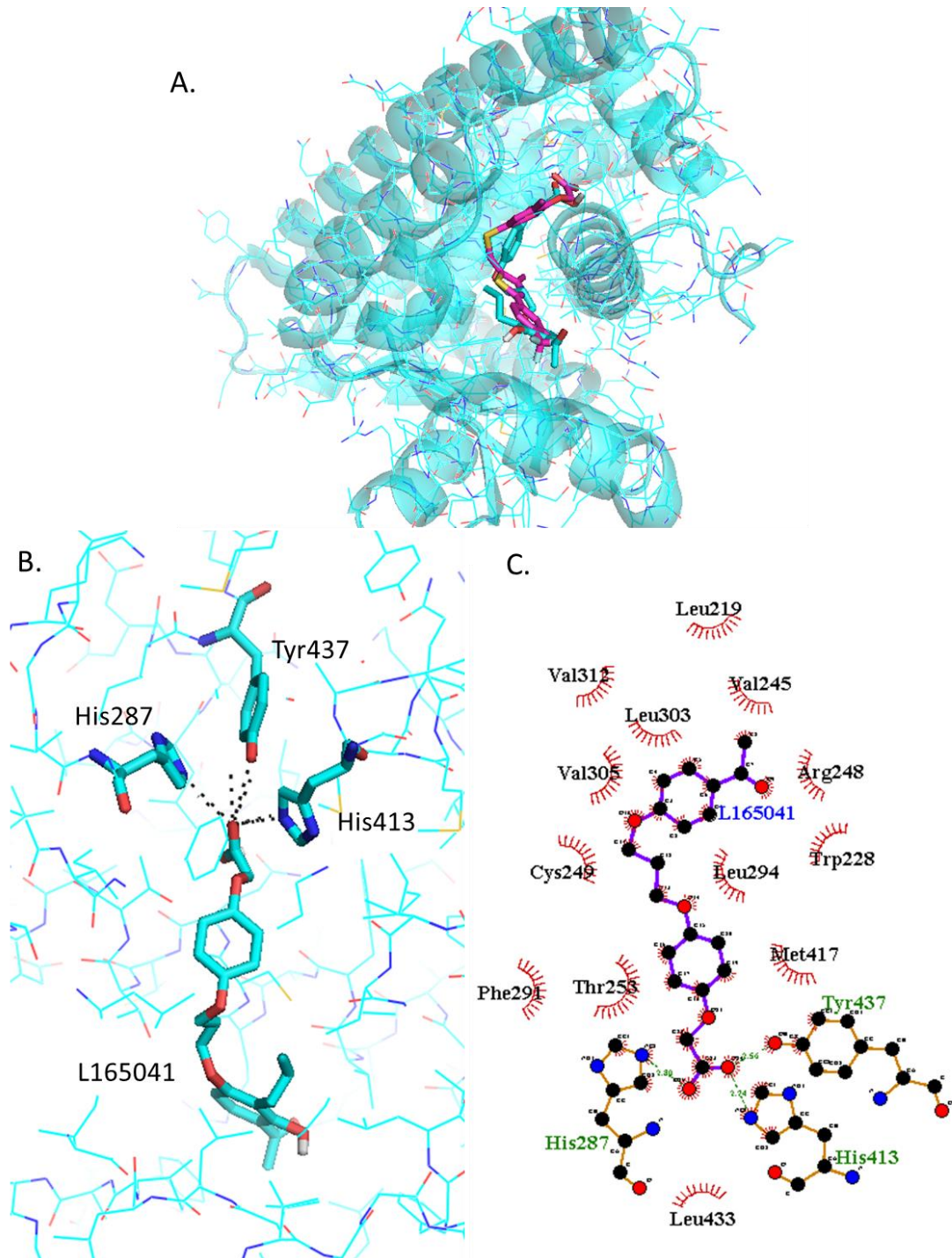
Figure 5.3 Analysis of L-165042 docked into PPARβ/δ (PBD:3TKM). A) Representation of the most stable L-165041 docking conformation (cyan sticks) compared to the GW0742 of the crystal structure (pink). B) 3D detail of the amino acids forming polar bindings with L-165041 calculated by Pymol. C) Schematic 2D representation of the interaction between PPARβ/δ LBD and -L-165041 calculated using Ligplot+. The green dashed lines indicate polar interactions and the red spoked arcs indicate hydrophobic interactions. Color coding of atoms: red O, Blue N, mustard S, pink C of GW0742 from the crystal structure, cyan sticks C of L-165041 docked into the crystal structure, cyan lines C from PPARβ/δ.

5.2.1.3 Docking of GSK3787

GSK3787 binds in a slightly different place than GW0742, although there is some overlapping of the binding sites, as shown in Figure 5.4 A. Also, the amino acids involved in the polar interaction of GSK3787 predicted by Pymol, Thr252 and Asn307, are different to those of the agonists (Figure 5.4 B) as well as the residues that interact with the hydrophobic tail of GSK3787 (Figure 5.4 C).
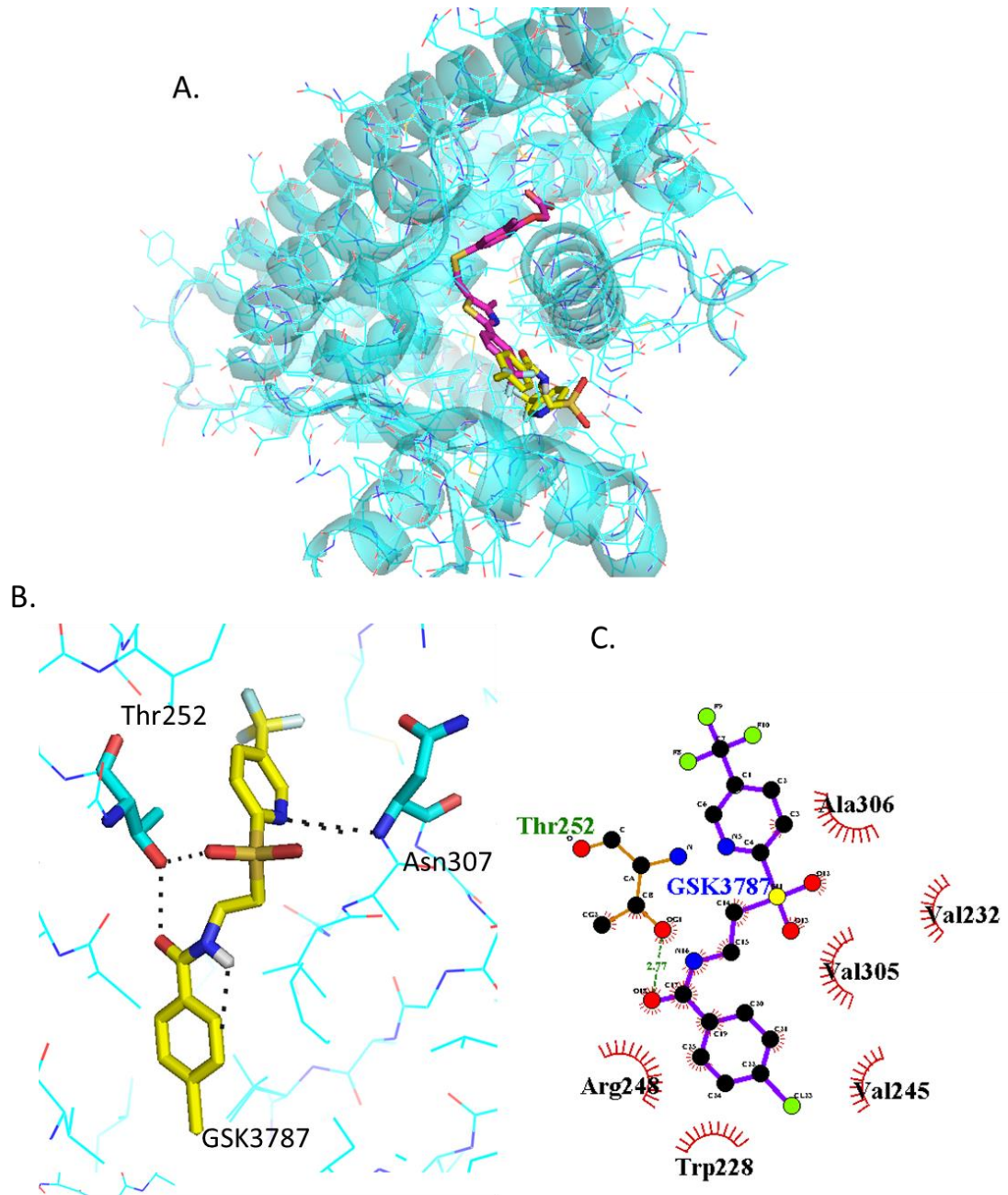
Figure 5.4 Analysis of GSK3787 docked into PPARβ/δ (PBD:3TKM). A) Representation of the most stable GSK3787 docking conformation (yellow) compared to the GW0742 of the crystal structure (pink). B) 3D detail of the amino acids forming polar bindings with GSK3787 calculated by Pymol. C) Schematic 2D representation of the interaction between PPARβ/δ LBD and GSK3787 calculated using Ligplot+. The green dashed lines indicate polar interactions and the red spoked arcs indicate hydrophobic interactions. Color coding of atoms: red O, Blue N, mustard S, pink C of GW0742 from the crystal structure, yellow C of GSK3787 docked into the crystal structure, cyan C from PPARβ/δ.

5.2.1.4 Docking of GSK0660

GSK0660 binds very close but not in the same binding site as GW0742, as shown in Figure 5.5 A. The amino acids involved in the polar bindings with GSK0660, Thr252, Asn307, Arg248 and Ala306, are again different to those for the agonists, although two of them are common with GSK3787 (Figure 5.5 B). Ligplot+ predicts slightly different polar binding profile (Figure 5.5 C), probably because these two softwares use different algorithms for binding prediction, although still show hydrophobic interactions common with GSK3787, such as Trp228, Val305 and Ala306.
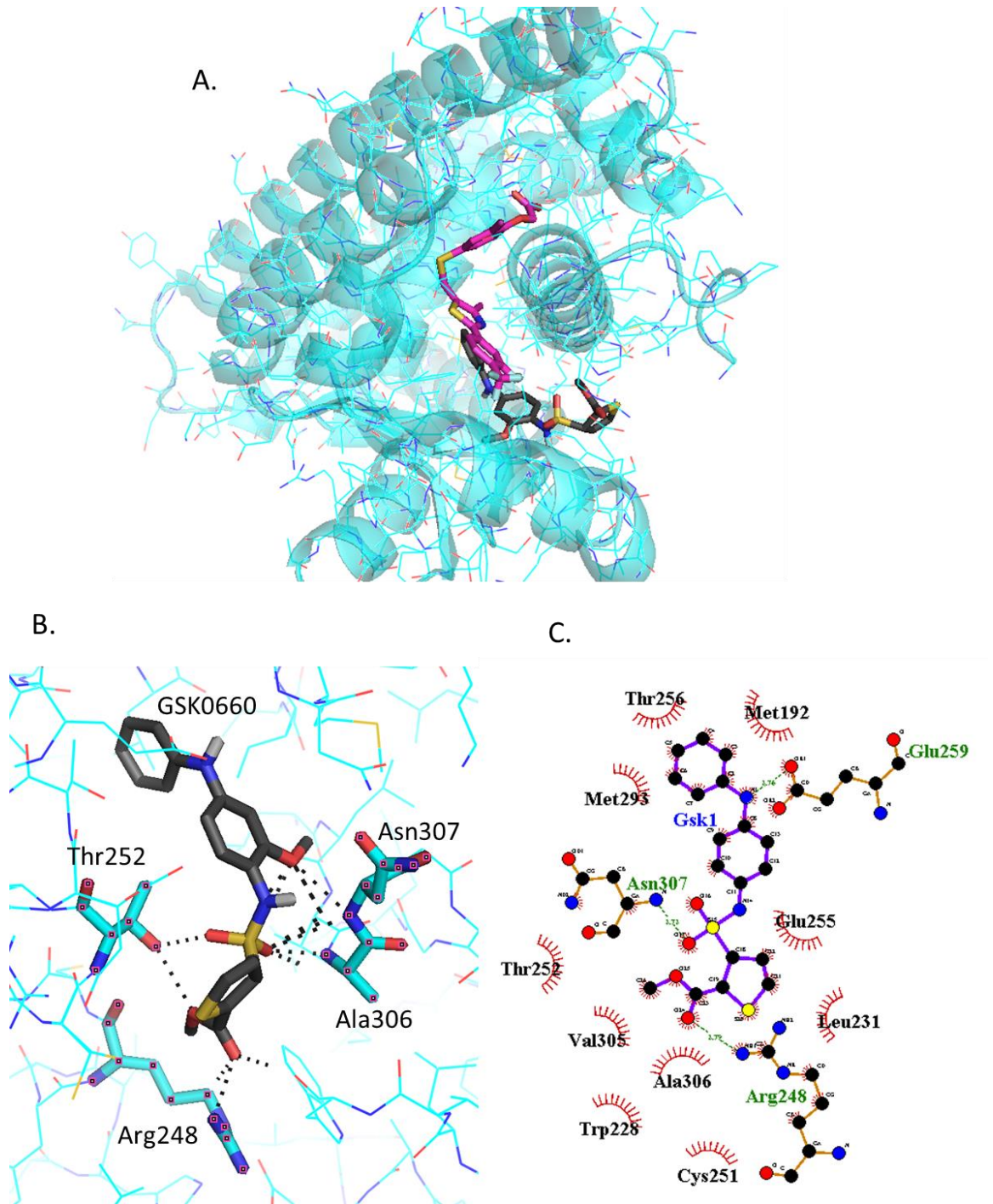
Figure 5.5 Analysis of GSK0660 docked into PPARβ/δ (PBD:3TKM). A) Representation of the most stable GSK0660 docking conformation (grey) compared to the GW0742 of the crystal structure (pink). B) 3D detail of the amino acids forming polar bindings with GSK0660 calculated by Pymol. C) Schematic 2D representation of the interaction between PPARβ/δ LBD and GSK0660 calculated using Ligplot+. The green dashed lines indicate polar interactions and the red spoked arcs indicate hydrophobic interactions Color coding of atoms: red O, Blue N, mustard S, pink C of GW0742 from the crystal structure, grey C of GSK0660 docked into the crystal structure, cyan C from PPARβ/δ.

5.2.2 Docking of two PPARβ/δ ligands simultaneously

The possibility of binding a second ligand after the first ligand was bound in the most stable orientation was investigated next. To do that, the best hit from previous docking was used, assigned Ligand 1, and then a second molecule was docked, assigned Ligand 2. The aim was to mimic the conditions of the experiments performed in this thesis and predict what could have happened at molecular level. When the tissues were treated with only one ligand there is only one option for two ligands to bind, but when two different ligands are present at the same time either of them can bind first into the binding pocket. All these ligand-binding possibilities were considered and resumed in Table 5.2, the results are summarised in Table 5.3.

Table 5.2 Possible order the ligands could have bound to PPARβ/δ in the experiments performed in this thesis.

Treatment	Ligand 1	Ligand 2
GW0742	GW0742	GW0742
GSK3787	GSK3787	GSK3787
GW0742+GSK3787	GW0742	GSK3787
	GSK3787	GW0742
L-165041	L-165041	L-165071
GSK0660	GSK0660	GSK0660
L-165041+GSK0660	L-165041	GSK0660
	GSK0660	L-165041

Table 5.3 Docking prediction of binding affinities and amino acids forming polar interactions with the PPARβ/δ ligands bound into the LBD. The affinity of the binding was predicted by Autodock Vina and the best hit was analysed on Pymol.

Ligand 1			Ligand 2		
Molecule	**Affinity (Kcal/mol)**	**Aa with polar interactions**	**Molecule**	**Affinity (Kcal/mol)**	**Aa with polar interactions**
GW0742	-11.1	His287 His413 Tyr437	GW0742	-8.5	Arg258
			GSK3787	-7.7	Trp228 Thr252
GSK3787	-9.1	Thr252 Asn307	GW0742	-8.1	Trp228 Lys229
			GSK3787	-7.4	Thr253 His413
L-165041	-8.7	His287 His413 Tyr437	L-165041	-8.3	Met192 Cys251 Thr252 Thr256 Ile290 Ala306
			GSK0660	-6.5	Arg198 Asn339
GSK0660	-8.6	Arg248 Thr252 Ala306 Asn307	L-165041	-8.1	Thr253 His413
			GSK0660	-8.9	Thr252 Thr253

A further analysis on Pymol was done for each option.

5.2.2.1 Analysis of GW0742 and GSK3787 docked into GW0742-bound

PPARβ/δ

After GW0742 is bound in the most stable orientation within the PPARβ/δ-LBD, GW0742 and GSK3787 can still bind at favourable energies (-8.5 kcal/mol and -7.7 kcal/mol respectively), although at very different binding sites to the most stable one and forming polar interactions with different residues, as shown in Figure 5.6.
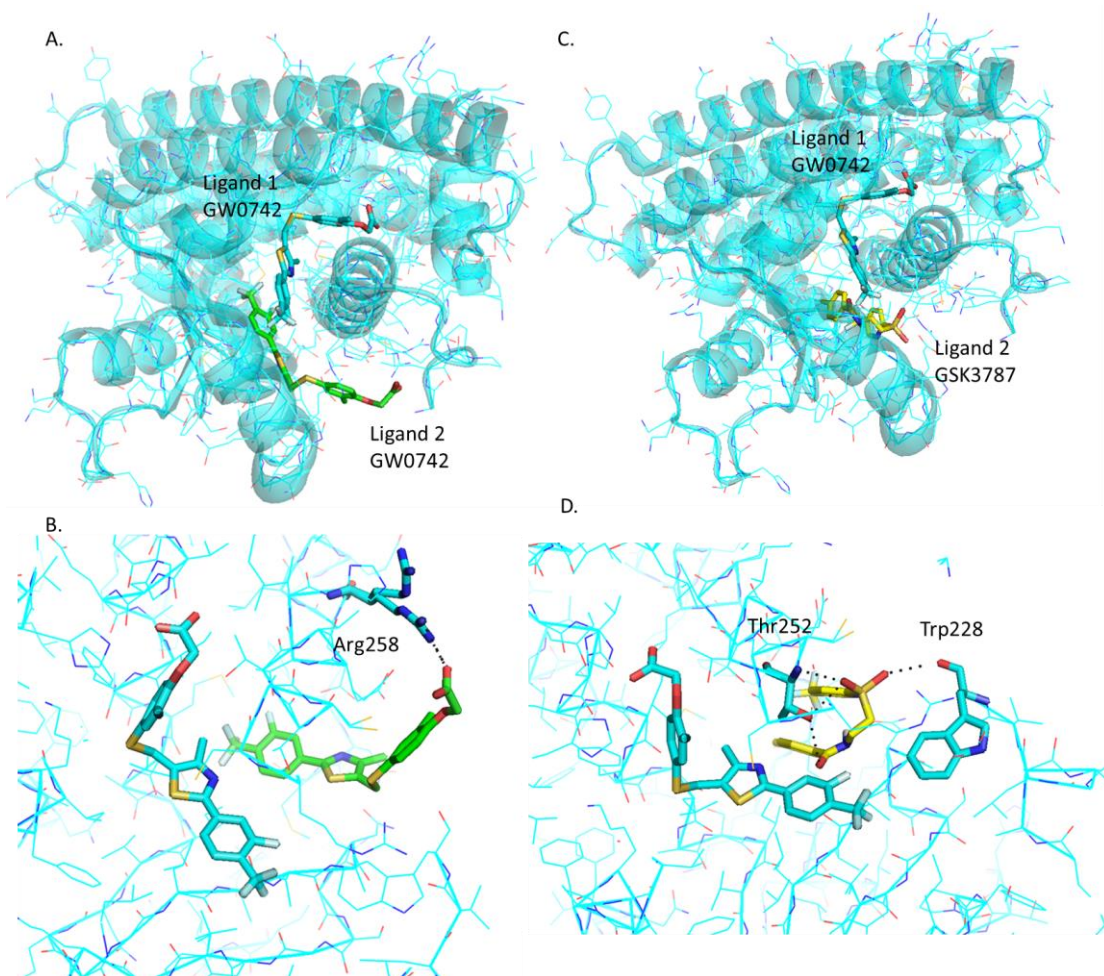
Figure 5.6 Analysis of GW0742 and GSK3787 docked into PPARβ/δ+GW0742. A second molecule of GW0742 (A, B) or GSK3787 (C, D) was docked into the LBD of PPARβ/δ containing one molecule of GW0742. A) Representation of how two GW0742 molecules bind into the PPARβ/δ binding pocket at same time. B) Detail of the amino acids interacting with the second molecule of GW0742. C) Representation of how one molecule of GW0742 first and then one molecule of GSK3787 bind into the PPARβ/δ binding pocket at same time. D) Detail of the amino acids interacting with the second molecule of GSK3787. Color coding of atoms: red O, Blue N, mustard S, cyan C PPARβ/δ and GW0742 that binds first within the binding pocket, green C of GW0742 that binds second into the binding pocket, yellow C of GSK3787 that binds second into the binding pocket.

5.2.2.2 Analysis of GW0742 and GSK3787 docked into GSK3787-bound

PPARβ/δ

GW072 and GSK3787 can also bind into the binding pocket after GSK3787 at favourable energies (-8.1 kcal/mol and -7.4 kcal/mol respectively) and the binding site is also different to the most stable ones (Figure 5.7), but interestingly the binding site is also different to the previous one, when GW0742 is bound first into the binding pocket instead of GSK3787.
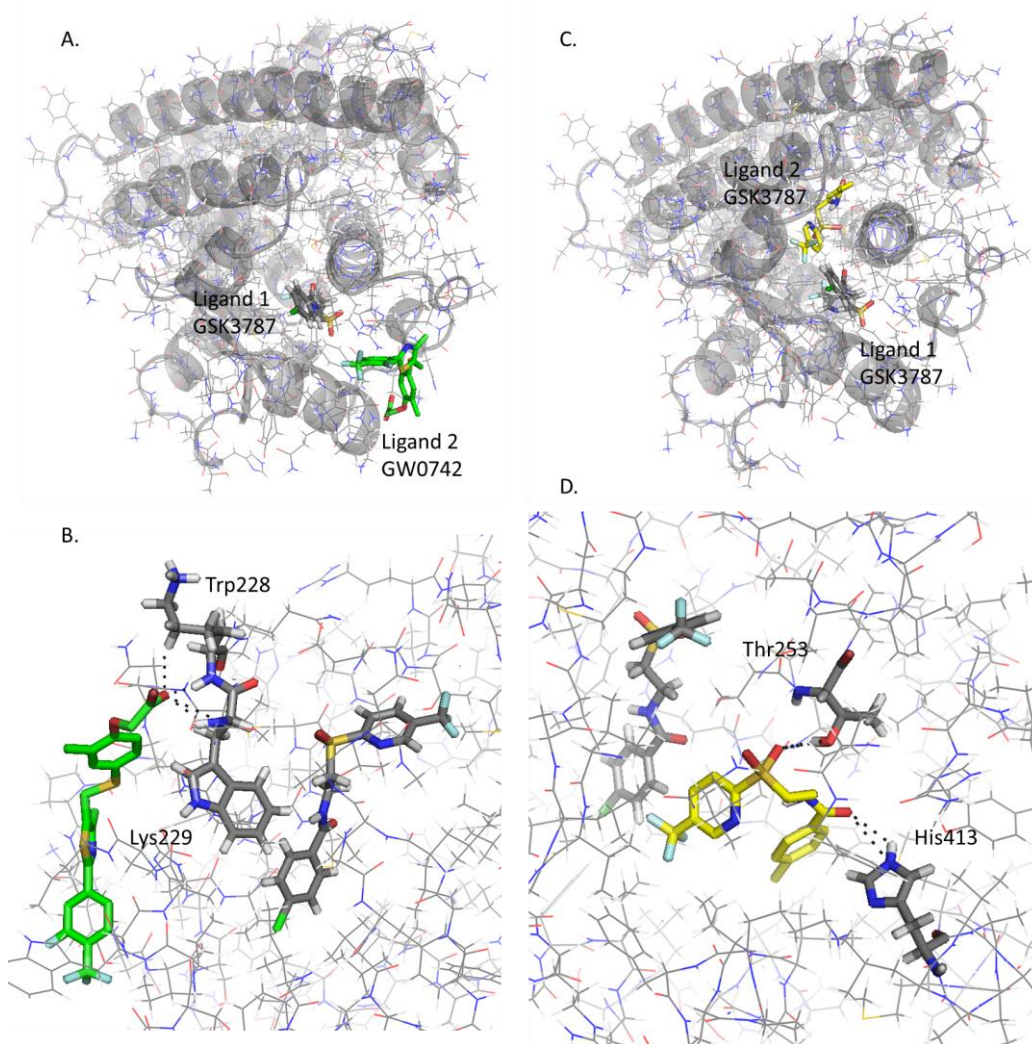
Figure 5.7 Analysis of GW0742 and GSK3787 docked into PPARβ/δ+GSK3787. A second molecule of GW0742 (A, B) or GSK3787 (C, D) was docked into the LBD of PPARβ/δ containing one molecule of GSK3787. A) Representation of how one molecule of GSK3787 first and then one molecule of GW0742 bind into the PPARβ/δ binding pocket at same time. B) Detail of the amino acids interacting with the second molecule of GW0742. C) Representation of how two molecules of GSK3787 bind into the PPARβ/δ binding pocket at same time. D) Detail of the amino acids interacting with the second molecule of GSK3787. Color coding of atoms: red O, Blue N, mustard S, grey C PPARβ/δ and GSK3787 that binds first within the binding pocket, green C of GW0742 that binds second into the binding pocket, yellow C of GSK3787 that binds second into the binding pocket.

5.2.2.3 Analysis of L-165041 and GSK0660 docked into L-165041-bound

   PPARβ/δ

When L-165041 is bound to the ligand binding pocket first, a second molecule of L-165041 or GSK0660 can bind with favourable energies (-8.3 kcal/mol and -6.5 kcal/mol respectably) and again, forming polar interactions with different residues. The most interesting finding is that GSK0660, although still in the PPARβ/δ-LBD, it binds outside the binding pocket (Figure 5.8).
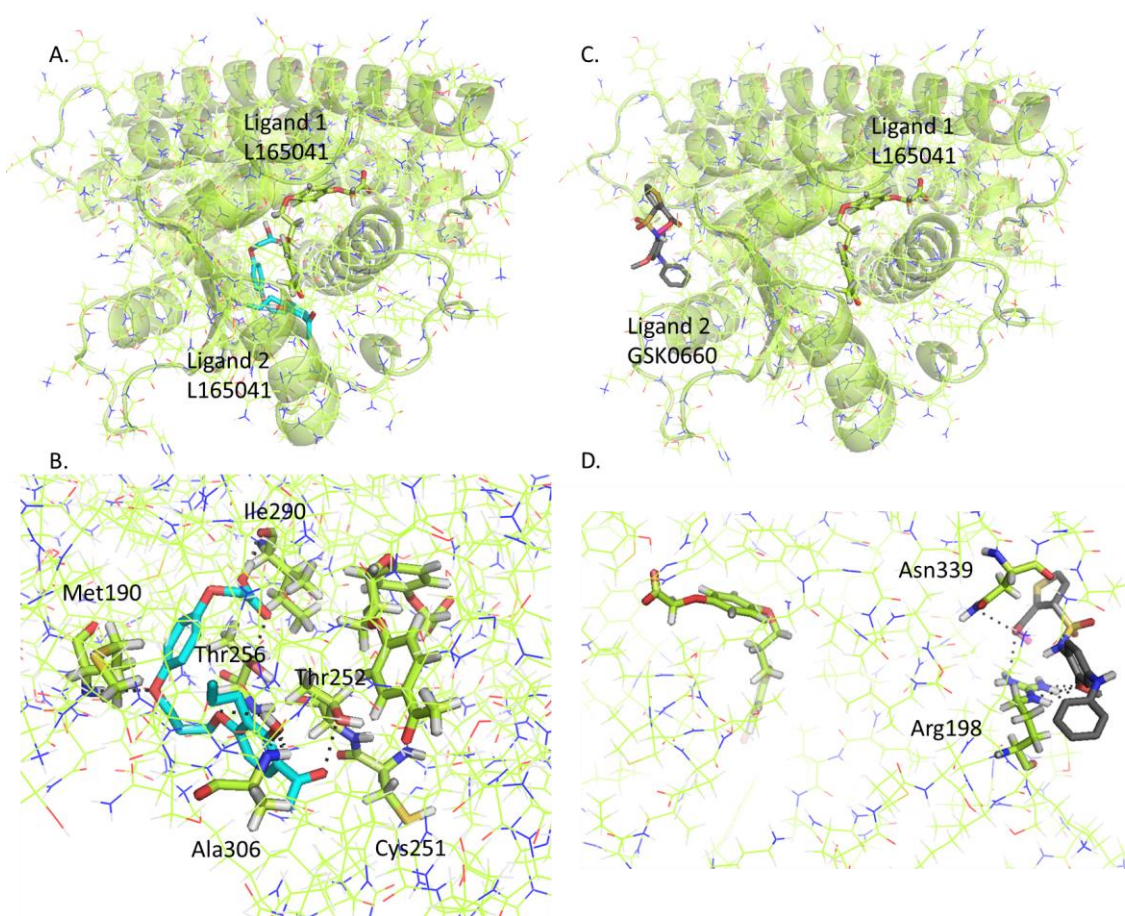
Figure 5.8 Analysis of L-165041 and GSK0660 docked into PPARβ/δ+L-165041. A second molecule of L-165041 (A, B) or GSK0660 (C, D) was docked into the LBD of PPARβ/δ containing one molecule of L-165041. A) Representation of how two L-165041 molecules bind into the PPARβ/δ binding pocket at same time. B) Detail of the amino acids interacting with the second molecule of L-165041. C) Representation of how one molecule of L-165041 first and then one molecule of GSK0660 bind into the PPARβ/δ binding pocket at same time. D) Detail of the amino acids interacting with the second molecule of GSK0660. Color coding of atoms: red O, Blue N, mustard S, yellow C PPARβ/δ and L-165041 that binds first within the binding pocket, cyan C of L-165041 that binds second into the binding pocket, grey C of GSK0660 that binds second into the binding pocket.

5.2.2.4 Analysis of L-165041 and GSK0660 docked into GSK0660-bound

PPARβ/δ

L-165041 and GSK0660 can also bind within the binding pocket at favourable energies (-8.1 kcal/mol and -8.9 kcal/mol respectively) after GSK0660 is bound in the most stable orientation (Figure 5.9), but again the binding site is different to previously when L-165041 was bound first.
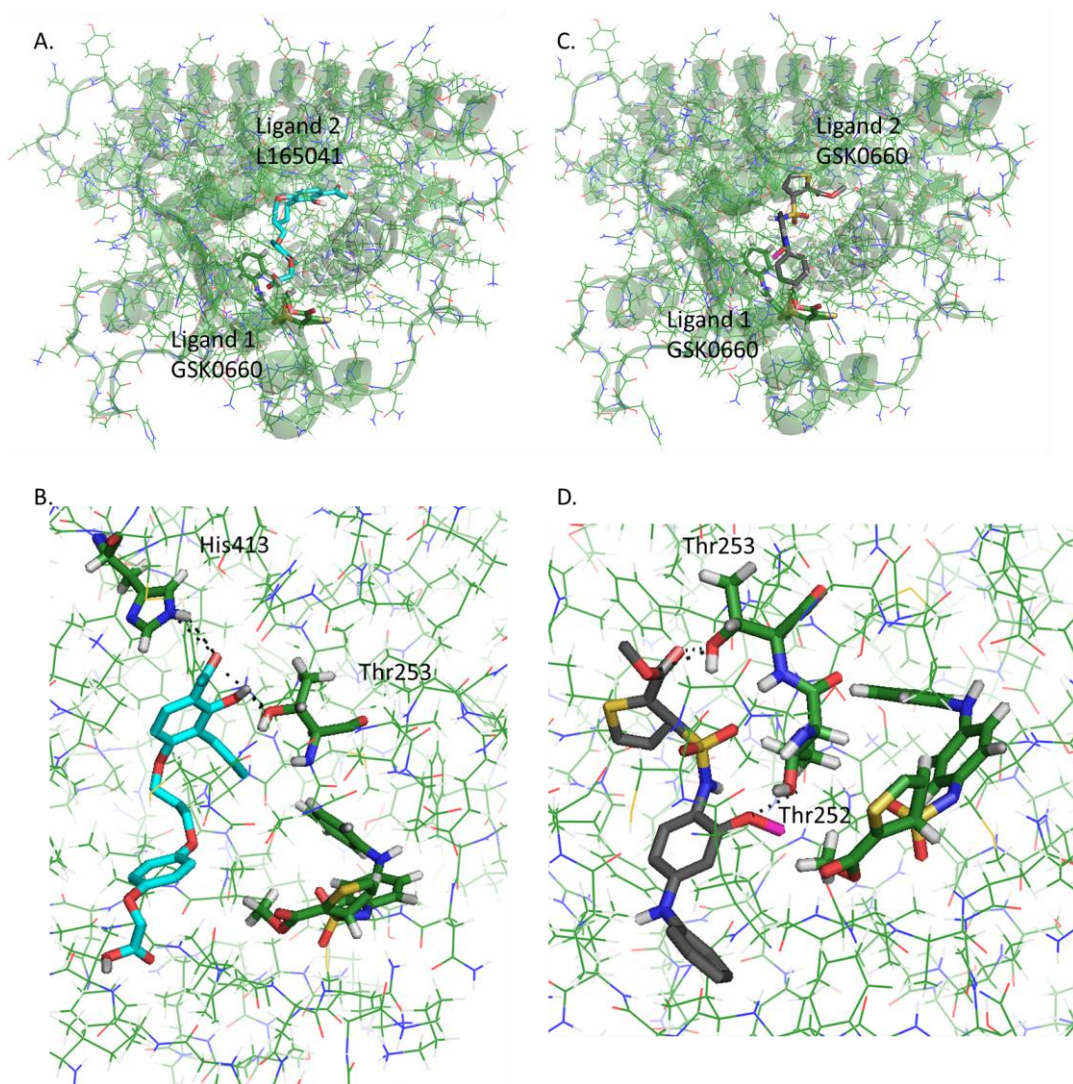
Figure 5.9 Analysis of L-165041 and GSK0660 docked into PPARβ/δ+GSK0660. A second molecule of L-165041 (A, B) or GSK0660 (C, D) was docked into the LBD of PPARβ/δ containing one molecule of GSK0660. A) Representation of how one molecule of GSK0660 first and then one molecule of L-165041 bind into the PPARβ/δ binding pocket. B) Detail of the amino acids interacting with the second molecule of L-165041. C) Representation of how two molecules of L-165041 bind into the PPARβ/δ binding pocket at same time. D) Detail of the amino acids interacting with the second molecule of GSK0660. Color coding of atoms: red O, Blue N, mustard S, green C PPARβ/δ and GSK0660 that binds first within the binding pocket, cyan C of L-165041 that binds second into the binding pocket, grey C of GSK0660 that binds second into the binding pocket.

5.3   Discussion

This chapter aims to gain a deeper understanding of the interaction of the PPARβ/δ binding pocket with different ligands, which might help explaining the different responses after PPARβ/δ activation.

To do that the four PPARβ/δ ligands used in this thesis, two agonists (GW0742 and L-165042) and two antagonists (GSK3787 and GSK0660) were docked into the PPARβ/δ binding site. The PPARβ/δ crystal structure used for the docking experiments was co-crystallized with GW0742, which was used as a control to validate the performance of the docking. The most stable pose of GW0742 predicted by Autodock Vina overlaps perfectly with the GW0742 of the crystal structure, and the polar head of GW0742 interacts with the same residues described by the author of the crystal structure (Batista *et al.* 2012), indicating that the docking protocol followed is good.

The main finding of this docking experiment is that the agonists and antagonists have a different binding profile within the binding pocket. GW0742 and L-165041 dock in the same binding place, while GSK3787 only partially overlaps GW0742 and GSK0660 binds very close but not in the very same site as GW0742. But far more interesting is the fact that the same three amino acids His287, His413 and Tyr437 form polar interactions with the two agonists docked, but they do not bind the antagonists in any of the poses predicted by docking. Furthermore, the amino acids Thr252 and Asn307 are more prone to bind the antagonists and are not predicted to bind GW0742.

This finding agrees with previous results were GW0742 was docked to another PPARβ/δ crystal structure (PDB: 3GZ9) using another docking software (Glide), and the same three amino acids bound GW0742 (Perez-Diaz *et al.* 2016). What is

more, several studies co-crystallised PPARβ/δ with different agonists both synthetic, such as iloprost (Jin *et al.* 2011), the fibrate GW2433 (Xu *et al.* 1999), or GW501516 (Wu *et al.* 2017) and natural PPARβ/δ agonists such as with eicosapentaenoic acid (EPA) (Xu *et al.* 1999), and in all cases the agonists showed polar bindings with the same three amino acids His287, His413 and Tyr437.

It is worth mentioning another study where the authors selected 5 compounds that potentially bound PPARβ/δ and performed a luciferase transactivation assay to biologically test if these compounds activate PPARβ/δ. They further analysed two of them by docking and molecular dynamics (MD) simulation, one compound that activated PPARβ/δ (Compound 1) and another one that did not activate PPARβ/δ (Compound 2). The docking and MD simulation results for the Compound 1 showed and interaction with His287, His413 and Tyr437, and the results for Compound 2 showed and interaction with Thr252 (Maltarollo *et al.* 2015).

This suggests the possibility that the different binding profile between agonists and antagonists can provoke a different 3D conformational change that might explain why PPARβ/δ binds to co-repressors instead of co-activators and *vice versa*.

Taking all this into account it can be hypothesised that a ligand that shows a high binding affinity and is predicted to form polar bonds with His287, His413 and Tyr437 will most likely behave as agonist. On the contrary, if one ligand shows high binding affinity but it is predicted to bind other residues such as Thr252 and Asn307 it is more likely that it will behave as antagonist. While there is a number of studies and PPARβ/δ crystal structures that support the first part of the hypothesis, it would be very useful to have PPARβ/δ crystal structures co-crystallized with antagonists to confirm the second part of this claim.

Some researchers mentioned the possibility that more than one ligand can simultaneously fit in the PPARβ/δ binding pocket (Nandhikonda *et al.* 2013). This option was tested using the *in silico* methods available.

The treatment of tissues with only GW0742 allows two possibilities: the binding of one or two molecules into LBD. If a second molecule of GW0742 binds to PPARβ/δ, this molecule is predicted to bind no too far from the most stable binding site and with the same binding affinity and residue interaction (Arg258) than the 8th best pose predicted for the first molecule. Similarly, when only GSK3787 is present in the treatment, a second molecule of GSK3787 is predicted to bind also not far away from its most stable binding site and with favourable binding affinity, and what is more, it will still form polar bonds with Thr252, an amino acid that is predicted to bind GSK3787 in five out of eight most stable poses predicted by docking, including the first three.

For the treatment of tissues with GW0742+GSK3787 all the options mentioned above still apply but two more options are available: GW0742 binds first and GSK3787 after or GSK3787 binds first and GW0742 after. When GW0742 binds first, GSK3787 can still bind very close to its most stable binding site with a very favourable binding affinity, and what is more, still binds the residue Thr252. If GSK3787 binds first, GW0742 is predicted to bind very far away from the most stable binding site, at the entrance of the binding pocket, and as a consequence it will have a very different binding profile forming polar bonds with Trp228 and Lys229, two residues that did not show any interaction with ligands before.

Similar analysis can be done with the other pair of agonist and antagonist. The treatment with L-165041 can lead to the binding of one or two molecules at same time; if a second molecule of L-165041 binds, it will interact with the same residues as the second most stable pose (Met192, Thr252, Thr256, Ile290 and Ala306) also

at similar binding affinity. When tissues are treated with GSK0660, a second molecule can bind very close to the most stable orientation, with similar binding affinity and also, they will share the amino acid Thr252 to form polar bindings.

If tissues are treated with L-165041+GSK0660 and L-165041 binds first, GSK0660 can still bind the LBD but outside the binding pocket, forming polar interactions with Arg198 and Asn336 and at much lower binding affinity. If GSK0660 binds first, L-165041 can bind very close to its most stable binding pose with very favourable affinity binding and interacting with Thr253 and His413.

Looking at the docking scores and molecular poses of the ligands, all possibilities described above have very favourable energies for it to happen. That opens a whole new scenario of possibilities that could dramatically change the 3D conformation of PPARβ/δ in ways that have not been thought of before, resulting in the binding of different co-regulators, which ultimately could change the PPARβ/δ response from induction to trans-repression or *vice versa*.

However, although tempting, it would be very venturous to conclude that these bindings are likely to happen only based on docking results. Docking is a very useful tool but only provides the calculated binding affinity, in other words, how well the ligand binds into the binding site. But there are other factors that can affect the likelihood of the ligands binding the binding site, such as the mobility of the molecules.

Molecular dynamics (MD) simulation is a technique for the calculation of 'movement' of the complex. It takes into account how the shape of the molecules can change with time, because a ligand can have a very good binding affinity but, because of the movement, it might 'fly' away from the binding pocket. For that reason, MD simulation is probably an essential validation that needs to be done before making any further conclusion from the docking results.

5.3.1 Conclusion

In this chapter it is described a characteristic PPARβ/δ-ligand binding profile which is different for agonists and antagonists. PPARβ/δ agonists form polar bonds with His287, His413 and Tyr437, while antagonists are more promiscuous about which amino acids they bind to, although they are very prone to bind Thr252 and Asn307. This is a new finding that can help to do better predictions about the agonist/antagonist behaviour of new drugs targeting PPARβ/δ.

To our knowledge, this is the first time that the possibility of binding two ligands simultaneously into the binding pocket is explored. The results suggest that this possibility is very likely to happen with very favourable affinity energies, and it is worth considering when designing and interpreting experiments where PPARβ/δ is ligand-activated. However, more experiment such as MD simulation need to be done to verify the results

Chapter 6: General discussion

PPARβ/δ is a nuclear receptor widely expressed which is involved in lipid metabolism, glucose metabolism, insulin sensitivity, inflammation, and cell proliferation, and it is emerging as a therapeutic target for the treatment of disorders associated with metabolic syndrome or diabetes. There is also an increased interest about the non-genomic effects of PPARβ/δ on hypertension, a life-threatening condition that can appear either spontaneously for still not known reasons or as a consequence of other diseases such as diabetes. Although there are no marketed drugs targeting PPARβ/δ yet, the interest on PPARβ/δ continues and in recent years several compounds were developed, and few reached clinical trials.

Because PPARβ/δ is a receptor involved in so many important biological functions its regulation can affect a number of different molecular pathways at the same time, so it is very important to fully understand its mechanism of action. However, there are great discrepancies in the literature about its role and its functioning both at genomic and non-genomic level.

This thesis aims to expand the knowledge on PPARβ/δ to better understand its mechanism of action at different levels using a multidisciplinary range of techniques including pharmacological, molecular and computational methods, which might give some clues for the development of new drugs and treatments.

6.1   Non-genomic effects of PPARβ/δ.

The non-genomic effects of PPARβ/δ ligands on vascular tone was the first focus of investigation. Pharmacological methods such as organ bath and myography were used because they are the *ex vivo* techniques most physiologically similar to an *in vivo* living organism where the conditions can be controlled and the responses measured accurately. Two main types of arteries were investigated, aorta and mesenteric arteries as a model of systemic and resistance vasculature respectively from healthy and STZ-induced diabetic rats.

As a result of the experiments, further evidence that PPARβ/δ significantly reduces hypercontraction in a non-genomic manner was provided but, to our knowledge, this is the first time to determine and publish that 100 nM GW0742 is the minimum concentration needed to perceive these beneficial effects.

It was also found that the incubation of aorta and mesenteric arteries in high glucose for 30 min did not have any effect in vascular contractility and the influence of high glucose to the impairment of contraction of STZ-diabetic vessels is the result of a prolonged exposure rather than punctual peaks of elevated glucose levels.

Additional evidence that aorta and mesenteric arteries contraction is dysfunctional in STZ-diabetic rat model was provided. But further to this, new evidence of the different mechanistic pathways used by different contraction agents that change with the type of vessel and health condition was found. According to the data, the impairment of the RhoA/ROCK pathway contributes the most to the dysfunction of the aorta contraction in diabetes; on the contrary, other pathways such as PI3K/Akt/eNOS or potassium channels might have more relevance in the dysfunction of the mesenteric arteries in diabetes.

It was also described the pathways used by PPARβ/δ to dilate the vessels. In large systemic arteries such as aorta, GW0742 activates PPARβ/δ which will cause the vascular dilation through the PI3K/Akt/eNOS pathway in STZ-diabetic model. GW0742 mediates the dilation of the artery in part by the inhibition of RhoA/ROCK activity in Naïve contracted arteries but not in STZ-diabetic arteries, although it is not clear if this mechanism is PPARβ/δ dependent. Besides, GW0742-mediated dilation of aorta involves potassium channels more in the diabetic state, but whether this GW0742-dependent dilation is PPARβ/δ-mediated or it is an off-target effect is still to be determined.

In resistance arteries such as mesenteric arteries, GW0742 activates PPARβ/δ which inhibits the contraction through the PI3K/Akt/eNOS pathway in Naïve and possibly STZ-diabetic tissues. Additionally, GW0742 inhibits the RhoA/ROCK pathway in STZ-diabetic mesenteric arteries in a PPARβ/δ-independent manner and regulates the potassium channels in Naïve mesenteric arteries, although it is not known if the regulation of potassium channels is PPARβ/δ-dependent or an off-target effect.

To our knowledge, this is the first study comparing the vascular reactivity of systemic and resistance arteries from healthy and STZ-induced diabetic animals looking at three different pathways at same time and analysing the effect of PPARβ/δ in all of them. The results exposed here may help to lead new therapeutic approaches for the treatment of hypertension.

6.2   Genomic effects of PPARβ/δ

The mechanism of action of PPARβ/δ at genomic level was explored next. Based on the literature it was hypothesised that PPARβ/δ can act as a molecular switch between induction and trans-repression and depending on which pathway is

triggered the tissue will have pro- or anti- response. To test the hypothesis, and again based on the literature, the regulation of the inflammatory response by PPARβ/δ on different lung tissues using a variety of molecular techniques was investigated.

In the lung three main tissues were identified: pulmonary artery, bronchi and parenchyma. All three tissues were dissected from the same lung and treated in parallel. The inflammation was induced with LPS and regulated with different PPARβ/δ ligands. Surprisingly, it was found that the most anti-inflammatory effect of PPARβ/δ was observed when an agonist and antagonist were present at same time, and also that PPARβ/δ seems to play a more important role on the regulation of inflammation in pulmonary artery than bronchi or parenchyma.

Following the hypothesis, it was interpreted that the presence of agonists and antagonist simultaneously provokes a conformational change on PPARβ/δ that switches PPARβ/δ from a pro-inflammatory state to an anti-inflammatory state. Next step was to link the pro- and anti-inflammatory responses with the induction or trans-repression mechanism of action of PPARβ/δ.

To do that, the regulation of the transcription of the selected marker genes for each mechanism of action was studied, and the results indicated that the induction was more responsible for the pro-inflammatory response and trans-repression for the anti-inflammatory response. This regulation was clearer in the pulmonary artery than in the other two tissues, which fits with the weaker inflammatory regulation by PPARβ/δ observed in bronchi and parenchyma.

It is worth pointing out that in pulmonary artery the differences on gene transcription of marker genes for trans-repression were borderline to be significantly different between treatments, but they showed not to be regulated by PPARβ/δ in parenchyma. NF-κB and Bcl-6 regulate a long list of genes, and the analysis of a

few selected marker genes is only a small part of a much bigger picture, indicating that there is a potential lack of information. Moreover, it would not be surprising that NF-κB and Bcl-6 regulate a different cluster of genes depending on the tissue, suggesting the need of a different marker gene per tissue. It all indicates that, although reliable, qRT-PCR provides limited information about the PPARβ/δ molecular switch.

A better alternative to this approach is the co-immunoprecipitation of PPARβ/δ. By analysing the protein that is bound to PPARβ/δ, whether it is RXR (induction mode) or NF-κB (trans-repression mode), and how it changes with the treatment and even tissue can demonstrate which pathway has been activated or repressed. What is more, it could also provide data of additional trans-repression pathways by detecting other transcription factors bound to PPARβ/δ, such as Bcl-6 or AP-1. In that way it is possible to draw the full picture of the PPARβ/δ molecular switch and how it changes with treatments and even with tissues, independently of the genes regulated by them. Unfortunately, due to the non-reliable antibodies anti-PPARβ/δ available this approach was not successful.

6.3 *In silico* modelling of PPARβ/δ

Next interest was to find out what happens in the PPARβ/δ binding pocket and how PPARβ/δ is activated/repressed after ligand binding, as well as the possibility of accommodating more than one ligand simultaneously into the binding pocket. For these questions computational methods such as docking were used.

First of all, a different binding profile for agonists and antagonists was described, which might cause a different 3D conformation of PPARβ/δ that could explain the interaction with co-repressors instead of co-activators and *vice versa*. To our knowledge, the different agonist/antagonist binding profile to PPARβ/δ has not

been described before and it might help to predict the behaviour of a ligand with a high binding affinity.

Also, the possibility of two agonists binding at same time into the PPARβ/δ binding pocket was explored. According to the results, all the options studied seem feasible with favourable binding energies, suggesting the need of being more cautious when designing and interpreting the results of experiments using PPARβ/δ ligands, although more experiments need to be done to verify this result.

6.4   Conclusion

This thesis reveals a multidisciplinary approach for the study of PPARβ/δ that provides novel information about its functioning both at genomic and non-genomic level. The findings of this study can potentially help the drug discovery industry for a better prediction of the behaviour of new drugs and can also help developing new treatments targeting PPARβ/δ for hypertension or metabolic diseases.

6.5   Future work

It would be very useful to perform experiments in order to prove or disprove some of the conclusions of this thesis, such as:

- Co-immunoprecipitate PPARβ/δ under the same conditions used in this thesis to have the full picture of the PPARβ/δ molecular switch.
- Co-crystallise PPARβ/δ with antagonists to verify the antagonist binding profile described.
- Perform a MD simulation of PPARβ/δ with two ligands simultaneously, same combinations used in this thesis.

References

(2005). "Diagnosis and classification of diabetes mellitus." <u>Diabetes Care</u> **28 Suppl 1**: S37-42.

Aarenstrup, L., Flindt, E. N., Otkjaer, K., Kirkegaard, M., Andersen, J. S. and Kristiansen, K. (2008). "HDAC activity is required for p65/RelA-dependent repression of PPARdelta-mediated transactivation in human keratinocytes." <u>J Invest Dermatol</u> **128**(5): 1095-1106.

Adhikary, T., Kaddatz, K., Finkernagel, F., Schonbauer, A., Meissner, W., Scharfe, M., Jarek, M., Blocker, H., Muller-Brusselbach, S. and Muller, R. (2011). "Genomewide analyses define different modes of transcriptional regulation by peroxisome proliferator-activated receptor-beta/delta (PPARbeta/delta)." <u>PLoS One</u> **6**(1): e16344.

Adhikary, T., Wortmann, A., Schumann, T., Finkernagel, F., Lieber, S., Roth, K., Toth, P. M., Diederich, W. E., Nist, A., Stiewe, T., Kleinesudeik, L., Reinartz, S., Muller-Brusselbach, S. and Muller, R. (2015). "The transcriptional PPARbeta/delta network in human macrophages defines a unique agonist-induced activation state." <u>Nucleic Acids Res</u> **43**(10): 5033-5051.

Agrawal, R. (2014). "The first approved agent in the Glitazar's Class: Saroglitazar." <u>Curr Drug Targets</u> **15**(2): 151-155.

Ahmad, J., Odin, J. A., Hayashi, P. H., Chalasani, N., Fontana, R. J., Barnhart, H., Cirulli, E. T., Kleiner, D. E. and Hoofnagle, J. H. (2017). "Identification and characterization of fenofibrate-induced liver injury." <u>Dig Dis Sci</u> **62**(12): 3596-3604.

Ali, F. Y., Davidson, S. J., Moraes, L. A., Traves, S. L., Paul-Clark, M., Bishop-Bailey, D., Warner, T. D. and Mitchell, J. A. (2006). "Role of nuclear receptor signaling in platelets: antithrombotic effects of PPARbeta." <u>Faseb j</u> **20**(2): 326-328.

Ali, F. Y., Hall, M. G., Desvergne, B., Warner, T. D. and Mitchell, J. A. (2009). "PPARbeta/delta agonists modulate platelet function via a mechanism involving PPAR receptors and specific association/repression of PKCalpha--brief report." <u>Arterioscler Thromb Vasc Biol</u> **29**(11): 1871-1873.

Altieri, P., Spallarossa, P., Barisione, C., Garibaldi, S., Garuti, A., Fabbi, P., Ghigliotti, G. and Brunelli, C. (2012). "Inhibition of doxorubicin-induced senescence by PPARdelta activation agonists in cardiac muscle cells: cooperation between PPARdelta and Bcl6." <u>PLoS One</u> **7**(9): e46126.

An, H. J., Lee, B., Kim, S. M., Kim, D. H., Chung, K. W., Ha, S. G., Park, K. C., Park, Y. J., Kim, S. J., Yun, H. Y., Chun, P., Yu, B. P., Moon, H. R. and Chung, H. Y. (2018). "A PPAR pan agonist, MHY2013 alleviates age-related hepatic lipid accumulation by promoting fatty acid oxidation and suppressing inflammation." <u>Biol Pharm Bull</u> **41**(1): 29-35.

Araki, E., Yamashita, S., Arai, H., Yokote, K., Satoh, J., Inoguchi, T., Nakamura, J., Maegawa, H., Yoshioka, N., Tanizawa, Y., Watada, H., Suganami, H. and Ishibashi, S. (2018). "Effects of pemafibrate, a novel selective PPARalpha modulator, on lipid and glucose metabolism in patients

with type 2 diabetes and hypertriglyceridemia: A randomized, double-blind, placebo-controlled, phase 3 trial." <u>Diabetes Care</u> **41**(3): 538-546.

Archer, S. L., Souil, E., Dinh-Xuan, A. T., Schremmer, B., Mercier, J. C., El Yaagoubi, A., Nguyen-Huu, L., Reeve, H. L. and Hampl, V. (1998). "Molecular identification of the role of voltage-gated K+ channels, Kv1.5 and Kv2.1, in hypoxic pulmonary vasoconstriction and control of resting membrane potential in rat pulmonary artery myocytes." <u>J Clin Invest</u> **101**(11): 2319-2330.

Aronoff, S., Rosenblatt, S., Braithwaite, S., Egan, J. W., Mathisen, A. L. and Schneider, R. L. (2000). "Pioglitazone hydrochloride monotherapy improves glycemic control in the treatment of patients with type 2 diabetes: a 6-month randomized placebo-controlled dose-response study. The Pioglitazone 001 Study Group." <u>Diabetes Care</u> **23**(11): 1605-1611.

Astakhova, A. A., Chistyakov, D. V., Pankevich, E. V. and Sergeeva, M. G. (2015). "Regulation of cyclooxygenase 2 expression by agonists of PPAR nuclear receptors in the model of endotoxin tolerance in astrocytes." <u>Biochemistry (Mosc)</u> **80**(10): 1262-1270.

Atkinson, M. A. and Leiter, E. H. (1999). "The NOD mouse model of type 1 diabetes: as good as it gets?" <u>Nat Med</u> **5**(6): 601-604.

Bao, X. C., Fang, Y. Q., You, P., Zhang, S. and Ma, J. (2014). "Protective role of peroxisome proliferator-activated receptor beta/delta in acute lung injury induced by prolonged hyperbaric hyperoxia in rats." <u>Respir Physiol Neurobiol</u> **199**: 9-18.

Barish, G. D., Atkins, A. R., Downes, M., Olson, P., Chong, L. W., Nelson, M., Zou, Y., Hwang, H., Kang, H., Curtiss, L., Evans, R. M. and Lee, C. H. (2008). "PPARdelta regulates multiple proinflammatory pathways to suppress atherosclerosis." <u>Proc Natl Acad Sci U S A</u> **105**(11): 4271-4276.

Barlaka, E., Gorbe, A., Gaspar, R., Paloczi, J., Ferdinandy, P. and Lazou, A. (2015). "Activation of PPARbeta/delta protects cardiac myocytes from oxidative stress-induced apoptosis by suppressing generation of reactive oxygen/nitrogen species and expression of matrix metalloproteinases." <u>Pharmacol Res</u> **95-96**: 102-110.

Barroso, E., Eyre, E., Palomer, X. and Vazquez-Carrera, M. (2011). "The peroxisome proliferator-activated receptor beta/delta (PPARbeta/delta) agonist GW501516 prevents TNF-alpha-induced NF-kappaB activation in human HaCaT cells by reducing p65 acetylation through AMPK and SIRT1." <u>Biochem Pharmacol</u> **81**(4): 534-543.

Batista, F. A., Trivella, D. B., Bernardes, A., Gratieri, J., Oliveira, P. S., Figueira, A. C., Webb, P. and Polikarpov, I. (2012). "Structural insights into human peroxisome proliferator activated receptor delta (PPAR-delta) selective ligand binding." <u>PLoS One</u> **7**(5): e33643.

Bays, H. E., Schwartz, S., Littlejohn, T., 3rd, Kerzner, B., Krauss, R. M., Karpf, D. B., Choi, Y. J., Wang, X., Naim, S. and Roberts, B. K. (2011). "MBX-8025, a novel peroxisome proliferator receptor-delta agonist: lipid and other metabolic effects in dyslipidemic overweight patients treated with and without atorvastatin." <u>J Clin Endocrinol Metab</u> **96**(9): 2889-2897.

Bellani, G., Laffey, J. G., Pham, T., Fan, E., Brochard, L., Esteban, A., Gattinoni, L., van Haren, F., Larsson, A., McAuley, D. F., Ranieri, M., Rubenfeld, G., Thompson, B. T., Wrigge, H., Slutsky, A. S.

and Pesenti, A. (2016). "Epidemiology, Patterns of Care, and Mortality for Patients With Acute Respiratory Distress Syndrome in Intensive Care Units in 50 Countries." Jama **315**(8): 788-800.

Berger, J., Leibowitz, M. D., Doebber, T. W., Elbrecht, A., Zhang, B., Zhou, G., Biswas, C., Cullinan, C. A., Hayes, N. S., Li, Y., Tanen, M., Ventre, J., Wu, M. S., Berger, G. D., Mosley, R., Marquis, R., Santini, C., Sahoo, S. P., Tolman, R. L., Smith, R. G. and Moller, D. E. (1999). "Novel peroxisome proliferator-activated receptor (PPAR) gamma and PPARdelta ligands produce distinct biological effects." J Biol Chem **274**(10): 6718-6725.

Berhanu, P., Kipnes, M. S., Khan, M. A., Perez, A. T., Kupfer, S. F., Spanheimer, R. C., Demissie, S. and Fleck, P. R. (2006). "Effects of pioglitazone on lipid and lipoprotein profiles in patients with type 2 diabetes and dyslipidaemia after treatment conversion from rosiglitazone while continuing stable statin therapy." Diab Vasc Dis Res **3**(1): 39-44.

Birenbaum, M. D. A., Tesse, P. D. A., Loyer, P. D. X., Michelet, M. D. P. D. P., Andriantsitohaina, P. D. R., Heymes, P. D. C., Riou, M. D. P. D. B. and Amour, M. D. P. D. J. (2008). "Involvement of β3-adrenoceptor in altered β-adrenergic response in senescent heart: role of nitric oxide synthase 1–derived nitric oxide." Anesthesiology **109**(6): 1045-1053.

Bishop-Bailey, D. (2000). "Peroxisome proliferator-activated receptors in the cardiovascular system." Br J Pharmacol **129**(5): 823-834.

Bishop-Bailey, D. and Bystrom, J. (2009). "Emerging roles of peroxisome proliferator-activated receptor-beta/delta in inflammation." Pharmacol Ther **124**(2): 141-150.

Bishop-Bailey, D. and Hla, T. (1999). "Endothelial cell apoptosis induced by the peroxisome proliferator-activated receptor (PPAR) ligand 15-deoxy-Delta12, 14-prostaglandin J2." J Biol Chem **274**(24): 17042-17048.

Bojic, L. A., Burke, A. C., Chhoker, S. S., Telford, D. E., Sutherland, B. G., Edwards, J. Y., Sawyez, C. G., Tirona, R. G., Yin, H., Pickering, J. G. and Huff, M. W. (2014). "Peroxisome proliferator-activated receptor delta agonist GW1516 attenuates diet-induced aortic inflammation, insulin resistance, and atherosclerosis in low-density lipoprotein receptor knockout mice." Arterioscler Thromb Vasc Biol **34**(1): 52-60.

Braissant, O., Foufelle, F., Scotto, C., Dauca, M. and Wahli, W. (1996). "Differential expression of peroxisome proliferator-activated receptors (PPARs): tissue distribution of PPAR-alpha, -beta, and -gamma in the adult rat." Endocrinology **137**(1): 354-366.

Brouwers, O., Niessen, P. M., Haenen, G., Miyata, T., Brownlee, M., Stehouwer, C. D., De Mey, J. G. and Schalkwijk, C. G. (2010). "Hyperglycaemia-induced impairment of endothelium-dependent vasorelaxation in rat mesenteric arteries is mediated by intracellular methylglyoxal levels in a pathway dependent on oxidative stress." Diabetologia **53**(5): 989-1000.

Bruning, J. B., Chalmers, M. J., Prasad, S., Busby, S. A., Kamenecka, T. M., He, Y., Nettles, K. W. and Griffin, P. R. (2007). "Partial agonists activate PPARγ using a helix 12 independent mechanism." Structure **15**(10): 1258-1271.

Budzyn, K., Paull, M., Marley, P. D. and Sobey, C. G. (2006). "Segmental differences in the roles of rho-kinase and protein kinase C in mediating vasoconstriction." J Pharmacol Exp Ther **317**(2): 791-796.

Burgess, D. C., Hunt, D., Li, L., Zannino, D., Williamson, E., Davis, T. M., Laakso, M., Kesaniemi, Y. A., Zhang, J., Sy, R. W., Lehto, S., Mann, S. and Keech, A. C. (2010). "Incidence and predictors of silent myocardial infarction in type 2 diabetes and the effect of fenofibrate: an analysis from the Fenofibrate Intervention and Event Lowering in Diabetes (FIELD) study." Eur Heart J **31**(1): 92-99.

Cariou, B., Hanf, R., Lambert-Porcheron, S., Zair, Y., Sauvinet, V., Noel, B., Flet, L., Vidal, H., Staels, B. and Laville, M. (2013). "Dual peroxisome proliferator-activated receptor alpha/delta agonist GFT505 improves hepatic and peripheral insulin sensitivity in abdominally obese subjects." Diabetes Care **36**(10): 2923-2930.

Cariou, B., Zaïr, Y., Staels, B. and Bruckert, E. (2011). "Effects of the new dual PPARα/δ agonist GFT505 on lipid and glucose homeostasis in abdominally obese patients with combined dyslipidemia or impaired glucose metabolism." Diabetes Care **34**(9): 2008-2014.

Castillero, E., Alamdari, N., Aversa, Z., Gurav, A. and Hasselgren, P. O. (2013). "PPARbeta/delta regulates glucocorticoid- and sepsis-induced FOXO1 activation and muscle wasting." PLoS One **8**(3): e59726.

Chandra, V., Huang, P., Hamuro, Y., Raghuram, S., Wang, Y., Burris, T. P. and Rastinejad, F. (2008). "Structure of the intact PPAR-γ–RXR-α nuclear receptor complex on DNA." Nature **456**: 350.

Chang, K. S. and Stevens, W. C. (1992). "Endothelium-dependent increase in vascular sensitivity to phenylephrine in long-term streptozotocin diabetic rat aorta." Br J Pharmacol **107**(4): 983-990.

Chang, Y. T., Chen, C. L., Lin, C. F., Lu, S. L., Cheng, M. H., Kuo, C. F. and Lin, Y. S. (2013). "Regulatory role of GSK-3 beta on NF- kappa B, nitric oxide, and TNF- alpha in group A streptococcal infection." Mediators Inflamm **2013**: 720689.

Chen, Y., Chen, H., Birnbaum, Y., Nanhwan, M. K., Bajaj, M., Ye, Y. and Qian, J. (2017). "Aleglitazar, a dual peroxisome proliferator-activated receptor-alpha and -gamma agonist, protects cardiomyocytes against the adverse effects of hyperglycaemia." Diab Vasc Dis Res **14**(2): 152-162.

Chin, J., Hong, J. Y., Lee, J., Hwang, H., Ko, H., Choi, H., Hahn, D., Ko, J., Nam, S.-J., Tak, J., Ham, J. and Kang, H. (2010). "Selective peroxisome proliferator-activated receptor δ isosteric selenium agonists as potent anti-atherogenic agents in vivo." Bioorganic & Medicinal Chemistry Letters **20**(24): 7239-7242.

Chiquette, E., Ramirez, G. and Defronzo, R. (2004). "A meta-analysis comparing the effect of thiazolidinediones on cardiovascular risk factors." Arch Intern Med **164**(19): 2097-2104.

Choi, H. D. and Shin, W. G. (2014). "Safety and efficacy of statin treatment alone and in combination with fibrates in patients with dyslipidemia: a meta-analysis." Curr Med Res Opin **30**(1): 1-10.

Clark, A. R. and Belvisi, M. G. (2012). "Maps and legends: the quest for dissociated ligands of the glucocorticoid receptor." Pharmacol Ther **134**(1): 54-67.

Cole, W. C. and Welsh, D. G. (2011). "Role of myosin light chain kinase and myosin light chain phosphatase in the resistance arterial myogenic response to intravascular pressure." Archives of Biochemistry and Biophysics **510**(2): 160-173.

Coll, T., Alvarez-Guardia, D., Barroso, E., Gomez-Foix, A. M., Palomer, X., Laguna, J. C. and Vazquez-Carrera, M. (2010). "Activation of peroxisome proliferator-activated receptor-{delta} by GW501516 prevents fatty acid-induced nuclear factor-{kappa}B activation and insulin resistance in skeletal muscle cells." Endocrinology **151**(4): 1560-1569.

Coll, T., Rodriguez-Calvo, R., Barroso, E., Serrano, L., Eyre, E., Palomer, X. and Vazquez-Carrera, M. (2009). "Peroxisome proliferator-activated receptor (PPAR) beta/delta: a new potential therapeutic target for the treatment of metabolic syndrome." Curr Mol Pharmacol **2**(1): 46-55.

Coneski, P. N. and Schoenfisch, M. H. (2012). "Nitric oxide release: Part III. Measurement and reporting." Chemical Society Reviews **41**(10): 3753-3758.

Cronet, P., Petersen, J. F. W., Folmer, R., Blomberg, N., Sjöblom, K., Karlsson, U., Lindstedt, E.-L. and Bamberg, K. (2001). "Structure of the PPARα and -γ ligand binding domain in complex with AZ 242; ligand selectivity and agonist activation in the PPAR family." Structure **9**(8): 699-706.

Dai, S., Robitaille, C., Bancej, C., Loukine, L., Waters, C. and Baclic, O. (2010). "Executive summary--report from the Canadian Chronic Disease Surveillance System: hypertension in Canada, 2010." Chronic Dis Can **31**(1): 46-47.

Degenhardt, T., Saramaki, A., Malinen, M., Rieck, M., Vaisanen, S., Huotari, A., Herzig, K. H., Muller, R. and Carlberg, C. (2007). "Three members of the human pyruvate dehydrogenase kinase gene family are direct targets of the peroxisome proliferator-activated receptor beta/delta." J Mol Biol **372**(2): 341-355.

Degueurce, G., D'Errico, I., Pich, C., Ibberson, M., Schutz, F., Montagner, A., Sgandurra, M., Mury, L., Jafari, P., Boda, A., Meunier, J., Rezzonico, R., Brembilla, N. C., Hohl, D., Kolios, A., Hofbauer, G., Xenarios, I. and Michalik, L. (2016). "Identification of a novel PPARbeta/delta/miR-21-3p axis in UV-induced skin inflammation." EMBO Mol Med **8**(8): 919-936.

DePaoli, A. M., Higgins, L. S., Henry, R. R., Mantzoros, C. and Dunn, F. L. (2014). "Can a selective PPARγ modulator improve glycemic control in patients with type 2 Diabetes with fewer side effects compared with pioglitazone?" Diabetes Care **37**(7): 1918-1923.

Desreumaux, P., Dubuquoy, L., Nutten, S., Peuchmaur, M., Englaro, W., Schoonjans, K., Derijard, B., Desvergne, B., Wahli, W., Chambon, P., Leibowitz, M. D., Colombel, J. F. and Auwerx, J. (2001). "Attenuation of colon inflammation through activators of the retinoid X receptor (RXR)/peroxisome proliferator-activated receptor gamma (PPARgamma) heterodimer. A basis for new therapeutic strategies." J Exp Med **193**(7): 827-838.

Di-Poi, N., Tan, N. S., Michalik, L., Wahli, W. and Desvergne, B. (2002). "Antiapoptotic role of PPARbeta in keratinocytes via transcriptional control of the Akt1 signaling pathway." Mol Cell **10**(4): 721-733.

Di Paola, R., Briguglio, F., Paterniti, I., Mazzon, E., Oteri, G., Militi, D., Cordasco, G. and Cuzzocrea, S. (2011). "Emerging role of PPAR-beta/delta in inflammatory process associated to experimental periodontitis." <u>Mediators Inflamm</u> **2011**: 787159.

Di Paola, R., Crisafulli, C., Mazzon, E., Esposito, E., Paterniti, I., Galuppo, M., Genovese, T., Thiemermann, C. and Cuzzocrea, S. (2010). "GW0742, a high-affinity PPAR -beta/delta agonist, inhibits acute lung injury in mice." <u>Shock</u> **33**(4): 426-435.

Ding, G., Cheng, L., Qin, Q., Frontin, S. and Yang, Q. (2006). "PPARdelta modulates lipopolysaccharide-induced TNFalpha inflammation signaling in cultured cardiomyocytes." <u>J Mol Cell Cardiol</u> **40**(6): 821-828.

Dunn, S. E., Bhat, R., Straus, D. S., Sobel, R. A., Axtell, R., Johnson, A., Nguyen, K., Mukundan, L., Moshkova, M., Dugas, J. C., Chawla, A. and Steinman, L. (2010). "Peroxisome proliferator-activated receptor delta limits the expansion of pathogenic Th cells during central nervous system autoimmunity." <u>J Exp Med</u> **207**(8): 1599-1608.

Edwards, C. J. and Williams, E. (2010). "The role of interleukin-6 in rheumatoid arthritis-associated osteoporosis." <u>Osteoporos Int</u> **21**(8): 1287-1293.

El-Awady, M. S., El-Agamy, D. S., Suddek, G. M. and Nader, M. A. (2014). "Propolis protects against high glucose-induced vascular endothelial dysfunction in isolated rat aorta." <u>J Physiol Biochem</u> **70**(1): 247-254.

Elsner, M., Guldbakke, B., Tiedge, M., Munday, R. and Lenzen, S. (2000). "Relative importance of transport and alkylation for pancreatic beta-cell toxicity of streptozotocin." <u>Diabetologia</u> **43**(12): 1528-1533.

Erdmann, E., Califf, R., Gerstein, H. C., Malmberg, K., Ruilope, L., Schwartz, G. G., Wedel, H., Volz, D., Ditmarsch, M., Svensson, A. and Bengus, M. (2015). "Effects of the dual peroxisome proliferator-activated receptor activator aleglitazar in patients with Type 2 Diabetes mellitus or prediabetes." <u>Am Heart J</u> **170**(1): 117-122.

Fajas, L., Fruchart, J. C. and Auwerx, J. (1998). "PPARgamma3 mRNA: a distinct PPARgamma mRNA subtype transcribed from an independent promoter." <u>FEBS Lett</u> **438**(1-2): 55-60.

Fan, Y., Wang, Y., Tang, Z., Zhang, H., Qin, X., Zhu, Y., Guan, Y., Wang, X., Staels, B., Chien, S. and Wang, N. (2008). "Suppression of pro-inflammatory adhesion molecules by PPAR-delta in human vascular endothelial cells." <u>Arterioscler Thromb Vasc Biol</u> **28**(2): 315-321.

Farley, K. S., Wang, L. F., Law, C. and Mehta, S. (2008). "Alveolar macrophage inducible nitric oxide synthase-dependent pulmonary microvascular endothelial cell septic barrier dysfunction." <u>Microvasc Res</u> **76**(3): 208-216.

Fedorova, L. V., Sodhi, K., Gatto-Weis, C., Puri, N., Hinds, T. D., Jr., Shapiro, J. I. and Malhotra, D. (2013). "Peroxisome proliferator-activated receptor delta agonist, HPP593, prevents renal necrosis under chronic ischemia." <u>PLoS One</u> **8**(5): e64436.

Feng, X., Gao, X., Jia, Y., Zhang, H., Xu, Y. and Wang, G. (2016). "PPAR-α agonist fenofibrate decreased RANTES levels in type 2 diabetes patients with hypertriglyceridemia." Medical Science Monitor : International Medical Journal of Experimental and Clinical Research **22**: 743-751.

Filippatos, T. D. and Elisaf, M. S. (2015). "Safety considerations with fenofibrate/simvastatin combination." Expert Opin Drug Saf **14**(9): 1481-1493.

Fonseca, V. A., Valiquett, T. R., Huang, S. M., Ghazzi, M. N. and Whitcomb, R. W. (1998). "Troglitazone monotherapy improves glycemic control in patients with type 2 diabetes mellitus: a randomized, controlled study. The Troglitazone Study Group." J Clin Endocrinol Metab **83**(9): 3169-3176.

Foreman, J. E., Chang, W. C., Palkar, P. S., Zhu, B., Borland, M. G., Williams, J. L., Kramer, L. R., Clapper, M. L., Gonzalez, F. J. and Peters, J. M. (2011). "Functional characterization of peroxisome proliferator-activated receptor-beta/delta expression in colon cancer." Mol Carcinog **50**(11): 884-900.

Forman, B. M., Chen, J. and Evans, R. M. (1997). "Hypolipidemic drugs, polyunsaturated fatty acids, and eicosanoids are ligands for peroxisome proliferator-activated receptors alpha and delta." Proc Natl Acad Sci U S A **94**(9): 4312-4317.

Forman, B. M., Goode, E., Chen, J., Oro, A. E., Bradley, D. J., Perlmann, T., Noonan, D. J., Burka, L. T., McMorris, T., Lamph, W. W., Evans, R. M. and Weinberger, C. (1995). "Identification of a nuclear receptor that is activated by farnesol metabolites." Cell **81**(5): 687-693.

Galuppo, M., Di Paola, R., Mazzon, E., Genovese, T., Crisafulli, C., Paterniti, I., Cuzzocrea, E., Bramanti, P., Kapoor, A., Thiemermann, C. and Cuzzocrea, S. (2010). "Role of PPAR-delta in the development of zymosan-induced multiple organ failure: an experiment mice study." J Inflamm (Lond) **7**: 12.

Geiger, L. N., Dunsford, W. S., Lewis, D. J., Brennan, C., Liu, K. C. and Newsholme, S. J. (2009). "Rat carcinogenicity study with GW501516, a PPAR delta agonist." Toxicol Sci **108**(SUPPL.): 895.

Girroir, E. E., Hollingshead, H. E., He, P., Zhu, B., Perdew, G. H. and Peters, J. M. (2008). "Quantitative expression patterns of peroxisome proliferator-activated receptor-beta/delta (PPARbeta/delta) protein in mice." Biochem Biophys Res Commun **371**(3): 456-461.

Goldberg, A. C., Schonfeld, G., Feldman, E. B., Ginsberg, H. N., Hunninghake, D. B., Insull, W., Jr., Knopp, R. H., Kwiterovich, P. O., Mellies, M. J., Pickering, J. and et al. (1989). "Fenofibrate for the treatment of type IV and V hyperlipoproteinemias: a double-blind, placebo-controlled multicenter US study." Clin Ther **11**(1): 69-83.

Gomaraschi, M., Ossoli, A., Adorni, M. P., Damonte, E., Niesor, E., Veglia, F., Franceschini, G., Benghozi, R. and Calabresi, L. (2015). "Fenofibrate and extended-release niacin improve the endothelial protective effects of HDL in patients with metabolic syndrome." Vascul Pharmacol **74**: 80-86.

Goto, Y., Kakizaki, M. and Masaki, N. (1976). "Production of spontaneous diabetic rats by repetition of selective breeding." Tohoku J Exp Med **119**(1): 85-90.

Grundy, S. M. (2016). "Metabolic syndrome update." Trends Cardiovasc Med **26**(4): 364-373.

Grygiel-Gorniak, B. (2014). "Peroxisome proliferator-activated receptors and their ligands: nutritional and clinical implications--a review." Nutr J **13**: 17.

Gu, Y., Li, X., He, T., Jiang, Z., Hao, P. and Tang, X. (2014). "The antifibrosis effects of peroxisome proliferator-activated receptor delta on rat corneal wound healing after excimer laser keratectomy." PPAR Res **2014**: 464935.

Gu, Y., Tang, X., Xie, L., Meng, G. and Ji, Y. (2016). "Aliskiren improves endothelium-dependent relaxation of thoracic aorta by activating PI3K/Akt/eNOS signal pathway in SHR." Clin Exp Pharmacol Physiol **43**(4): 450-458.

Ham, S. A., Yoo, T., Hwang, J. S., Kang, E. S., Lee, W. J., Paek, K. S., Park, C., Kim, J. H., Do, J. T., Lim, D. S. and Seo, H. G. (2014). "Ligand-activated PPARdelta modulates the migration and invasion of melanoma cells by regulating Snail expression." Am J Cancer Res **4**(6): 674-682.

Hamblin, M., Chang, L., Fan, Y., Zhang, J. and Chen, Y. E. (2009). "PPARs and the cardiovascular system." Antioxid Redox Signal **11**(6): 1415-1452.

Han, J. K., Kim, H. L., Jeon, K. H., Choi, Y. E., Lee, H. S., Kwon, Y. W., Jang, J. J., Cho, H. J., Kang, H. J., Oh, B. H., Park, Y. B. and Kim, H. S. (2013). "Peroxisome proliferator-activated receptor-delta activates endothelial progenitor cells to induce angio-myogenesis through matrix metallo-proteinase-9-mediated insulin-like growth factor-1 paracrine networks." Eur Heart J **34**(23): 1755-1765.

Han, J. K., Lee, H. S., Yang, H. M., Hur, J., Jun, S. I., Kim, J. Y., Cho, C. H., Koh, G. Y., Peters, J. M., Park, K. W., Cho, H. J., Lee, H. Y., Kang, H. J., Oh, B. H., Park, Y. B. and Kim, H. S. (2008). "Peroxisome proliferator-activated receptor-delta agonist enhances vasculogenesis by regulating endothelial progenitor cells through genomic and nongenomic activations of the phosphatidylinositol 3-kinase/Akt pathway." Circulation **118**(10): 1021-1033.

Harrington, L. S., Moreno, L., Reed, A., Wort, S. J., Desvergne, B., Garland, C., Zhao, L. and Mitchell, J. A. (2010). "The PPARbeta/delta agonist GW0742 relaxes pulmonary vessels and limits right heart hypertrophy in rats with hypoxia-induced pulmonary hypertension." PLoS One **5**(3): e9526.

Haskova, Z., Hoang, B., Luo, G., Morgan, L. A., Billin, A. N., Barone, F. C., Shearer, B. G., Barton, M. E. and Kilgore, K. S. (2008). "Modulation of LPS-induced pulmonary neutrophil infiltration and cytokine production by the selective PPARbeta/delta ligand GW0742." Inflamm Res **57**(7): 314-321.

He, T., Smith, L. A., Lu, T., Joyner, M. J. and Katusic, Z. S. (2011). "Activation of peroxisome proliferator-activated receptor-{delta} enhances regenerative capacity of human endothelial progenitor cells by stimulating biosynthesis of tetrahydrobiopterin." Hypertension **58**(2): 287-294.

Hellmold, H., Zhang, H., Andersson, U., Blomgren, B., Holland, T., Berg, A. L., Elebring, M., Sjogren, N., Bamberg, K., Dahl, B., Westerberg, R., Dillner, B., Tugwood, J., Tugwood, J., Roberts, R., Lundholm, E., Camejo, G., Skanberg, I. and Evans, J. (2007). "Tesaglitazar, a PPARalpha/gamma agonist, induces interstitial mesenchymal cell DNA synthesis and fibrosarcomas in subcutaneous tissues in rats." Toxicol Sci **98**(1): 63-74.

Helsen, C. and Claessens, F. (2014). "Looking at nuclear receptors from a new angle." Molecular and Cellular Endocrinology **382**(1): 97-106.

Henriksen, K., Byrjalsen, I., Qvist, P., Beck-Nielsen, H., Hansen, G., Riis, B. J., Perrild, H., Svendsen, O. L., Gram, J., Karsdal, M. A. and Christiansen, C. (2011). "Efficacy and safety of the PPARgamma partial agonist balaglitazone compared with pioglitazone and placebo: a phase III, randomized, parallel-group study in patients with type 2 diabetes on stable insulin therapy." Diabetes Metab Res Rev **27**(4): 392-401.

Henry, R. R., Buse, J. B., Wu, H., Durrwell, L., Mingrino, R., Jaekel, K., El Azzouzi, B., Andjelkovic, M. and Herz, M. (2015). "Efficacy, safety and tolerability of aleglitazar in patients with type 2 diabetes: pooled findings from three randomized phase III trials." Diabetes Obes Metab **17**(6): 560-565.

Henry, R. R., Lincoff, A. M., Mudaliar, S., Rabbia, M., Chognot, C. and Herz, M. (2009). "Effect of the dual peroxisome proliferator-activated receptor-alpha/gamma agonist aleglitazar on risk of cardiovascular disease in patients with type 2 diabetes (SYNCHRONY): a phase II, randomised, dose-ranging study." Lancet **374**(9684): 126-135.

Higashiyama, H., Billin, A. N., Okamoto, Y., Kinoshita, M. and Asano, S. (2007). "Expression profiling of peroxisome proliferator-activated receptor-delta (PPAR-delta) in mouse tissues using tissue microarray." Histochem Cell Biol **127**(5): 485-494.

Hollingshead, H. E., Morimura, K., Adachi, M., Kennett, M. J., Billin, A. N., Willson, T. M., Gonzalez, F. J. and Peters, J. M. (2007). "PPARbeta/delta protects against experimental colitis through a ligand-independent mechanism." Dig Dis Sci **52**(11): 2912-2919.

Home, P. D., Pocock, S. J., Beck-Nielsen, H., Curtis, P. S., Gomis, R., Hanefeld, M., Jones, N. P., Komajda, M. and McMurray, J. J. (2009). "Rosiglitazone evaluated for cardiovascular outcomes in oral agent combination therapy for type 2 diabetes (RECORD): a multicentre, randomised, open-label trial." Lancet **373**(9681): 2125-2135.

Huang, C. J., Liu, I. M. and Cheng, J. T. (2007). "Increase of peroxisome proliferator-activated receptor delta gene expression in the lungs of streptozotocin-induced diabetic rats." Pulm Pharmacol Ther **20**(1): 69-74.

Humbert, X., Dolladille, C., Sassier, M., Valnet-Rabier, M. B., Vial, T., Guitton, E., Page, A., Sole, E., Auriche, P., Coquerel, A., Alexandre, J. and Fedrizzi, S. (2017). "Fibrates and risk of venous thromboembolism: Case/no-case study in French pharmacovigilance database." Therapie **72**(6): 677-682.

Hwang, J. S., Eun, S. Y., Ham, S. A., Yoo, T., Lee, W. J., Paek, K. S., Do, J. T., Lim, D. S. and Seo, H. G. (2015). "PPARdelta modulates oxLDL-induced apoptosis of vascular smooth muscle cells through a TGF-beta/FAK signaling axis." Int J Biochem Cell Biol **62**: 54-61.

Iida, S., Taguchi, H., Watanabe, N., Kushiro, T. and Kanmatsuse, K. (2001). "Insulin-induced relaxation of rat mesenteric artery is mediated by Ca(2+)-activated K(+) channels." Eur J Pharmacol **411**(1-2): 155-160.

IJpenberg, A., Jeannin, E., Wahli, W. and Desvergne, B. (1997). "Polarity and specific sequence requirements of peroxisome proliferator-activated receptor (PPAR)/retinoid X receptor heterodimer binding to DNA. A functional analysis of the malic enzyme gene PPAR response element." J Biol Chem **272**(32): 20108-20117.

Inoue, T., Kohro, T., Tanaka, T., Kanki, Y., Li, G., Poh, H. M., Mimura, I., Kobayashi, M., Taguchi, A., Maejima, T., Suehiro, J., Sugiyama, A., Kaneki, K., Aruga, H., Dong, S., Stevens, J. F., Yamamoto, S., Tsutsumi, S., Fujita, T., Ruan, X., Aburatani, H., Nangaku, M., Ruan, Y., Kodama, T. and Wada, Y. (2014). "Cross-enhancement of ANGPTL4 transcription by HIF1 alpha and PPAR beta/delta is the result of the conformational proximity of two response elements." Genome Biol **15**(4): R63.

Issemann, I. and Green, S. (1990). "Activation of a member of the steroid hormone receptor superfamily by peroxisome proliferators." Nature **347**(6294): 645-650.

Ito, M. K. (2015). "Long-chain omega-3 fatty acids, fibrates and niacin as therapeutic options in the treatment of hypertriglyceridemia: A review of the literature." Atherosclerosis **242**(2): 647-656.

Jani, R. H., Pai, V., Jha, P., Jariwala, G., Mukhopadhyay, S., Bhansali, A. and Joshi, S. (2014). "A multicenter, prospective, randomized, double-blind study to evaluate the safety and efficacy of Saroglitazar 2 and 4 mg compared with placebo in type 2 diabetes mellitus patients having hypertriglyceridemia not controlled with atorvastatin therapy (PRESS VI)." Diabetes Technol Ther **16**(2): 63-71.

Jiang, Z. Y., Lin, Y. W., Clemont, A., Feener, E. P., Hein, K. D., Igarashi, M., Yamauchi, T., White, M. F. and King, G. L. (1999). "Characterization of selective resistance to insulin signaling in the vasculature of obese Zucker (fa/fa) rats." J Clin Invest **104**(4): 447-457.

Jimenez, R., Sanchez, M., Zarzuelo, M. J., Romero, M., Quintela, A. M., Lopez-Sepulveda, R., Galindo, P., Gomez-Guzman, M., Haro, J. M., Zarzuelo, A., Perez-Vizcaino, F. and Duarte, J. (2010). "Endothelium-dependent vasodilator effects of peroxisome proliferator-activated receptor beta agonists via the phosphatidyl-inositol-3 kinase-Akt pathway." J Pharmacol Exp Ther **332**(2): 554-561.

Jin, L., Lin, S., Rong, H., Zheng, S., Jin, S., Wang, R. and Li, Y. (2011). "Structural basis for iloprost as a dual peroxisome proliferator-activated receptor alpha/delta agonist." J Biol Chem **286**(36): 31473-31479.

Jove, M., Laguna, J. C. and Vazquez-Carrera, M. (2005). "Agonist-induced activation releases peroxisome proliferator-activated receptor beta/delta from its inhibition by palmitate-induced nuclear factor-kappaB in skeletal muscle cells." Biochim Biophys Acta **1734**(1): 52-61.

Juhl, C. B., Hollingdal, M., Pørksen, N., Prange, Å., Lönnqvist, F. and Schmitz, O. (2003). "Influence of rosiglitazone treatment on β-cell function in type 2 diabetes: Evidence of an increased ability of glucose to entrain high-frequency insulin pulsatility." Journal of Clinical Endocrinology and Metabolism **88**(8): 3794-3800.

Jung, Y. R., Lee, E. K., Kim, D. H., Park, C. H., Park, M. H., Jeong, H. O., Yokozawa, T., Tanaka, T., Im, D. S., Kim, N. D., Yu, B. P., Mo, S. H. and Chung, H. Y. (2015). "Upregulation of collagen expression via PPARbeta/delta activation in aged skin by magnesium lithospermate B from Salvia miltiorrhiza." J Nat Prod **78**(8): 2110-2115.

Kahn, S. E., Haffner, S. M., Heise, M. A., Herman, W. H., Holman, R. R., Jones, N. P., Kravitz, B. G., Lachin, J. M., O'Neill, M. C., Zinman, B. and Viberti, G. (2006). "Glycemic durability of rosiglitazone, metformin, or glyburide monotherapy." N Engl J Med **355**(23): 2427-2443.

Kahremany, S., Livne, A., Gruzman, A., Senderowitz, H. and Sasson, S. (2015). "Activation of PPARdelta: from computer modelling to biological effects." Br J Pharmacol **172**(3): 754-770.

Kanda, T., Wakino, S., Homma, K., Yoshioka, K., Tatematsu, S., Hasegawa, K., Takamatsu, I., Sugano, N., Hayashi, K. and Saruta, T. (2006). "Rho-kinase as a molecular target for insulin resistance and hypertension." Faseb j **20**(1): 169-171.

Kapoor, A., Collino, M., Castiglia, S., Fantozzi, R. and Thiemermann, C. (2010). "Activation of peroxisome proliferator-activated receptor-beta/delta attenuates myocardial ischemia/reperfusion injury in the rat." Shock **34**(2): 117-124.

Kapoor, A., Shintani, Y., Collino, M., Osuchowski, M. F., Busch, D., Patel, N. S., Sepodes, B., Castiglia, S., Fantozzi, R., Bishop-Bailey, D., Mota-Filipe, H., Yaqoob, M. M., Suzuki, K., Bahrami, S., Desvergne, B., Mitchell, J. A. and Thiemermann, C. (2010). "Protective role of peroxisome proliferator-activated receptor-beta/delta in septic shock." Am J Respir Crit Care Med **182**(12): 1506-1515.

Kawamori, R., Matsuhisa, M., Kinoshita, J., Mochizuki, K., Niwa, M., Arisaka, T., Ikeda, M., Kubota, M., Wada, M., Kanda, T., Ikebuchi, M., Tohdo, R. and Yamasaki, Y. (1998). "Pioglitazone enhances splanchnic glucose uptake as well as peripheral glucose uptake in non-insulin-dependent diabetes mellitus." Diabetes Research and Clinical Practice **41**(1): 35-43.

Kawano, K., Hirashima, T., Mori, S., Saitoh, Y., Kurosumi, M. and Natori, T. (1992). "Spontaneous long-term hyperglycemic rat with diabetic complications. Otsuka Long-Evans Tokushima Fatty (OLETF) strain." Diabetes **41**(11): 1422-1428.

Keller, H., Devchand, P. R., Perroud, M. and Wahli, W. (1997). "PPAR alpha structure-function relationships derived from species-specific differences in responsiveness to hypolipidemic agents." Biol Chem **378**(7): 651-655.

Khozoie, C., Borland, M. G., Zhu, B., Baek, S., John, S., Hager, G. L., Shah, Y. M., Gonzalez, F. J. and Peters, J. M. (2012). "Analysis of the peroxisome proliferator-activated receptor-beta/delta (PPARbeta/delta) cistrome reveals novel co-regulatory role of ATF4." BMC Genomics **13**: 665.

Kim, D. J., Akiyama, T. E., Harman, F. S., Burns, A. M., Shan, W., Ward, J. M., Kennett, M. J., Gonzalez, F. J. and Peters, J. M. (2004). "Peroxisome proliferator-activated receptor beta (delta)-dependent regulation of ubiquitin C expression contributes to attenuation of skin carcinogenesis." J Biol Chem **279**(22): 23719-23727.

Kim, H. J., Kim, M. Y., Hwang, J. S., Kim, H. J., Lee, J. H., Chang, K. C., Kim, J. H., Han, C. W., Kim, J. H. and Seo, H. G. (2010). "PPARdelta inhibits IL-1beta-stimulated proliferation and migration of vascular smooth muscle cells via up-regulation of IL-1Ra." Cell Mol Life Sci **67**(12): 2119-2130.

Kim, M. Y., Kang, E. S., Ham, S. A., Hwang, J. S., Yoo, T. S., Lee, H., Paek, K. S., Park, C., Lee, H. T., Kim, J. H., Han, C. W. and Seo, H. G. (2012). "The PPARdelta-mediated inhibition of angiotensin II-induced premature senescence in human endothelial cells is SIRT1-dependent." Biochem Pharmacol **84**(12): 1627-1634.

Kitazawa, T., Semba, S., Huh, Y. H., Kitazawa, K. and Eto, M. (2009). "Nitric oxide-induced biphasic mechanism of vascular relaxation via dephosphorylation of CPI-17 and MYPT1." J Physiol **587**(Pt 14): 3587-3603.

Kliewer, S. A., Umesono, K., Noonan, D. J., Heyman, R. A. and Evans, R. M. (1992). "Convergence of 9-cis retinoic acid and peroxisome proliferator signalling pathways through heterodimer formation of their receptors." Nature **358**(6389): 771-774.

Klingler, C., Zhao, X., Adhikary, T., Li, J., Xu, G., Haring, H. U., Schleicher, E., Lehmann, R. and Weigert, C. (2016). "Lysophosphatidylcholines activate PPARdelta and protect human skeletal muscle cells from lipotoxicity." Biochim Biophys Acta **1861**(12 Pt A): 1980-1992.

Kojetin, D. J., Matta-Camacho, E., Hughes, T. S., Srinivasan, S., Nwachukwu, J. C., Cavett, V., Nowak, J., Chalmers, M. J., Marciano, D. P., Kamenecka, T. M., Shulman, A. I., Rance, M., Griffin, P. R., Bruning, J. B. and Nettles, K. W. (2015). "Structural mechanism for signal transduction in RXR nuclear receptor heterodimers." Nature Communications **6**: 8013.

Kong, A. P., Yamasaki, A., Ozaki, R., Saito, H., Asami, T., Ohwada, S., Ko, G. T., Wong, C. K., Leung, G. T., Lee, K. F., Yeung, C. Y. and Chan, J. C. (2011). "A randomized-controlled trial to investigate the effects of rivoglitazone, a novel PPAR gamma agonist on glucose-lipid control in type 2 diabetes." Diabetes Obes Metab **13**(9): 806-813.

Krey, G., Braissant, O., L'Horset, F., Kalkhoven, E., Perroud, M., Parker, M. G. and Wahli, W. (1997). "Fatty acids, eicosanoids, and hypolipidemic agents identified as ligands of peroxisome proliferator-activated receptors by coactivator-dependent receptor ligand assay." Mol Endocrinol **11**(6): 779-791.

Krogsdam, A. M., Nielsen, C. A., Neve, S., Holst, D., Helledie, T., Thomsen, B., Bendixen, C., Mandrup, S. and Kristiansen, K. (2002). "Nuclear receptor corepressor-dependent repression of peroxisome-proliferator-activated receptor delta-mediated transactivation." Biochem J **363**(Pt 1): 157-165.

Laghezza, A., Piemontese, L., Tortorella, P. and Loiodice, F. (2019). "An update about the crucial role of stereochemistry on the effects of Peroxisome Proliferator-Activated Receptor ligands." Eur J Med Chem **176**: 326-342.

Lagu, B., Kluge, A. F., Goddeeris, M. M., Tozzo, E., Fredenburg, R. A., Chellur, S., Senaiar, R. S., Jaleel, M., Babu, D. R. K., Tiwari, N. K., Takahashi, T. and Patane, M. A. (2017). "Highly selective peroxisome proliferator-activated receptor delta (PPARdelta) modulator demonstrates improved safety profile compared to GW501516." Bioorg Med Chem Lett.

Larsen, P. J., Lykkegaard, K., Larsen, L. K., Fleckner, J., Sauerberg, P., Wassermann, K. and Wulff, E. M. (2008). "Dissociation of antihyperglycaemic and adverse effects of partial perioxisome proliferator-activated receptor (PPAR-γ) agonist balaglitazone." European Journal of Pharmacology **596**(1-3): 173-179.

Lawrence, T. (2009). "The nuclear factor NF-kappaB pathway in inflammation." Cold Spring Harb Perspect Biol **1**(6): a001651.

Lee, C. H., Olson, P., Hevener, A., Mehl, I., Chong, L. W., Olefsky, J. M., Gonzalez, F. J., Ham, J., Kang, H., Peters, J. M. and Evans, R. M. (2006). "PPARdelta regulates glucose metabolism and insulin sensitivity." Proc Natl Acad Sci U S A **103**(9): 3444-3449.

Lee, M., Saver, J. L., Towfighi, A., Chow, J. and Ovbiagele, B. (2011). "Efficacy of fibrates for cardiovascular risk reduction in persons with atherogenic dyslipidemia: a meta-analysis." Atherosclerosis **217**(2): 492-498.

Lenzen, S. (2008). "The mechanisms of alloxan- and streptozotocin-induced diabetes." Diabetologia **51**(2): 216-226.

Lewis, J. D., Habel, L., Quesenberry, C., Mamtani, R., Peng, T., Bilker, W. B., Hedderson, M., Nessel, L., Vaughn, D. J., Strom, B. L. and Ferrara, A. (2014). "Proteinuria testing among patients with diabetes mellitus is associated with bladder cancer diagnosis: Potential for unmeasured confounding in studies of pioglitazone and bladder cancer." Pharmacoepidemiology and Drug Safety **23**(6): 636-645.

Li, H., Chai, Q., Gutterman, D. D. and Liu, Y. (2003). "Elevated glucose impairs cAMP-mediated dilation by reducing Kv channel activity in rat small coronary smooth muscle cells." Am J Physiol Heart Circ Physiol **285**(3): H1213-1219.

Li, X., Li, J., Li, Z., Sang, Y., Niu, Y., Zhang, Q., Ding, H. and Yin, S. (2016). "Fucoidan from Undaria pinnatifida prevents vascular dysfunction through PI3K/Akt/eNOS-dependent mechanisms in the l-NAME-induced hypertensive rat model." Food Funct **7**(5): 2398-2408.

Li, Y., Connolly, M., Nagaraj, C., Tang, B., Bálint, Z., Popper, H., Smolle-Juettner, F. M., Lindenmann, J., Kwapiszewska, G., Aaronson, P. I., Wohlkoenig, C., Leithner, K., Olschewski, A. and Olschewski, A. (2012). "Peroxisome proliferator–activated receptor–β/δ, the acute signaling factor in prostacyclin-induced pulmonary vasodilation." American Journal of Respiratory Cell and Molecular Biology **46**(3): 372-379.

Liang, Y. J., Chen, C. Y., Juang, S. J., Lai, L. P., Shyu, K. G., Wang, B. W., Liu, S. Y. and Leu, J. G. (2010). "Peroxisome proliferator-activated receptor delta agonists attenuated the C-reactive protein-induced pro-inflammation in cardiomyocytes and H9c2 cardiomyoblasts." Eur J Pharmacol **643**(1): 84-92.

Liang, Y. J., Chen, S. A. and Jian, J. H. (2011). "Peroxisome proliferator-activated receptor delta downregulates the expression of the receptor for advanced glycation end products and pro-inflammatory cytokines in the kidney of streptozotocin-induced diabetic mice." Eur J Pharm Sci **43**(1-2): 65-70.

Liepinsh, E., Vilskersts, R., Zvejniece, L., Svalbe, B., Skapare, E., Kuka, J., Cirule, H., Grinberga, S., Kalvinsh, I. and Dambrova, M. (2009). "Protective effects of mildronate in an experimental model of type 2 diabetes in Goto-Kakizaki rats." Br J Pharmacol **157**(8): 1549-1556.

Lim, H. J., Lee, S., Park, J. H., Lee, K. S., Choi, H. E., Chung, K. S., Lee, H. H. and Park, H. Y. (2009). "PPAR delta agonist L-165041 inhibits rat vascular smooth muscle cell proliferation and migration via inhibition of cell cycle." Atherosclerosis **202**(2): 446-454.

Lim, H. J., Moon, I. and Han, K. (2004). "Transcriptional cofactors exhibit differential preference toward peroxisome proliferator-activated receptors alpha and delta in uterine cells." Endocrinology **145**(6): 2886-2895.

Liu, G., Li, X., Li, Y., Tang, X., Xu, J., Li, R., Hao, P. and Sun, Y. (2013). "PPARdelta agonist GW501516 inhibits PDGF-stimulated pulmonary arterial smooth muscle cell function related to pathological vascular remodeling." Biomed Res Int **2013**: 903947.

Liu, W., Liu, B., Liu, S., Zhang, J. and Lin, S. (2016). "Sphingosine-1-phosphate receptor 2 mediates endothelial cells dysfunction by PI3K-Akt pathway under high glucose condition." Eur J Pharmacol **776**: 19-25.

Long, G. G., Reynolds, V. L., Dochterman, L. W. and Ryan, T. E. (2009). "Neoplastic and non-neoplastic changes in F-344 rats treated with Naveglitazar, a gamma-dominant PPAR alpha/gamma agonist." Toxicol Pathol **37**(6): 741-753.

MacKenzie, A., Cooper, E. J. and Dowell, F. J. (2008). "Differential effects of glucose on agonist-induced relaxations in human mesenteric and subcutaneous arteries." Br J Pharmacol **153**(3): 480-487.

Makino, S., Kunimoto, K., Muraoka, Y., Mizushima, Y., Katagiri, K. and Tochino, Y. (1980). "Breeding of a non-obese, diabetic strain of mice." Jikken Dobutsu **29**(1): 1-13.

Maltarollo, V. G., Togashi, M., Nascimento, A. S. and Honorio, K. M. (2015). "Structure-based virtual screening and discovery of new PPARdelta/gamma dual agonist and PPARdelta and gamma agonists." PLoS One **10**(3): e0118790.

Mandard, S. and Patsouris, D. (2013). "Nuclear control of the inflammatory response in mammals by peroxisome proliferator-activated receptors." PPAR Res **2013**: 613864.

Mangialardi, G., Katare, R., Oikawa, A., Meloni, M., Reni, C., Emanueli, C. and Madeddu, P. (2013). "Diabetes causes bone marrow endothelial barrier dysfunction by activation of the RhoA-Rho-associated kinase signaling pathway." Arterioscler Thromb Vasc Biol **33**(3): 555-564.

Mathews, C. E., Langley, S. H. and Leiter, E. H. (2002). "New mouse model to study islet transplantation in insulin-dependent diabetes mellitus." Transplantation **73**(8): 1333-1336.

Meissner, M., Hrgovic, I., Doll, M. and Kaufmann, R. (2011). "PPARdelta agonists suppress angiogenesis in a VEGFR2-dependent manner." Arch Dermatol Res **303**(1): 41-47.

Misra, P., Qi, C., Yu, S., Shah, S. H., Cao, W. Q., Rao, M. S., Thimmapaya, B., Zhu, Y. and Reddy, J. K. (2002). "Interaction of PIMT with transcriptional coactivators CBP, p300, and PBP differential role in transcriptional regulation." J Biol Chem **277**(22): 20011-20019.

Montanari, R., Saccoccia, F., Scotti, E., Crestani, M., Godio, C., Gilardi, F., Loiodice, F., Fracchiolla, G., Laghezza, A., Tortorella, P., Lavecchia, A., Novellino, E., Mazza, F., Aschi, M. and Pochetti, G. (2008). "Crystal structure of the peroxisome proliferator-activated receptor gamma (PPARgamma) ligand binding domain complexed with a novel partial agonist: a new region of the hydrophobic pocket could be exploited for drug design." J Med Chem **51**(24): 7768-7776.

Moraes, L. A., Piqueras, L. and Bishop-Bailey, D. (2006). "Peroxisome proliferator-activated receptors and inflammation." Pharmacol Ther **110**(3): 371-385.

Morales-Cano, D., Moreno, L., Barreira, B., Pandolfi, R., Chamorro, V., Jimenez, R., Villamor, E., Duarte, J., Perez-Vizcaino, F. and Cogolludo, A. (2015). "Kv7 channels critically determine coronary artery reactivity: left-right differences and down-regulation by hyperglycaemia." Cardiovasc Res **106**(1): 98-108.

Mordes, J. P., Bortell, R., Blankenhorn, E. P., Rossini, A. A. and Greiner, D. L. (2004). "Rat models of type 1 diabetes: genetics, environment, and autoimmunity." Ilar j **45**(3): 278-291.

Moreno-Indias, I., Tinahones, F. J., Clemente-Postigo, M., Castellano-Castillo, D., Fernandez-Garcia, J. C., Macias-Gonzalez, M., Queipo-Ortuno, M. I. and Cardona, F. (2017). "Molecular effect of fenofibrate on PBMC gene transcription related to lipid metabolism in patients with metabolic syndrome." Clin Endocrinol (Oxf) **86**(6): 784-790.

Mosesson, M. W. and Amrani, D. L. (1980). "The structure and biologic activities of plasma fibronectin." Blood **56**(2): 145-158.

Mou, D., Yang, H., Qu, C., Chen, J. and Zhang, C. (2016). "Pharmacological activation of peroxisome proliferator-activated receptor-delta increases sphingomyelin synthase activity in THP-1 macrophage-derived foam cell." Inflammation **39**(4): 1538-1546.

Nakamura, M. and Yamada, K. (1967). "Studies on a diabetic (KK) strain of the mouse." Diabetologia **3**(2): 212-221.

Nakhooda, A. F., Like, A. A., Chappel, C. I., Murray, F. T. and Marliss, E. B. (1977). "The spontaneously diabetic Wistar rat. Metabolic and morphologic studies." Diabetes **26**(2): 100-112.

Nandhikonda, P., Yasgar, A., Baranowski, A. M., Sidhu, P. S., McCallum, M. M., Pawlak, A. J., Teske, K., Feleke, B., Yuan, N. Y., Kevin, C., Bikle, D. D., Ayers, S. D., Webb, P., Rai, G., Simeonov, A., Jadhav, A., Maloney, D. and Arnold, L. A. (2013). "Peroxisome proliferation-activated receptor delta agonist GW0742 interacts weakly with multiple nuclear receptors, including the vitamin D receptor." Biochemistry **52**(24): 4193-4203.

Neels, J. G. and Grimaldi, P. A. (2014). "Physiological functions of peroxisome proliferator-activated receptor beta." Physiol Rev **94**(3): 795-858.

Nesto, R. W., Bell, D., Bonow, R. O., Fonseca, V., Grundy, S. M., Horton, E. S., Le Winter, M., Porte, D., Semenkovich, C. F., Smith, S., Young, L. H. and Kahn, R. (2004). "Thiazolidinedione use, fluid retention, and congestive heart failure: a consensus statement from the American Heart Association and American Diabetes Association." Diabetes Care **27**(1): 256-263.

Neumann, A., Weill, A., Ricordeau, P., Fagot, J. P., Alla, F. and Allemand, H. (2012). "Pioglitazone and risk of bladder cancer among diabetic patients in France: A population-based cohort study." Diabetologia **55**(7): 1953-1962.

Nissen, S. E. and Wolski, K. (2007). "Effect of rosiglitazone on the risk of myocardial infarction and death from cardiovascular causes." N Engl J Med **356**(24): 2457-2471.

Nissen, S. E., Wolski, K. and Topol, E. J. (2005). "Effect of muraglitazar on death and major adverse cardiovascular events in patients with type 2 diabetes mellitus." Jama **294**(20): 2581-2586.

Northcott, C. A., Hayflick, J. S. and Watts, S. W. (2004). "PI3-kinase upregulation and involvement in spontaneous tone in arteries from DOCA-salt rats: is p110delta the culprit?" Hypertension **43**(4): 885-890.

Northcott, C. A., Poy, M. N., Najjar, S. M. and Watts, S. W. (2002). "Phosphoinositide 3-kinase mediates enhanced spontaneous and agonist-induced contraction in aorta of deoxycorticosterone acetate-salt hypertensive rats." Circ Res **91**(4): 360-369.

Nullens, S., De Man, J., Bridts, C., Ebo, D., Francque, S. and De Winter, B. (2018). "Identifying therapeutic targets for sepsis research: A characterization study of the inflammatory players in the cecal ligation and puncture model." Mediators Inflamm **2018**: 5130463.

Oelze, M., Knorr, M., Schuhmacher, S., Heeren, T., Otto, C., Schulz, E., Reifenberg, K., Wenzel, P., Munzel, T. and Daiber, A. (2011). "Vascular dysfunction in streptozotocin-induced experimental diabetes strictly depends on insulin deficiency." J Vasc Res **48**(4): 275-284.

Oliver, W. R., Jr., Shenk, J. L., Snaith, M. R., Russell, C. S., Plunket, K. D., Bodkin, N. L., Lewis, M. C., Winegar, D. A., Sznaidman, M. L., Lambert, M. H., Xu, H. E., Sternbach, D. D., Kliewer, S. A., Hansen, B. C. and Willson, T. M. (2001). "A selective peroxisome proliferator-activated receptor delta agonist promotes reverse cholesterol transport." Proc Natl Acad Sci U S A **98**(9): 5306-5311.

Olson, E. J., Pearce, G. L., Jones, N. P. and Sprecher, D. L. (2012). "Lipid effects of peroxisome proliferator-activated receptor-delta agonist GW501516 in subjects with low high-density lipoprotein cholesterol: characteristics of metabolic syndrome." Arterioscler Thromb Vasc Biol **32**(9): 2289-2294.

Ooi, E. M., Watts, G. F., Sprecher, D. L., Chan, D. C. and Barrett, P. H. (2011). "Mechanism of action of a peroxisome proliferator-activated receptor (PPAR)-delta agonist on lipoprotein metabolism in dyslipidemic subjects with central obesity." J Clin Endocrinol Metab **96**(10): E1568-1576.

Ozkan, M. H. and Uma, S. (2005). "Inhibition of acetylcholine-induced EDHF response by elevated glucose in rat mesenteric artery." Life Sci **78**(1): 14-21.

Padilla, J., Jenkins, N. T., Vieira-Potter, V. J. and Laughlin, M. H. (2013). "Divergent phenotype of rat thoracic and abdominal perivascular adipose tissues." Am J Physiol Regul Integr Comp Physiol **304**(7): R543-552.

Palkar, P. S., Borland, M. G., Naruhn, S., Ferry, C. H., Lee, C., Sk, U. H., Sharma, A. K., Amin, S., Murray, I. A., Anderson, C. R., Perdew, G. H., Gonzalez, F. J., Muller, R. and Peters, J. M. (2010). "Cellular and pharmacological selectivity of the peroxisome proliferator-activated receptor-beta/delta antagonist GSK3787." Mol Pharmacol **78**(3): 419-430.

Park, J., Lee, S. E., Hur, J., Hong, E. B., Choi, J. I., Yang, J. M., Kim, J. Y., Kim, Y. C., Cho, H. J., Peters, J. M., Ryoo, S. B., Kim, Y. T. and Kim, H. S. (2015). "M-CSF from cancer cells induces fatty acid synthase and PPARbeta/delta activation in tumor myeloid cells, leading to tumor progression." Cell Rep.

Patel, H., Giri, P., Patel, P., Singh, S., Gupta, L., Patel, U., Modi, N., Shah, K., Jain, M. R., Srinivas, N. R. and Patel, P. (2017). "Preclinical evaluation of saroglitazar magnesium, a dual PPAR-alpha/gamma agonist for treatment of dyslipidemia and metabolic disorders." Xenobiotica: 1-10.

Pathan, N., Hemingway, C. A., Alizadeh, A. A., Stephens, A. C., Boldrick, J. C., Oragui, E. E., McCabe, C., Welch, S. B., Whitney, A., O'Gara, P., Nadel, S., Relman, D. A., Harding, S. E. and Levin, M. (2004). "Role of interleukin 6 in myocardial dysfunction of meningococcal septic shock." Lancet **363**(9404): 203-209.

Pauciullo, P., Marotta, G., Rubba, P., Cortese, C., Caruso, M. G., Gnasso, A., Fischetti, A., Motti, C. and Mancini, M. (1990). "Serum lipoproteins, apolipoproteins and very low density lipoprotein subfractions during 6-month fibrate treatment in primary hypertriglyceridaemia." J Intern Med **228**(5): 425-430.

Pechery, A., Fauconnet, S., Bittard, H. and Lascombe, I. (2016). "Apoptotic effect of the selective PPARbeta/delta agonist GW501516 in invasive bladder cancer cells." Tumour Biol **37**(11): 14789-14802.

Perez-Diaz, N. and Mackenzie, L. S. (2015). "Linking induction and transrepression of PPARβ/δ with cellular function." Anual Research & Review in Biology **6**(4): 253-263.

Perez-Diaz, N., Pushkarsky, I., Oweis, N., Lione, L. A. and Mackenzie, L. S. (2018). "The non-genomic effects of the PPARβ/δ; Agonist GW0742 on streptozotocin treated rat aorta." Current Molecular Pharmacology **11**(2): 149-154.

Perez-Diaz, N., Zloh, M., Patel, P. and Mackenzie, L. S. (2016). "In silico modelling of prostacyclin and other lipid mediators to nuclear receptors reveal novel thyroid hormone receptor antagonist properties." Prostaglandins Other Lipid Mediat **122**: 18-27.

Piqueras, L., Reynolds, A. R., Hodivala-Dilke, K. M., Alfranca, A., Redondo, J. M., Hatae, T., Tanabe, T., Warner, T. D. and Bishop-Bailey, D. (2007). "Activation of PPARbeta/delta induces endothelial cell proliferation and angiogenesis." Arterioscler Thromb Vasc Biol **27**(1): 63-69.

Piqueras, L., Sanz, M. J., Perretti, M., Morcillo, E., Norling, L., Mitchell, J. A., Li, Y. and Bishop-Bailey, D. (2009). "Activation of PPARbeta/delta inhibits leukocyte recruitment, cell adhesion molecule expression, and chemokine release." J Leukoc Biol **86**(1): 115-122.

Pollock, C. B., Yin, Y., Yuan, H., Zeng, X., King, S., Li, X., Kopelovich, L., Albanese, C. and Glazer, R. I. (2011). "PPARdelta activation acts cooperatively with 3-phosphoinositide-dependent protein kinase-1 to enhance mammary tumorigenesis." PLoS One **6**(1): e16215.

Puigserver, P., Wu, Z., Park, C. W., Graves, R., Wright, M. and Spiegelman, B. M. (1998). "A Cold-Inducible Coactivator of Nuclear Receptors Linked to Adaptive Thermogenesis." Cell **92**(6): 829-839.

Qu, D., Liu, J., Lau, C. W. and Huang, Y. (2014). "Differential mechanisms for insulin-induced relaxations in mouse posterior tibial arteries and main mesenteric arteries." Vascul Pharmacol **63**(3): 173-177.

Quintela, A. M., Jimenez, R., Gomez-Guzman, M., Zarzuelo, M. J., Galindo, P., Sanchez, M., Vargas, F., Cogolludo, A., Tamargo, J., Perez-Vizcaino, F. and Duarte, J. (2012). "Activation of peroxisome

proliferator-activated receptor-beta/-delta (PPARbeta/delta) prevents endothelial dysfunction in type 1 diabetic rats." <u>Free Radic Biol Med</u> **53**(4): 730-741.

Quintela, A. M., Jimenez, R., Piqueras, L., Gomez-Guzman, M., Haro, J., Zarzuelo, M. J., Cogolludo, A., Sanz, M. J., Toral, M., Romero, M., Perez-Vizcaino, F. and Duarte, J. (2014). "PPARbeta activation restores the high glucose-induced impairment of insulin signalling in endothelial cells." <u>Br J Pharmacol</u> **171**(12): 3089-3102.

Rao, M. Y., Soliman, H., Bankar, G., Lin, G. and MacLeod, K. M. (2013). "Contribution of Rho kinase to blood pressure elevation and vasoconstrictor responsiveness in type 2 diabetic Goto-Kakizaki rats." <u>J Hypertens</u> **31**(6): 1160-1169.

Ratner, R. E., Parikh, S. and Tou, C. (2007). "Efficacy, safety and tolerability of tesaglitazar when added to the therapeutic regimen of poorly controlled insulin-treated patients with type 2 diabetes." <u>Diab Vasc Dis Res</u> **4**(3): 214-221.

Reboldi, G., Gentile, G., Manfreda, V. M., Angeli, F. and Verdecchia, P. (2012). "Tight blood pressure control in diabetes: evidence-based review of treatment targets in patients with diabetes." <u>Curr Cardiol Rep</u> **14**(1): 89-96.

Reddi, A. S. and Camerini-Davalos, R. A. (1988). "Hereditary diabetes in the KK mouse: an overview." <u>Adv Exp Med Biol</u> **246**: 7-15.

Rees, D. A. and Alcolado, J. C. (2005). "Animal models of diabetes mellitus." <u>Diabet Med</u> **22**(4): 359-370.

Renaud, J. P., Rochel, N., Ruff, M., Vivat, V., Chambon, P., Gronemeyer, H. and Moras, D. (1995). "Crystal structure of the RAR-gamma ligand-binding domain bound to all-trans retinoic acid." <u>Nature</u> **378**(6558): 681-689.

Riahi, Y., Kaiser, N., Cohen, G., Abd-Elrahman, I., Blum, G., Shapira, O. M., Koler, T., Simionescu, M., Sima, A. V., Zarkovic, N., Zarkovic, K., Orioli, M., Aldini, G., Cerasi, E., Leibowitz, G. and Sasson, S. (2015). "Foam cell-derived 4-hydroxynonenal induces endothelial cell senescence in a TXNIP-dependent manner." <u>J Cell Mol Med</u> **19**(8): 1887-1899.

Rodriguez-Calvo, R., Serrano, L., Coll, T., Moullan, N., Sanchez, R. M., Merlos, M., Palomer, X., Laguna, J. C., Michalik, L., Wahli, W. and Vazquez-Carrera, M. (2008). "Activation of peroxisome proliferator-activated receptor beta/delta inhibits lipopolysaccharide-induced cytokine production in adipocytes by lowering nuclear factor-kappaB activity via extracellular signal-related kinase 1/2." <u>Diabetes</u> **57**(8): 2149-2157.

Romanowska, M., al Yacoub, N., Seidel, H., Donandt, S., Gerken, H., Phillip, S., Haritonova, N., Artuc, M., Schweiger, S., Sterry, W. and Foerster, J. (2008). "PPARdelta enhances keratinocyte proliferation in psoriasis and induces heparin-binding EGF-like growth factor." <u>J Invest Dermatol</u> **128**(1): 110-124.

Romanowska, M., Reilly, L., Palmer, C. N., Gustafsson, M. C. and Foerster, J. (2010). "Activation of PPARbeta/delta causes a psoriasis-like skin disease in vivo." <u>PLoS One</u> **5**(3): e9701.

Ruddy, J. M., Akerman, A. W., Kimbrough, D., Nadeau, E. K., Stroud, R. E., Mukherjee, R., Ikonomidis, J. S. and Jones, J. A. (2017). "Differential hypertensive protease expression in the thoracic versus abdominal aorta." J Vasc Surg **66**(5): 1543-1552.

Saini, V. (2010). "Molecular mechanisms of insulin resistance in type 2 diabetes mellitus." World J Diabetes **1**(3): 68-75.

Sandhu, S. K., Volinia, S., Costinean, S., Galasso, M., Neinast, R., Santhanam, R., Parthun, M. R., Perrotti, D., Marcucci, G., Garzon, R. and Croce, C. M. (2012). "miR-155 targets histone deacetylase 4 (HDAC4) and impairs transcriptional activity of B-cell lymphoma 6 (BCL6) in the Emu-miR-155 transgenic mouse model." Proc Natl Acad Sci U S A **109**(49): 20047-20052.

Sandu, O. A., Ito, M. and Begum, N. (2001). "Selected contribution: insulin utilizes NO/cGMP pathway to activate myosin phosphatase via Rho inhibition in vascular smooth muscle." J Appl Physiol (1985) **91**(3): 1475-1482.

Schelleman, H., Bilker, W. B., Brensinger, C. M., Wan, F., Yang, Y. X. and Hennessy, S. (2010). "Fibrate/Statin initiation in warfarin users and gastrointestinal bleeding risk." Am J Med **123**(2): 151-157.

Schild, R. L., Schaiff, W. T., Carlson, M. G., Cronbach, E. J., Nelson, D. M. and Sadovsky, Y. (2002). "The activity of PPAR gamma in primary human trophoblasts is enhanced by oxidized lipids." J Clin Endocrinol Metab **87**(3): 1105-1110.

Schnegg, C. I., Kooshki, M., Hsu, F.-C., Sui, G. and Robbins, M. E. (2012). "PPARδ prevents radiation-induced proinflammatory responses in microglia via transrepression of NF-κB and inhibition of the PKCα/MEK1/2/ERK1/2/AP-1 pathway." Free Radical Biology and Medicine **52**(9): 1734-1743.

Schreiber, J., Jenner, R. G., Murray, H. L., Gerber, G. K., Gifford, D. K. and Young, R. A. (2006). "Coordinated binding of NF-κB family members in the response of human cells to lipopolysaccharide." Proceedings of the National Academy of Sciences **103**(15): 5899-5904.

Serrano-Marco, L., Chacon, M. R., Maymo-Masip, E., Barroso, E., Salvado, L., Wabitsch, M., Garrido-Sanchez, L., Tinahones, F. J., Palomer, X., Vendrell, J. and Vazquez-Carrera, M. (2012). "TNF-alpha inhibits PPARbeta/delta activity and SIRT1 expression through NF-kappaB in human adipocytes." Biochim Biophys Acta **1821**(9): 1177-1185.

Seth, A., Steel, J. H., Nichol, D., Pocock, V., Kumaran, M. K., Fritah, A., Mobberley, M., Ryder, T. A., Rowlerson, A., Scott, J., Poutanen, M., White, R. and Parker, M. (2007). "The Transcriptional Corepressor RIP140 Regulates Oxidative Metabolism in Skeletal Muscle." Cell Metabolism **6**(3): 236-245.

Shan, W., Palkar, P. S., Murray, I. A., McDevitt, E. I., Kennett, M. J., Kang, B. H., Isom, H. C., Perdew, G. H., Gonzalez, F. J. and Peters, J. M. (2008). "Ligand activation of peroxisome proliferator-activated receptor beta/delta (PPARbeta/delta) attenuates carbon tetrachloride hepatotoxicity by downregulating proinflammatory gene expression." Toxicol Sci **105**(2): 418-428.

Shearer, B. G., Steger, D. J., Way, J. M., Stanley, T. B., Lobe, D. C., Grillot, D. A., Iannone, M. A., Lazar, M. A., Willson, T. M. and Billin, A. N. (2008). "Identification and characterization of a selective

peroxisome proliferator-activated receptor β/δ (NR1C2) antagonist." <u>Molecular Endocrinology</u> **22**(2): 523-529.

Shearer, B. G., Wiethe, R. W., Ashe, A., Billin, A. N., Way, J. M., Stanley, T. B., Wagner, C. D., Xu, R. X., Leesnitzer, L. M., Merrihew, R. V., Shearer, T. W., Jeune, M. R., Ulrich, J. C. and Willson, T. M. (2010). "Identification and characterization of 4-chloro-N-(2-{[5-trifluoromethyl)-2-pyridyl]sulfonyl}ethyl)benzamide (GSK3787), a selective and irreversible peroxisome proliferator-activated receptor δ (PPARδ) antagonist." <u>Journal of Medicinal Chemistry</u> **53**(4): 1857-1861.

Sheppard, K. A., Phelps, K. M., Williams, A. J., Thanos, D., Glass, C. K., Rosenfeld, M. G., Gerritsen, M. E. and Collins, T. (1998). "Nuclear integration of glucocorticoid receptor and nuclear factor-kappaB signaling by CREB-binding protein and steroid receptor coactivator-1." <u>J Biol Chem</u> **273**(45): 29291-29294.

Soccio, Raymond E., Chen, Eric R. and Lazar, Mitchell A. (2014). "Thiazolidinediones and the promise of insulin sensitization in type 2 diabetes." <u>Cell Metabolism</u> **20**(4): 573-591.

Soliman, H., Nyamandi, V., Garcia-Patino, M., Varela, J. N., Bankar, G., Lin, G., Jia, Z. and MacLeod, K. M. (2015). "Partial deletion of ROCK2 protects mice from high-fat diet-induced cardiac insulin resistance and contractile dysfunction." <u>Am J Physiol Heart Circ Physiol</u> **309**(1): H70-81.

Song, L., Zou, Y. and Cao, Z. (2018). "Comparison of two different models of sepsis induced by cecal ligation and puncture in rats." <u>J Surg Res</u> **229**: 277-282.

Steinberg, H. O., Brechtel, G., Johnson, A., Fineberg, N. and Baron, A. D. (1994). "Insulin-mediated skeletal muscle vasodilation is nitric oxide dependent. A novel action of insulin to increase nitric oxide release." <u>J Clin Invest</u> **94**(3): 1172-1179.

Stephen, R. L., Gustafsson, M. C., Jarvis, M., Tatoud, R., Marshall, B. R., Knight, D., Ehrenborg, E., Harris, A. L., Wolf, C. R. and Palmer, C. N. (2004). "Activation of peroxisome proliferator-activated receptor delta stimulates the proliferation of human breast and prostate cancer cell lines." <u>Cancer Res</u> **64**(9): 3162-3170.

Stott, J. B., Jepps, T. A. and Greenwood, I. A. (2014). "KV7 potassium channels: a new therapeutic target in smooth muscle disorders." <u>Drug Discovery Today</u> **19**(4): 413-424.

Sun, N., Wang, H. and Wang, L. (2015). "Vaspin alleviates dysfunction of endothelial progenitor cells induced by high glucose via PI3K/Akt/eNOS pathway." <u>Int J Clin Exp Pathol</u> **8**(1): 482-489.

Széles, L., Póliska, S. r., Nagy, G., Szatmari, I., Szanto, A., Pap, A., Lindstedt, M., Santegoets, S. J. A. M., Rühl, R., Dezső, B. z. and Nagy, L. s. (2010). "Research resource: transcriptome profiling of genes regulated by RXR and its permissive and nonpermissive partners in differentiating monocyte-derived dendritic cells." <u>Molecular Endocrinology</u> **24**(11): 2218-2231.

Szkudelski, T. (2001). "The mechanism of alloxan and streptozotocin action in B cells of the rat pancreas." <u>Physiol Res</u> **50**(6): 537-546.

Sznaidman, M. L., Haffner, C. D., Maloney, P. R., Fivush, A., Chao, E., Goreham, D., Sierra, M. L., LeGrumelec, C., Xu, H. E., Montana, V. G., Lambert, M. H., Willson, T. M., Oliver, W. R., Jr. and Sternbach, D. D. (2003). "Novel selective small molecule agonists for peroxisome proliferator-

activated receptor delta (PPARdelta)--synthesis and biological activity." <u>Bioorg Med Chem Lett</u> **13**(9): 1517-1521.

Takata, Y., Liu, J., Yin, F., Collins, A. R., Lyon, C. J., Lee, C. H., Atkins, A. R., Downes, M., Barish, G. D., Evans, R. M., Hsueh, W. A. and Tangirala, R. K. (2008). "PPARdelta-mediated antiinflammatory mechanisms inhibit angiotensin II-accelerated atherosclerosis." <u>Proc Natl Acad Sci U S A</u> **105**(11): 4277-4282.

Tan, N. S., Icre, G., Montagner, A., Bordier-ten-Heggeler, B., Wahli, W. and Michalik, L. (2007). "The nuclear hormone receptor peroxisome proliferator-activated receptor beta/delta potentiates cell chemotactism, polarization, and migration." <u>Mol Cell Biol</u> **27**(20): 7161-7175.

Tan, N. S., Vazquez-Carrera, M., Montagner, A., Sng, M. K., Guillou, H. and Wahli, W. (2016). "Transcriptional control of physiological and pathological processes by the nuclear receptor PPARbeta/delta." <u>Prog Lipid Res</u> **64**: 98-122.

Tanaka, T., Yamamoto, J., Iwasaki, S., Asaba, H., Hamura, H., Ikeda, Y., Watanabe, M., Magoori, K., Ioka, R. X., Tachibana, K., Watanabe, Y., Uchiyama, Y., Sumi, K., Iguchi, H., Ito, S., Doi, T., Hamakubo, T., Naito, M., Auwerx, J., Yanagisawa, M., Kodama, T. and Sakai, J. (2003). "Activation of peroxisome proliferator-activated receptor δ induces fatty acid β-oxidation in skeletal muscle and attenuates metabolic syndrome." <u>Proceedings of the National Academy of Sciences</u> **100**(26): 15924-15929.

Taylor, P. D. and Poston, L. (1994). "The effect of hyperglycaemia on function of rat isolated mesenteric resistance artery." <u>Br J Pharmacol</u> **113**(3): 801-808.

Taylor, P. D., Wickenden, A. D., Mirrlees, D. J. and Poston, L. (1994). "Endothelial function in the isolated perfused mesentery and aortae of rats with streptozotocin-induced diabetes: effect of treatment with the aldose reductase inhibitor, ponalrestat." <u>Br J Pharmacol</u> **111**(1): 42-48.

Tian, X. Y., Wong, W. T., Wang, N., Lu, Y., Cheang, W. S., Liu, J., Liu, L., Liu, Y., Lee, S. S., Chen, Z. Y., Cooke, J. P., Yao, X. and Huang, Y. (2012). "PPARdelta activation protects endothelial function in diabetic mice." <u>Diabetes</u> **61**(12): 3285-3293.

Toell, A., Kroncke, K. D., Kleinert, H. and Carlberg, C. (2002). "Orphan nuclear receptor binding site in the human inducible nitric oxide synthase promoter mediates responsiveness to steroid and xenobiotic ligands." <u>J Cell Biochem</u> **85**(1): 72-82.

Toral, M., Romero, M., Jiménez, R., Robles-Vera, I., Tamargo, J., Martínez, M. C., Pérez-Vizcaíno, F. and Duarte, J. (2016). "Role of UCP2 in the protective effects of PPARβ/δ activation on lipopolysaccharide-induced endothelial dysfunction." <u>Biochemical Pharmacology</u> **110–111**: 25-36.

Trifilieff, A., Bench, A., Hanley, M., Bayley, D., Campbell, E. and Whittaker, P. (2003). "PPAR-alpha and -gamma but not -delta agonists inhibit airway inflammation in a murine model of asthma: in vitro evidence for an NF-kappaB-independent effect." <u>Br J Pharmacol</u> **139**(1): 163-171.

Truitt, K. E., Goldberg, R. B., Rosenstock, J., Chou, H. S., Merante, D., Triscari, J. and Wang, A. C. (2010). "A 26-week, placebo- and pioglitazone-controlled, dose-ranging study of rivoglitazone, a novel thiazolidinedione for the treatment of type 2 diabetes." <u>Curr Med Res Opin</u> **26**(6): 1321-1331.

Ueda, H., Ikegami, H., Yamato, E., Fu, J., Fukuda, M., Shen, G., Kawaguchi, Y., Takekawa, K., Fujioka, Y., Fujisawa, T. and et al. (1995). "The NSY mouse: a new animal model of spontaneous NIDDM with moderate obesity." Diabetologia **38**(5): 503-508.

Usuda, D. and Kanda, T. (2014). "Peroxisome proliferator-activated receptors for hypertension." World J Cardiol **6**(8): 744-754.

Vazquez-Carrera, M. (2016). "Unraveling the effects of PPARbeta/delta on insulin resistance and cardiovascular disease." Trends Endocrinol Metab **27**(5): 319-334.

Vorn, R. and Yoo, H. Y. (2017). "Effects of high glucose with or without other metabolic substrates on alpha-adrenergic contractions in rat mesenteric and femoral arteries." Korean J Physiol Pharmacol **21**(1): 91-97.

Vosper, H., Patel, L., Graham, T. L., Khoudoli, G. A., Hill, A., Macphee, C. H., Pinto, I., Smith, S. A., Suckling, K. E., Wolf, C. R. and Palmer, C. N. (2001). "The peroxisome proliferator-activated receptor delta promotes lipid accumulation in human macrophages." J Biol Chem **276**(47): 44258-44265.

Walsh, C. T., Radeff-Huang, J., Matteo, R., Hsiao, A., Subramaniam, S., Stupack, D. and Brown, J. H. (2008). "Thrombin receptor and RhoA mediate cell proliferation through integrins and cysteine-rich protein 61." The FASEB Journal **22**(11): 4011-4021.

Wang, C., Zhou, G. and Zeng, Z. (2014). "Effects of peroxisome proliferator-activated receptor-beta/delta on sepsis induced acute lung injury." Chin Med J (Engl) **127**(11): 2129-2137.

Wang, D., Fu, L., Ning, W., Guo, L., Sun, X., Dey, S. K., Chaturvedi, R., Wilson, K. T. and DuBois, R. N. (2014). "Peroxisome proliferator-activated receptor delta promotes colonic inflammation and tumor growth." Proc Natl Acad Sci U S A **111**(19): 7084-7089.

Wang, D., Wang, H., Guo, Y., Ning, W., Katkuri, S., Wahli, W., Desvergne, B., Dey, S. K. and DuBois, R. N. (2006). "Crosstalk between peroxisome proliferator-activated receptor delta and VEGF stimulates cancer progression." Proc Natl Acad Sci U S A **103**(50): 19069-19074.

Wang, L. Y., Niu, Z. Z., Hu, B. X., Wu, J. M., Jiang, X., Hu, X. F., Huang, W. H., Ouyang, J., Yu, L. and Qiu, X. Z. (2011). "Long-term intraperitoneal injection of lipopolysaccharide induces high expression of Id2 in the brain of mice." Mol Biol Rep **38**(6): 4193-4196.

Wang, X., Hao, Y., Wang, X., Wang, L., Chen, Y., Sun, J. and Hu, J. (2016). "A PPARdelta-selective antagonist ameliorates IMQ-induced psoriasis-like inflammation in mice." Int Immunopharmacol **40**: 73-78.

Wang, Y.-X., Lee, C.-H., Tiep, S., Yu, R. T., Ham, J., Kang, H. and Evans, R. M. (2003). "Peroxisome-proliferator-activated receptor δ activates fat metabolism to prevent obesity." Cell **113**(2): 159-170.

Ware, L. B. and Matthay, M. A. (2000). "The acute respiratory distress syndrome." N Engl J Med **342**(18): 1334-1349.

Wepler, M., Hafner, S., Scheuerle, A., Reize, M., Groger, M., Wagner, F., Simon, F., Matallo, J., Gottschalch, F., Seifritz, A., Stahl, B., Matejovic, M., Kapoor, A., Moller, P., Calzia, E., Georgieff, M.,

Wachter, U., Vogt, J. A., Thiemermann, C., Radermacher, P. and McCook, O. (2013). "Effects of the PPAR-beta/delta agonist GW0742 during resuscitated porcine septic shock." Intensive Care Med Exp **1**(1): 28.

Wu, C. C., Baiga, T. J., Downes, M., La Clair, J. J., Atkins, A. R., Richard, S. B., Fan, W., Stockley-Noel, T. A., Bowman, M. E., Noel, J. P. and Evans, R. M. (2017). "Structural basis for specific ligation of the peroxisome proliferator-activated receptor delta." Proc Natl Acad Sci U S A **114**(13): E2563-e2570.

Wu, K., Yang, Y., Liu, D., Qi, Y., Zhang, C., Zhao, J. and Zhao, S. (2016). "Activation of PPARgamma suppresses proliferation and induces apoptosis of esophageal cancer cells by inhibiting TLR4-dependent MAPK pathway." Oncotarget.

Wu, T. T., Niu, H. S., Chen, L. J., Cheng, J. T. and Tong, Y. C. (2016). "Increase of human prostate cancer cell (DU145) apoptosis by telmisartan through PPAR-delta pathway." Eur J Pharmacol **775**: 35-42.

Xie, Z., Gong, M. C., Su, W., Xie, D., Turk, J. and Guo, Z. (2010). "Role of calcium-independent phospholipase A2beta in high glucose-induced activation of RhoA, Rho kinase, and CPI-17 in cultured vascular smooth muscle cells and vascular smooth muscle hypercontractility in diabetic animals." J Biol Chem **285**(12): 8628-8638.

Xie, Z., Su, W., Guo, Z., Pang, H., Post, S. R. and Gong, M. C. (2006). "Up-regulation of CPI-17 phosphorylation in diabetic vasculature and high glucose cultured vascular smooth muscle cells." Cardiovasc Res **69**(2): 491-501.

Xu, H. E., Lambert, M. H., Montana, V. G., Parks, D. J., Blanchard, S. G., Brown, P. J., Sternbach, D. D., Lehmann, J. M., Wisely, G. B., Willson, T. M., Kliewer, S. A. and Milburn, M. V. (1999). "Molecular recognition of fatty acids by peroxisome proliferator-activated receptors." Mol Cell **3**(3): 397-403.

Xu, H. E., Lambert, M. H., Montana, V. G., Plunket, K. D., Moore, L. B., Collins, J. L., Oplinger, J. A., Kliewer, S. A., Gampe, R. T., Jr., McKee, D. D., Moore, J. T. and Willson, T. M. (2001). "Structural determinants of ligand binding selectivity between the peroxisome proliferator-activated receptors." Proc Natl Acad Sci U S A **98**(24): 13919-13924.

Yang, L., Zhou, J., Ma, Q., Wang, C., Chen, K., Meng, W., Yu, Y., Zhou, Z. and Sun, X. (2013). "Knockdown of PPAR delta gene promotes the growth of colon cancer and reduces the sensitivity to bevacizumab in nude mice model." PLoS One **8**(4): e60715.

Yin, L., Busch, D., Qiao, Z., van Griensven, M., Teuben, M., Hildebrand, F., Pape, H. C. and Pfeifer, R. (2018). "Dose-dependent effects of peroxisome proliferator-activated receptors beta/delta agonist on systemic inflammation after haemorrhagic shock." Cytokine **103**: 127-132.

Yu, K., Bayona, W., Kallen, C. B., Harding, H. P., Ravera, C. P., McMahon, G., Brown, M. and Lazar, M. A. (1995). "Differential activation of peroxisome proliferator-activated receptors by eicosanoids." J Biol Chem **270**(41): 23975-23983.

Yuan, J. X., Aldinger, A. M., Juhaszova, M., Wang, J., Conte, J. V., Jr., Gaine, S. P., Orens, J. B. and Rubin, L. J. (1998). "Dysfunctional voltage-gated K+ channels in pulmonary artery smooth muscle cells of patients with primary pulmonary hypertension." Circulation **98**(14): 1400-1406.

Yue, X., Wu, M., Jiang, H., Hao, J., Zhao, Q., Zhu, Q., Saren, G., Zhang, Y. and Zhang, X. (2016). "Endothelial lipase is upregulated by interleukin-6 partly via the p38 MAPK and p65 NF-kappaB signaling pathways." Mol Med Rep **14**(3): 1979-1985.

Zhang, J., Fu, M., Zhu, X., Xiao, Y., Mou, Y., Zheng, H., Akinbami, M. A., Wang, Q. and Chen, Y. E. (2002). "Peroxisome proliferator-activated receptor delta is up-regulated during vascular lesion formation and promotes post-confluent cell proliferation in vascular smooth muscle cells." J Biol Chem **277**(13): 11505-11512.

Zhang, J. S., Herreros-Villanueva, M., Koenig, A., Deng, Z., de Narvajas, A. A., Gomez, T. S., Meng, X., Bujanda, L., Ellenrieder, V., Li, X. K., Kaufmann, S. H. and Billadeau, D. D. (2014). "Differential activity of GSK-3 isoforms regulates NF-kappaB and TRAIL- or TNFalpha induced apoptosis in pancreatic cancer cells." Cell Death Dis **5**: e1142.

Zhao, Y. Y., Weir, M. A., Manno, M., Cordy, P., Gomes, T., Hackam, D. G., Juurlink, D. N., Mamdani, M., Moist, L., Parikh, C. R., Paterson, J. M., Wald, R., Yao, Z. and Garg, A. X. (2012). "New fibrate use and acute renal outcomes in elderly adults: a population-based study." Ann Intern Med **156**(8): 560-569.

Zheng, Z., Yu, S., Zhang, W., Peng, Y., Pu, M., Kang, T., Zeng, J., Yu, Y. and Li, G. (2017). "Genistein attenuates monocrotaline-induced pulmonary arterial hypertension in rats by activating PI3K/Akt/eNOS signaling." Histol Histopathol **32**(1): 35-41.

Zhu, B., Ferry, C. H., Blazanin, N., Bility, M. T., Khozoie, C., Kang, B. H., Glick, A. B., Gonzalez, F. J. and Peters, J. M. (2014). "PPARbeta/delta promotes HRAS-induced senescence and tumor suppression by potentiating p-ERK and repressing p-AKT signaling." Oncogene **33**(46): 5348-5359.

Zhu, B., Ferry, C. H., Markell, L. K., Blazanin, N., Glick, A. B., Gonzalez, F. J. and Peters, J. M. (2014). "The nuclear receptor peroxisome proliferator-activated receptor-beta/delta (PPARbeta/delta) promotes oncogene-induced cellular senescence through repression of endoplasmic reticulum stress." J Biol Chem **289**(29): 20102-20119.

Zhu, Y., Qi, C., Calandra, C., Rao, M. S. and Reddy, J. K. (1996). "Cloning and identification of mouse steroid receptor coactivator-1 (mSRC-1), as a coactivator of peroxisome proliferator-activated receptor gamma." Gene Expr **6**(3): 185-195.

Zhu, Y., Qi, C., Jain, S., Rao, M. S. and Reddy, J. K. (1997). "Isolation and characterization of PBP, a protein that interacts with peroxisome proliferator-activated receptor." J Biol Chem **272**(41): 25500-25506.

Zingarelli, B., Piraino, G., Hake, P. W., O'Connor, M., Denenberg, A., Fan, H. and Cook, J. A. (2010). "Peroxisome proliferator-activated receptor {delta} regulates inflammation via NF-{kappa}B signaling in polymicrobial sepsis." Am J Pathol **177**(4): 1834-1847.

Ziv, E., Shafrir, E., Kalman, R., Galer, S. and Bar-On, H. (1999). "Changing pattern of prevalence of insulin resistance in Psammomys obesus, a model of nutritionally induced type 2 diabetes." <u>Metabolism</u> **48**(12): 1549-1554.
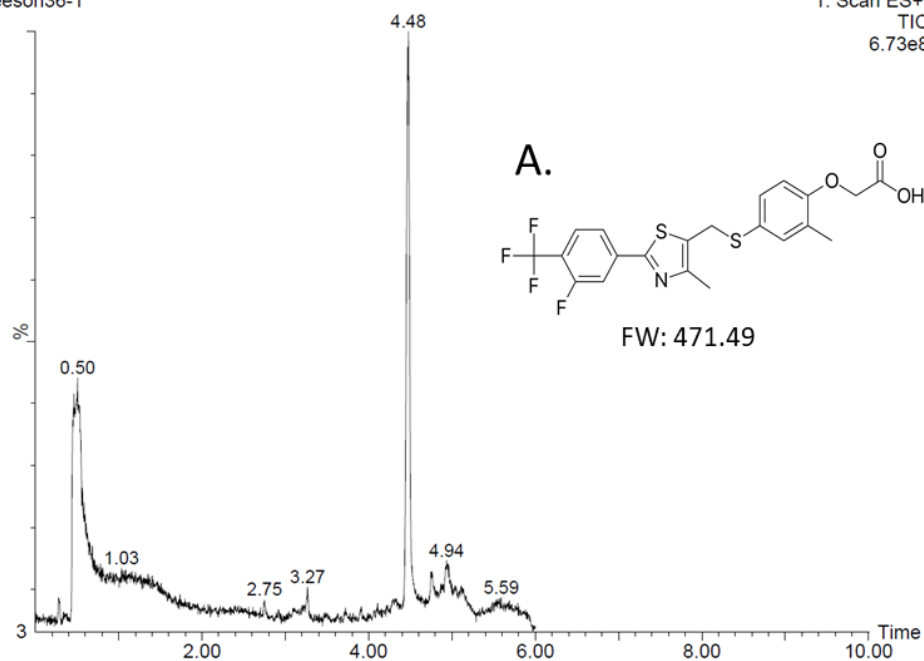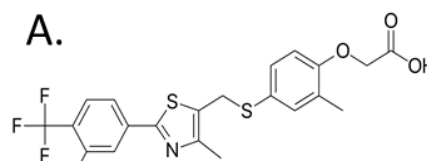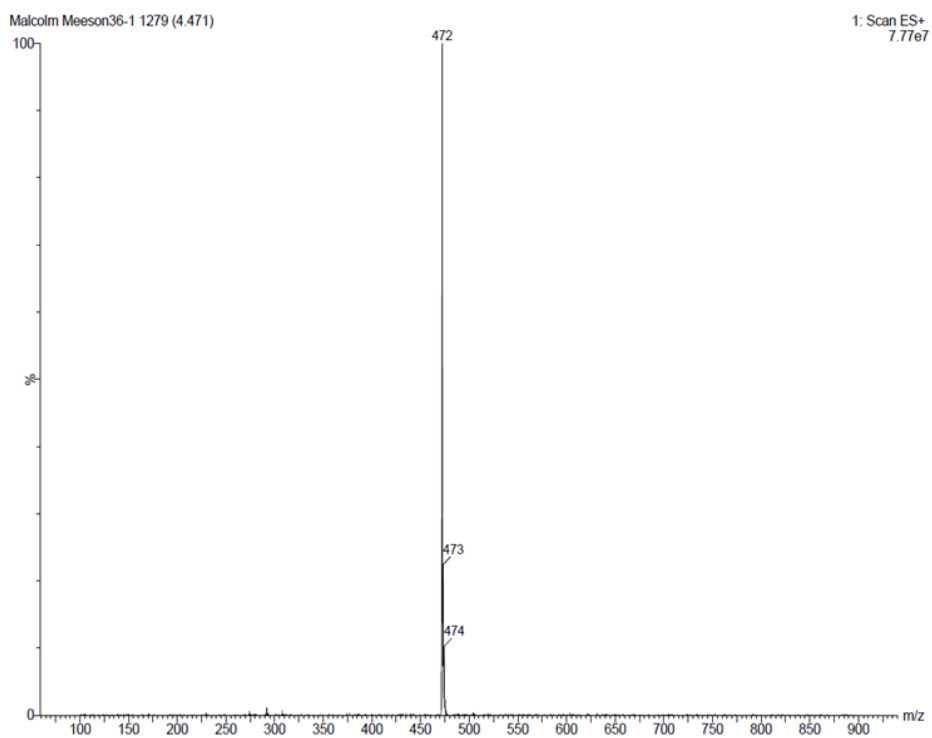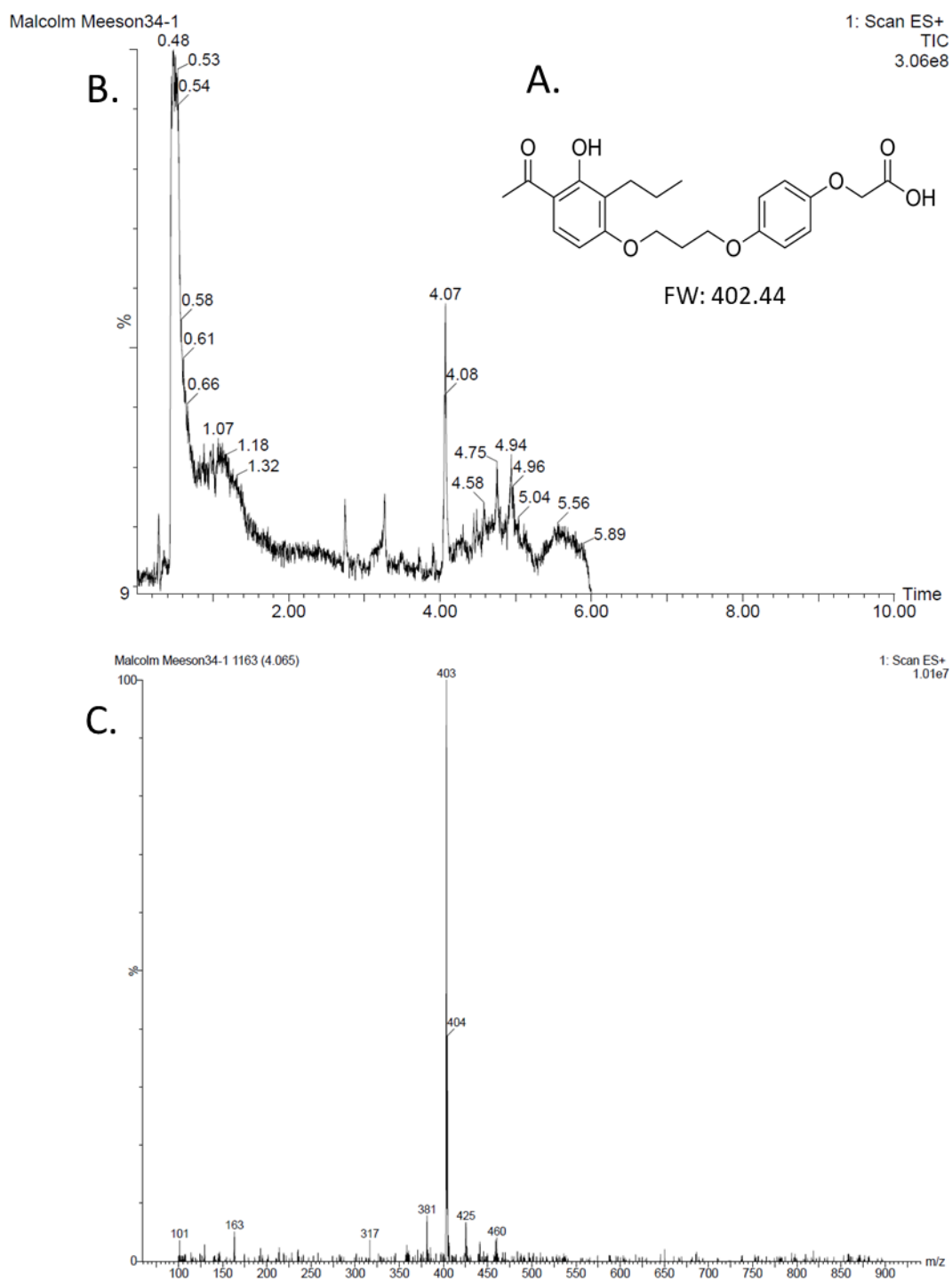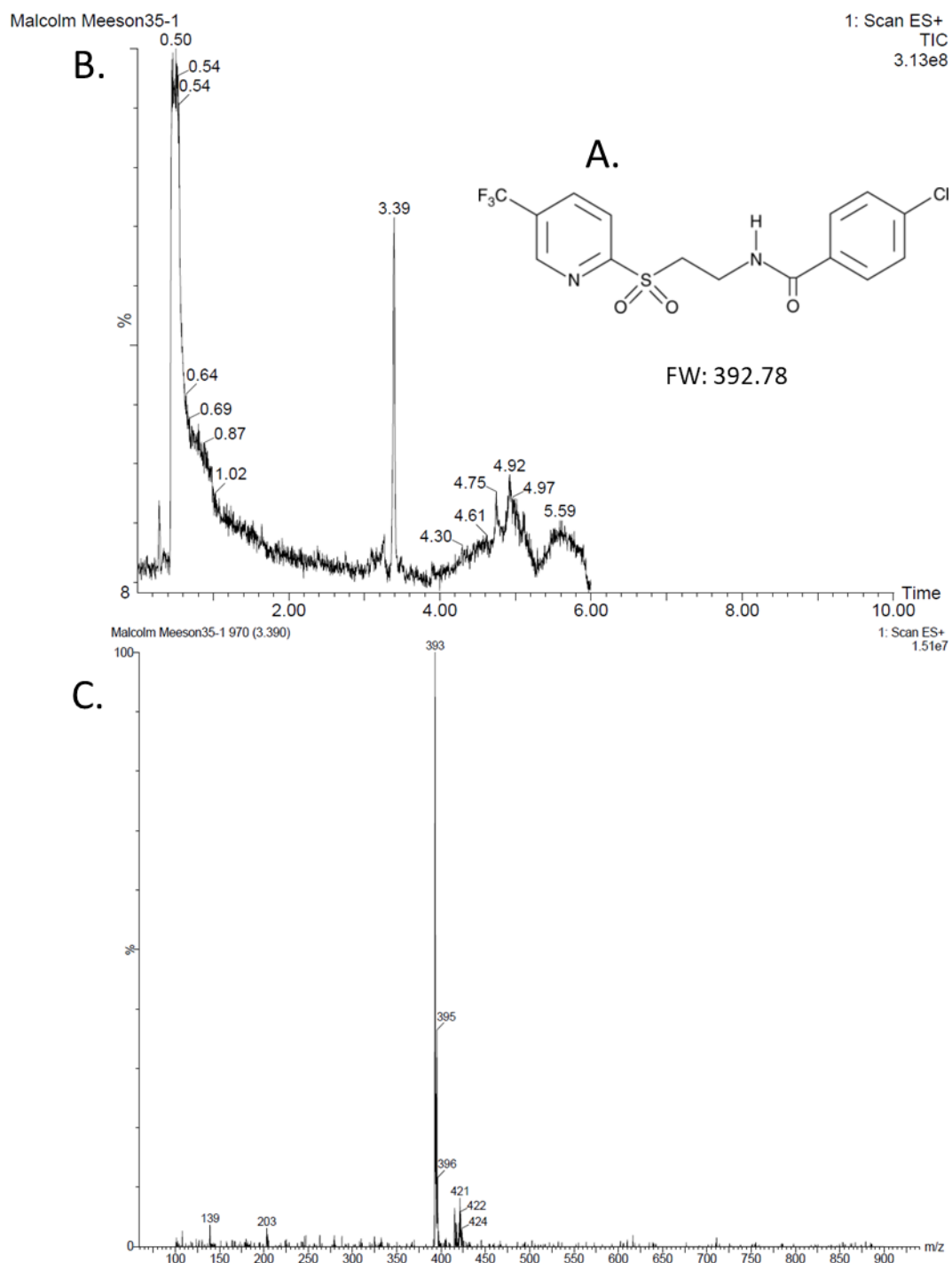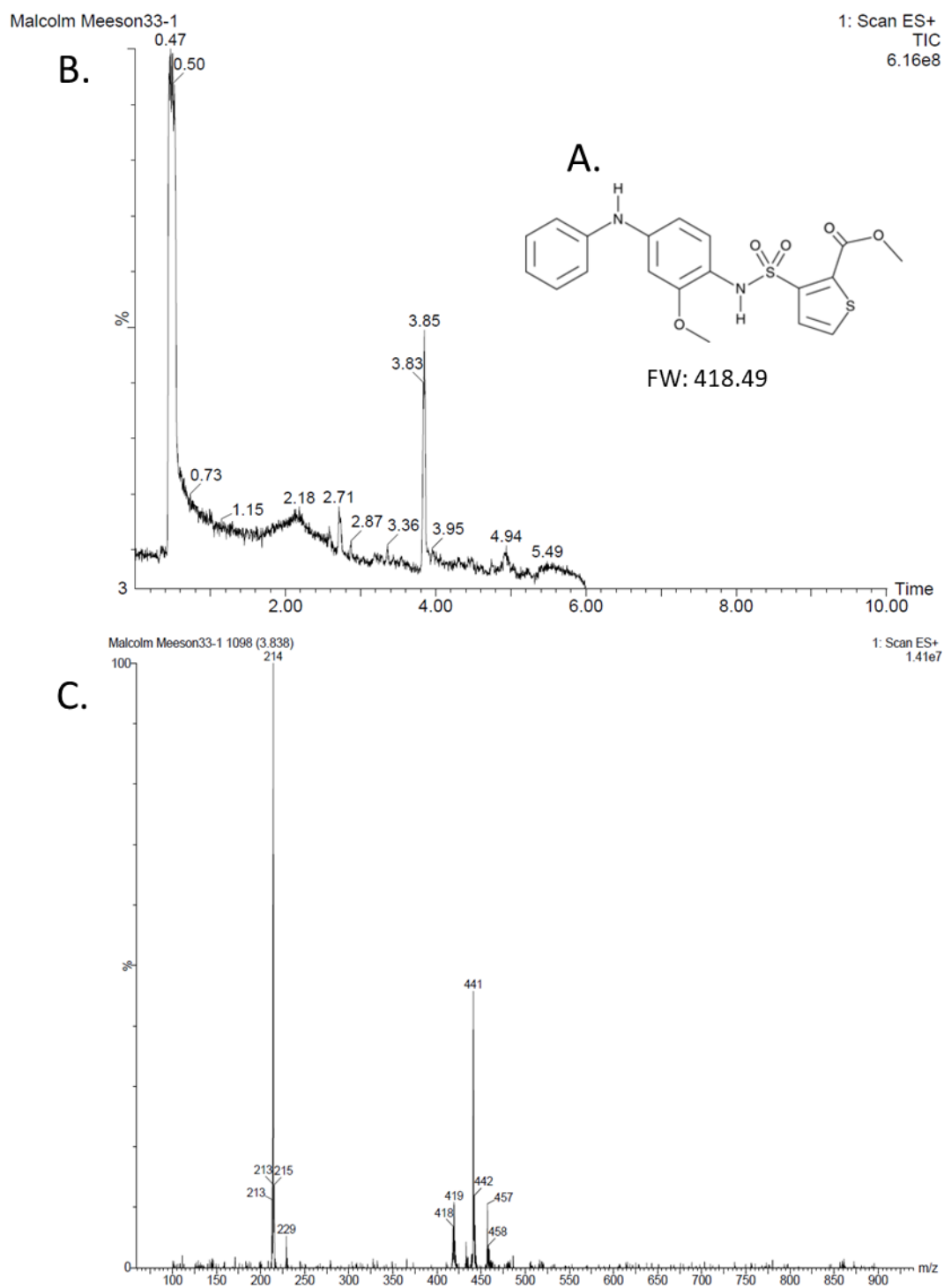
Appendix A

GW0742

B.

A.

FW: 471.49

C.

Figure 1. GW0742 mass spectrometry results. A sample of 0.1 mg/mL GW0742 in DMSO was run in a mass spectrophotometer. A) GW0742 structure and molecular weight. B) UV spectrum. C) Mass spectrum at the time of the largest peak

L-165041

Figure 2. L-165041 mass spectrometry results. A sample of 0.1 mg/mL L-165041 in DMSO was run in a mass spectrophotometer. A) L-165041 structure and molecular weight. B) UV spectrum. C) Mass spectrum at the time of the largest peak
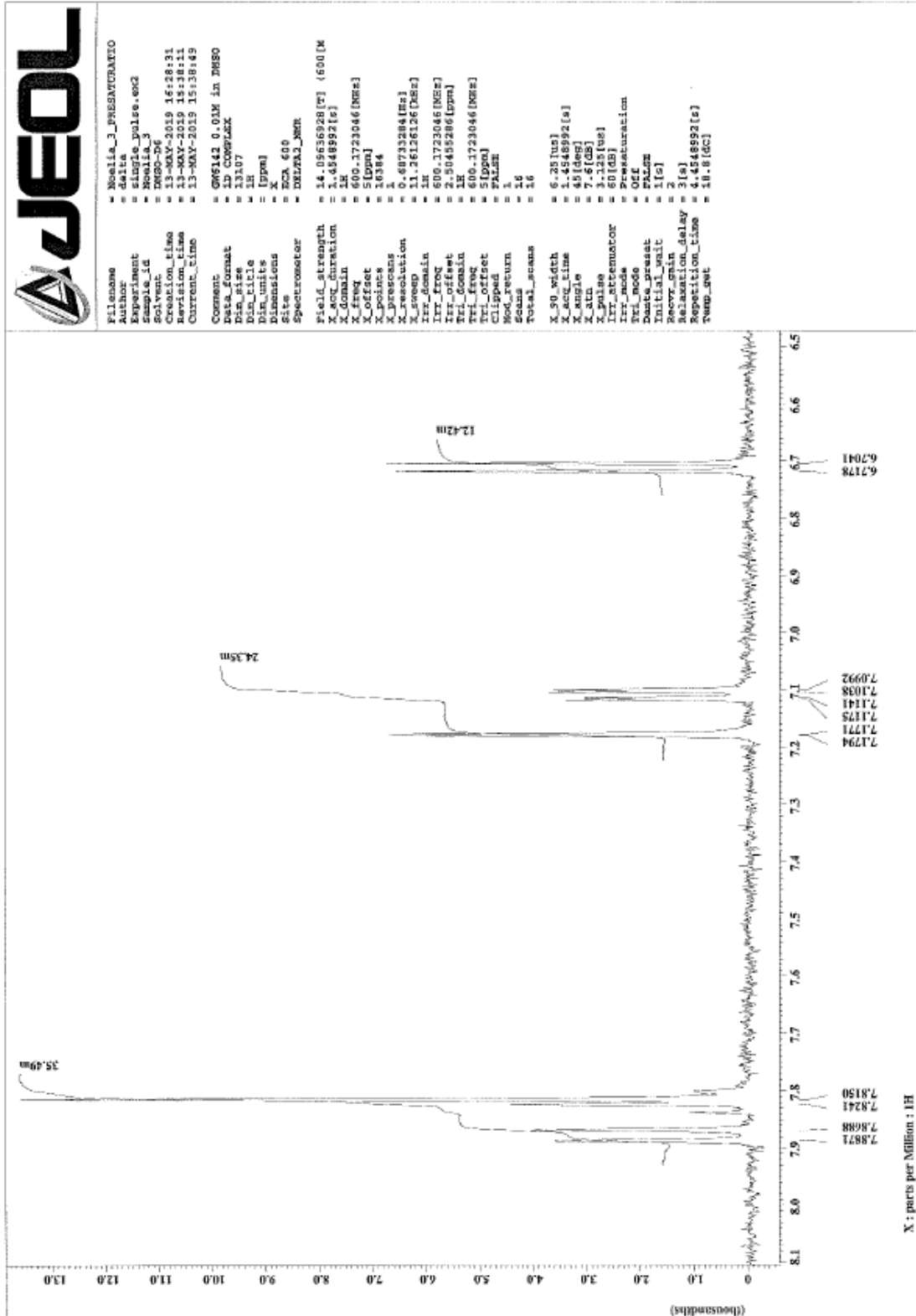
GSK3787

Figure 3 . GSK3787 mass spectrometry results. A sample of 0.1 mg/mL GSK3787 in DMSO was run in a mass spectrophotometer. A) GSK3787 structure and molecular weight. B) UV spectrum. C) Mass spectrum at the time of the largest peak

GSK0660

Figure 4. GSK0660 mass spectrometry results. A sample of 0.1 mg/mL GSK0660 in DMSO was run in a mass spectrophotometer. A) GSK0660 structure and molecular weight. B) UV spectrum. C) Mass spectrum at the time of the largest peak
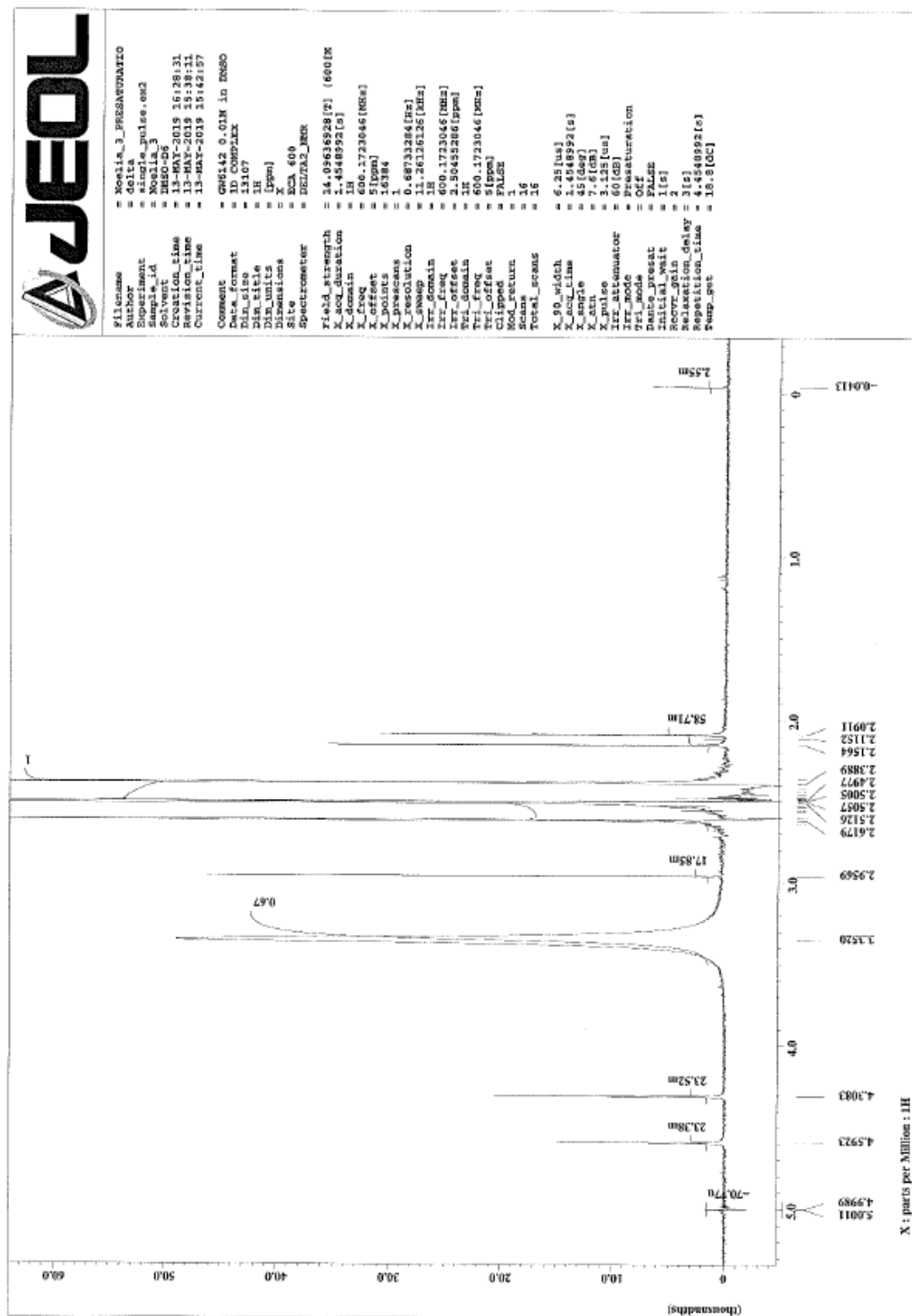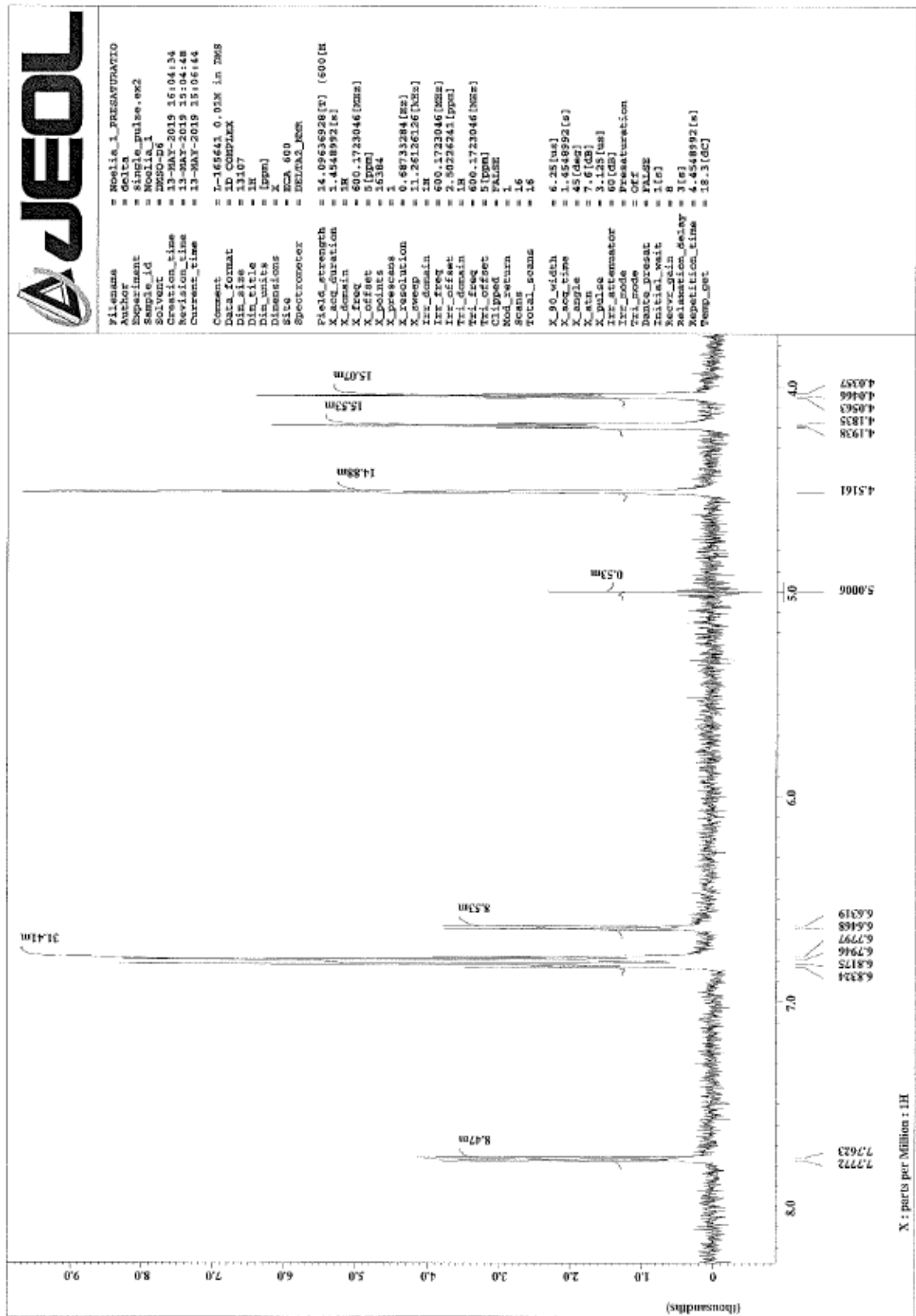
Appendix B

GW0742

A.
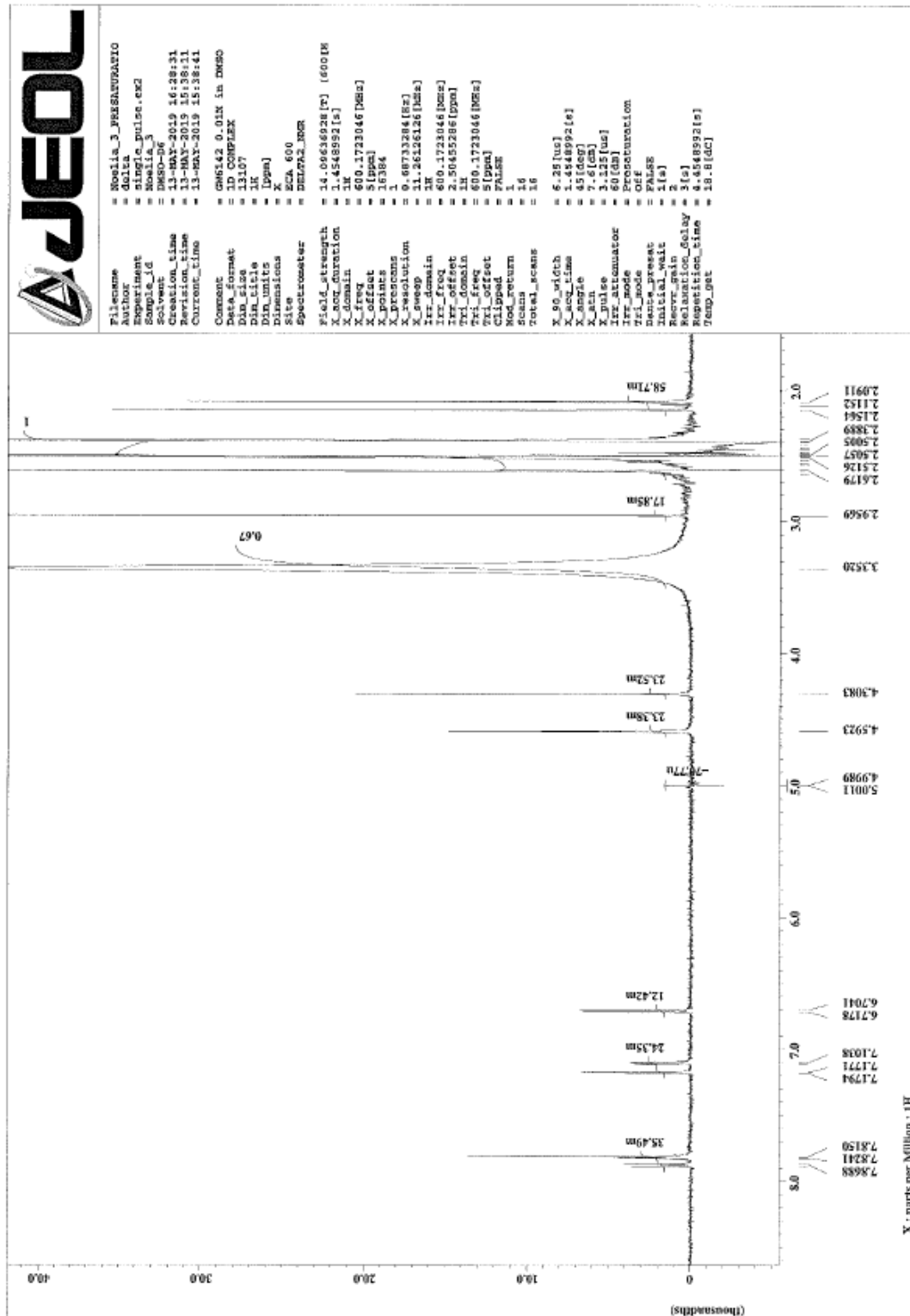
B.

C.

Figure 1. H-NMR spectrum of GW0742. A sample of 1 mg GW0742 in deuterated DMSO was run for NMR spectroscopy. A) Wide spectrum B, C) Spectrum zoom in.
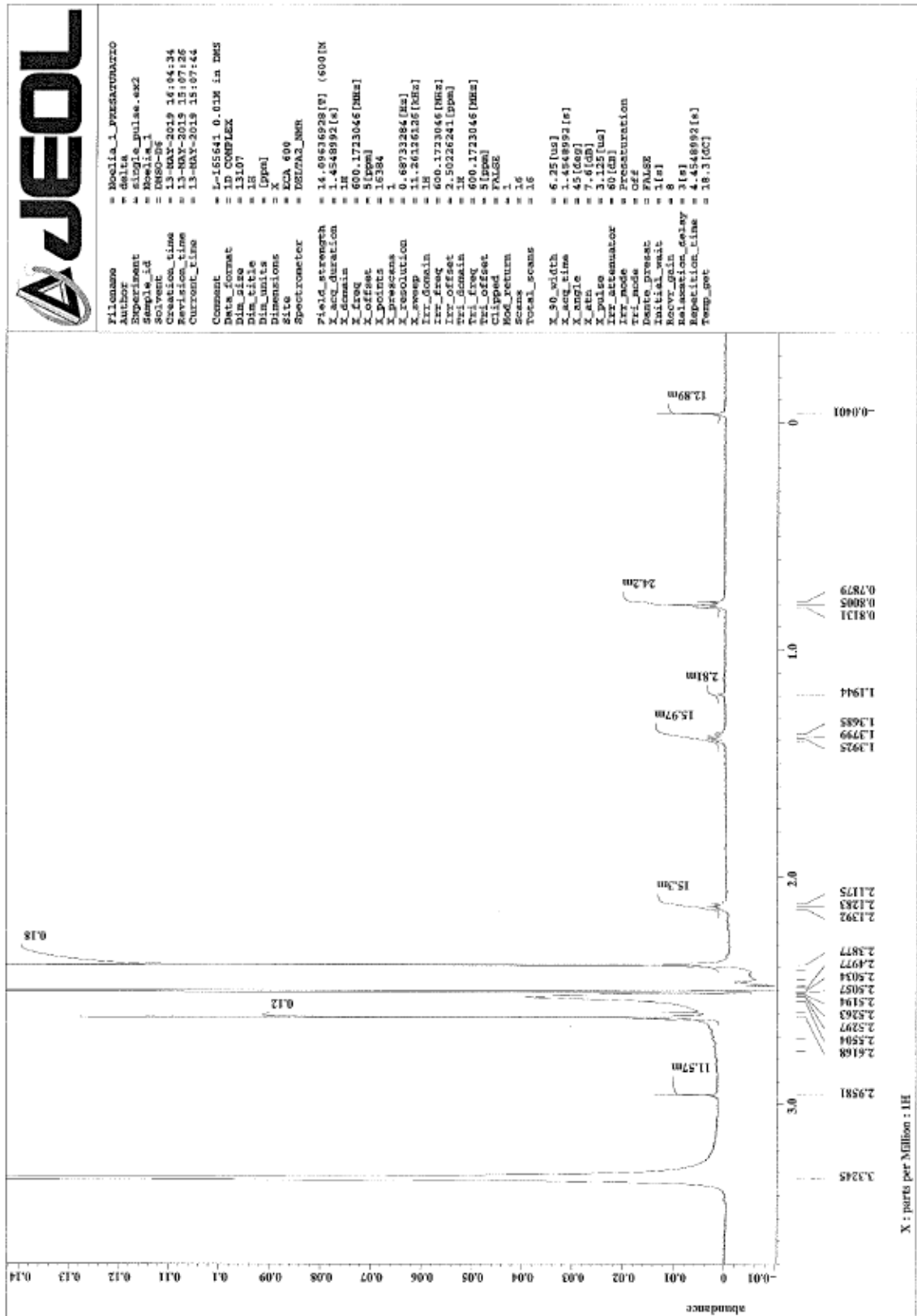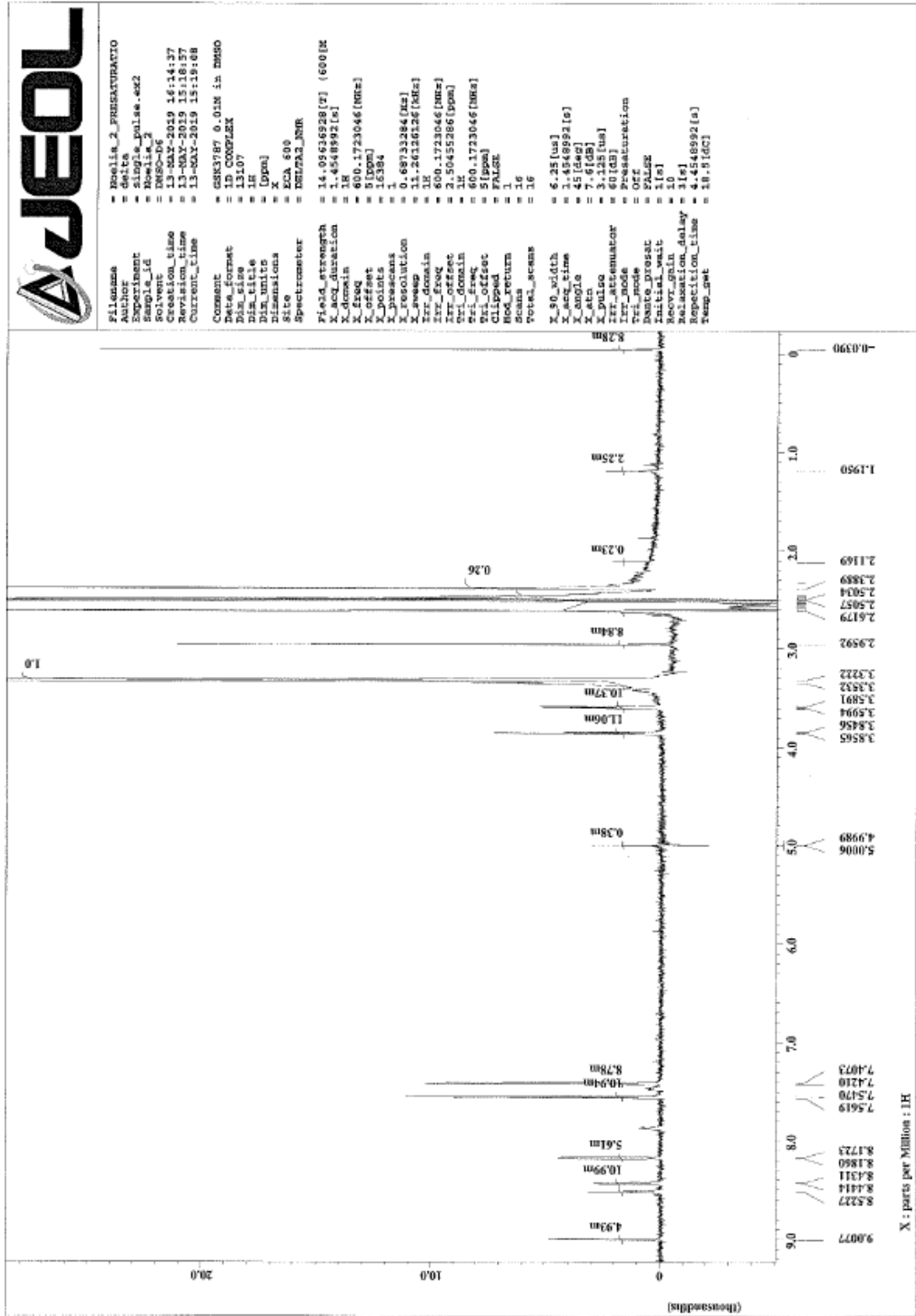
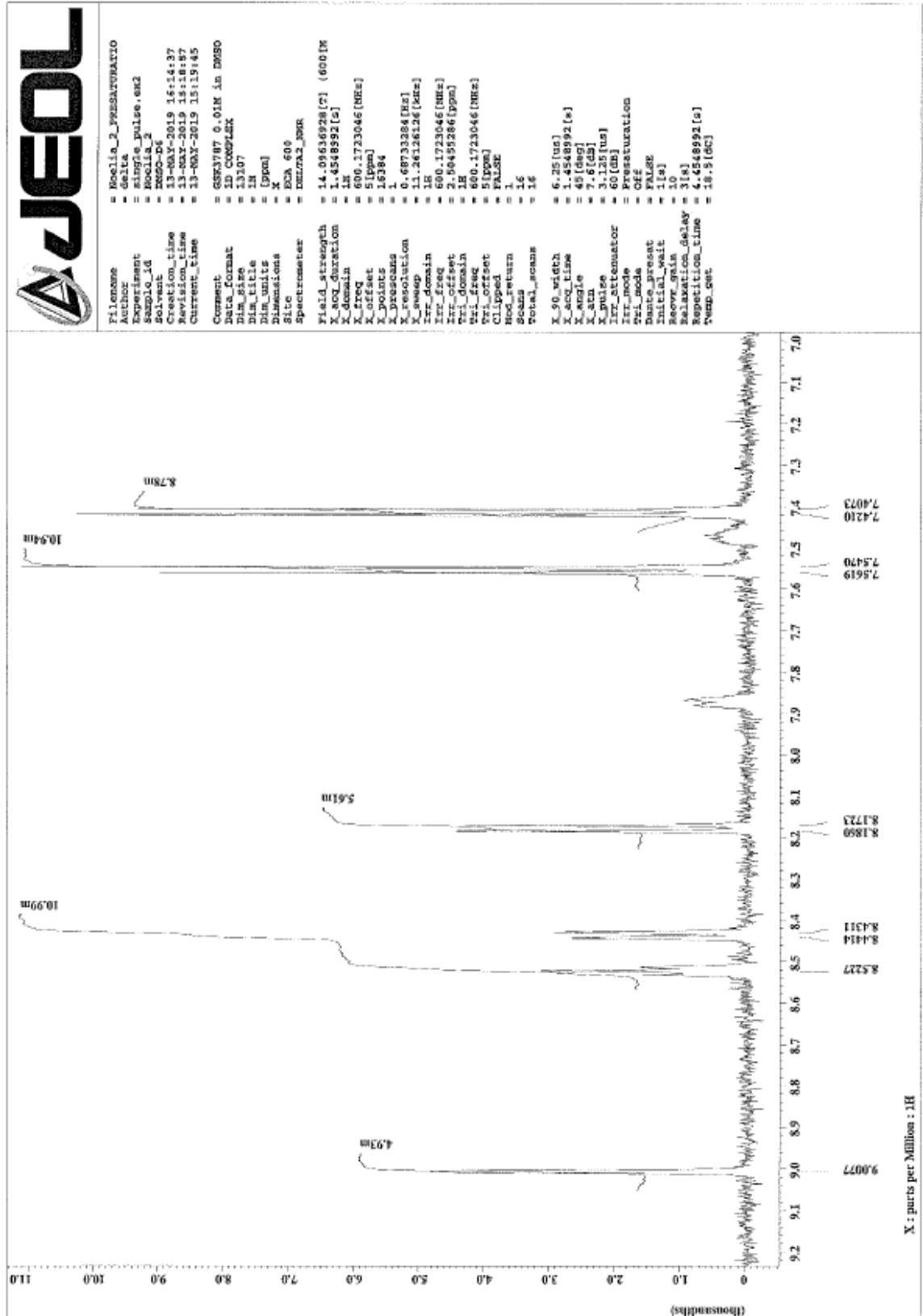**L-165041**

A.

B.

C.

D.

Figure 2. H-NMR spectrum of L-165041. A sample of 1 mg L-165041 in deuterated DMSO was run for NMR spectroscopy. A) Wide spectrum B, C, D) Spectrum zoom in.
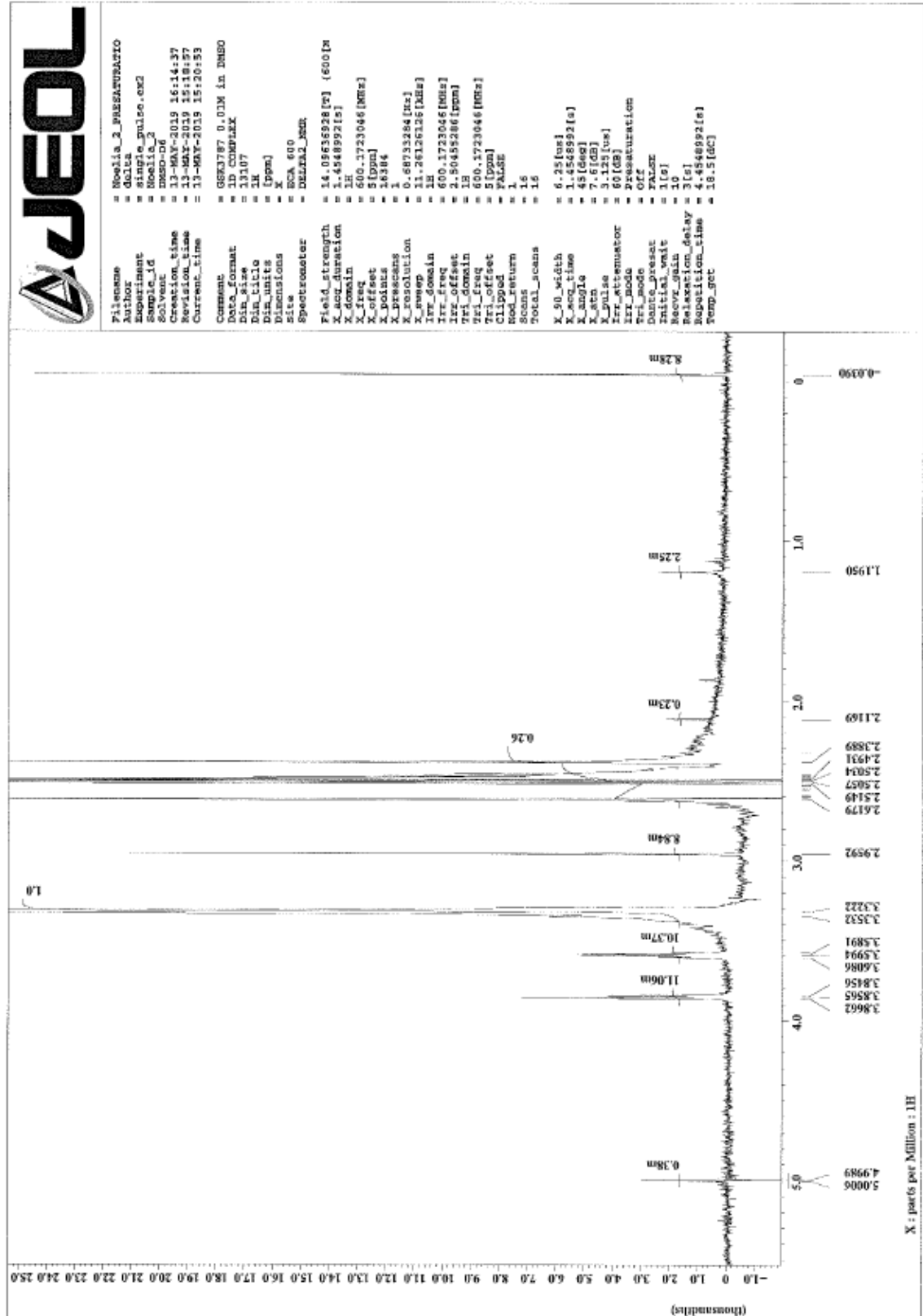
GSK3787

A.

B.

C.

D.

Figure 3 . H-NMR spectrum of GSK3787. A sample of 1 mg GSK3787 in deuterated DMSO was run for NMR spectroscopy. A) Wide spectrum B, C, D) Spectrum zoom in.

GSK0660

A.

B.

Figure 4. H-NMR spectrum of GSK0660. A sample of 1 mg GSK0660 in deuterated DMSO was run for NMR spectroscopy. A) Wide spectrum B) Spectrum zoom in.